Ministero dell'Università
e della Ricerca

Dipartimento di Scienze
Fisiche ed Astronomiche

Università degli Studi
di Palermo

DIPARTIMENTO DI SCIENZE FISICHE ED ASTRONOMICHE

DOTTORATO DI RICERCA IN FISICA - XIX CICLO

EFFECTS OF METAL IONS ON AGGREGATION PROCESSES OF WHEY PROTEINS

S.S.D FIS/07

Giovanna Navarra

Palermo, febbraio 2008

Supervisore: prof. Maurizio Leone

Coordinatore: prof. Natale Robba

To Giancarlo and Alessandro

Contents

List of Abbreviations

0.5Cu-BLG 3.3 mM BLG with 0.5 mM $CuCl_2$ in solution, pH 4 and 2.5

10Cu-BLG(BSA)…3.3 mM BLG (1mM BSA) cold gel induced by 10mM $CuCl_2$

10Zn-BLG(BSA)…3.3 mM BLG (1mM BSA) cold gel induced by 10mM $ZnCl_2$

30Cu-BLG(BSA)…3.3 mM BLG (1mM BSA) cold gel induced by 30mM $CuCl_2$

30Zn-BLG(BSA)…3.3 mM BLG (1mM BSA) cold gel induced by 30mM $ZnCl_2$

3Cu-BLG 3.3 mM BLG with 3 mM $CuCl_2$ in solution, pH 4 and 2.5

Aβ Amyloid β(-peptide)

A-BLG 3.3 mM BLG cold gel induced by glucono-δ-lactone (0.42%w/w)

A-BSA 1 mM BSA cold gel induced by glucono-δ-lactone (0.42% w/w)

AD Alzheimer disease

BLG Bovine β-Lactoglobulin

BSA Bovine Serum Albumin

Cu-BLG 3.3 mM BLG with 1 mM $CuCl_2$ in solution, pH 7

Cu-BSA 1 mM BSA with 0.3 mM $CuCl_2$ in solution, pH 7

DLS Dynamic Light Scattering

ΔAbs Differential Absorption Intensity

FTIR Fourier Transform Infrared (absorption)

HSA Human Serum Albumin

MES 2-(N-morpholino)ethanesulfonic acid

NEMO N-ethylmorpholine

pI Isoelectric point

WPI Whey Protein Isolate

Zn-BLG 3.3 mM BLG with 1 mM $ZnCl_2$ in solution

Zn-BSA 1 mM BSA with 0.3 mM $ZnCl_2$ in solution, pH = 7

Overview

Protein aggregation processes have been subject of several studies because of their relevance in many fields of the scientific and technological research, from medicine to alimentary sciences. These recent researches have shown that these kinds of processes involve several mechanisms: for example, conformational and structural changes at single protein level, nucleation processes and protein-protein interactions with consequent formation of new intermolecular bonds. These mechanisms acting on different scales of time and space may evolve in different phases and be interconnected [**Manno et al., 2004**; **San Biagio et al., 1999**, **Militello et al. 2003**]. Under specific destabilizing conditions, all proteins seem to have the ability to "misfold" and subsequently assemble themselves in ordered sovramolecular aggregates known as Amyloid fibrils [**Arai et al., 1999**, **Fandrich et al., 2001**]. Amyloid fibril formation appears to be a fundamental event in the etiology of different pathologies (amyloidos) such as Parkinson's, Alzheimer's and Creutzfeldt-Jacob diseases. All these pathologies are related to abnormous extracellular deposition of amyloid fibrils [**Kelly 1998**, **Uversky et al., 2001**, **Foguel et al., 2003**]. It is important to note that also globular proteins with no homology to each other or to the disease-associated proteins have the ability to form fibrils resembling those extracted from diseased tissue [**Arai et al. 1999**].

In this framework, the presence of metal ions in the protein solutions can lead to different aggregation and/or denaturation processes respect to the one peculiar of the protein, being these differences dependent on the kind of metal and on its concentration. Metal ions have an active role both in thermal aggregation and cold set gelation processes. These processes are quite different, but both are based on the proteins ability to form aggregates.

In the field of biomedical sciences, great interest has been devoted to the study of the effects induced by metal ions on the formation of fibrils and on the mechanisms at the base of the proteins aggregation. Indeed, the presence of metal

ions, together with the amyloid fibrils formation, appears to be one of the fundamental aspects in the etiology of different pathologies (amyloidos) such as the already mentioned diseases. It has been observed that the senile plaques typical of the Alzheimer disease contain high quantities of metal ions such Cu^{+2}, Fe^{+3} e Zn^{+2} (the last one being the most abundant). The role of these ions has not been yet clarified but several evidences indicate a their implication in the arising of the pathogenic disease: for example, the fibrils formation by beta amyloid peptide, (i.e. the main component of the plaques) results to be sizeably accelerated by zinc and copper ions presence [**Bush et al., 1994**; **Mantyh et al., 1993**]. For this reason, it appears clear that these ions could have significant consequences on unfolding and/or on aggregation processes.

Moreover, metal ions could be able to affect aggregates structure typology on a macroscopic scale. For instance, iron ions induce "cold gelation" processes in aggregate structures rising from β-Lactoglobulin (BLG), which is one of the main constituent of ruminant milk whey [**Remondetto et al., 2003**].

Recently, the researchers' interest has moved towards the cold gelation of proteins; in fact, this alternative way to obtain gels from proteins has immediate applications in food technology and engineering. This process is very important in biotechnology and, in particular, in tissue engineering because its last gelation step does not require high temperatures, so allowing the cell growth. The cold gelation of whey protein is relevant in the food technology. Whey protein gels are widely used in food as gelling agents, emulsifiers, texture modifiers, thickening agents and foaming agents. In addition to their functional characteristics, they also have the advantages of a high nutritive value and are generally recognized as safe status; for this reason, they are generally referred to as "label friendly" ingredients. In this sense, the addition of metal ions to solutions can be considered as an important tool to induce cold gelation of proteins. For this reason, a suitable knowledge of the processes that form the basis should allow to rule the mechanical and sensorial properties of the gels by varying the kind and the concentration of metal ions.

The aim of this PhD research work has been the study of the role of metal ions, in particular copper and zinc ions, during the aggregation processes (thermal aggregation and cold-set gelation) of some model-proteins earlier profusely characterized, as well as β-Lactoglobulin (BLG), and Bovine Serum Albumin (BSA). For this reason, the conformational changes at level of the secondary and tertiary structures, have been analysed via the time evolution of Amide I′ and Amide II bands profiles, monitored by Fourier Transform infrared (FTIR) absorption spectroscopy, while the growth of aggregates has been monitored by dynamic light scattering, through the time evolution of the scattering intensity and the z-average diameter of the species in solution, mainly focusing the interest on the differences related to the presence of the metal ions in solution during the aggregation process. Cold-set gels induced by metal ions have been studied too; in particular, the aggregates dimension and the conformational changes induced by the heating treatment, being the first step of the formation of a cold-induced gel, have been characterized and the mechanical properties of the gels induced by the addition of metal ions have been investigated by rheological measurements.

This work is part of the research activities of the molecular biophysics group of the Dept. of Physical and Astronomical Sciences (DSFA) in Palermo. This group has a relevant scientific expertise in the study of the conformational changes involved in the aggregation processes of different proteins [**Militello et al. 2003**, and **2004**, **Vetri et al., 2005**, **2007a** and **2007b**, **Librizzi 2005** and **2007**].

Outline of the thesis

This thesis is organized in 6 chapters. In chapter 1, a general introduction on the aggregation and gelation processes of the proteins even in presence of metal ions has been reported. In chapter 2, the main details on the protein solution and gels preparation and on the selected experimental settings are reported together with the basic theoretical background of the used techniques. In chapters 3 and 4, the experimental results concerning the influence of metal ions on thermal aggregation of BLG and BSA, obtained in several experimental conditions, are reported and discussed. Chapter 5 contains the results concerning the characterization of cold-set gels of BLG and BSA induced by the addition of copper or zinc ions to the pre-heated solutions. Finally, the main results are summarized in chapter 6.

Chapter 1

Scientific background

1.1 The proteins: a brief description

Proteins perform many vital functions and for this reason, they are usually indicated as the "molecules of the life". Indeed, their function is fundamental also for the correct performance of important physiological tasks. In this framework, a single protein molecule is considered as a component with a well-defined stoichiometry and geometry and which is not easily dissociated. Each protein is formed by a specific polypeptide chain. Every polypeptide is characterized by a distinct amino acids composition and sequence; in particular, 20 amino acids are common to all living organism on earth. This design strategy enables a vast array of different molecules to be efficiently constructed by a single type of factor in the cell, the ribosome, by controlling the order in which the amino acids are joined into the polypeptide chain using information encoded in DNA [**Vendruscolo et al., 2003**].

Amino acids are organic composts made by an carbon atom, C_α, at which a carboxylic group, COOH, an amidic group, NH_2, an hydrogen atom and a *residue* identifying the particular amino acid (as shown in figure 1.1) are bonded to. Different amino acids associate themselves covalently with peptidic bonds creating an amino acids chain (figure 1.2), via a condensation process through which a water molecule is made free. Amino acids chain forming the complete covalent structure of the protein defines its *primary structure*. Geometrical disposition of some locally ordered parts of the protein forms the *secondary structures*. These are regular structures that show a particular symmetry. The only symmetric three dimensional structure that can be constructed from a linear chain of chiral building blocks is an helix. These helices are held together by hydrogen bonds between the amino hydrogen atoms (the hydrogen bonds donors) and the carboxyl oxygen atoms (the hydrogen bonds acceptors). This kind of secondary structure, shown in figure 1.3, is called *α-helix*. A different and not symmetric secondary structure is represented by *β-sheet*, shown in figure 1.4; every strand of sheet is a regular and continuous two-fold helical structure, with hydrogen-bonding interactions between strands holding the sheet together. The residues involved in neither of these structures are often called "*random coil*" for sake of a better description, even though their structure may be far from random. Usually, this not ordered structure in the native state of the protein performs the links between the ordered secondary structures or it is in a more mobile part of the protein because of its functional works.

The secondary structure defines the geometry of the protein skeleton, also named backbone. The three-dimensional arrangement of the whole structure of the protein builds the *tertiary structure*. This includes a description not only of the local symmetric structure, but also of the spatial location of all residues as far as it is possible. Finally, the non covalent association of polypeptides forming a multimeric complex defines the *quaternary structure* of a protein. This level of structure is described mainly by the types and number of polypeptide subunits.

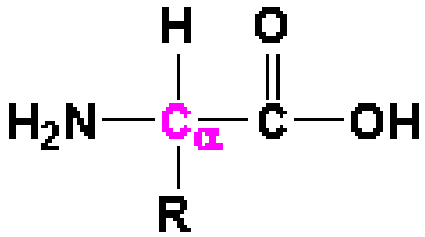

Figure 1.1: Schematic representation of one amino acid;
R is the residue that identifies it.

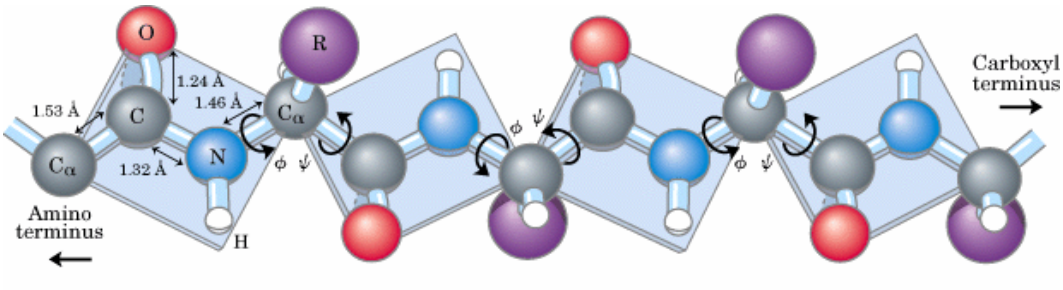

Figure 1.2: Geometry of peptide bond (identified by the cyan square in figure) and of the polypeptide chain.

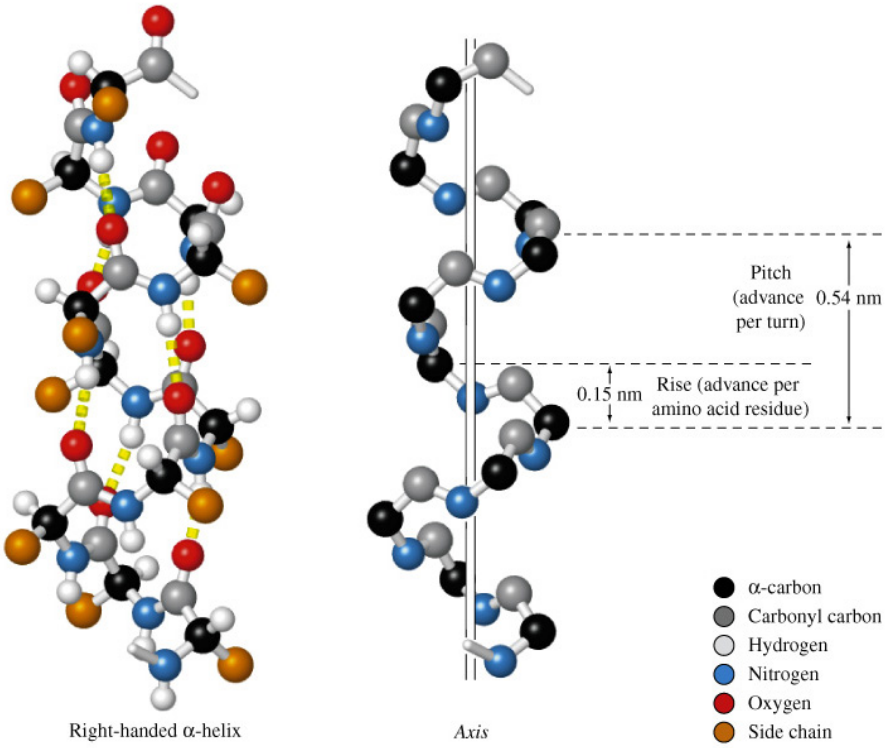

Figure 1.3: α-helix structures.

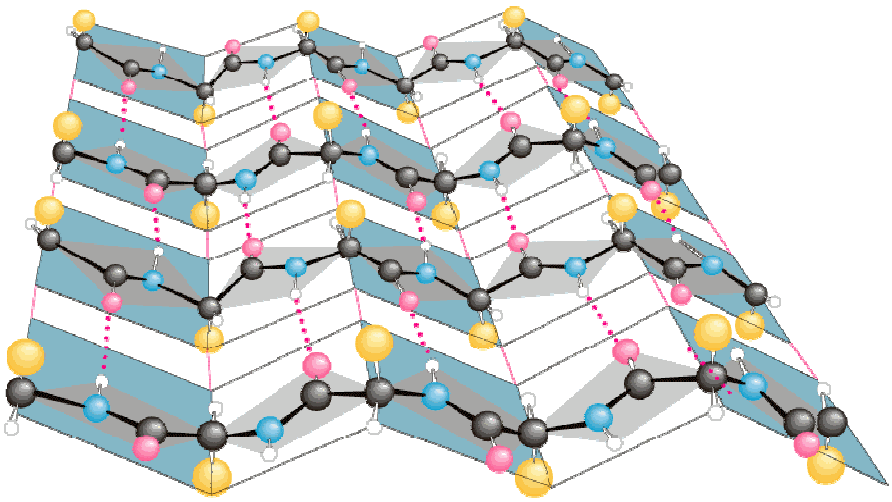

Figure 1.4: β-sheet structures.

The most complete description possible of a molecule in solution is its *conformation.* This word indicates what it is known about preferred orientations of groups which are in principle capable of movement by internal rotation. The conformation is generally an average over energetically accessible molecular structures, also considering the solvent molecules surrounding the proteins (proteins - solvent system).

Each protein, constituted by a specific polypeptide chain, folds in one way only after its synthesis; the native structure of a protein is the structure that it assumes after its natural folding in physiological conditions. The folding pathway is determined by the protein sequence and by the energetic interactions existing between the several secondary structures. These interactions stabilize the tertiary and quaternary structures of the protein molecule. Native functional state of the protein is thermodynamically stable; it can be considered as a function of state and does not depend on the process. This state should be at the global minimum of free energy relative to all other states accessible (correspond to different conformations) on that time scale [**Dill 1990**].

Different kinds of energetic interactions drive and stabilize the assembly of the proteins. Long-range and short-range interactions are involved in protein folding. These can be repulsive or attractive interactions.

An extremely repulsive interaction appears when many atoms have close separations and their electron clouds overlap [**Israelachvili 1992, Bryant et al, 1998**]. This kind of interaction determines how nearly the atoms can pack together. *Steric overlap interactions* play a role in determining the possible conformations of the protein in solution: a protein molecule can not assume any spatial disposition with two or more segments occupying the same place. An attractive interaction is represented by *van der Waals interactions*, which are interactions between existing or induced dipoles. They play a minor role in determining the final conformation of the protein since the van der Waals interactions are almost the same in the folded and unfolded states.

Hydrogen bonds play a fundamental role in the protein folding; in particular, they give a big contribution to the stability of the secondary structures, such as α–helices, of the tertiary structure and also the bonds between protein and solvent occur through them [**Dill 1990, Bryant et al., 1998**].

The main role in determining the conformation and the interactions of protein molecules in solution is played by the *Hydrofobic interactions*. They manifest themselves as strong attractive forces between non-polar groups separated by water. Actually, they are due to the capability of water molecules to form relatively strong hydrogen bonds with other water molecules, whereas non-polar molecules can only form relatively weak van der Waals bonds with their neighbors [**Israelachvili 1992, Bryant et al, 1998**]. When a non-polar molecule is introduced into water, a rearrangement of the water molecules in its immediate vicinity is induced; this rearrangement changes both the interaction energy and entropy of the system. The energetic changes due to the contanct of the non-polar molecules with water are thermodynamically unfavorable and for this reason the system tends to minimize the contact area between water and non-polar groups, producing an attractive force between the non-polar groups [**Dill 1990, Bryant et al., 1998**].

Electrostatic interactions act between species which have a permanent electrical charge. Generally, these interactions can be attractive or repulsive depending on the charge sign. The sign, magnitude and distribution of the charge on a protein molecule is governed principally by the pH of the aqueous solution [**Howell 1992**]. Proteins are negatively charged above their isoelectric point (pI); below, it they are positively charged and, at the isoelectric point, they have no net charge (although they still have some regions of positive charge and other regions of negative charge) [**Koning et al., 1992**]. Electrostatic interactions are also involved when a polyvalent ion simultaneously binds to the surface of at least two protein molecules that have the same charge, so realizing a bridging ion. These polyvalent ions may be low molecular weight species, such as Ca^{2+}, Mg^{2+}, or Al^{3+}, or high molecular weight biopolymers, such as polysaccharides or other proteins. The

presence of these ions in solution promotes the association since it reduces the magnitude of the electrostatic interactions through electrostatic screening [**Bryant et al., 1998, Remondetto et al., 2003**].

Covalent bonds, which have an important role in the stabilization of specific protein domains, are intra-molecular *S-S disulfide bridges.* These bonds are principally formed in alkaline conditions because of the SH groups oxidation of two residues of Cysteine. The interaction so created is very strong (≈ 200 kJ) and, when present, is responsible of the high stability of the polypeptide chain of the protein. Moreover, this kind of bond can also occur between residues of Cysteine of different protein molecules, in such a way realizing stable aggregates.

The main contribute opposing the folding of globular proteins is the entropy associated with the greater number of configurational states that an unfolded protein can take up relatively to the folded protein [**Dill 1990, Bryant et al., 1998**].

The general characteristics of the most important molecular interactions between protein molecules, above mentioned, are summarized in table 1.1:

Type	Sign[a]	Strength	Range	pH	I.S.	Temperature
Hydrophobic	A	Strong	Long	No	No	Increases
Electrostatic	R	Weak→Strong	Short→Long	Yes	Decreases	Increases
H-bonding	A	Weak	Short	No	No	Decreases
Van der Waals	A	Weak	Short	No	No	-
Steric repulsion	R	Strong	Short	No	No	-
Disulfide bonds	A	Very strong	Short	Yes	No	Increases

[a] A, attractive, R, repulsive
[b] Depends on pH and ionic strength (I.S.)

Tab. 1.1: General characteristics of molecular interactions between two similar protein molecules in aqueous solution [**Bryant et al., 1998**].

1.2 Proteins aggregation processes

Protein aggregation is a possible consequence of cellular existence and it is an important factor in a variety of pharmaceutical and biotechnological processes. Almost all proteins tend to aggregate in opportune experimental conditions, but in different ways and to different extents under different settings. Aggregation processes depend on several factors, such as temperature, pH value, protein concentration, ionic strength, presence of cosolutes [**Aymard et al., 1996, Fink 199**8, **Kusumoto et al., 1998**, **Renard et al.,1998, Hoffmann et al., 1999, Vaiana et al., 2001, Baussay et al., 2004, Manno et al., 2004**. **Militello et al., 2004**]. Proteins aggregation is a process resulting by different interconnected mechanisms occurring on different hierarchical scales [**San Biagio et al., 1999, Chiti et al., 2002, Militello et al., 2003 and 2004, Manno et al., 2004, Vetri et al., 2005**]. Conformational and structural changes of protein molecules, formation of intermolecular bonds and nucleation processes are involved in the aggregates building. In order to understand which are the equilibrium and dynamic aspects of proteins aggregation, it is important to know the forces driving the protein-protein association and to be able to regulate them. The dynamic aspects of the aggregation process involve protein changes both on a microscopic scale, such as structural and conformational changes, and on macroscopic scale, as result of intermolecular interactions. Moreover, these different typologies of changes can be not independent, since small changes in local configuration could allow a great stereo-reorganization of macro-molecules. This complex process is not yet totally understood and many efforts have been made in this direction by the scientists in order to increase the knowledge of a multistage process such as the aggregation process, which is based on the protein-protein interactions and highly affected by the protein-solvent interaction. It is widely accepted that the first step leading to aggregation is in most cases a partial unfolding of the proteins. For example, in thermally induced aggregation, this process is activated by the increasing of temperature [**Allain et al., 1999, Chiti et al., 2002, de la Fuente et al., 2002, Carrotta et al., 2003, Militello et al.,2004, Dobson 2004**, **Visschers et al., 2005**]. The partial unfolding of

the protein causes the exposition of sites, like hydrophobic surfaces or thiol groups (SH), inaccessible in the native form and having nevertheless a dominant role in the aggregation processes. The formation of aggregates via noncovalent interactions and via thiol/disulfide exchange reactions may occur simultaneously or sequentially, but it is experimentally very difficult to distinguish between these steps. However, it is generally accepted that at neutral pH thiol/disulfide exchange reactions, leading to the formation of intermolecular disulfide bonds, are involved [**Yu et al., 1985, Ozaki et al., 1987, Li et al., 1991, Liu et al., 1994 Hoffmann et al.,1997 Hoffmann et al., 1999, Otte et al., 2000**]. These exchange reactions can be described like having got three steps, i.e. an initiation, a propagation and a termination step [**Hoffmann et al., 1999, Roefs and de Kruif 1994**]. The initiation step consists in the partial opening of the protein that exposes the SH group; this one can become reactive consequently to an irreversible reaction. In the propagation step, the reactive thiol group reacts via a thiol/disulfide exchange reaction with one of the two intra-molecular disulfide bonds of a non-reactive protein molecule. As a result, an intermolecular disulfide bond is formed and a new reactive thiol group becomes accessible. The termination step occurs when two reactive intermediates react with each other, forming a polymer without a reactive thiol group. A scheme of this reaction is shown in figure 1.5. The aggregates formed through this reaction are irreversible and very stable.

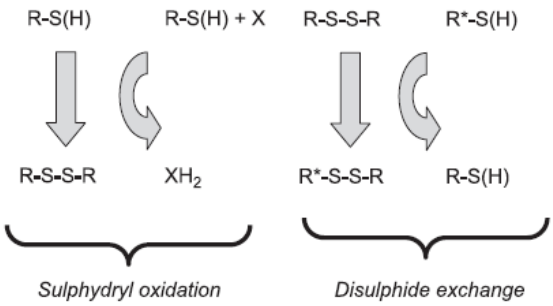

Figure 1.5: Scheme of a sulphydryl oxidation and a disulfide exchange reaction. Figure from **Visschers et al., 2005**.

The occurring of conformational changes on the protein secondary structure is usually associated to the partial unfolding process. In most cases, these conformational changes lead to the formation of aggregates with β-richer structures. Indeed, it has been observed that the aggregation induces an increase in the amount of secondary β-sheet structures, and a decrease of the α-helices ones [**Fang et al., 1997, Fink 1998, Militello et al., 2004, Yan et al., 2006**]. Also for native all-β proteins, a significant new β structure, related to the intermolecular interactions, was observed; typically, this amounted to ~20-25% of the total secondary structure. So, it can be considered that the aggregation process evolves through β-sheet-like interactions. It has been observed that proteins with a richer native β-structures and with a greater number of hydrophobic residues have a greater tendency to the creation of aggregates [**Fink 1998, Chiti et al., 2002**]. Nevertheless, what it has been said before is not a prerogative of all-β proteins only, but all-α and α+β proteins too create aggregates through β-sheet-like interactions after a conversion of the structure at secondary level from α-type to β-type, as it was experimental observed for BLG and BSA [**Allain et al., 1999, Militello et al., 2003 and 2004, Navarra et al., 2007**]. However, the way through which the conformational changes take part in the aggregation pathways is not yet completely clear.

The interest on the comprehension of the complex mechanisms leading to the aggregation resides certainly in the field of the basic research, and it is growing also in biomedical and biotechnological fields. Indeed, it is well known that under suitable experimental conditions all proteins are able to undergo a "mis-folding" and then to assemble themselves in ordered aggregates, named amyloid fibrils [**Arai et al., 1999, Fandrich et al., 2002**]. These structures have similar morphologies (long, unbranched and often twisted structures of a few nm in diameter) and a characteristic "cross beta" X-ray fibre diffraction pattern [**Sunde et al., 1997**]. Their core structure is composed of β-sheets having strands running perpendicular to the fibril axis. Recent studies have suggested that the ability of the polypeptide chains to form such structures is common, and indeed can be considered a generic feature

of the polypeptide chains and as a consequence of all proteins **[Chiti et al., 1999, Jimenez et al., 1999, Fandrich et al., 2002, Goers et al., 2002]**. The fibrillar aggregates are strictly related with the manifestation of many degenerative pathologies, such as Parkinson, Alzheimer and Creutzfeldt-Jacob diseases. All these diseases result fundamentally from errors in the production, regulation or degragation of protein molecules [**Chiti et al., 1999, Dobson 1999 and 2004, Vendruscolo et al., 2003, Stefani 2004, Uversky et al., 2004**]. Moreover, some of these pathologies are accompanied by peculiar morphological manifestations like formation of senile plaques in the brain, amyloidosis of brain vessels and intra-neuronal deposits of amyloid fibrils.

From an industrial point of view, proteins aggregation is relevant in a variety of biotechnological processes and pharmaceutical applications, including formation and renaturation of inclusion bodies and formulation and storage stability of protein drugs.

Food industry has recently spent great efforts to increase the own knowledge of the complex mechanisms characterizing the aggregation processes of the whey proteins. Whey proteins, whose BLG and BSA are some of the main components , are widely used in foods as gelling agents, emulsifiers, texture modifiers, thickening agents and foaming agents [**Kinsella et al 1989, Bryant et al., 1998, Alting 2003, Alting et al., 2003a**]. The growing preference of consumers for more tasty, healthy, convenient, and natural food products has provided the dairy industry an unique opportunity to develop and supply milk protein ingredients to improve the functional properties of food products. Food scientists have recognized the importance of understanding the molecular basis of proteins functionality and this has given great impulse to the development of protein ingredients. In particular, during some food manufacturing processes, whey proteins undergo heat treatments that could activate aggregation processes. The inevitable heat treatments used during the processing and preservation of whey protein products can seriously affect the native state and stability of the whey proteins. Consequently, a better understanding of their behaviour during heating is essential to control their properties and characteristics

during the recovery and application of whey products. In order to optimize heat treatments ensuring proper functional and nutritional uses of whey protein products, detailed information about the kinetics and the mechanism of the unfolding and the aggregation of whey proteins is needed. Moreover, we want to underline that a heat treatment can also be the first step of the creation of protein gels and, in particular, of cold induced gels by metals. Spectroscopic techniques, like absorption and emission spectroscopy, FTIR spectroscopy together with light scattering and microscopy are useful combined tools to explore these complex processes [**Militello et al. 2003**, and **2004**, **Vetri et al., 2005**, **2007a** and **2007b**, **Librizzi 2005** and **2007, Navarra et al., 2007 and 2008**].

1.2.1 Role of metal ions

During the recent years, studies of the influence of metals on aggregation processes have been developed more and more. Long since, metal ion mediated protein aggregation processes are known to occur in a variety of biological and processing environments. Some of these are *in vitro* precipitation of β-amyloid protein by aluminium ions [**Kawahara 2001 and 2003**], copper-induced aggregation of β-Lactoglobulin [**Bouhallab et al., 2004**] and of whey proteins, in general [**Barbut et al., 1993**, **Hongsprabhas et al. 1997a, 1997b, 1998 and 1999, Remondetto et al., 2003**]. However, very recently, the interest towards this research argument is ever increasing because of the involvement of certain metal ions in developing of some degenerative pathologies, such as Alzheimer disease (AD) [**Paik et al., 1999, Miura et al., 2000, Suzuki et al., 2001, Stellato et al., 2006, Fox et al., 2007**], and Parkinson's disease [**Paik et al., 1999**]. As it has been already said, some of these pathologies are accompanied by peculiar morphological manifestations like formation of senile plaques in the brain, amyloidosis of brain vessels and intra-neuronal deposits of amyloid fibrils. A microparticle-induced X-ray emission analysis of multiple brain regions has shown that Fe, Zn, and Cu ions are significantly concentrated in the neurophil of AD patients and are further concentrated within the core and periphery of senile

plaques [**Danscher et al., 1997, Lovell et al., 1998, Miura et al., 2000, Religa et al., 2006**]. Their role has not been fully understood yet, but it has been speculated to be crucial in the pathological effects of Alzheimer disease [**Bush et al., 1994, Kaiser 1994, Bush et al., 1995, Fitzgerald 1995, Maggio et al., 1995**, **Multhaup et al., 1996**].

On the other hand, not only metals reflect on physiological factors that can influence negatively the protein structure, but also transition metals especially are essential for the survival of the organism by participating in various biologically important redox reactions. Therefore, a coveted goal should be clarifying which is the role of the metal ions in the origin of degenerative disease and in which way their physiological function is converted in a harmful function because of the same redox reactions or direct molecular interactions with bio-macromolecules.

Considering that the main component of the AD amyloid plaques is the β-amyloid peptide (Aβ), the scientific research that has investigated the metal-Aβ interactions and the structural coordination of the metal with this crucial peptide is wide [**Miura et al., 2000, Suzuki et al., 2001, Comai et al., 2003, Stellato et al., 2006, Garai et al., 2006 and 2007**]. The metals deposited in senile plaques in largest amounts are copper, iron and zinc. Cu^{2+} and Zn^{2+} metals ions have a different physiological role and it has been observed that, in vitro, both promote (zinc more than copper) aggregation in amyloid fibrils and/or in amorphous aggregates [**Bush et al., 1994, Huang et al., 1997, Tjernberg et al., 1999, Suzuki et al., 2001, Comai et al., 2003, Bouhallab et al., 2004, Raman et al., 2005, Danielsson et al., 2007, Wang et al., 2007**]. Copper is one of the most abundant transition metals present in living systems, and Cu^{2+} ions are known to play a key role in the working mechanism of several important metalloenzymes, such as galactose oxidase and superoxide dismutase. A driving force in the activity of these enzymes is the folding of a peptide, which consists of amino acid side chains, around the Cu^{2+} cation [**Mesu et al., 2006**]. Zinc is second only to iron in terms of abundance and importance in biological systems. The Zn^{2+} cation plays a structural as well as a catalytical role in proteins. It plays a structural role in the proteins of zinc finger family, which are involved in nucleic acid binding and gene regulation [**Berg et al., 1996**]. In addition, zinc carries out an essential function in

many enzymes and virtually in all aspects of metabolism [**Foley et al., 2007**]. It is noteworthy to underline that in a study carried out on the toxicity of the β-amyloid peptide in presence of copper(Cu/Aβ), it has been observed that this metal can assume a bivalent function depending on the Cu/Aβ concentration ratio: the Raman spectrum of a metal–Aβ complex in presence both of Zn^{2+} and Cu^{2+} shows that the cross-linking of Aβ via binding of Zn^{2+} to the N_{τ} atom of histidine is prevented by chelation of Cu^{2+} by the N_{π} atom of histidine and nearby amide nitrogens. The strongest inhibitory effect is at a Cu/Aβ molar ratio of around 4. For a ratio greater than 4, Cu^{2+} itself promotes the Aβ aggregation by binding to the phenolate oxygen of Tyr10 [**Suzuki et al., 2001**]. Stellato and co-workers have made clear a different role of zinc and copper [**Stellato et al., 2006**]: experimental measurements of X-ray absorption spectroscopy have shown different metal binding site structures in β-amyloid peptides according to whether they are complexed with Cu^{2+} or Zn^{2+} ions. While the geometry around copper is stably consistent with an intra-peptide binding with three metal-coordinated Histidine residues, the zinc coordination mode depends on specific status of the solution. In particular, different sample preparations lead to different geometries around the absorber experimental monitored, which are compatible with either an intra- or an interpeptide coordination mode. This result reinforces the hypothesis assigning different physiological roles to the two metals, with zinc favouring peptide aggregation and, as a consequence, plaque formation [**Stellato et al., 2006**]. It is necessary to point out that controversial ideas are present in the scientific world on the role and influence of metal ions in aggregation processes; the same metal can assume a promoter or inhibitor role in the aggregation, being still not clear the conditions and the mechanism of its different action. Moreover, Zn^{2+} induces the Aβ aggregation at acidic-to-neutral pH, while Cu^{2+} is an effective inducer only at mildly acidic pH [**Miura et al., 2000**]. Under mildly acidic conditions, as in the physiological acidosis following an inflammatory process, copper is preferentially bound [**Atwood et al., 1998**]. Even if there is no doubt that the metals bind Aβ peptide and promote peptide

precipitation in appropriate experimental conditions [**Bush et al., 1994, Esler et al., 1996, Paik et al., 1999, Miura et al., 2000, Qin et al., 2003, Bouhallab et al., 2004**], studies with very low concentrations of copper and zinc (few micromolar) have shown that they can reduce Aβ toxicity for cultured mammalian neurons [**Lovell et al., 1999, Moreira et al., 2000, Yoshiike et al., 2001, House et al., 2004**]. Through a not clear mechanism, zinc ions destabilize the formation of soluble amyloid-β aggregates [**Garai et al., 2006 and 2007**], like oligomeric aggregates, which greater neurotoxicity in respect to the fibrillar forms has been speculated in several scientific works [**Hoshi et al., 2003, Cleary et al., 2005, Garai et al., 2006, Carrotta et al., 2006**].

The generally accepted argumentation on the divalent metals role in protein aggregation is based on their ability to act as bridges, as well as to provide an electrostatic screening between the negatively charged groups of the neighbouring protein molecules [**Iyer et al., 1996, Hongsprabhas et al., 1997a, 1997b, 1998 and 1999, Bryant et al., 1998, Remondetto et al., 2003**]. Nevertheless, also monovalent ions can have a promoting effect on the aggregates formation. Indeed, proteins aggregation is generally promoted by the electrostatic screening due to the action of monovalent and/or divalent ions. However, a concentration of divalent ions much lower than monovalent one is enough in order to cause aggregation: divalent ions are much more effective at screening electrostatic interactions and have a greater ability to form salt bridges than monovalent ones [**Bryant et al., 1998, Remondetto et al., 2003**]. A higher salt concentration should change the distance distribution of the repulsive forces and thus the energy barriers. The loss of repulsive forces makes it possible for the charged protein molecules to get close enough to interact via noncovalent forces with a low potential energy [**Remondetto et al., 2003**].

Protein sites mainly involved in the coordination with positively charged metal ions are negatively charged sites, such as the carboxylic groups, the primary amino group of polypeptide chain skeleton and same residues of certain amino acids. The most relevant amino acid showing to have a great affinity in binding metal ions is Histidine [**Miura et al., 2000, Morante et al., 2004, Mesu et al., 2006**]. A

study of **Mesu et al., 2006**, on the structural coordination between copper(II) and Histidine (His) complexes in aqueous solutions has shown that, in highly acidic conditions, Cu^{2+} and His are present as free ions, but around pH = 2, coordination starts via the deprotonated carboxylic acid group. Coordination of the imidazole ring begins around pH = 3 and leads to the formation of the mixed ligand complexes $Cu^{2+}[H_2his^0(O_c,N_{am})][Hhis^-(O_c,N_{am},N_{im})]$ and $Cu^{2+}[Hhis^-(N_{am},N_{im})][Hhis^-(O_c,N_{am},N_{im})]$ around pH = 5. It has been demonstrated that coordination of the imidazole ring occurs predominantly via the N_π atom. At pH ~ 7, the double-tridentate ligand complex $Cu^{2+}[Hhis^-(O_c,N_{am},N_{im})]_2$ is the most abundant species, whose molecular structure with the N atoms in the equatorial plane and the O atoms in the axial position is reported in figure 1.6 [**Miura et al., 2000, Suzuky et al., 2001, Mesu et al., 2006**]. A penta-coordination between copper (II) and Aβ peptide has been turned out in a computational study [**Stellato et al., 2006**]. As can be seen in figure 1.7, the metal ion is coordinated to three nitrogens, belonging to three Histidine residues, and two oxygen atoms, one belonging to the oxygen of a Tyrosine residue (Tyr 10) and the remaining one possibly belonging to either OH^- (water) or to some amino acidic residue different from the bound Histidine and Tyrosine [**Stellato et al., 2006**]. A coordination of the copper with α prion protein involving the equatorial binding of two His-Gly dipeptides has emerged from computational and experimental studies [**Morante et al., 2004**]. Moreover, the observed copper(II)-induced self oligomerization of α-synuclein has been attributed to a specific copper coordination with C-terminus of the protein [**Paik et al., 1999**]. **Bertran et al., 1999** have shown that Cu^{2+} binds also Glycine, with a bidentated coordination of the metal with the oxygen atoms of the COO^- group [**Bertran et al., 1999**]. As far as the coordination properties of zinc are concerned, it ha been observed that Zn(II) binds to the N_τ atom of the histidine imidazole ring of Aβ- peptide and this peptide aggregates via the formation of intermolecular His(N_τ)-Zn(II)-His(N_τ) bridges, according the molecular structure in figure 1.8 [**Miura et al., 2000, Suzuki et al., 2001**].

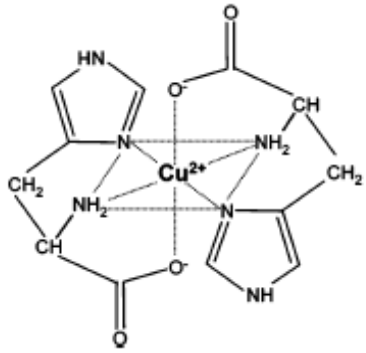

Figure 1.6: Proposed molecular structure of Cu^{2+}/his complex at pH~7. Figure from **Mesu et al., 2006**.

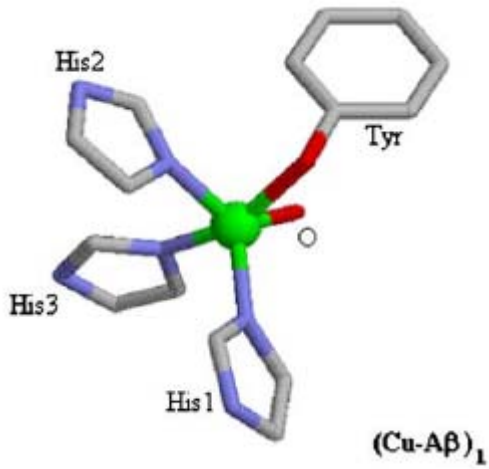

Figure 1.7: Schematic picture of the molecular arrangement around the copper (green) ion. The following abbreviations are used for the residues bound to the ion: His Histidine, Tyr Tyrosine. Figure from **Stellato et al., 2006**.

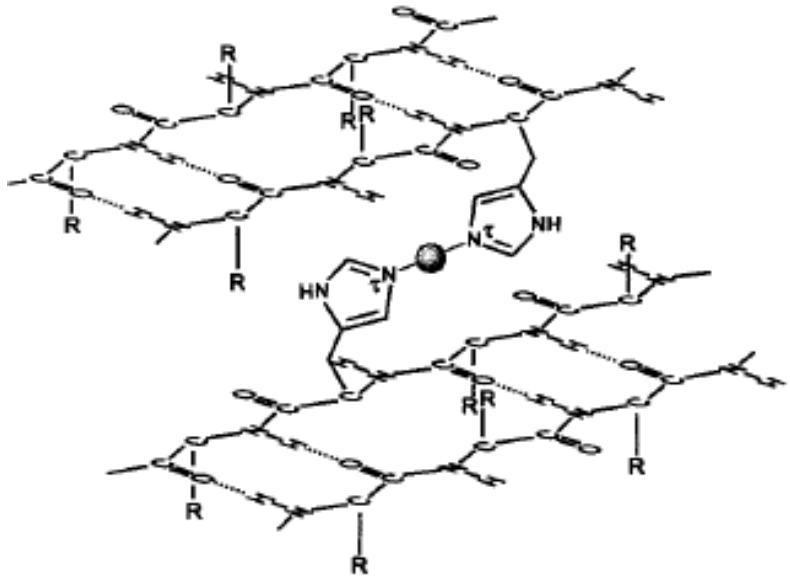

Figure 1.8: A possible model for the insoluble aggregates of Zn(II)-Aβ formed at neutral-to-acidic pH. β-Sheets of Aβ are cross-linked with His(N_τ)-metal-His(N_τ) bridges. The metal ion is shown as a ball. Figure from **Miura et al., 2000**.

Stellato et al., 2006 have also made an investigation on the coordination of zinc and Aβ- peptide, finding that unlike Cu ions, Zn ions can realize two different hexa-coordinations, both reported in figure 1.9. In the first hexa-coordination, one also finds a N atom belonging to a Histidine residue and three oxygen atoms, one belonging to the oxygen of a Tyrosine residue. The other Zn hexa-coordination mode is obtained by two N atoms belonging to two Histidine residues and four oxygen atoms, one belonging to the oxygen of a Tyrosine residue and the remaining three either to water or to amino acidic residues different from Histidine and Tyrosine residues [**Stellato et al., 2006**]. Moreover, one of the most commonly found ligands in zinc catalytic binding sites is Cysteine, with others being Histidine, Aspartic acid and Glutamic acid [**Morante et al., 2004, Mesu et al., 2006, Stellato et al., 2006, Foley et al., 2007**].

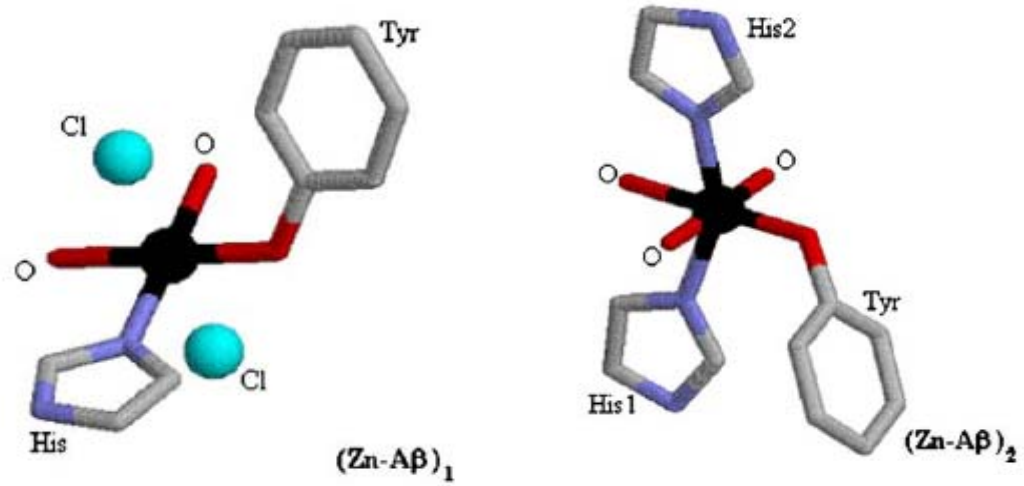

Figure 1.9: Schematic pictures of the molecular arrangement around the zinc (black) ion. The following abbreviations are used for the residues bound to the ion: His Histidine, Tyr Tyrosine. Figure from **Stellato et al., 2006**.

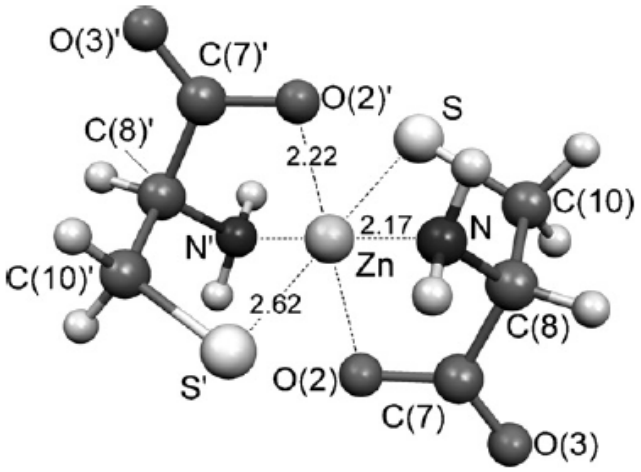

Figure 1.10: Optimized structure of the Zn(Cys)2 complex. Atomic distances are given in Angstroms. Figure from **Foley et al., 2007**

Raman measurements have shown that NH and CO groups of cysteine may be involved in complexation, as well as the COO^- and NH^{3+} groups in the case of terminal cysteine [**Folay et al., 2007**]. In particular, spectra analysis directly demonstrates the deprotonation of the SH and NH^{3+} cysteine groups upon zinc binding. Spectral evidence for the COO^- group participating in the zinc coordination has also been found. These results are consistent with a hexa-coordination of the metal in the zinc–cysteine complex that is reported in figure 1.10 [**Folay et al., 2007**].

In view of the controversial actions attributed to both metals and to the different coordination ways with Aβ-peptide, and proteins in general, and considering that these differences might influence the protein-protein interactions, the study of the aggregation processes affected by metal ions of some model-proteins, such as BLG and BSA, is crucial because it could help in clarifying via experimental studies performed *in vitro* the role played by metals *in vivo* before their deposition in the senile plaques.

1.3 Proteins Gelation processes

Many globular proteins have the ability to form gels. It is well known that under appropriate conditions, native proteins can undergo conformational changes associated with partial unfolding or denaturation that may lead to aggregation [**Militello et al., 2003 and 2004, Vetri et al., 2005 and 2007, Euston et al., 2007**] and, above a critical protein concentration, to gelation [**Mulvihill et al., 1987, Ziegler et al., 1990, Bryant et al., 1998, Le Bon et al., 1999, Allain et al., 1999, Gosal et al., 2000, Doi 1993, Sittikijyothin et al., 2007, San Biagio et al 1996 and 1999**].

Gels have been defined as soft, deformable elastic solids consisting of a connected network of either small particles or large molecules [**Hongsprabhas et al., 1999**]. Other definitions which are referred to in this thesis were given by Ziegler and Foegeding (1990), who defined a gel as "a continuous network of macroscopic dimensions immersed in a liquid medium and exhibiting no steady-state flow", and

Wong (1989), who defined gelation as an "aggregation of denatured molecules with a certain degree of order, resulting in the formation of a continuous network".

Substantially, it is possible to distinguish between heat- and cold-induced gels. Actually, gelation processes can be also induced by an increase of pressure [**Van Camp et al., 1997, Ipsen et al., 2002**], but only heat- and cold-gels have the most relevant application in food technology and for this reason a wide literature is focused on the study of their properties in order to understand the general mechanisms leading to the gel formation. In fact, the perception of texture during consumption is determined by the size and the spatial arrangement of the structural elements of food, their mechanical properties and their response to the dynamic conditions during consumption. For the same reason, the mainly studied gels come from whey proteins, such as Whey Protein Isolate (WPI) [**Hongsprabhas et al., 1997, 1998, and 1999, Marangoni et al., 2000, Doucet et al., 2003, Alting et al., 2000, 2003a, 2003b, 2004**], β-Lactoglobulin (BLG) [**Dufour et al., 1998**, **Renard et al., 1999, Leung Sok Line et al., 2005**, **Veerman et al. 2003a, Remondetto et al., 2003, Alting et al., 2002**] and Bovine Serum Albumin (BSA) [**Donato et al., 2005**], which are widely used as ingredients in foods because of their unique functional properties, i.e. emulsification, gelation thickening, foaming and water-binding capacity. In a most recent period, they have also been used for encapsulation and protection of sensitive materials and pH-sensitive hydrogels for the controlled delivery of biologically-active drugs [**Gunasekeran et al., 2006 and 2007**].

Obviously, basic research scientists too show great interest in the study of gels properties in order to make clearer the equilibrium between protein-protein and protein-water interactions and balance between attractive and repulsive forces, that are necessarily required for the formation of a gel matrix [**Allain et al., 1999**].

During the last 30 years, some of the most widely studied physico-chemical properties have included the chemical nature of the constituent amino acids, the secondary and tertiary structures of protein molecules and the stability and flexibility of these protein molecules. The macroscopic properties of a gel, however, are influenced by a hierarchy of factors, which cannot be directly linked to the

properties of individual protein molecules. The rheological behaviour of a particulate protein gel, for example, is influenced by the amount of protein present, the size, morphology and surface properties of the primary aggregating particles, and the interaction among these primary particles leading to the formation of a network. The importance of this structural hierarchy should not be overlooked. The physico-chemical properties of individual protein molecules, as well as environmental conditions (pH, temperature, ionic strength and species, solvent polarity and type), will influence the type of primary particles formed (morphology, size, surface properties), the interactions between them, and ultimately the resulting three-dimensional network structure. This network is largely responsible for the macroscopic rheological properties of gels [**Marangoni et al., 2000**].

1.3.1 Heat-induced gelation

Thermal gelation is commonly seen as a three-step process that can be intertwined: i) first, the native protein unfolds, exposing hydrophobic amino acid residues, favouring in this way the building of molecular pre-aggregates via disulfide bridges, hydrogen bonds and hydrophobic and/or van der Waals interactions; ii) then, the aggregation further proceeds with association of protein pre-aggregates, and iii) finally, when the protein concentration is sufficiently high, a three-dimensional network entrapping water is created [**Lefevre et al., 2000**]. Depending on the pH value and ionic strength of the medium, different kinds of gels have been obtained varying from transparent to turbid and opalescent "fine stranded" or "particulate" gels. Studies performed on heat-induced gels of BLG [**Renard et al., 1999, et al., Lefevre 2000, Gosal 2004a and 2004b, Sittikijyothin et al., 2007**] have permitted to establish that, in salt-free solutions, gels are transparent above pH 6 and below pH 4. They are composed of more or less flexible linear strands and for this reason are named "fine stranded" gels. Between pH 4 and 6, gels are opaque and characterized by a random association into large and almost spherical aggregates. They are named "particulate gels". Both typologies of gels are shown in

figure 1.11. Obviously, what said is strictly related to the charge distribution in the protein: when the pH value is far from isoelectric point of the protein (pI = 5.2 for BLG), this latter is charged and, consequently, the residual electrostatic repulsion between close protein molecules prevents aggregation. In this case, the intermolecular bonds may be principally formed via attractive hydrophobic interactions leading to the formation of aggregates in ordered "string-of-beads" or filamentous structures [**Doi 1993, Bryant et al., 1998**]. On the contrary, when pH is next to pI of the protein or the residual electrostatic repulsion between charged proteins is completely screened, the formation of largely spherical aggregates leading to "particulate gel" is promoted [**Lefevre et al., 2000**]. A dependence of the protein gel appearance and the electrostatic repulsion modulation from the pH value and the ionic strength is shown in figure 1.12. The different kinds of gels can be differentiated by rheological and other techniques investigating gels structure [**Renard et al., 1999, Marangoni et al., 2000, Gosal et al., 2000 2004a and 2004b, Remondetto et al., 2003, Donato et al., 2005, Sittikijyothin et al., 2007**], as well as by kinetics acquired during heat-treatment with Fourier Transform Infrared (FTIR) spectroscopy: fine stranded gels show different positions in the frequency of the aggregation band, indicating that hydrogen bonds are stronger for these aggregates than for particulate ones [**Lefevre et al., 2000, Remondetto et al., 2003**]. Interestingly, even for the same type of gel, differences in the mechanical properties were measured vs pH [**Clark et al., 1981**]. Indeed, the pH value has a large influence also in the formation of cold-induced gels.

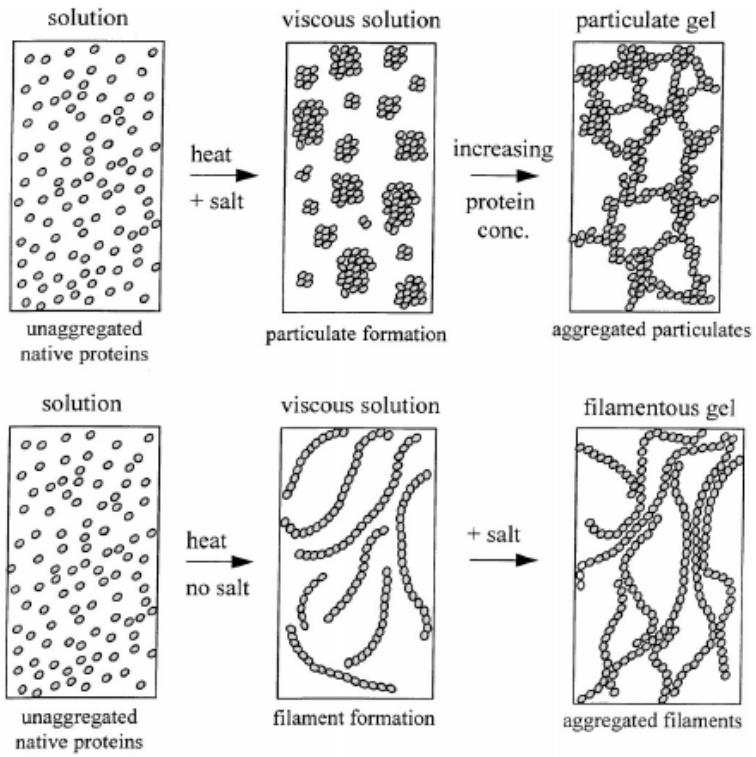

Figure 1.11: Development of particulate and fine stranded gel structures. Figure adapted from Bryant et al. 1998

.

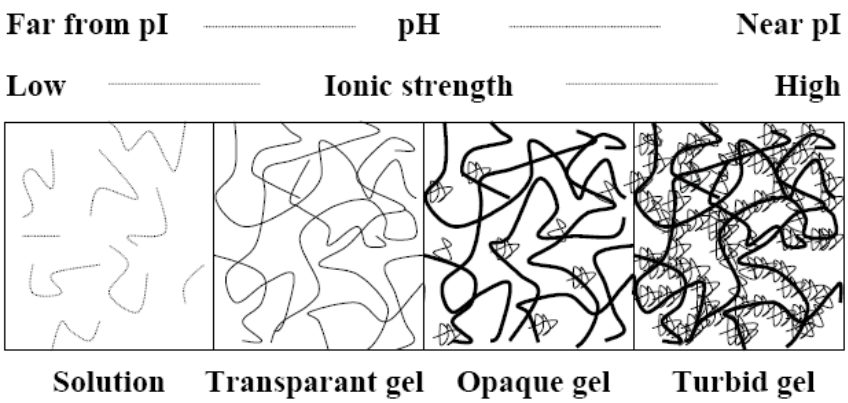

Figure 1.12: Relation between protein gel appearance and modulation of the electrostatic repulsion. Figure adapted from Doi and Kitabatake (1997).

1.3.2 Cold gelation

Cold gelation process is an alternative way to obtain gels from proteins having immediate applications in food technology and engineering, since the last gelation step does not need high temperature. The main feature of the process of cold gelation is that the (heat-induced) activation step of the proteins is uncoupled from the subsequent steps in the gelation process, differently from the heat-induced gelation, where the processes of unfolding, aggregation, and gelation are intertwined, as evident in figure 1.13.

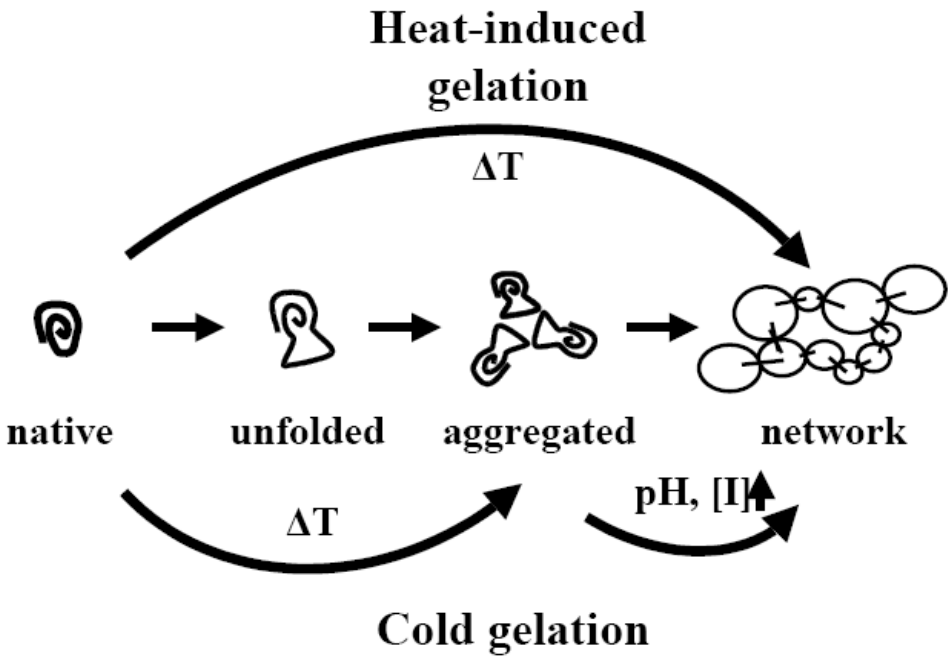

Figure 1.13: Scheme of steps involved in the formation of heat- and cold-induced gels. Figure adapted from Alting Thesis 2003.

In the first step of the cold gelation process, a stable dispersion of protein aggregates is obtained after heating of a solution of native proteins at a pH far from the pI, at low ionic strength (no salts added) and at a protein concentration such that no gel is formed. After cooling, the stable dispersion of aggregates is maintained. These aggregates constitute the structural units responsible for the three-dimensional

network of cold-set gels [**Remondetto et al., 2003**] and with this meaning, they will be named "pre-aggregates" in the following. In the second step, gelation can be induced at room temperature changing the solvent properties by decreasing temperature [**Allain et al., 1999**], adding salts [**Hongsprabhas et al., 1998b and 1999, Bryant et al., 2000, Remondetto et al., 2002 and 2003**], lowering pH [**Alting 2000, 2002, 2003a, 2003b, and 2004, Donato et al., 2007**], adding enzymes or chemical cross-linkers [**Doucet et al., 2003**] or increasing hydrostatic pressure [**Phillips et al., 1994, Totosaus et al., 2002**].

Besides pH value and ionic strength, other parameters have an influence on the properties of gels, such as the proteins concentration and the temperature at which the solution containing the pre-aggregates is prepared. The concentration of proteins in heat-denatured protein solution has a major influence on the properties of the viscous solutions, or gels, formed by adding salts. At relatively low protein concentration, the heat-denatured protein tends to form a viscous solution rather than a gel. As the protein concentration is increased, the viscosity of this solution increases. Above a critical protein concentration, the heat-denatured protein solution forms a gel rather than a viscous solution. A further increase in the protein concentration then leads to an increase in the Young's modulus and water-holding capacity of the gel [**Hongsprabhas et al., 1997a, Bryant et al., 1998**]. The temperature at which the gelation process is carried out also has an important influence on the rate of gelation and the structure of the gels formed. The gelation rate of cold-set gels formed by adding either NaCl or $CaCl_2$ to heat-denatured WPI solutions has been found to increase with increasing temperature [**Kitabatake et al., 1996, Hongsprabhas et al., 1997a, Van Camp et al., 1997**]. It has been suggested that this is due to the role played by the hydrophobic interactions in starting the initial aggregation of the protein filaments [**McClements et al., 1995**]. The hydrophobic attraction is relatively strong and at long range, and its magnitude increases as the temperature raises. Consequently, it is believed that this interaction plays an important role in determining the aggregation rate of the protein filaments. Regardless, once the gels

are formed, their strength tends to increase, as the temperature decreases [**Van Camp et al., 1997**]. This suggests that hydrophobic interactions play a dominant role in the initial stages of aggregation, but that non-hydrophobic interactions play a more important role in determining the final gel strength [**Bryant et al., 1998**].

The cold gelation process is induced principally by lowering the pH value towards pI of the proteins or by increasing the ionic strength caused by adding salts; both methods permit to decrease electrostatic repulsive forces that prevent them to get close and form aggregates [**Bryant et al., 1998, Remondetto et al., 2003**].

The lowering of pH value towards pI of protein solution is a crucial step in cold gelation induced by adding acid in the pre-heated protein solution. Acid-induced gels of Whey Protein Isolate (WPI) and β–Lactoglobulin (BLG) have been characterized by Alting in his PhD thesis work. Typically, an appropriate amount (dependent on the protein concentration) of glucono-δ-lactone as acidifier was added at room temperature and consequently the pH of the solution was gradually lowered from neutral pH to a pH about 5 (after ~24 h). This acidification induced gelation of the protein solution [**Alting et al., 2000, 2002 2003a, 2003b and 2004**]. The characterization of these gels has allowed to establish that the formation of disulfide bonds can occur during the second step of the acid-induced cold gelation process, though the reactions leading their formation proceed optimally under alkaline conditions. This has been tentatively attributed to a large increase of the effective local concentration during the gel state [**Alting et al., 2000**]. Gel hardness significantly decreases (by 10-fold) in gels prepared from thiol-blocked aggregates, even if micro-structural analysis does not reveal any difference respect to gels prepared from non-modified whey protein aggregates. This has allowed the authors to put forward a relatively simple model that could clarify disulfide bonds role in the formation of cold induced gels in very acidic conditions. They have postulated that the initial microstructure of gels is primarily determined by non-covalent interactions. The additional covalent disulfide bonds have only formed after gelation, probably via actived thiol-disulfide exchange reactions, and involved in stabilizing the network

(preventing of spontaneous rupture and syneresis) and increasing the gel rigidity [**Alting et al., 2000, Visschers et al., 2005**]. Moreover, Alting et al. have also verified the importance of the net charge of the protein in the gelation process [**Alting et al., 2002**], characterizing gels of BLG formed after having modified chemically the net-charge of the protein aggregates, either by succinylation of the primary amino groups or by methylation of the carboxylic acid groups. This study has also demonstrated that the isoelectric point of the protein affects the formation of additional disulfide bonds having this a clear effect on the properties of the gel.

1.3.3 Metals-induced cold gelation

Cold gels formed after adding metals in pre-heated protein solution belong obviously to the more general category of salt-induced cold gels. During the most recent years, research activity on the salt-induced cold gels has focused on metals-induced gelation, since only recently the importance of the metals for human health has been accepted. Some metals are essential for a correct metabolism and their total absence in the human organism induces acute diseases. Even if the concentration of metals used to induce cold gelation is not physiological, clarifying the mechanisms at the base of the gelation processes activated by adding metals in pre-heated solution of biocompatible proteins, such as whey proteins, is important both in the basic research area and in possible applications in food technology and engineering.

The first step of the cold gelation process, consisting in the pre-heating of the solution that causes the protein molecules to open their structure and interact with each other, is common for all cold-induced gels. In the second step, salt is added to cooled protein solution to form salt-induced gels at room temperature. The function of salt could be to screen the repulsive forces between the aggregated protein molecules, which can then form gel. It may also aid in the formation of salt bridges between charged groups on proteins. Besides charge dispersion, a divalent salt, such as $CaCl_2$, induces cross-linking of proteins and thus promotes gelation at much lower concentrations than a monovalent salt [**Mulvihill et al., 1988, Hongsprabhas et**

al., 1997a, Bryant et al., 2000]. From studies performed on cold-set Whey Protein Isolate gels prepared with Ca^{2+} it has been turned out that the amount of salt used to form a cold-set gel, rather than the reactive sulphydryl groups [**Hongsprabhas et al., 1997a**], is likely to be the main factor of structure and spatial organization of protein aggregates. Indeed, at lower salt concentration, the increase in aggregates size and network connectivity over time was achieved by clustering of adjacent aggregates, while, at higher salt concentration (about 10-fold), the increase in aggregates size and connectivity was achieved by enlargement of aggregates which formed connected paths and filled up interstitial spaces [**Hongsprabhas et al., 1997a and 1999**]. Other studies confirm that the network formation processes are governed by salt concentration, resulting in different gelation mechanisms and in various structure types [**Remondetto, et al., 2002, and 2003**], which determine the water-holding capacity (WHC), permeability, texture, and appearance of the gel [**Bryant et al., 2000**]. **Marangoni et al., 2000**, have investigated the structure of gels as a function of protein and salt concentration, finding that particle size decreases as a function of increasing protein concentration and increases as a function of increasing salt concentrations. Moreover, they observed that the rate of aggregation in presence of $CaCl_2$ is longer than in presence of NaCl and that the mass fractal dimension [1] of gels formed in presence of $CaCl_2$ was greater than that formed in presence of NaCl. These results suggested a greater amount of order in $CaCl_2$ gels, possibly due to the cross-linking effect of Ca^{2+} [**Marangoni et al., 2000**].

Through rheological measurements, **Remondetto et al. 2003** showed that the cold gel formation of BLG (~3 mM) with the addition of divalent iron is achieved via two molecular mechanisms, which are both modulated by the iron concentration. At 30 mM of iron, gel formation is essentially controlled by van der Waals interactions, while at 10 mM of iron, hydrophobic interactions predominate. At these two concentrations, disulfide bonds contribute to gel consolidation, the effect being

[1] Fractal dimension, D, is a statistical quantity that gives an indication of how completely a fractal appears to fill space. For colloidal aggregates, which behave as stochastic mass-fractals on a scale which is large compared to the primary particle size, dimensional fractal is related to the slope of the log-log plot of the macroscopic elastic constant vs of the volume fraction or concentration **[Marangoni et al., 2000]**.

more pronounced at 10 mM of iron. Moreover, they have observed that these mechanisms lead to the formation of gels with different microstructures. At the higher iron concentration, a strong and rapid decrease in the repulsion forces is produced, resulting in random aggregation. At the lower iron concentration, the iron diminishes the superficial charge of both molecules and aggregated molecules, facilitating the interaction among hydrophobic regions and leading to the growth of the aggregation in the preferential direction and to filamentous gel formation [**Bryant et al., 1998, Remondetto et al., 2003**]. According **Remondetto et al., 2003**, two hypothesis may explain this behaviour: either divalent cations act as bridges between the negatively charged carboxylic groups on neighbouring β-lg molecules, as previously proposed [**Bryant et al., 1998, Marangoni et al., 2000**] or cations alter the ionic force. However, if the formation of bridges is essential to network formation, the increase in the metal ions concentration would result in the rise in the elasticity, which is contrary to their data showing that ionic force plays a major role in the formation (i.e., in support of the second hypothesis). Moreover, only the second hypothesis helps to explain why cold-induced gelation needs to occur at a divalent cations concentration that is lower than that of monovalent cations [**Kitabatake et al., 1996, Bryant et al., 2000**]. Therefore, **Remondetto et al. 2003** conclude that the predominant role of the metals is to alter the ionic force, rather than to act as bridges between the negatively charged carboxylic groups of protein molecules.

A new multistep Ca^{2+}-induced cold gelation process, starting with the protein in its fibrillar form, allows to form gel with very low protein concentration. Moreover, in these gels critical percolation, determined using rheological measurements, is an order of magnitude lower than in the conventional cold gelation method [V**eerman et al., 2003a**].

The effects of the metals in cold-set gels can be improved also by adding of oil before metal, inducing the formation of an emulsion gel. Emulsion gels with high storage modulus **G'** and good water-holding capacity (WHC) were obtained by raising the oil concentration. In contrast, an increase in salt concentration reduces

the WHC and changes the structure of the emulsion gel from fine-stranded to random aggregates. Oil content in the emulsion leads to a greater number of oil globules fitted into the gel matrix, which serves as many anchor points that strengthening the three-dimensional network. In such a way, oil and calcium are both clearly involved in the cold-set BLG emulsion gel network building process. Thus, results show that it is possible to manipulate the final gel characteristics by adjusting the proportion of oil included in the matrix and the amount of added calcium. [**Leung Sok Line et al., 2005**].

These novel routes open possibilities for the efficient use of protein gels as food ingredients in general.

1.4 Investigated whey proteins

The proteins used in this thesis work are β-Lactoglobulin A (BLG) and Bovine Serum Albumin (BSA). Both are globular proteins, usually employed as model-proteins: their structure has been well characterized and their behaviour in making aggregates and gels as a function of different experimental conditions has been extensively investigated. For these reasons, they have been considered appropriate proteins in order to study the effects of the metals on the aggregation and gelation processes. BLG and BSA are some of the main constituents of milk whey. Whey proteins constitute about 20% of bovine milk, the remaining part is composed by different types of caseins. The main characteristics of some whey proteins are summarized in tables 1.2.

Protein	% in milk	MW (Da)	Secondary strucutre	pI	S-S Bridges	Thiol (S-H)
β-Lactoglobulin	≈ 12	18350	15% α-helices 50% β-sheets	5.2	2	1
α-Lactalbumin	≈ 5	14174	50% α-helices 6% β-sheets		4	0
Bovine Serum Albumin	≈ 1.2	66000	67% α-helices 31% random coil	5.1	17	1

[Carter et al., 1994, Fang et al., 1998, Militello et al., 2004 and 2005]

Tab 1.2: Features of some proteins of bovine milk

Both BLG and BSA undergo conformational changes when exposed to high temperature [**Militello et al., 2003 and 2004, Vetri et al., 2005, 2007a and 2007b**]. In absence of thermal denaturation, both are soluble up to very acidic conditions [**Aymard et al., 1999**]. This feature makes their application in food manufacturing proper as gelling agents, emulsifiers, texture modifiers, thickening agents and foaming agents [**Kinsella et al., 1989**], replacing biopolymers, that have not the same nutritive value but are currently used.

1.4.1 Bovine β-Lactoglobulin

β-Lactoglobulin belongs to lipocalins family [**Flower et al., 2000**]. The principal characteristic of lipocalin family proteins is their ability, due to their structure, to bind small lipophilic molecules by locking up them in their hydrophobic pocket to reduce to minimum its contact with the solvent [**Pervaiz et al., 1987, Flower, 1996**]. Although the BLG function biological remains elusive [**Kontopidis et al., 2004**], this protein is known for its capacity to bind molecules such as the retionic acid [**Kontopidis et al., 2002**] and various hydrophobic ligands including the fatty acids and liposoluble vitamins. As a consequence, it is not surprising that it can also bind other hydrophobic molecules such as cholesterol and steroids [**Kontopidis et al., 2004**, **Flower et al., 2000**, **Sawyer et al., 2000, Pervaiz et al., 1987**]. It was suggested that one of the functions of the BLG is that to bind non-polar molecules to protect and transport them, through the acid environment of the stomach, towards the basic environment of the intestine **[Perez et al., 1995]**.

The primary structure of BLG is composed by 162 amino acids and its molecular weight is about 18.3 kDa **[Brownlow et al., 1997, Kontopidis et al., 2004]**. The X-ray crystallography and small-angle x-ray scattering studies have revealed that BLG, in the dimeric conformation, is an approximately prolate ellipsoid with a length of 69 Å and a width of 36 Å. Alternatively, the dimer can be described by two impinging spheres with a radius of 18 Å **[Verheul et al., 1999]**. The globular conformation of BLG is a consequence of an uniform distribution of non-polar, polar

and ionic residues which makes it possible for the hydrophobic residues to set in the inner core of the protein **[Cheftel et al., 1985]**.

The secondary structure of BLG was determined by using several experimental techniques, such as Circular Dichroism **[Dong et al., 1998]**, Infrared Spectroscopy **[Fang et al., 1997, Dong et al., 1998, Subirade et al., 1998]**, Crystallography **[Brownlow et al., 1997]**. It is composed of 15% of α-helices, 50% of β-strands and ~20% of reverse turns **[Vetri et al., 2005]**. This structure occurs in the form of eight antiparallel β-sheets (indicated from A to H in figure 1.14) which are rolled up to form a barrel in the calyx shape, whose interior is hydrophobic **[Brownlow et al., 1997, Wong et al., 1996]**. Inside the β-barrel is the hydrophobic ligand site.

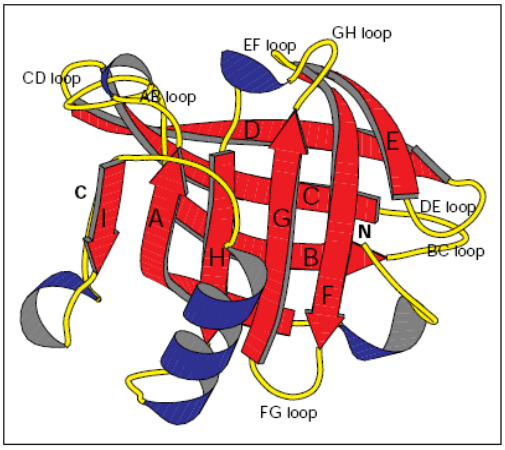

Figure 1.14: Molecular structure of β-Lactoglobulin monomer.
Figure from **Brownlow et al., 1997**.

The more external β-sheet, named I, is involved in the formation of BLG dimers via non covalent link of two monomers, the single monomer having a radius of gyration of about 1.5 nm **[Carrotta et al., 2003]**; dimers constitute the most probable quaternary structure of the protein at neutral pH **[Brownlow et al., 1997, de la Fuente et al., 2002, Hoffmann et al., 1999, Piazza et al., 2002, Kontopidis et al., 2004]**.

BLG contains two disulphide bridges (S-S) between the residues Cys66-Cys160 and Cys106-Cys119 and one free thiol group (SH) very reactive in position 121. S-S bridges together with hydrogen bonds stabilize the native tertiary structure

of the protein [**Papiz et al., 1986, Dill 1990, Bryant et al., 1998**] and, in appropriate experimental conditions, drive its aggregation process [**Yu et al., 1985, Ozaki et al., 1987, Li et al., 1991, Griffin et al., 1993, Roefs et al., 1994, Hoffmann et al., 1999, Vetri et al., 2005**]. Moreover, two tryptophans are present inside BLG; the first one (trp61) is found in an external zone, practically exposed to the solvent, while the second one (trp19) is in the core of a hydrophobic cavity [**Brownlow et al., 1997, Renard et al., 1998, Vetri et al., 2005**].

The quaternary structure of BLG is strictly dependent on the pH value: at pH values from 5 to 8, the dimer is the most stable conformation of BLG at room temperature, although small proportions of higher aggregates (e.g., tetramers) may be present as well [**Hoffmann et al., 1999, Panick et al., 1999**]. Below pH 3.5 the protein conformation is essentially monomeric. The dissociation leading to monomeric subunits is driven by non-specific interactions, such as electrostatic repulsion **[Verheul et al., 1999, Aymard et al., 1999]**. From pH 3.5 to 5.2, a reversible aggregation of BLG resulting in the formation of octamers has been observed, especially at low temperature (4 °C) [**Renard et al., 1999, Verheul et al., 1999**]. Around pH 7.5 the BLG conformation changes reversibly, as first described by Tanford et al., 1959; this so called *Tanford transition* is reported to be associated with the titration of one buried carboxyl group per monomer and with changes in the environment of a tyrosine residue and a free cysteine group. A pH rise above 8 induces time-dependent, irreversible aggregation of BLG caused by the formation of intermolecular disulfide bonds leading to the appearance of tetramers in solution [**Verheul et al., 1999**].

There are 7 variable genetics which are distinguished from/to each other because of the substitution of certain amino acids. Variable A and B are most frequently met; they are different in the positions 64 (Asp/Gly), which is in a flexible loop, and 118 (Val/Ala) at the beginning of the layer H [**Brownlow et al., 1997**].

Figure 1.15 presents the BLG charge. It is known that several peptide areas of BLG are rich in amino acids positively (arginine, histidine and lysin) or negatively charged (acid glutamic and asparagine) giving origin to charged zones on the

surface of the protein **[Brownlow et al., 1997]**. This charge distribution is dramatically dependent on the pH value. The isoelectric point, pI, is 5.2 [**Bryant et al. 1998**, **Renard et al., 1998**].

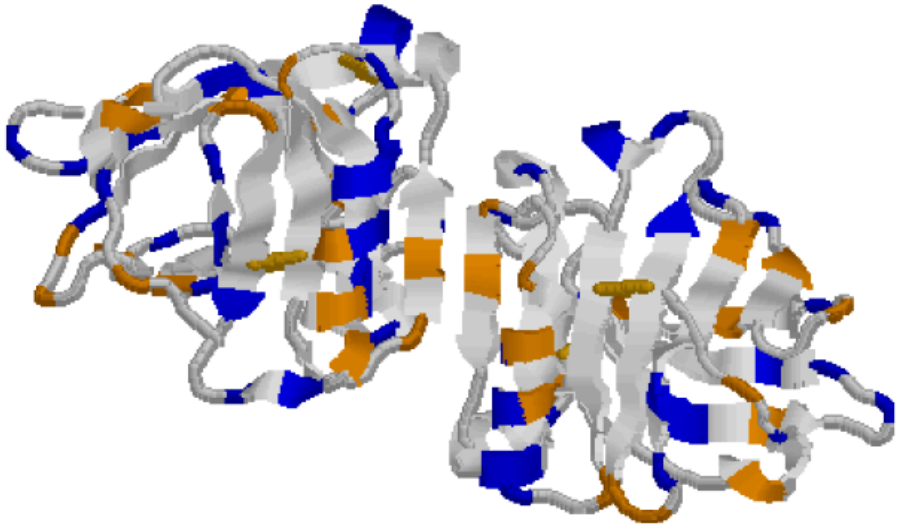

Figure 1.15: Three-dimensional structure of dimeric β-Lactoglobulin at neutral pH showing the charge distribution. Positively charged amino acids are in blue; negatively charged amino acids are in orange; neutral amino acids are in white. Figure from **Brownlow et al., 1997**.

Thermal aggregation of β–Lactoglobulin

When subjected to heat-treatment, BLG protein units undergo aggregation and denaturation processes as a function of temperature value **[Iametti et al., 1996, de La Fuente et al., 2000, Vetri et al., 2005]**.

The first stage of denaturation, at about 40 °C and at neutral pH, is characterized by the dissociation of dimers in monomers **[Iametti et al., 1996]**. As the temperature increases from 50 to 70 °C, a sequence of conformational changes occurs. The secondary structure is modified because of the conversion of the unique α–helical structure in β-structure evolving towards intermolecular β–sheets with the proceeding of the aggregation process induced by the temperature increase. A partial unfolding, caused by rupture of hydrogen bonds, uncovers the Cys121 thiol

group; at about 50 °C one tryptophanil (trp) residue is exposed, the unfolding being completely reversible; and finally at 70 °C the second trp is exposed, this last unfolding being irreversible **[Hambling et al., 1992, Iametti et al., 1996, Wong et al., 1996]**. In this reactive state, the molecule undergoes various reactions of aggregation including the formation of intermolecular disulphide bridges and interactions between the exposed hydrophobic areas [**Relkin 1998**, **Verheul et al., 1998, Vetri et al., 2005**]. For longer times of treatment at 80 °C, oxidation processes occur, starting exchange processes between a thiol group and a disulphide bridge of various molecules [**Relkin 1998**]. The aggregates are also steadied by ionic interactions and hydrogen bonds **[Wong et al., 1996]**. A study carried out by differential scanning calorimetric associated with spectroscopic measurements has revealed that the two domains unfold independently according to a mechanism where an equilibrium step is followed by an irreversible transition **[Fessas et al., 2001]**.

The unfolding of the protein caused by high temperature and resulting in exposure and activation of free sulphydryl groups is regarded as the rate-limiting step in the aggregation process [**Griffin et al., 1993, Roefs et al., 1994, Iametti et al., 1996, de la Fuente et al., 2002**].

The model proposed by Roefs and Kruif (1994) is based on the association of monomeric subunits. It consists of three steps:

$$B_2 \leftrightarrow B \rightarrow B^{SH} \qquad (1)$$

$$B + B_i^{SH} \rightarrow B_{i+1}^{SH} \quad i \geq 1 \qquad (2)$$

$$B_i^{SH} + B_j^{SH} \rightarrow B_{i+j} \quad i, j \geq 1 \qquad (3)$$

The starting step (1) is characterized by a number of reversible reactions followed by an irreversible reaction. In the reversible reaction, BLG dimer (B_2) splits into monomers (B). This is followed by the exposure of the free sulphydryl group of native BLG, which makes the protein reactive (B^{SH}). The propagation reaction (2) corresponds to the build-up of aggregates via thiol/disulphide exchange reactions

between an activated BLG intermediate, with a free reactive thiol group (SH), and a native non-reactive BLG. In the final step (3), two active intermediates react and form a larger disulphide-linked polymer, without an exposed reactive thiol group. This reaction scheme accounts for the formation of aggregates in which the monomers are linearly linked, but the aggregates are not stiff rods and may even have a spherical shape. The order of this reaction is 1.5. This model holds for BLG dissolved in water at neutral pH and heated at about 65 °C **[Hoffmann et al., 1996]**.

Later and different studies performed by Bauer and co-researchers revealed the presence of metastable intermediate oligomers formed in the early steps of BLG thermal aggregation **[Bauer et al., 1998, and 2000, Carrotta et al., 2001 and 2003]**. The intermediates show typical molten globule features (secondary structure content similar to the native state one and less tight packing of the side chains). These oligomers are central in the aggregation process; indeed, it was demonstrated that they rapidly form aggregates upon heating in absence of monomeric proteins [**Bauer et al., 2000**]. The model used by the authors to understand the data suggests a linear association of monomers in oligomers via disulfide bridges and a formation of aggregates nucleus from four oligomers via non-covalent interactions **[Bauer et al., 1998, and 2000, Carrotta et al., 2001 and 2003]**. This behaviour deviates from the model proposed by Roefs and Kruif, 1994, according to which the aggregates grow directly by association of monomers through intermolecular disulfide bonds. Moreover, at higher temperatures, the formation of reactive monomers would be very fast and, as a consequence, the rate of the final reaction would also be faster (shorter propagation), so that only relatively small aggregates would be formed via this pathway **[Schokker et al., 1999]**. This mechanism would be applicable only if the temperature is high enough to dissociate and unfold the BLG molecules very rapidly so that the aggregation reaction becomes rate limited. Consequently, aggregation would not be limited to the formation of linear aggregates; branched aggregates could be formed **[de la Fuente et al., 2002]**. This would be in agreement with the heat-induced BLG aggregation studies, in which the formation of rod-like

aggregates was observed **[Aymard et al., 1996, Gimel et al., 1994]**. Static and dynamic light scattering measurements showed that the formation of BLG aggregates upon heating the solution at neutral pH occurs via two-step process **[Gimel et al., 1994, Aymard et al., 1996, Le Bon et al., 1999]**. Heat-induced denaturation would lead to the formation of small clusters with a size independent of concentration, temperature and ionic strength. Then, these clusters would aggregate and form self-similar structures with a broad size distribution. The internal dynamics of these aggregates were shown to be intermediate between those of flexible coils and rigid aggregates **[Gimel et al., 1994, Aymard et al., 1996, Le Bon et al., 1999]**. No evidence for a similar two-step aggregation process has been observed in the formation of BLG aggregates at pH 2 through static and dynamic light scattering **[Aymard et al., 1999]**; in this case, polydisperse aggregates, whose structure is strongly influenced by the ionic strength, are formed with a rigid rod-like local structure having mass per unit length close to that of a string of BLG monomers but with a somewhat larger diameter.

In this outlook, the role played by the different types of interaction in the aggregation process is not fully understood and contrasting ideas are present. Hoffmann et al. 1997 showed that a large proportion of high-molecular-mass aggregates, formed in water at near neutral pH and at 65 °C, are created by intermolecular disulphide bridges, while non covalent interactions have less importance. Other studies put in evidence the important role played by thiol group principally as initiator of thiol/disulphide exchange reactions mainly promoted at higher pH values **[Iametti et al., 1996, Hoffmann et al., 1996 and 1999, Kitabatake et al., 2001, Vetri et al., 2005, Visschers et al., 2005]**. However, the aggregation models explaining the presence of intermediate oligomers in aggregation pathway assign a predominant role also to non-covalent interactions, such as hydrophobic interactions **[Iametti et al., 1996, Schokker et al., 1999, Bauer et al., 2000, Vetri et al., 2005]**. Other authors reported that the non-covalent interactions become more important at higher temperature (> 90 °C) and only the use of lower temperature gave a greater

relevance to the disulphide interactions **[Kitabatake et al., 2001, de la Fuente et al., 2002]**.

The aggregation and denaturation processes are affected by several parameters besides temperature, such as pH, ionic strength, which can change the process pathway.

The critical temperature of denaturation of the BLG is > 70 °C at neutral pH **[Euston et al., 2007]** but it can vary according to the pH. With a basic pH, stability decreases and denaturation temperature goes down to 50 °C for a pH 9. This is due to an increase in the reactivity of the thiols groups **[Verheul et al., 1998, de la Fuente et al., 2002]**. With an acid pH, thermal stability of the native BLG increases **[Verheul et al., 1998, de la Fuente et al., 2002]** because the molecule is more compact and it is stabilized by several hydrogen bonds **[Renard et al., 1998, de la Fuente et al., 2002]**. Moreover, at an acid pH, the thiol groups are not reactive ($pK_a = 7.5$) **[Tanford et al., 1959, Hoffmann et al., 1999]**. Thus, the aggregates formed with pH < 6.5 are maintained primarily by hydrophobic interactions and hydrogen bonds. With pH < 3, the thermal denaturation is partially reversible if the treatment is not too severe (temperature belove 80 °C) **[Euston et al., 2007]**.

The ionic force plays an important role in the thermal stability of BLG. In general all salts, in appropriate concentrations, promote aggregation via hydrophobic interactions by a reduction of the electrostatic repulsions **[Bryant et al., 1998, Remondetto et al., 2003]**. At acidic conditions, a low increase in the ionic force prevents the denaturation by a steadying effect (salting-in) which stabilizes dimeric conformation **[Fox 1989]**, but with higher concentrations aggregation is favoured (salting-out) **[Verheul et al., 1998]**. Finally, it was found that with pH > pI ions can interact, binding the carboxylic groups of protein and affecting the reactivity of the grouping thiol **[Bouhallab et al., 2004]**.

1.4.2 Bovine Serum Albumin

Bovine Serum Albumin (BSA) is the most abundant protein in plasma proteins and moreover it is a protein of the bovine milk whey. It plays a number of important biological roles including the binding and transport of essential, therapeutic and toxic metals **[Peters, 1996]**. Moreover, it is capable to bind an extraordinarily wide range of metabolites, drugs and other organic compounds. Transporting fatty acids is the main function of serum albumin **[Channu et al., 1999]**. A number of studies are focused on the structure and on the multifunctional binding properties of Serum Albumins **[Foster 1977, Peters 1985]**. BSA forms covalent adducts with various metal ions, such as Cu^{2+}, Ni^{2+}, Zn^{2+}, and Co^{2+}. The binding of these metals to serum albumin has been widely reported **[Zhou et al., 1994, Sadler et al., 1996, Liang et al., 2001, Liu et al., 2005]**. It is clear from previous publications **[Zhou et al., 1994, Sadler et al., 1996, Liang et al., 2001, Andrè et al., 2004, Liu et al., 2005]** that serum albumin has a variety of metal sites with different specificities, although the reported data are somewhat ambiguous. Notwithstanding, at least two binding sites for Cu^{2+} and Zn^{2+} have been identified in hydrophobic cavities of the molecules **[Sadler et al., 1994, Bal et al., 1998, Zhang et al., 2002, Stewart et al., 2003]**.

Information on the structure of BSA are determined by the structural studies performed on Human Serum Albumin (HSA), whose structure has been crystallized **[Carter et al., 1994, Curry et al., 1999]**. BSA and HSA have, indeed, a tight homology in the primary sequence and structure; while, the observed differences are, for example, the substitution of two residues having however the same hydrophobic nature and so not influencing the structure.

BSA constituted by 582 amino acids has a molecular weight of 66.28 KD **[Peters 1985, Gelamo et al., 2000]** and its structural shape is ellipsoidal with dimension 40 Å - 140 Å. The BSA molecule is made up of three homologous domains (I, II, III) which are divided into nine loops (L1-L9) by 17 disulphide bonds.

The secondary structure of BSA is predominantly alpha-helical (67%) with the remaining polypeptide occurring in turns and extended or flexible regions

between sub-domains with no beta-sheets **[Carter et al., 1994]**. Domains I and II and domains II and III are connected through helical extensions, creating the two longest helices in albumin.

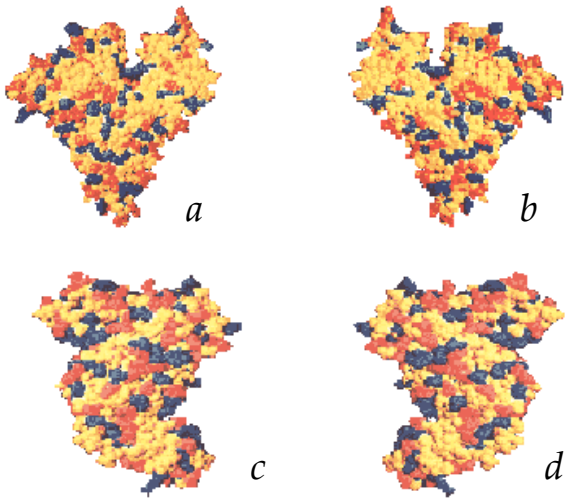

Figure 1.16: Space filling model of the bovine serum albumin molecule with basic residues colored in blue, acidic residues in red, and neutral ones in yellow. (a) Front view, (b) back view, (c) left side, and (d) right side **[Carter et al., 1994]**.

17 disulphide bridges inside protein make stable the tertiary structure at neutral pH and room temperature but do not prevent significant changes in shape and size as a function of pH and temperature **[Foster 1977, Carter et al., 1994]**. A free thiol group (Cys34) is also present in the protein structure; it has been verified that this one has a relevant role in thermal aggregation pathways of BSA in appropriate experimental conditions **[Militello et al., 2003]**.

As depicted in **Carter et al., 1994**, and shown in figure 1.16, the albumin molecule is not uniformly charged within the primary structure. Unlike the asymmetric charge distribution on the primary structure, the distribution on the tertiary structure seems fairly uniform. Its isoelectric point is around 4.9 **[Putnam 1975, Peters 1996, Taboada et al., 2004, Brewer et al., 2005]**.

BSA shows several conformational isomerisations as a function of pH, illustrated in figure 1.17; some of these are physiological. Because of the great

number of charged amino acids in primary sequence of albumins, lots of these modifications must be attributed to the break of ionic couples caused by a change of pH value. In particular, pH 4.5 marks the transition from "native" (N) to "fast" (F) form, for which a decrease of the helical structures is observed. When pH decreases more and more, the structure is more and more open and, at pH 2.7, the protein assumes the "expanded" conformation (E). Finally, at pH 9, albumin changes conformation to the "basic" form (B).

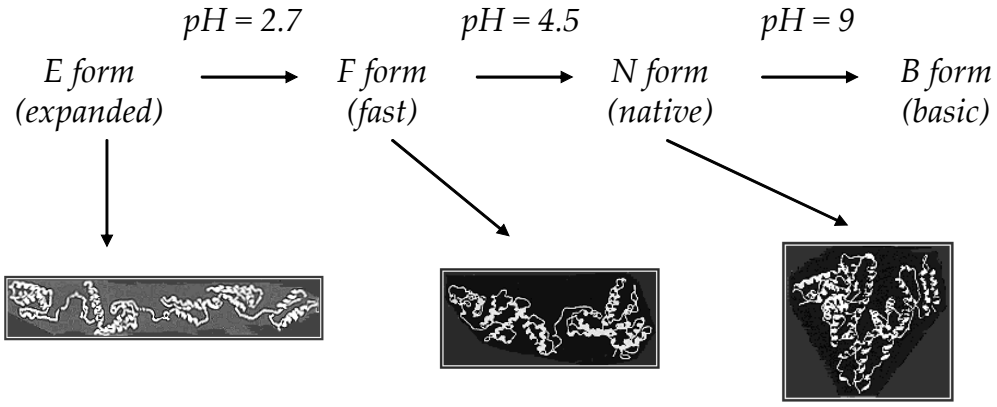

Figure 1.17: Different conformational isomerisation of BSA as a function of pH [Carter et al., 1994].

BSA, as well as many other globular proteins, has the tendency to aggregate in macromolecular assemblies when subjected to a temperature increase **[Barone et al., 1992].** Thermal aggregation of BSA appears to be a multiple interaction and cross-feedback among different processes occurring on different length-scales, namely: i) protein conformational changes (possibly including oligomer formation); ii) nucleation and growth of aggregates (fibrils, fibers, gels, amorphous deposits) and iii) the liquid-liquid demixing (LLD) phase transition **[Bulone et al., 1993, San Biagio et al., 1991, 1996 and 1999, Manno et al., 1999 and 2001, Vaiana et al., 2003 and 2004]**.

In appropriate experimental conditions, thermal aggregation of BSA is characterized by the conformational changes of its native structure from a structure prevalently constituted by α-helices to a more open β-rich structure. These changes

are overall modulated by the pH value, the temperature, the time of heating, the protein concentration and other variables **[Barone et al., 1995, Giancola et al., 1997, Veerman et al., 2003b, Militello et al., 2004, Vetri et al., 2007a]**. For example at two different pH values, a reversible denaturation is observed when BSA undergoes a heat-treatment at around 80 °C, while an irreversible denaturation is observed when the protein is heated for a longer period at 60 °C **[Barone et al., 1992, Gelamo et al., 2000, Kosa et al., 1998]**. In particular, when the temperature increases, electrostatic interactions result unchanged, whereas the contribution of hydrophobic interactions increases, due to their entropic origin **[Jaenicke 1990]**. The role of sulphydryl group, Cys34, in the associative processes has been also investigated. Blocking of the free sulphydryl, Cys-34, with iodoacetamide, cysteine, or glutathione prevents the occurrence of mixed disulphides in aged albumin, as well as the occurrence of the albumin dimer **[Peters 1985]**. Moreover, **Militello et al. 2003** observed, in low concentration regime and at pH 6.2, that in BSA-Fluorescein-5-Malemide conjugate, where free thiol group bound covalently with fluorescein cannot be available to form intermolecular bonds, the aggregation and the conformational change characteristic of non-modified BSA aggregation (from α to β-rich structures) are now prevented.

Aggregative behaviour of BSA is mainly modulated by the pH, which has already a strong influence on BSA structure as well. Again, in low concentration regime **Vetri et al. 2007** made a study on BSA thermal aggregation at pH 4.7 and 5.7 following kinetic of the emission of tryptophans present in the protein. The authors found that the "incipit" of BSA aggregation is not driven by nucleation mechanisms and, at these pH values, it is mainly due to hydrophobic interactions. These interactions are favoured by the exposure of hydrophobic residues induced by the conformational changes, which have the common feature of being the step for initiating intermolecular cross-linking interactions also without changes in secondary structure.

In high concentration regime, **Militello et al., 2004** followed thermal aggregation of this protein at different pH value by FTIR Spectroscopy, in order to monitor conformational changes of the secondary and tertiary structures, and by Dynamic Light Scattering, in order to have information on the average dimension of aggregates. The authors found that when the pH approaches to the pI of the protein the aggregation mechanism becomes more disordered. In particular, at pH values far from the pI of the protein, the aggregation mechanism proceeds in an ordered way to form β-aggregates mostly comig from the α-helix changes and producing aggregates of small dimensions. At pH values approaching the pI, the aggregation mechanism is more disordered and other aggregates of larger dimensions add to the smaller ones; moreover, a spectral disorder is also observed, when the larger species appear, probably coming from increased amount of random coil structures **[Militello et al., 2004]**.

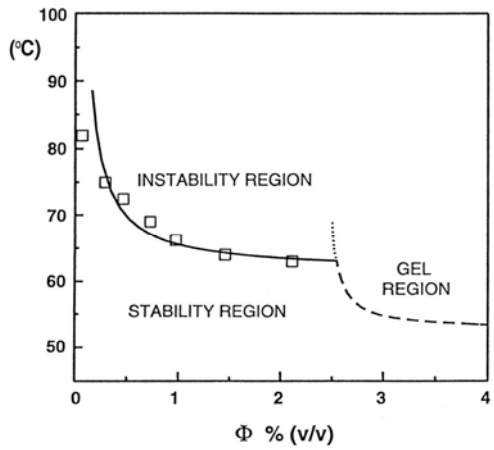

Figure 1.18: Phase diagram of BSA solution **[San Biagio et al., 1996]**.

In high concentration regime, it must be not neglected the role of thermodynamic instability of proteins solutions against liquid-liquid demixing (LLD) in protein aggregation **[San Biagio et al., 1996 and 1999, Manno et al., 2001, Militello et al., 2003, Vaiana et al., 2003]** and its dependence on above parameters affecting aggregation pathway **[Bulone et al., 1993, Manno et al., 2004]**. In figure 1.18 the temperature-versus-concentration phase diagram obtained for BSA in **San**

Biagio et al. 1996 is shown. Spinodal curve separates a phase of homogeneous solution from a phase of LLD instability. Results obtained by **Vaiana et al., 2004** viewed together with those of **San Biagio et al., 1996 and 1999** show that aggregation occurs with the formation of oligomers behaving as larger units (or "aggregation building blocks") and, exhibiting their own collective behavior with spinodal instability, critical divergences, demixing and final cross-linking and aggregation. These results highlight that the aggregation process evolves from individual proteins to oligomers and to aggregates and therefore that it is remarkably more complex than the plain stepwise accretion that could at first sight be inferred from the non-nucleated character of oligomerization itself **[Vaiana et al., 2004]**.

1.5 Problems and Goals

The themes treated in this PhD thesis are based on the investigation of metal contributions to aggregation processes, such as thermal aggregation and cold-gelation of proteins are. As it has been already said, the interest towards these topics is much recent. In particular, the protein aggregation in presence of metal ions has received much attention because of the discovery of an active contribution of metals in the arise of some degenerative pathologies [**Mantyh et al., 1993, Bush et al., 1994**]. While, the recent interest toward cold-induced gels of protein is due to the more and more increasing demand of consumers for more convenient, healthy, tasty and natural food products created via the use of "label-friend" ingredients, such as the whey proteins [**Bryant et al., 1998, Alting 2003, Alting et al., 2003**].

In this scenario, which has been widely described in this chapter, some contrasting information on the effects induced by metals on the protein thermal aggregation in presence of metal ions and on the cold-set gels are encountered. For example, if the metal/protein interaction is considered, the metal can assume the role either of promoter or of inhibitor of the aggregation process as a function of different experimental conditions [**Bush et al., 1994, Suzuki et al., 2001, House et al.,**

2004, Stellato et al., 2006]. While, with respect to the metal-induced cold gels a different dependence of the viscoelastic properties of gels has been observed as a function of metal concentration [**Marangoni et al., 2000, Remondetto et al., 2003**]. Finally and mainly as concerns the study of metal effect on thermal aggregation, the most part of scientific investigations has been carried out on a unique biological system, β-amyloid peptide. Indeed, as it has been already said, the abnourmous extracellular deposition of amyloid fibrils, related to several neurodegenerative pathologies, has origin from the amyloid aggregation of β-peptides.

Thus, in this young research field, our pioneer studies intend to add a contribute in order to clarify the role and the effects of metal ions in protein aggregation processes, through a comparative study carried out in the same experimental conditions, involving two model proteins, such as BLG and BSA, characterized by different features. This choice is motivated by the supposition that the interaction between protein and metal cannot be affected by the metal kind only, but that the protein nature must have an important role. In particular, BLG has mainly a β-kind secondary structure and it is characterized by a different quaternary structure as a function of pH. The latter influences the evolution of the aggregation process. BSA has a α-kind secondary structure and it has been selected because of its ability to bind various metal ions in inner hydrophobic sites, such as Cu^{2+} and Zn^{2+}. This aspect could characterize and justify different behaviours of metal ions in the interaction with protein.

With this aim, the effects of metals on the aggregation processes both of BLG and of BSA (thermal aggregation and cold-gelation) have been studied at neutral pH. Moreover, the effects of metal ions presence during thermal aggregation of BLG have been investigated as a function of pH too. The experimental approach has been explained in the overview section and the used experimental techniques will be described in the following chapter.

Chapter 2

Materials and Methods

2.1 Samples preparation

2.1.1 Proteins solutions

β-lactoglobulin A from bovine milk was obtained from Sigma-Aldrich. The powdered protein was dissolved in *(i)* a 20 mM MES buffer, made in D_2O (99.9%, Aldrich) and titred with KOH up to pD 7 or *(ii)* in 20 mM N-ethylmorpholine (NEMO), made in D_2O (99.9%, Aldrich) titred with formic acid until to pD 4 or 2.5. pD is pH meter reading + 0.4 correction. The final concentration of protein was 3.3 mM (60 mg/ml). $CuCl_2$ or $ZnCl_2$ (99.999%, Sigma-Aldrich) 0.1 M was diluted in buffer at 1% and its final concentration was 1 mM. The freshly prepared samples,

centrifuged (2000 rpm for 8 minutes) and filtered (0.20 μm), were divided in two aliquots for IR and scattering measurements, respectively. The temperature selected for the monitoring of the thermal aggregation at neutral pH was 60 °C, while 42 °C and 50 °C were the selected temperatures at pH 4 and 2.5, respectively. D_2O solutions were used to avoid the IR spectral overlaps between Amide I band and the strong absorption band of water in the region 1650 cm^{-1}.

Bovine Serum Albumin was obtained from Sigma-Aldrich. Powdered protein was dissolved in *(i)* a 20 mM MES buffer, made in D_2O (99.9%, Aldrich) and titred with KOH until to pD 7 or *(ii)* in 20 mM N-ethylmorpholine (NEMO), made in D_2O (99.9%, Aldrich) titred with formic acid until to pD 4 or 2.5. The final concentration of protein was 1 mM (66 mg/ml). $CuCl_2$ or $ZnCl_2$ (99.999%, Sigma-Aldrich) 0.1 M or 0.03 mM was diluted in buffer at 1% and its final concentration was 1 mM or 0.3 mM, in order to obtain a [metal]/ [protein] ratio of 1:1 and 0.3 : 1, the latter being the same investigated for BLG. The freshly prepared samples, centrifuged (2000 rpm for 8 minutes) and filtered (0.20 μm), were divided in two aliquots for IR and scattering measurements, respectively. The temperature selected for all the measurements was 58 °C. D_2O solutions were used to avoid the IR spectral overlaps between Amide I band and strong absorption band of water in the region around 1650 cm^{-1}.

The selected temperatures of protein incubation were different since the activation temperature of the aggregation process is dramatically dependent on the protein and on the experimental conditions. Here, the selected temperature was the more suitable one in order to study the thermal aggregation and, especially, the metal ions effects on this latter at different experimental conditions.

2.1.2 Gels

The procedure employed for the preparation of the BLG or BSA gels was the same except for the protein molar concentration, 3.3 mM for BLG and 1 mM for BSA, and for the heating temperature, 60 °C for BLG and 58 °C for BSA.

The protein solution was prepared through the procedure described above and leading to pH 7. After the centrifugation and the filtration, the freshly samples were divided in two aliquots for IR and scattering kinetics in order to characterize the pre-heating phase of native protein solution. In order to form reactive pre-aggregates leading to gels formation, we prepared another protein solution of about 1.5 ml. This was made using H_2O instead of D_2O and after incubation at selected temperature for two hours under weak stirring.

$CuCl_2$ or $ZnCl_2$ (99.999%, Sigma-Aldrich) 0.1 or 0.3 mM in bi-distilled water were added to the several aliquots of the same protein pre-heated solutions after cooling at room temperature, obtaining a final concentration of 10 or 30 mM.

2.2 Experimental methods

As we have already said, Dynamic Light Scattering measurements were realized on the protein solutions in order to obtain information on the time evolution of the mean dimension of the aggregates. The structural and the conformational changes at secondary and tertiary level were studied by the time evolution of Amide I' and Amide II bands profiles respectively, monitored by infrared absorption spectroscopy. Rheological measurements were carried out in order to study viscoelastic properties of the gels.

2.2.1 Dynamic Light Scattering:

a) Theoretical background

The Dynamic Light Scattering (DLS) technique measures the time-dependent fluctuations of the scattered light intensity occurring because of the particles are undergoing random Brownian motion. Analysis of these intensity fluctuations enables the determination of the diffusion coefficients distribution of the particles, which can be converted into a size distribution using established theories that will be briefly summarized in the following.

DLS provides important information about the structure and the aggregation process of a protein. For example, it makes possible to follow the changes in protein quaternary structure as a function of pH by the diameter size distribution of the particles in solution. The most important information for this thesis work concerns the characterization of the evolution of the aggregation process via the kinetics of the scattered light intensity, the Z-average diameter and the diameter size distribution of the particles in solution. DLS enables to determine also the melting point of the protein, defined as the temperature at which thermal denaturation occurs; this is easily monitored with light scattering instrumentation because of the molecular weight dependence on the scattering intensity. It is important to remind that the increase of the molecular weight of a protein during thermal denaturation can be due to the association, for example, of hydrophobic residues of different protein units exposed to the solvent after the partial unfolding of the protein induced by the temperature increase. The z-average diameter is the weighted mean hydrodynamic size of the ensemble collection of particles measured by DLS. In experimental conditions leading to the protein aggregation, changes in Z-average diameter indicate that the aggregation results in an increase of the mean dimension of the aggregates. The diameter size distribution allows us to follow the time evolution of the dimension of the single species present in solution.

In DLS measurements single photons are detected and correlated. Correlation is a statistical method for measuring the degree of non- randomness in an apparently random data set. The autocorrelation function is the convolution of the intensity signal with itself as a function of time. When applied to a time dependent intensity trace, as measured in dynamic light scattering, the correlation coefficients, $G(\tau)$, are calculated as shown below, where I is the intensity, t is the time, and τ is the so called delay time:

$$G(\tau) = \int_0^\infty I(t)I(t+\tau)dt\,. \qquad (2.1)$$

The shift time (τ) is often referred to as delay time since it represents the delay between the "original" and the "shifted" signals. The continuous intensity correlation function cannot be directly measured, but it can be approximated with discrete points obtained by a summation over the duration of the experiment. The expression giving an approximation of the continuous autocorrelation function is shown below, which holds true for both linear and arbitrary delay times:

$$G_k(\tau_k) = \sum_{i=0} I(t_i) I(t_i + \tau_k) \tag{2.2}$$

If the intensity statistic of the measured signal is Gaussian (which is true for all diffusion and for most of the random processes), the autocorrelation function can be expressed according to the Siegert relation. This states that the normalized intensity autocorrelation function can be expressed as the sum of 1 and the square of the field autocorrelation function, $g(\tau)$, scaled with a coherence factor γ expressing the efficiency of the photon collection system:

$$G(\tau) = 1 + \gamma g(\tau)^2 \tag{2.3}$$

When $g(\tau)$ can be approximated with a single exponential, the expression assumes the form shown below, where A is the amplitude or intercept of the correlation function, B is the baseline, D is the diffusion coefficient, q is the scattering vector, λ_0 is the vacuum laser wavelength, $\tilde{n}$ is the medium refractive index, θ is the scattering angle, K is the Boltzmann constant, T is the absolute temperature, η is the viscosity of the medium, and R_H is the hydrodynamic radius.

$$G_2(\tau) = \langle I(t) \bullet I(t+\tau) \rangle = A[1 + B\exp(-2\Gamma\tau)] \tag{2.4}$$

$$\Gamma = Dq^2, \qquad q = \frac{4\pi\tilde{n}}{\lambda_0}\sin\left(\frac{\theta}{2}\right), \qquad D = \frac{KT}{6\pi\eta R_H}. \tag{2.5 a, b, c}$$

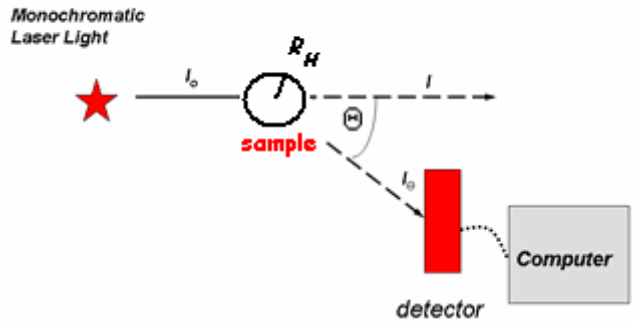

Figure 2.1: Scheme of a scattering process. The particle is approximated with a sphere having *hydrodynamic diameter*, R_H.

Therefore, by this technique it is possible to measure the diffusion coefficient D of particles in solution and as a consequence (see 2.5c) the hydrodynamic radius through the fluctuations of the detected light intensity. A scheme of a scattering process of monochromatic light by a particle is illustrated in figure 2.1. The relations above reported are valid in absence of multiple scattering. Moreover, an important hypothesis behind this relation is that the particles in solution are spheres moving in a regime of laminar viscous friction, where η is the viscosity of the medium; therefore, the measured hydrodynamic radius is the effective radius of a sphere having a diffusion coefficient equal to the measured one. It is important to stress that the right dimension of the object in solution is determined by the gyration radius, because the hydrodynamic radius is usually greater due to a not removable moisturizing shell around the protein **[Wilkins et al., 1999, Berne et al., 1976]**.

The theoretical approach in order to obtain the Z-average diameter from the autocorrelation function consists in the use of the Cumulant analysis, while the particle size distribution can be determined by a deconvolution of the measured intensity autocorrelation function of the sample. Usually, this deconvolution is accomplished using a non-negatively constrained least squares (NNLS) fitting algorithm, common example being CONTIN algorithm **[Provencher 1982]**. Concerning the results shown in this Thesis work, the particle size distributions have been reported as well as derived by the original software of the instrument,

while a Cumulants analysis has been performed on the autocorrelation functions in order to eliminate some artefacts present in the determination of the Z-average diameter. In the following, we will briefly illustrate the steps leading to the determination of Z-average diameter and diameter size distribution.

In the Cumulants approach, the exponential fitting expression in (2.4) is expanded in order to account for polydispersity or peak broadening effects, as shown below:

$$G_2(\tau) = A\left[1 + B\exp(-2\Gamma\tau + \mu_2\tau^2)\right]. \tag{2.6}$$

This expression is there linearized and the data are fitted in the form shown in (2.7)

$$\begin{aligned} y(t) &= \frac{1}{2}\ln\left[G_2(\tau) - A\right] \cong \frac{1}{2}\ln\left[AB\exp(-2\langle\Gamma\rangle\tau + \mu_2\tau^2)\right] = \\ &\frac{1}{2}\ln\left[AB\right] - \langle\Gamma\rangle\tau + \frac{\mu_2}{2}\tau^2 = a_0 - a_1\tau + a_2\tau^2 \end{aligned} \tag{2.7}$$

The first Cumulant or moment (a_1) is used to calculate the intensity weighted Z-average mean size and the second moment (a_2) is used to determine a parameter defined as the polydispersity index (PdI) through the following relations:

$$Z_D = \frac{1}{a_1}\frac{KT}{3\pi\eta}\left[\frac{4\pi\tilde{m}}{\lambda_0}\sin\left(\frac{\theta}{2}\right)\right]^2, \qquad PdI = \frac{2a_2}{a_1^2}, \qquad B = \frac{\exp(2a_0)}{A} \tag{2.8 a,b,c}$$

It is important to stress that the Cumulants analysis algorithm does not yield a distribution, but it gives the intensity weighted Z-average.

In order to obtain the determination of the size distribution, it is necessary to refer to a not negatively constrained least squares fitting algorithm as CONTIN **[Provencher 1982]**. The ideal field correlation function of "hypothetical" identical diffusing spheres is given by a single exponential decay function with decay rate Γ determined by the diffusion coefficient and by the wave vector of the scattered light.

The main aim of the data inversion consists in finding the appropriate distribution of exponential decay functions which best describe the measured field correlation function. The fitting function for g_k consists of a summation of single exponential functions built as a grid of exponentials of decay rate Γ_i :

$$g_k^{fit} = \sum_i A_i \exp(\Gamma_i \tau_i) \tag{2.9}$$

The factor A_i is the area under the curve for each exponential contribution, and it represents the strength of that particular i^{th} exponential function. The best fit is found minimizing the deviation of the fitting function (ξ^2) from the measured data points:

$$\xi^2 = \sum_k \left[g_k - g_k^{fit}\right]^2 \sigma_k = \sum_k \left[g_k - \sum_i A_i \exp(\Gamma_i \tau_i) \right]^2 \sigma_k \tag{2.10}$$

The weighting factor σ_k is incorporated to place more emphasis on the strongly correlated, rather than the low correlated (and noisy), data points.

In order to identify the solution of A_i's in the grid of fitted g_k expressions, it is necessary to minimize the deviation with respect to each A_i and then solving the resulting system of equations:

$$\frac{\partial \xi^2}{\partial A_i} = 0 \tag{2.11}$$

A_i values are there found using an iterative approach with some imposed constraints, which will not be listed here. The normalized display of A_i vs R_i, hydrodynamic radius (or Ai vs diameter), is the intensity particle size distribution displayed within the Intensity PSD Report in the Zetasizer Nano software (see figure 2.2).

			Diam. (nm)	% Intensity	Width (nm)
Z-Average (d.nm):	62.6	Peak 1:	65.8	100.0	15.5
PdI:	0.025	Peak 2:	0.00	0.0	0.00
Intercept:	0.950	Peak 3:	0.00	0.0	0.00

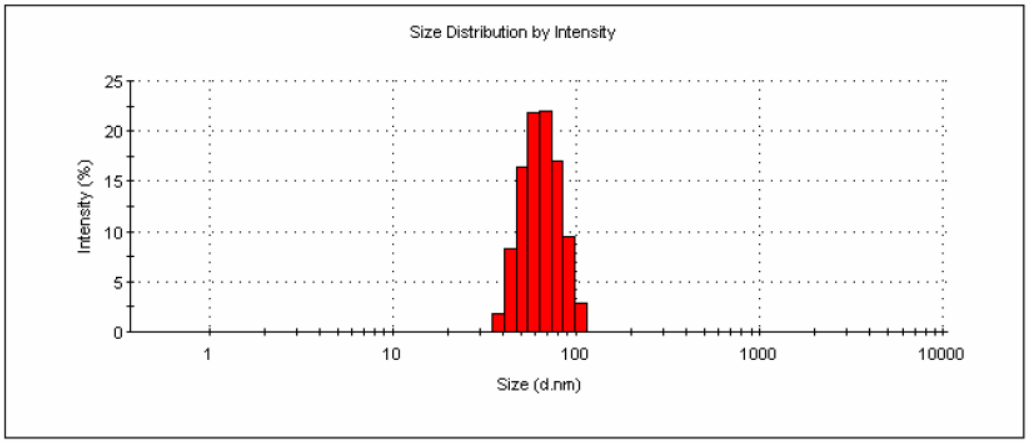

Figure 2.2: An excerpt from an Intensity PSD Report in the Zetasizer Nano software, and includes an example of the %Intensity histogram, along with the peak mean and standard deviation, derived from an NNLS deconvolution algorithm.

The average sizes displayed in the peak table are the intensity weighted averages, and are obtained directly from the size histogram using the following expression.

$$\langle R \rangle = \frac{\sum A_i R_i}{\sum A_i}. \tag{2.12}$$

The peak width or standard deviation (σ), indicative of the distribution in the peak, is also obtained directly from the histogram.

$$\sigma = \frac{\sqrt{\langle R^2 \rangle - \langle R \rangle^2}}{\langle R \rangle}, \qquad \text{where} \qquad \langle R^2 \rangle = \frac{\sum A_i R_i}{\sum A_i}. \tag{2.13}$$

In the following, the histogram in the diameter size distribution will be illustrated by a continuous line.

Then, through Mie theory with the use of the input parameter of the sample refractive index, it is possible to convert the intensity distribution into volume and number distributions **[Mie 1908, Bohren et al., 1983]**.

b) Experimental setting

Zetasizer Nano-S90 (Malvern Instruments) Dynamic Light Scattering Instrument was used. It is equipped with a He–Ne laser (λ= 633 nm) light source. The scattering angle is 90°. The sample compartment is completely self-enclosed and the temperature is automatically controlled. Kinetics were realized at fixed temperature, while temperature scanning was realized increasing the temperature of 1 °C every 5 minutes and starting measurements after an equilibration time of 3 minutes. From the exponential decay time of the photon autocorrelation functions ("correlation time") an effective hydrodynamic radius (R_H) of free diffusing particles in solution and a diameter size distribution were determined through the methods explained in the Theoretical background section (paragraph 2.2.1a). Kinetics allowed us to study the time evolution of the mean dimension of the aggregates and of the dimension of the single species in solution.

2.2.2 FTIR absorption:

a) Theoretical background

The treatment of the vibration of the molecules is a very complex problem. If this treatment is performed in terms of motion equation in the Lagrange form as a function of mass-adjusted cartesian displacement coordinates, it leads to a secular equation deriving by a non diagonal matrix which must be resolved. It is well known that its resolution is simplified using normal coordinates. Thus, it results that the vibrational problem can be considerably simplified by an appropriate choice of the coordinate systems. For example, a system of internal coordinates and symmetry coordinates is particularly useful. The difficulties encountered during the resolution of the problem can be overcome using a set of internal coordinates describing the bond distortions (such as bond stretching, angle deformations, and torsions). These coordinates do not contribute to the potential energy and result in zero roots in the solution to the vibrational problem. Thus, the size of the secular equation in internal coordinates is smaller and hence easier to solve. The use of

internal coordinates description allows to neglect the interactions of the rotational and vibrational energies of the molecule. This description of the vibrational problem has particular advantages in the biopolymers vibrational analysis and in the calculations of infrared intensities. The most commonly used internal coordinates consist of the following five types:

1. bond stretching coordinate representing a change in the length of a chemical bond (figure 2.3a);
2. in-plane bending coordinate representing a change in the angle between two chemical bonds having one atom in common (figure 2.3b);
3. out-of-plane bending coordinate representing a variation in the angle defined by two bonds with one atom in common and a third bond connected to the common atom (figure 2.3c);
4. torsion coordinate representing a variation in the dihedral angle between the plane determined by three consecutive bond connecting four atoms (figure 2.3d);
5. linear bend coordinate representing the bending of a linear three-atom bond (figure 2.3e).

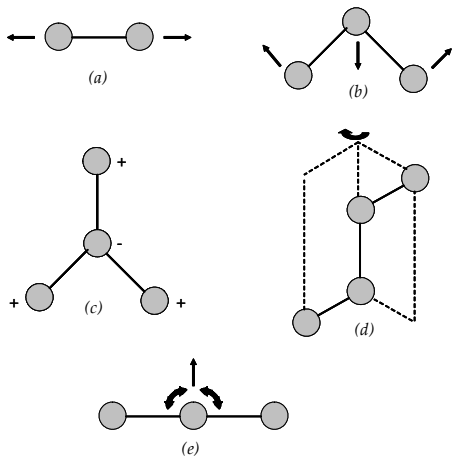

Figure 2.3: Definition of internal coordinates: *(a)* bond stretching; *(b)* valence angle bending; *(c)* out of plane bending or angle between a bond and a plane defined by two bonds; *(d)* torsion; *(e)* linear valance angle bending.

The vibrational absorption spectroscopy is based on the interaction between the described above vibrational molecular system and an electromagnetic radiation. Classical electrodynamics specifies that in order for a molecule to absorb radiation: *i)* the molecule must possess the same vibrational or rotational frequency of the electromagnetic radiation and *ii)* a change in the magnitude and/or direction of the dipole moment must take place. If both conditions are met, the vibration is termed as IR-active and an absorbance band is seen in the IR spectrum of the molecule. It is important underline that the IR bands are broadened also by rotational transitions occurring simultaneously to the vibrational ones. Because the rotational bands are much more closely spaced in terms of energy, a great number of molecules will populate excited rotational states at room temperature. The multiplicity of the rotational states is a Boltzmann distribution, and, thus, the number of different vibronic (vibronic + rotation) transitions is directly proportional to temperature.

The problem of the interaction between the electromagnetic radiation and molecules is treated solving the Schrodinger equation with the help of the Perturbation's theory. When a radiation field is present, there is a probability that a molecule exchanges energy with the field and appears in a quantum state different from its original one. This process is responsible for the appearance of spectra.

From a semi-classical point of view, the interaction between an electromagnetic wave and the matter is described by the Hamiltonian of the system expressed as following:

$$H = \frac{1}{2m}(\mathbf{p} - q\mathbf{A})^2 + q\varphi = H_0 + H'(t) \qquad (2.14)$$

This total Hamiltonian is considered as a sum of a component, H_0, describing the molecule in absence of external fields and of a component, $H'(t)$, which can be treated as a perturbation. $H'(t)$ depends on the vector potential $\mathbf{A}(\mathbf{r},t)$ according to the expression:

$$H'(t) = -\frac{i\hbar e}{m}\mathbf{A}\cdot\nabla + \frac{e^2}{2m}\mathbf{A}^2 \qquad (2.15)$$

where the term in $\mathbf{A}^2$ can be neglected in the weak field case.

An important approximation allowing to carry out the computation of the eigenfunctions related to a many-body problem, such as the molecular system, and associated to the Hamiltonian above reported is the *Born-Oppenheimer approximation* **[Rebane 1970, Weissbluth 1978, Bransden et al., 1983]**. This assumes that the total eigenfunctions $\Psi(\mathbf{r},\mathbf{R})$ of a molecular system can be factorized into two terms: an electronic wave function $\chi(\mathbf{r},\mathbf{R})$, depending on parametrically nuclear coordinates, **R**, and electronic coordinates **r** and a wave function $\varphi(R)$ associated to the nuclei and depending on their coordinates only:

$$\Psi(\mathbf{r},\mathbf{R})= \chi(\mathbf{r},\mathbf{R})\ \varphi(\mathbf{R}). \qquad (2.16)$$

The electronic wave function $\chi(\mathbf{r},\mathbf{R})$ depends on the electronic spin variables as well and are antisymmetric in respect to the electronic coordinates permutations. Assuming the system in a stable configuration and in the hypothesis of small nuclear motions (*harmonic approximation*), $\varphi(\mathbf{R})$ can be expressed in terms of normal vibrational modes **Q**, so that the nuclear wave function can be factorized as a product of N single harmonic oscillator eigenfunctions $\varphi_i(Q_i)$, characterized by the equilibrium position Q_{oi} and vibrational energy $E_i=h\nu$:

$$\varphi(\mathbf{Q})=\Pi^{N}_{i=1}\varphi_i(Q_i) \qquad (2.17)$$

and

$$E_{vib} = \sum_i E_i(Q_i) \qquad (2.18)$$

The separation of the electronic and nuclear motions depends on the large difference in mass between the electrons and nuclei. Since the former ones are much lighter, they have relatively greater velocities and their motion can be treated by assuming fixed positions of the nuclei. Conversely, the small nuclear oscillations, compared to inter-atomic distance, occur in an essentially averaged electron distribution.

By theoretical treatment, it results that the number of the molecules making per unit time the transition from the ground vibrational state, $\varphi_g(\mathbf{Q})$, to one of the upper vibrational states, $\varphi_u(\mathbf{Q})$, by absorbing radiation is

$$n_0 \cdot B_{g\to u} \cdot \rho(E) \cdot \delta(E - E_{ug}), \qquad (2.19)$$

where n_0 is the molecule volume density in the g state, ρ(E) is the energy density of the radiation field at the energy E, $E_{ug}= E_u-E_g$, and $B_{g\rightarrow u}$ is the transition probability , or the *Einstein coefficient*, *for absorption*, defined as

$$B_{g\rightarrow u} = \frac{16\pi^4}{3h^2}\cdot\frac{1}{4\pi\varepsilon_0}\cdot\left|F_{g\rightarrow u}\right|^2, \tag{2.20}$$

where, considering the *Electric Dipole approximation*, we can write:

$$F_{g\rightarrow u} = \left\langle \Psi_u \middle| \text{-}e\mathbf{r} \middle| \Psi_g \right\rangle = \left\langle \Psi_u \middle| \mathbf{M} \middle| \Psi_g \right\rangle. \tag{2.21}$$

In particular, let x, y, z be the axes of a coordinate system fixed in the molecule. If M_x, M_y, M_z are the three components of the electric dipole moment $\boldsymbol{M}$ of the molecule in the direction of the coordinate axes in a displaced position of the nuclei, and if M^0_x, M^0_y, M^0_z are the components of the electric dipole moment $\boldsymbol{M}^0$ in the equilibrium position, then, for sufficiently small displacements, M_x can be expanded:

$$M_x = M_x^0 + \sum_i \left(\frac{\partial M_x}{\partial Q_i}\right)_0 Q_i + \ldots \tag{2.22}$$

and similarly for M_y and M_z.

So, utilizing the expression 2.16 for the eigenfunctions, after its conversion in normal coordinates and the *Born-Oppenheimer approximation*, according to the 2.22, for each vibrational mode results:

$$\left\langle \chi_u(\{\mathbf{Q}_{0i}\},\mathbf{r}) \middle| \chi_g(\{\mathbf{Q}_{0i}\},\mathbf{r}) \right\rangle \frac{\partial M_x}{\partial Q_i}\bigg|_{Q_0} \left\langle \varphi_u(\{\mathbf{Q}_i\}) \middle| Q_i \middle| \varphi_g(\{\mathbf{Q}_i\}) \right\rangle, \tag{2.23}$$

where $\boldsymbol{Q}$ has been fixed to the equilibrium position of the ith nucleus, $\boldsymbol{Q_0}$, in the electronic wave function term. Similarly for M_y and M_z.

The dipole moment $\boldsymbol{M}$ of the molecule will change with the frequency of a normal vibration i (that is, this frequency will be active in the infrared) *if and only if* at least one of the derivates of the dipole moment components (M_x, M_y, M_z) is different from zero. The variation of the dipole moment of a vibrating molecule is strictly dependent on the molecule symmetry. If you consider a homonuclear diatomic molecule, such as CO_2, vibrations maintaining the symmetry induce no net change

in dipole moment; hence, no interaction with infrared radiation occurs for this motion. Conversely, in the asymmetric stretching vibration, the symmetry of the molecule is perturbed and there is a change in the net dipole moment, allowing infrared absorption.

FTIR spectroscopy of the Amides

The spectrum of a protein consists of contributions due to vibrational modes of lateral residues and to characteristic vibration modes of the backbone. Vibrational bands associated with the backbone vibrations, termed as *Amides*, are very important in order to determine the secondary structure of the protein by FTIR technique.

Theoretical calculations and the analysis of the experimental probes performed on the N-methylacetamide molecule (which is the simplest molecule containing a trans peptide group analogous to that in a polypeptide chain) have allowed to identify the characteristic bands of the CONH group, present in every protein backbone **[Miyazawa 1960]**. These bands, the Amides, are IR and Raman-active. In table 2.1 fundamental vibrational modes of the Amides for the molecule N-methylacetamide are listed with the theoretical and experimental frequency position. Obviously, in a protein these values are not much different. Moreover, the spectral positions of the Amides of a protein can undergo changes as a function of solvent; in particular, when the protein is dissolved in D_2O instead of H_2O, the hydrogen atoms of the protein make the exchange with deuterium's atoms of the solvent, inducing the displacement of the bands frequency associated to the modes involving these atoms. Shifted bands are termed Amide I', Amide II', etc. In figure 2.4 a spectrum of a protein dissolved in D_2O is shown. In this thesis we have mainly used FTIR spectroscopy to study Amide I' and II' in order to get insight on the structural changes of the investigated proteins. A short description of these two bands and of the main changes associated with aggregation processes follows in the text.

Vibrational mode	ν_{exp}(cm^{-1})	ν_{th}(cm^{-1})	Main contributions
Amide A	3236	3254	NH-s(100%)
Amide I	1653	1646	CO-s(83%), CN-s(15%), CCN-d(11%)
Amide II	1567	1515	NH-ib(49%), CN-s(33%), CO-ib(12%), CC-s-ib(10%), NC-s(9%)
Amide III	1299	1269	NH-ib(52%), CC-s(18%), CN-s(14%), CO-ib(11%)
NC stretch	1096	1070	NC-s(77%), CC-s(17%)
NC stretch CC stretch	881	908	NC-s(31%), CC-s(17%), CO-s(16%), CNC-d(14%), CCN-d(10%)
Amide V	725	721	CN-t(75%), NH-ob(38%)
Amide IV	627	637	CO-ib(44%), CC-s(34%), CNC-d(11%)
Amide VI	600	655	CO-ob(85%), CN-t(13%)
CNC-def	289	274	CNC-d(71%), CO-ib(19%), CCN-d(13%)
Amide VII	206	226	NH-ob(64%), CN-t(15%), CO-0b(12%)

Table 2.1: N.methylacetamide vibrational modes. Comparison from theoretical and experimental data. In the table only modes contributing for more 5% are included.
S: stretch; d: deformation; t: torsion; ib: in-plane bend; ob: out-of-plane bend **[Miyazawa 1960]**.

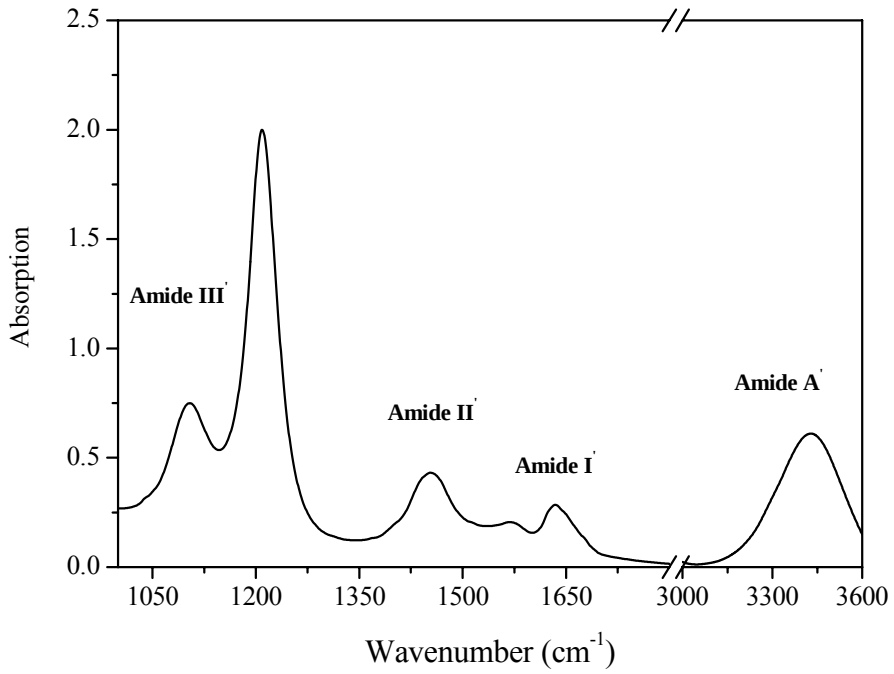

Figure 2.4: Fundamental bands of an IR spectrum (with D_2O as co-solvent) associated to a protein are termed *Amides*.

Amide II. The amide II vibration is an out-of phase combination of largely NH in-plane bending (ib) and CN stretching (s) with small contributions COib, CCs and CNs. Because of the large NHib contribution, N-deuteration has a great effect on the vibration modes, shifting the fundamental at about 1450cm^{-1} **[Grdadolnik et al., 2001]**. Because of deuteration deep effect on the Amide II mode, this can be used to monitor hydrogen exchange rates in proteins [**Militello et al., 2004**], characterizing the partial unfolding of the protein which can cause the proteins aggregation.

Amide I. The amide I vibration is an out-of phase combination of COs and CNs, with significant contributions from the C_αCN deformation (d) and less important contribution from C_αCs, CNC_αd and NHib. The position of this band is at about 1650 cm^{-1} in H_2O. The HOH bending of the water molecule is in the same spectral position of Amide I. In order to isolate these contributions, the observation of Amide I is performed in D_2O instead of H_2O.

The Amide I vibration, such as the Amide II one, is localized in the amidic group; in particular, both vibrations involve the CONH group only (i.e. Cα is not involved) and for this reason they are defined as localized vibrations. The vibration of a peptidic group interacts only with the same vibration of an adjacent group, introducing first order corrections in the frequencies values. The interactions between vibrational modes of different frequencies localized in adjacent groups lead to second order corrections in the frequencies values. Finally, not adjacent groups can interact through hydrogen-bonds, leading to first order correction too. The effects due to the coupling occur only if the transition momenta are almost parallel, like in the case of highly oriented peptides. The treatment of these effects can be developed using the perturbation theory, with the hypothesis that the frequency of the OCNH group can be considered as the not modified one added to a contribution due to the vibrational coupling **[Miyazawa 1960]**. Thus, the Amide I vibration is very sensitive to both H-bonding and dipole coupling. Since the amount of dipole coupling and H-bonding is determined by the secondary structures of the proteins, *shape, position and bandwidth of the Amides depend on the protein conformation.* The

Amide I position has been used to distinguish between β-sheet, α-helical and random coil structures **[Cai et al., 1999, Pelton et al., 2000]** and in order to study the conformational changes induced on the secondary structure of the protein by a particular experimental condition **[Fang et al., 1997 and 1998, Sun et al., 1997, Dong et al., 1998, Dufour et al., 1998, Taneva et al., 1999, Lefevré et al., 2003]**. In deed, as it is evident in figure 2.5, the Amide I of a all-α protein, such as BSA, and of a mainly-β one, such as BLG have very different conformations.

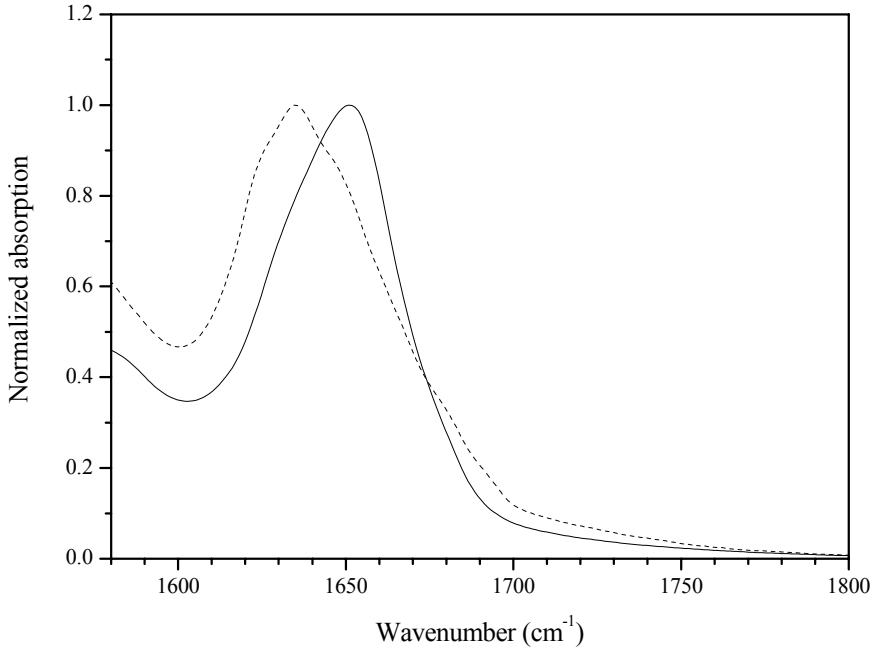

Figure 2.5: FTIR spectra of Bovine Serum Albumin (continuous line) and β-Lactoglobulin (dashed line).

Usually, Amide I band is the result of the overlap of several contributions deriving from the presence of different kinds of secondary structures, which can be isolated through a proper deconvolution of the band itself **[Cai et al., 1999, Pelton et al., 2000]**. The scientific literature is rich of studies devoted to the assignment of the different components to the different secondary structures **[Byler et al., 1986, Dong et al., 1990, Cai et al., 1999, Pelton et al., 2000]**. A scheme of these assignments is reported in table 2.2.

Secondary structure	Amide I position (cm^{-1})	Amide I′ position (cm^{-1})
β-sheet	1624-1643	1625-1640 1670-1680
α-helix	1650-1658	1651-1657
β-aggregates	1610-1620 1690-1698	1610-1623 1675-1695
β-turn	1665-1689	1670-1690
Random-coil	***1649-1652***	***1640-1650***

Table 2.2: IR bands assignment to the correspondent secondary structures **[Byler et al., 1986, Dong et al., 1990 and 1998, Fang et al., 1997, Subirade et al., 1998].**

Amide I′ and Amide II′ bands have been widely studied in order to monitor aggregation processes **[Fang et al., 1997, Qi et al., 1997, Subirade et al., 1998, Lefevre et al., 1999, Panick et al., 1999, Renard et al., 1999, Militello et al., 2004]**. Indeed, as it has been said, proteins aggregation process usually occurs after a partial opening of the protein, and simultaneously with conformational changes of the secondary structure. The partial unfolding of the protein induces the exchange between hydrogen atoms of the protein and deuterium atoms of the solvent, which can be monitored by the increase of Amide II′ and the decrease of Amide II in the infrared spectrum **[Kavanagh et al., 2000, Militello et al., 2004]**. In most cases, conformational changes associated to aggregation processes lead to the formation of aggregates with β-richer structures. Indeed, it has been observed that the aggregation induces an increase in the amount of secondary structure with IR components in the 1623-1637 cm^{-1}. This is the spectral region characterized by the vibrational activity of native β-sheet structures in the protein and of β-aggregated structures deriving by the instauration of intermolecular bonds between different protein units **[Fink 1998, Qi et al., 1997, Fang et al., 1997, Lefevrè et al., 1999, Allain et al., 1999, Militello et al., 2003 and 2004, Remondetto et al., 2003]**. Indeed, the aggregation of proteins housing α-helical structures usually occurs via conformational changes consisting in the conversion of these structures in β-type structures that subsequently form intermolecular bonds with the creation of β-aggregated structures. Thus, the changes in the Amide I′ bands can be considered a marker of the aggregation

processes, and for this reason, this band has been extensively studied in different experimental conditions causing the proteins aggregation **[Qi et al., 1997, Subirade et al., 1998, Lefevrè et al., 1999, Panick et al., 1999, Renard et al., 1999]**. Finally, the Amide I' study allows to reveal also the formation of a gel through the shift toward lower wavenumbers of the bands assigned to β-sheets and β-aggregated structures, indicating the instauration of stronger H-bonds due to the origination of an ordered network entrapping water **[Allain et al., 1999, Renard et al., 1999, Lefevrè et al., 2000, Remondetto et al., 2003]**.

b) Experimental setting

IR spectra were measured using Bruker Vertex 70 Fourier transform spectrophotometer, equipped with a MIR light globar source (i.e. an U shaped silicon carbide piece), with spectral resolution of 2 cm^{-1}. Each spectrum was averaged over 100 scans. All samples were placed between two CaF_2 windows, with a 0.05 mm Teflon spacer.

Spectra as obtained by the instrumental acquisition are affected by the strong absorption of the water vapour present into the sample camera. Even if the acquisition is realized under a constant flow of nitrogen, this contribution is not eliminated at all. Thus, the IR vapour spectrum must be subtracted to the absorption spectrum of the sample. The vapour absorption spectrum has been determined from the absorption spectrum of empty beam line.

In order to study the spectral region of Amide I' and Amide II and II', when necessary, a normalization procedure was done. This consisted in putting to zero the minimum value at about 1900 cm^{-1} and in making coincident the maximum value of the band assigned to DOD bending of D_2O (~1200 cm^{-1}), in order to eliminate probable differences in the absorption values due to a different amounts of sample used for the acquisition.

To obtain information on conformational changes of the secondary structures induced during the aggregation process driven by the temperature

increase, it is necessary to extrapolate the variations undergone by each of components the Amide I′ band isolating every single contribution. In order to identify the time variations of each overlapping component under the broad amides, differential spectra were obtained by subtracting to the spectrum at a generic time t, the spectrum at t_0 (where t_0 was 7 minutes, to reach thermal equilibrium):

$$\Delta Abs(t,\upsilon) = Abs(t,\upsilon) - Abs(t_0,\upsilon).$$

In figure 2.6 an absorption spectrum and a differential spectrum of BLG are shown, in order to make it evident that the differential spectra allow to distinguish the single contributions resulting overlapped in the absorption spectrum.

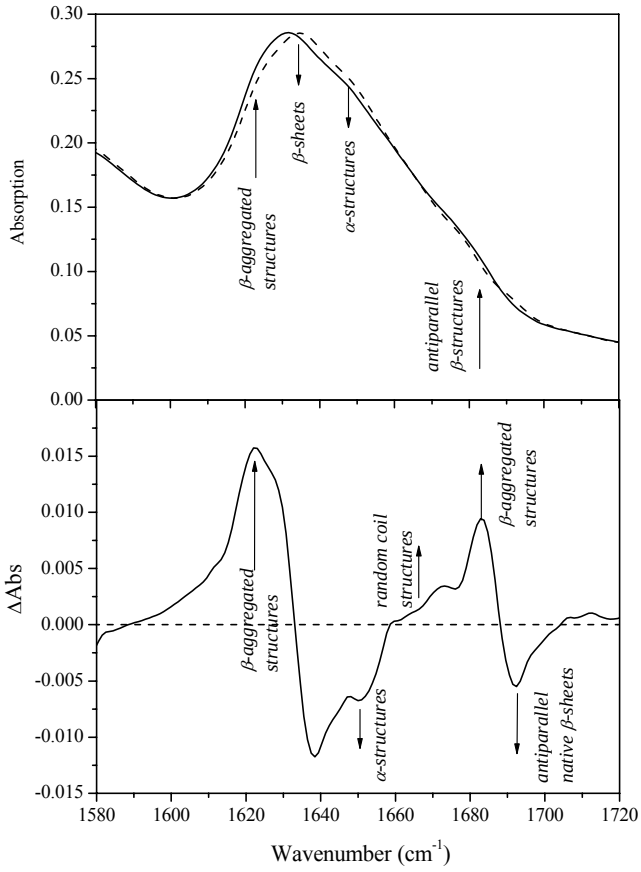

Figure 2.6: Position of the single contributions to the Amide I′ band evidenced in Absorption spectra (upper) and differential spectra (bottom) of β-Lactoglobulin realized at the start (dashed line) and at the end (continuous line) of thermal aggregation. Arrows indicate the expected variation of the contributions during the kinetic.

2.2.3 Rheology:

a) Theoretical background

Rheology is defined as the *science studying the deformation and flow of matter* **[Barnes et al., 2001]**; this science allows to investigate the viscoelastic properties of materials. Every material is influenced by external forces. Rheology deals with the relationship between force, deformation and time.

An ideal solid is elastic and its reaction (*shear strain*) to a *shear stress* is well described by Hooke's law. Indicating with G_0 the *rigidity modulus*, with τ the *shear stress*, with γ the *shear strain*, the relation $G_0 = \tau / \gamma$ is valid. For an ideal fluid (*Newtonian fluid),* τ is proportional to the rate of deformation (*shear rate*) $\dot{\gamma}$, and their proportionality coefficient is the viscosity η_0: $\tau = \eta_0 \cdot \dot{\gamma}$.

Actually, ideal solids or liquids are not encountered. All materials show mixed properties: they behave as solids or liquids depending on stress intensity and duration of stress applied **[Kavanagh et al. 1998]**. For example, for viscoelastic fluids, it is possible to perform an experimental test, known as "creep experiment". It is realized in regime of small deformations and it allows to apply a constant low stress and to determine a zero-shear viscosity from the linear strain-time region by plotting γ against time. The zero shear viscosity is influenced by the molecular structure of the investigated material. On the other hand, test in regime of large deformation concerns the study of a gel sample undergoing tension/compression or shear force, carried out up to yield point **[Kavanagh et al. 1998]**. These results provide equal or greater values than that obtained by small deformation measurements. The knowledge of the gels behaviour undergoing the latter test kind is important, since gel samples are often subjected in applications to stresses and strains well outside the linear viscoelastic region. However, the results shown in this thesis work have been obtained in linear viscoelastic region under the induction of small deformation.

The most unsophisticated models are based on the linearity hypothesis in order to describe the viscoelastic properties of the materials. The Maxwell model sums linearly the totally elastic deformations and completely viscous deformations.

The Voigt-Kelvin model sums linearly the elastic and viscous strains. The linearity hypothesis is based on a "superposition principle". This implies that the response (strain) at any time is directly proportional to the value of the initiating signal (stress) **[Barnes et al., 2001]**. In the linear theory of viscoelasticity, the differential equations are linear and the coefficients of the time differentials are constant even if strictly related to the material. Under these hypotheses, the linear theory is applicable only to small changes in the variables, and a general differential equation for linear viscoelasticity can be written as follows:

$$\left(1+\alpha_1\frac{\partial}{\partial t}+\alpha_2\frac{\partial}{\partial t^2}+\ldots+\alpha_n\frac{\partial}{\partial t^n}\right)\tau=\left(1+\beta_1\frac{\partial}{\partial t}+\beta_2\frac{\partial}{\partial t^2}+\ldots+\beta_m\frac{\partial}{\partial t^m}\right)\gamma\,, \qquad (2.24)$$

where $n=m$ or $n=m-1$ **[Barnes et al., 2001]**. Then, the solid linear behaviour (Hooke's law) is obtained if β_0 is the only non-zero parameter. If only α_1 (=τ_M) and β_1 (=η_0) are both non-zero parameters, the relation

$$\tau+\tau_M\dot{\tau}=\eta_0\dot{\gamma} \qquad (2.25)$$

can be written and after a rearrangement can assume the form

$$\dot{\gamma}=\frac{\dot{\tau}}{G_0}+\frac{\tau}{\eta_0}. \qquad (2.26)$$

τ_M is the called the "relaxation time" and $\eta_0=\lim_{\omega\to 0}\frac{G''}{\omega}$ is, as already said, the bulk viscosity. Rewriting this relation in frequencies domain, shear modulus is obtained:

$$G(\omega)=\frac{\tau(\omega)}{\gamma(\omega)}=\left(\frac{1}{G_0}-\frac{i}{\eta_0\omega}\right)^{-1}, \qquad (2.27)$$

where ω is a angular frequency of oscillation. This relation can conveniently be written in the form:

$$G=G'+iG''=\frac{\alpha^2\omega^2}{1+\alpha^2\omega^2}G_0+i\frac{\alpha\omega}{1+\alpha^2\omega^2}G_0=|G|\cdot e^{i\theta} \qquad (2.28)$$

with $$|G|=G_0\frac{(\omega\tau)}{\sqrt{1+(\omega\tau)^2}}, \quad \theta=arctg\frac{G''}{G'} \qquad (2.29)$$

where G' is the real part, representing a measure of the energy stored per cycle of deformation and its value reflects the solid-like or elastic behaviour of the tested material, G'' is the imaginary part, referring to the energy dissipated by the sample and it is associated with the fluid-like or viscous characteristic of the material **[Bell 1989, Tadros 1996, Leung Sok Line et al., 2005]**. Finally, θ is the phase angle corresponding to the response delay of the strain to the applied stress and it indicates the relative importance of viscous and elastic elements in the emulsion gels **[Leung Sok Line et al., 2005]**. For example, θ values of 0 and 90° are typical for perfect elastic solids and viscous liquids, respectively. When the value of G' is greater than the value of G'', θ is very small and the material is said to be predominantly elastic **[Chen et al., 1999]**.

The storage modulus (G'), the loss modulus (G'') and the phase angle (θ) have been widely studied in order to characterize the small deformation rheological properties of emulsion gels **[Gosal et al., 2000 and 2004, Leung Sok Line et al., 2005, Renard et al., 1999, Remondetto et al., 2003, Donato et al., 2005, and 2007, Marangoni et al., 2000, Sittikijyothin et al., 2007, Veerman et al., 2003a]**. The changes of these parameters as a function of temperature, frequency and time can be studied, allowing the comprehension of several aspects characterizing a gel.

One of the most powerful rheological methods to investigate the mechanical properties of materials is the frequency oscillatory test (mechanical spectra) in which both stress and strain vary sinusoidally with time. In these measurements, the strain is small enough and falls within the linear viscoelastic region, which is the region in which the measured rheological parameters are linearly dependent on the perturbation. Further, the time evolution of the mechanical spectra reflects the changes of the molecular structure of the system. The figure 2.7 shows the behaviour of G′ and G′′ as function of frequency for a gelling system. At the lowest frequencies the system is liquid; G′ and G′′ (with G′′>G′) growth with a slope of 2 and 1, respectively (continuous lines). When the sample molecular weight becomes

larger due to gelation (dotted lines), the relaxation domain shifts towards lowest frequencies and the plateau value becomes larger.

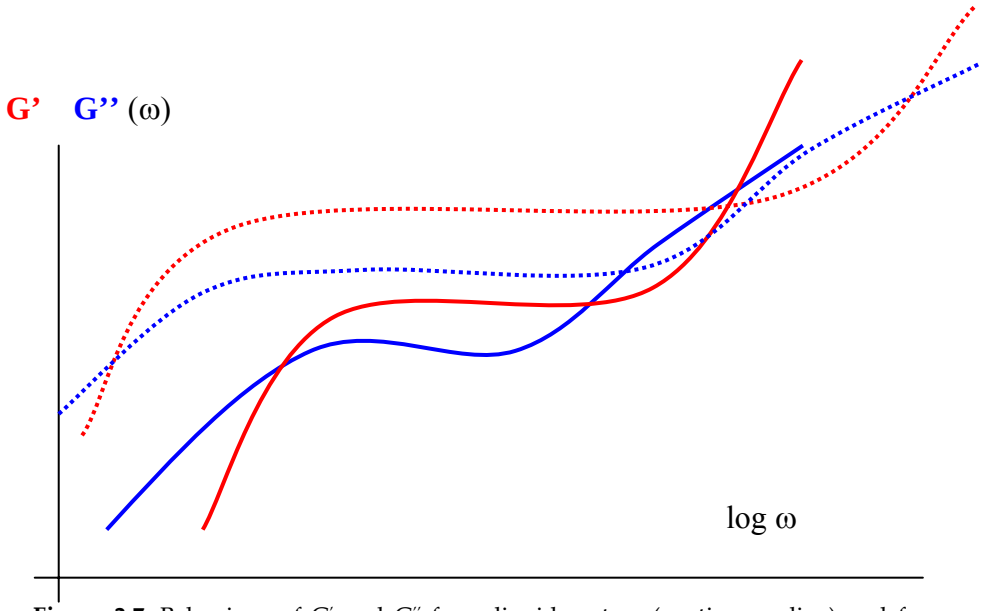

Figure 2.7: Behaviour of G′ and G″ for a liquid system (continuous line) and for a system which is forming a gel (dotted lines).

The behaviour of G', G'' and θ as a function of time permits to determine the gelation time, defined simply as the time when G' shows its initial fast increase **[Gosal et al., 2000]**. It has been recently recognised that the analysis of the frequency dependence of the mechanical spectrum of a gelling system (the trace of G′ and G″ vs. logω) can, in principle, lead to a phenomenological precise description of the gel point **[Panick et al., 1999]**.

b) Experimental setting

Rheological measurements were performed on a stress controlled AR 1000 rheometer (TA Instruments, USA) using a titanium-cone/plate geometry (angle 0.0174 rad, radius 20 mm, gap 26 μm).

Cycles of viscoelastic spectra, with a pause of 1 hour, were performed in the 0.1–200 rad/sec frequency range, at a strain of 1×10^{-3}, well within the linear viscoelastic region. The protein suspension with the added salt was gently stirred and placed on the rheometer plate, set at a temperature of 20°C. The thin sample air-

interface was coated with silicone oil to avoid water evaporation. The time evolution of the shear storage modulus (G′) and shear loss modulus (G′′) can be derived by the cycles of viscoelastic spectra selecting a specific frequency.

Chapter 3

Experimental results: Thermal aggregation of β-Lactoglobulin

3.1 β-Lactoglobulin samples at neutral pH

β-Lactoglobulin (BLG) is a protein characterized by different native conformations as a function of pH value. At neutral pH (pH = 7) the monomer/dimer equilibrium is shifted towards dimeric conformation. It is well known that, when subjected to heat-treatments, the protein undergoes changes of the secondary, tertiary and quaternary structures **[Wong et al., 1996; Hambling et al., 1992, Iametti et al., 1996, Fang et al., 1997, Qi et al., 1997, Subirade et al., 1998, Panick et al., 1999, Carrotta et al., 2001, Vetri et al.,2005]**. In order to investigate the metal ions effects on the heat-induced aggregation process, the first necessary step has consisted in the determination of the more appropriate experimental conditions for the study. Hence, in order to identify the more suitable temperature value, the changes of the scattered light by BLG solution in absence and in presence of metal ions in solution have been investigated as a function of temperature in the range 20 - 60 °C. In the following, we will indicate as BLG the solution of 3.3 mM BLG prepared in absence of metal ions; as Cu-BLG the solution of 3.3 mM BLG prepared in presence of 1 mM copper ions and, finally, as Zn-BLG the solution of 3.3 mM BLG prepared in presence of 1 mM zinc ions.

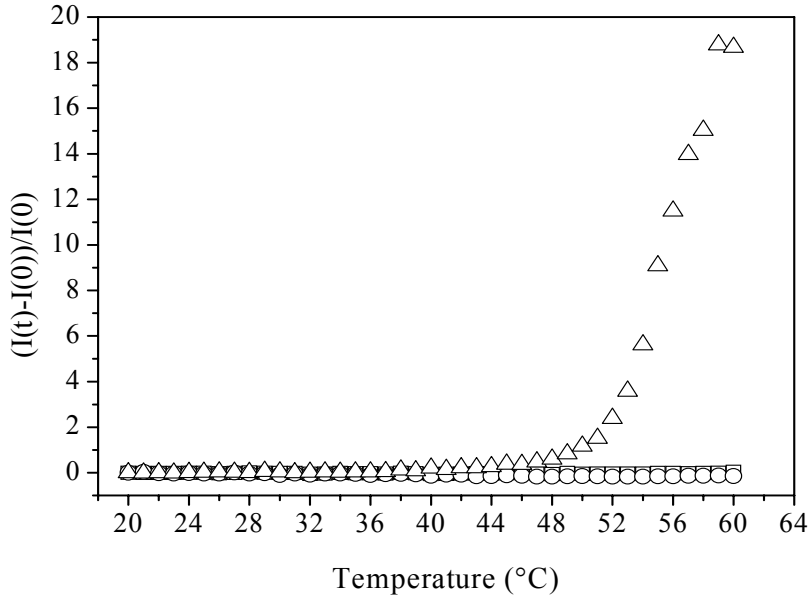

Figure 3.1: Normalized scattered intensity as a function of temperature at pH = 7 for (□) BLG, (○) Cu-BLG and (Δ) Zn-BLG. The experimental error is smaller than symbol dimension.

Temperature scans are shown in figure 1. As it can be seen, in the Zn-BLG sample, a rapid increase of intensity is evident, indicating an aggregation process starting at about 48 °C. For the other two samples, BLG and Cu-BLG, nothing occurs up to 60 °C. The fact that two ions, Zn^{2+} and Cu^{2+}, do not induce similar effects on the heat aggregation process excludes that the observed changes in Zn-BLG sample can be due to a pure electrostatic interaction between the positive charge of divalent metal ions and the partial negative charge of the protein (pH > pI = 5.1). Indeed, both metal ions have the same divalent nature and, at the same concentration, they cause an equal alteration of the ionic force[2] of the protein solution.

[2] Ionic force is defined according to the following equation:

$$\mu = \frac{1}{2}\sum_{i=1}^{n} C_i \times Z_i^2 \ ,$$

where C_i is active ionic concentration and Z_i is ionic charge **[Remondetto et al., 2003]**.

Since for Zn-BLG the aggregation kinetic induced at a temperature higher than 60 °C should be too fast, this temperature value has been selected to analyse the aggregation kinetics of all samples. In the following, we report induced changes of the secondary and tertiary structures and of the growth evolution of aggregates dimension of BLG at T = 60 °C and pH = 7. This is a required characterization before studying the influence of metal ions on the aggregation processes in the same experimental conditions.

3.1.1 Thermal aggregation

In figure 3.2 the time evolution of the normalized scattered intensity (fig. 3.2a) and of the average diameter of BLG (fig. 3.2b) are shown. As it can be seen, the number and the dimension of the aggregates in solution increase as a function of time. In particular, when the protein is subjected to an increasing temperature, an increase of the light scattering intensity (figure 3.2a) is observed since the first ten minutes of the kinetic. No lag time is present, in agreement with the results obtained by Bauer et al., 2000, in similar experimental conditions. The light scattering intensity and Z-average diameter as a function of time are characterized by two different phases. During the first three hours, they increase with a linear profile; in the remaining time, the diameter evolution follows a different behaviour. According to **Bauer et al., 2000**, the first phase is characterized by the formation of metastable intermediates, named oligomers, via linear association of reactive monomers induced by intermolecular S-S bonds and it can be well described by the model of Roefs and de Kruif (1994), (see paragraph 1.4.1). These oligomers have the typical features of molten globule states: secondary structure content similar to the native structure but less tight packing of the side chain **[Carrotta et al.,2001]**. A linear fit, made on the light scattered intensity during the first 180 minutes of the BLG kinetic (red line in figure 3.2a), confirms the linear increase of the intensity and, as a consequence, of the average mass of the particles in solution, thus suggesting a linear association of the proteins units during this first phase of the kinetic.

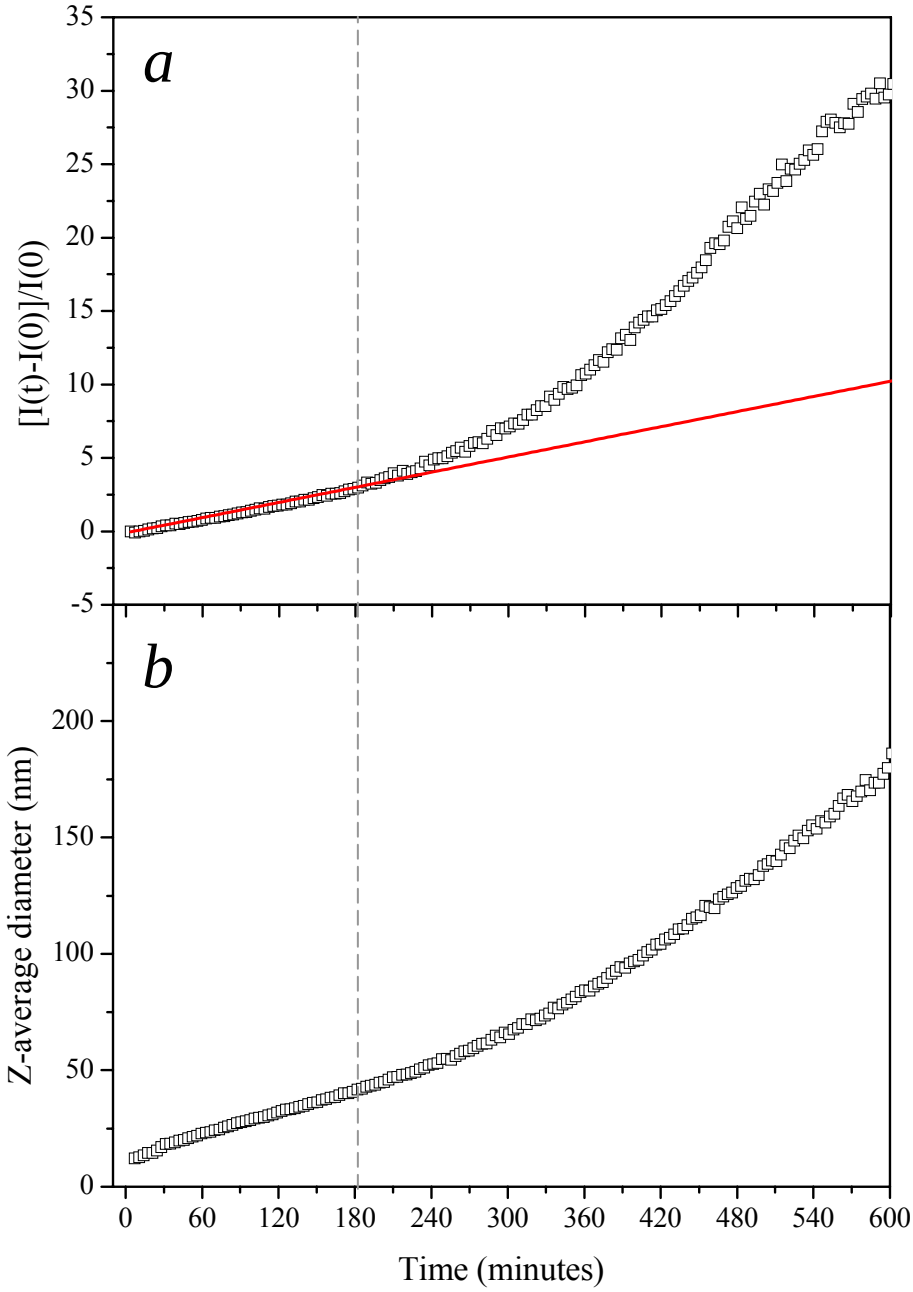

Figure 3.2: (a) Time evolution of the normalized scattered intensity and (b) of the Z-average diameter of BLG solution in MES 20 mM at pH = 7 heated at 60 °C. The experimental error is smaller than symbol dimension.Red line in (*a*) indicates the fit linear obtained for the BLG scattering intensity during the first 180 minutes.

The second phase is characterized by the formation of aggregates built from the association of metastable oligomers with different dimensions **[Bauer et al., 1998 and 2000, Carrotta et al., 2001 and 2003]**. The formation of the aggregates does not occur via intermolecular S-S bonds, but mainly via hydrophobic interactions; the assembly is nucleated with at least four oligomers in the nucleus **[Hoffmann et al., 1999, Bauer et al., 2000]**. This deviates from the model proposed by **Roefs and de Kruif (1994)**, in which aggregates grow by addition of monomers through intermolecular disulfide bonds. Indeed, the existence of the intermediates in the formation of BLG aggregates is sure **[Bauer et al., 1998 and 2000, Schokker et al., 1999 Carrotta et al., 2001 and 2003, D'Alfonso et al., 2002, Baussay et al., 2004]** and, moreover, the key role of these intermediates in the formation of the aggregates has been verified by the observation of aggregates building in absence of monomeric species in solution **[Bauer et al., 2000]**. However, aggregation is not limited to the formation of linear aggregates, but also branched aggregates can be formed, similarly to rod-like aggregates, whose presence has been revealed by other studies **[Griffin et al., 1993, Gimel et al., 1994, Aymard et al., 1996 and 1997]**.

The concept of fractals has been used to characterize the structure of the grown aggregates. The determination of the topological structure of a fractal object occurs according to the relation:

$$M(t) = aR_H^{df}(t) \qquad (3.1)$$

where the prefactor a depends on the local structure of the aggregates and their size distribution, M is the molecular mass of the aggregates, R_H is the hydrodynamic radius and df is the fractal dimension of the object **[Nicolai et al., 1993, Baussay et al., 2004]**. For example, when df is 1, the morphology of the studied object is *linear*, when df is equal to 3 the object morphology approaches to a *spherical* one. A scheme illustrating these morphologies kinds is reported in figure 3.3.

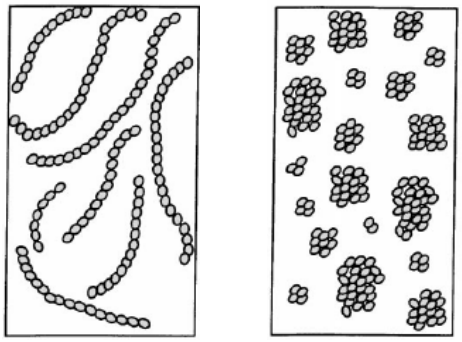

Figure 3.3: Morphologies of linear (on the left) and spherical aggregates (on the right) in solution.

The scattering measurements allow to have information about the structure of the aggregates of 60mg/ml BLG in MES 20 mM at pH = 7. Indeed, the "Mean count rate" of scattered photons is proportional to molecular mass of the aggregates. Thus, the plot of the mean count rate of scattered photons as a function of Z-average diameter in a logarithmic scale allows to determine the *df* as the slope of the straight line fitting the data, in analogy with the determination of the topological structure of a fractal object through its *fractal dimension.* In figure 3.4, the correlation between the mean count rate of scattered photons and z-average diameter is reported. The fit with a straight line has been made between about 25 and 180 nm of the z-average; at higher values, the scattered intensity profile approaches to a saturation value (see figure 3.2a). The extrapolation obtained for the slope of the straight line was 1.49 ± 0.01, a value consistent with the formation of a greater species via linear association of the native units, whose spatial conformation results by its folding. In terms of a nucleation and growth process, one can suppose that during the first three hours of protein incubation at 60°C when the scattered intensity depends linearly on the time, some long "fiberlike" aggregates only are observed, and after the reaching of a critical size, the growth process becomes relatively fast **[Aymard et al., 1999]**, leading to bigger aggregates around 200nm in size, in agreement with other authors **[Hoffmann et al., 1999, Le bon et al., 1999]**. This agreement is not invalidated if a different value of the incubation temperature is chosen, since it has been verified

that the temperature of the protein incubation affects the rate of aggregates formation but not their structure **[Baussay et al., 2004, Elofsson et al., 1996]**.

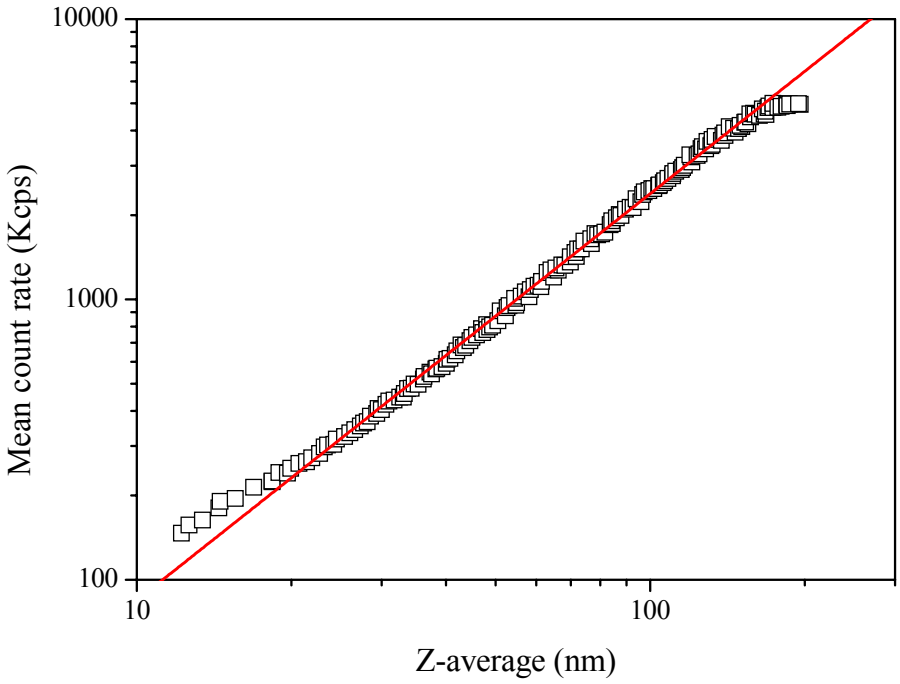

Figure 3.4: Scattering intensity as a function of Z-average diameter for BLG at pH = 7 and T = 60 °C. The experimental error is smaller than symbol dimension. The red line shows the fit linear Y=*a*+*b*x, where *b*=1.49±0.01.

Heat-induced changes of the secondary and tertiary structures have been monitored by FTIR measurements. In figure 3.5, FTIR absorption spectra of the protein are reported in the Amide II/Amide II' spectral region, at initial and final time of its incubation at 60 °C for about 5 hours. As indicated by the arrows in figure, Amide II decreases and Amide II' increases as a function of incubation time. This behavior is a marker of the partial opening of the protein and thus of the changes of the tertiary structure, during which the hydrogen atoms remained within the protein core undergo H-D exchange.

Contemporaneously, also changes of the secondary structure of the protein are induced by the temperature. These conformational changes were studied analyzing the time evolution of the Amide I' absorption band.

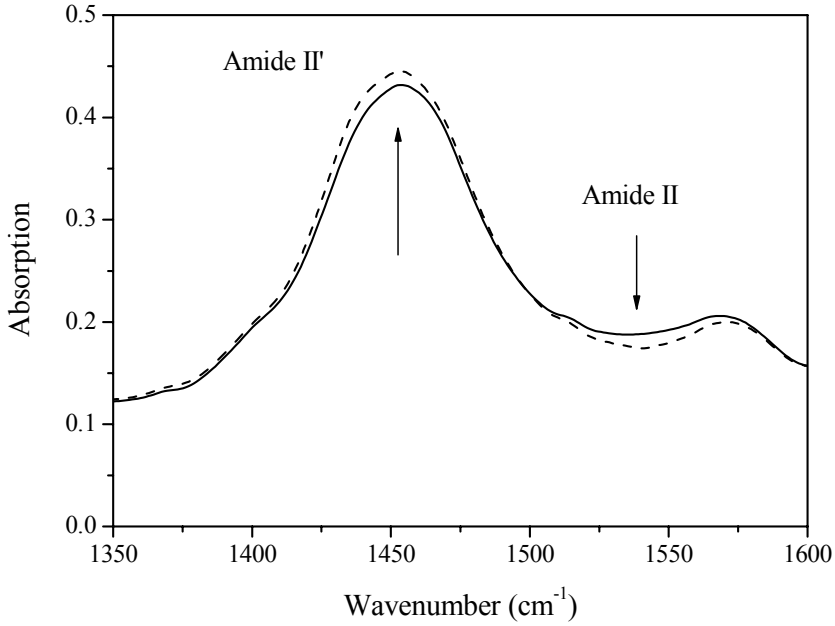

Figure 3.5: FTIR absorption spectra of BLG at pH = 7 at initial time (solid line) and after 5,5 hours (dashed line) of the incubation at T = 60 °C. The arrows indicate the Amide II and Amide II′ changes as a function of time.

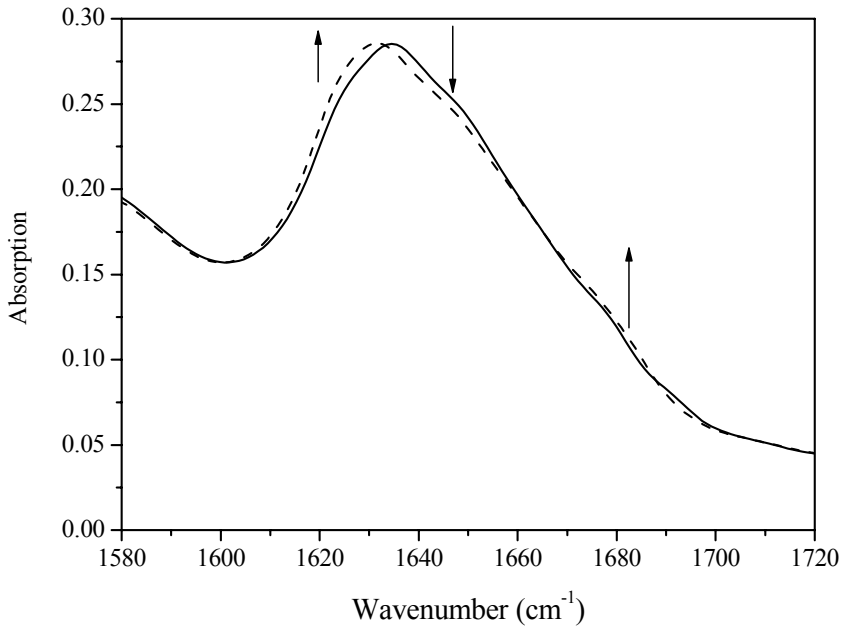

Figure 3.6: FTIR absorption spectra of BLG at pH = 7 at initial time (solid line) and after 5.5 hours (dashed line) of the incubation at T = 60 °C. The arrows indicate the Amide I′ changes as a function of time.

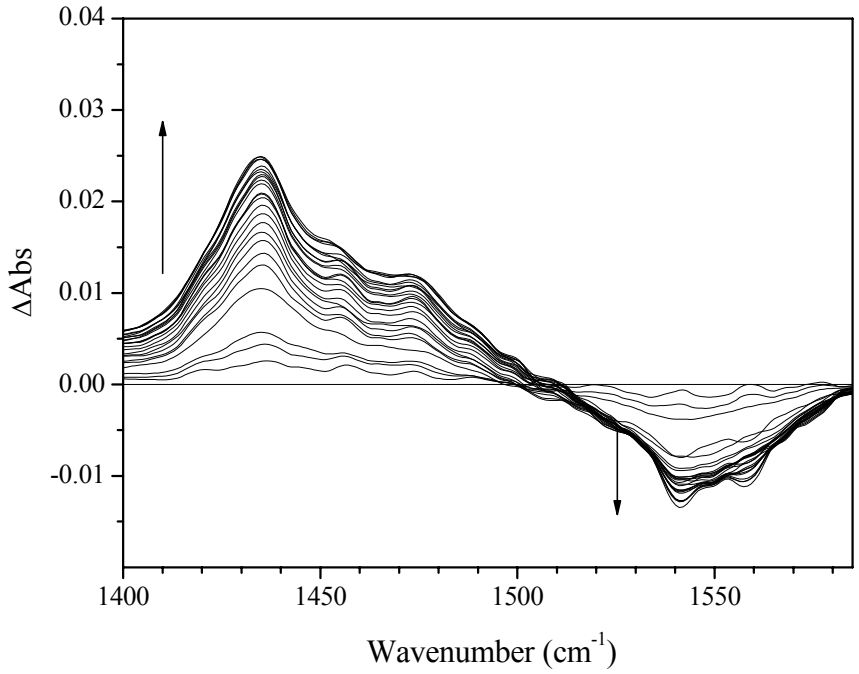

Figure 3.7: FTIR differential spectra of BLG at pH = 7 in the Amide II/Amide II′ during the incubation at T = 60 °C for 5 hours. The arrows indicate the Amide II and Amide II′ changes as a function of time.

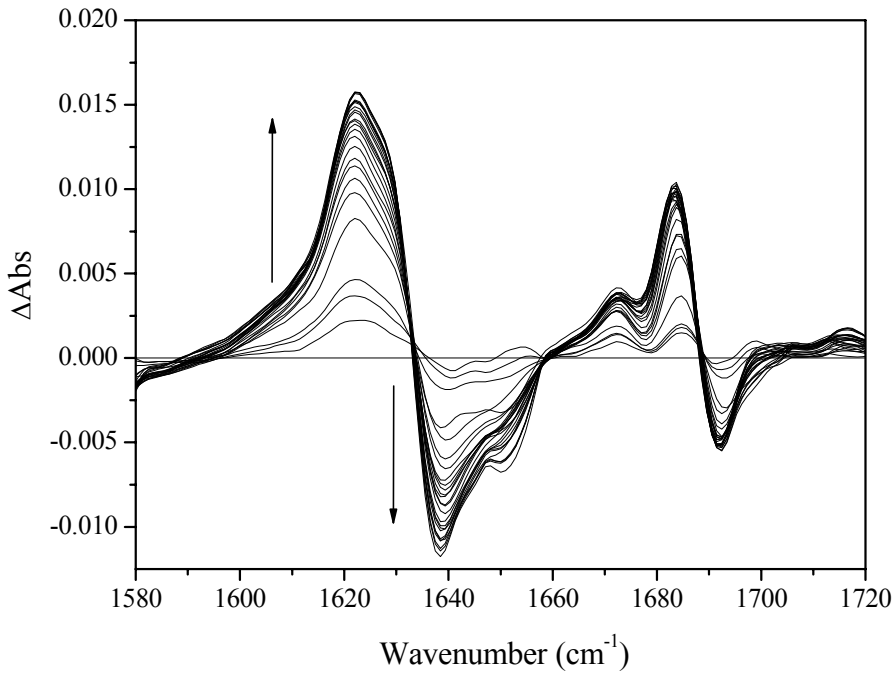

Figure 3.8: FTIR differential spectra of BLG at pH = 7 in the Amide I′ during the incubation at T = 60 °C for 5 hours. The arrows indicate the Amide I′ changes as a function of time.

As shown in figure 3.6, it is evident that the heat-treatment induces a conversion of the α-helix structures of the protein, (whose spectral contribution is at about 1650 cm^{-1}), in to β-sheets, (whose spectral contributions are in the region between 1620 - 1640 cm^{-1}); the increase of the components at about 1620 and 1680 cm^{-1} indicates the building of anti-parallel β-aggregated structures. To better highlight the changes of the main spectral components of the band, differential absorption spectra in the Amide II/Amide II' and Amide I' region are reported in figure 3.7 and 3.8 respectively. In figure 3.7, the H-D exchange results evident through the Amide II' and Amide II bands conversion related to a change of the molecular group performing vibration. In the spectral region between 1630 and 1660 cm^{-1}, shown in figure 3.8, the vibrational contributions of the α-helix, disordered random coil and intra-molecular native β-sheet structures fall and, as it is evident, the absorption intensity in this spectral region decreases as a function of time (as indicated by the arrow). Another negative contribution to the Amide I' band is present, at about 1690 cm^{-1} and assigned to native β-turn structures. The bands due to intermolecular aggregation are peaked at around 1623 and 1685 cm^{-1} and are assigned to vibrations of strongly bound intermolecular β-strands and of anti-parallel β-sheets, respectively. These bands increase as a function of time, giving evidence that aggregation occurs, as it can also be seen by light scattering measurements. The time evolution of the differential absorption intensity of Amide I' component, at 1623 cm^{-1}, and Amide II' component, at 1436 cm^{-1}, is shown in figure 3.9. It is evident that the partial opening process of BLG and the building of β-aggregates have similar kinetics. From the comparison of their time evolution appears that the process of the formation of β-aggregated structures slows down earlier than the protein opening one. However, both processes do not stop their evolution during the whole observed period.

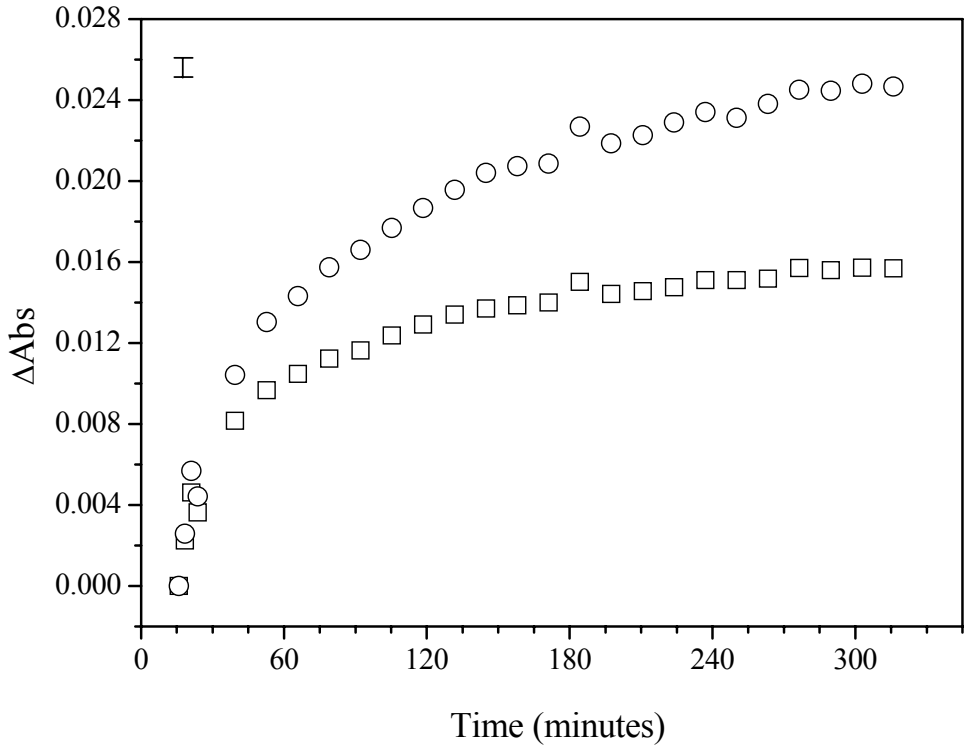

Figure 3.9: Time evolution of the FTIR differential absorption intensity of (□) Amide I′ components at 1623 cm^{-1} and (○) Amide II′ component at 1436 cm^{-1} of BLG at pH = 7 and T = 60 °C. Error bar at the top on the right is the experimental error estimated for differential absorption values.

3.1.2 Effects of the presence of copper or zinc

In this section the results relative to the effects induced by metal ions on the BLG thermal aggregation process above described are illustrated. We remind that we will indicate as BLG the solution of 3.3 mM BLG prepared without metal ions; while as Cu-BLG the solution of 3.3 mM BLG prepared with 1 mM copper ions; finally, we will call Zn-BLG the solution of 3.3 mM BLG prepared with 1 mM zinc ions.

In figure 3.10 the time evolution of the normalized scattered intensity and of the Z-average diameter is shown for BLG, Cu-BLG and Zn-BLG at pH = 7 and at T = 60 °C. In particular, figure 3.10a reports the time evolution of the total scattered intensity for the three samples, in the first 60 minutes. Again, a greater effect of zinc in comparison to copper has been revealed.

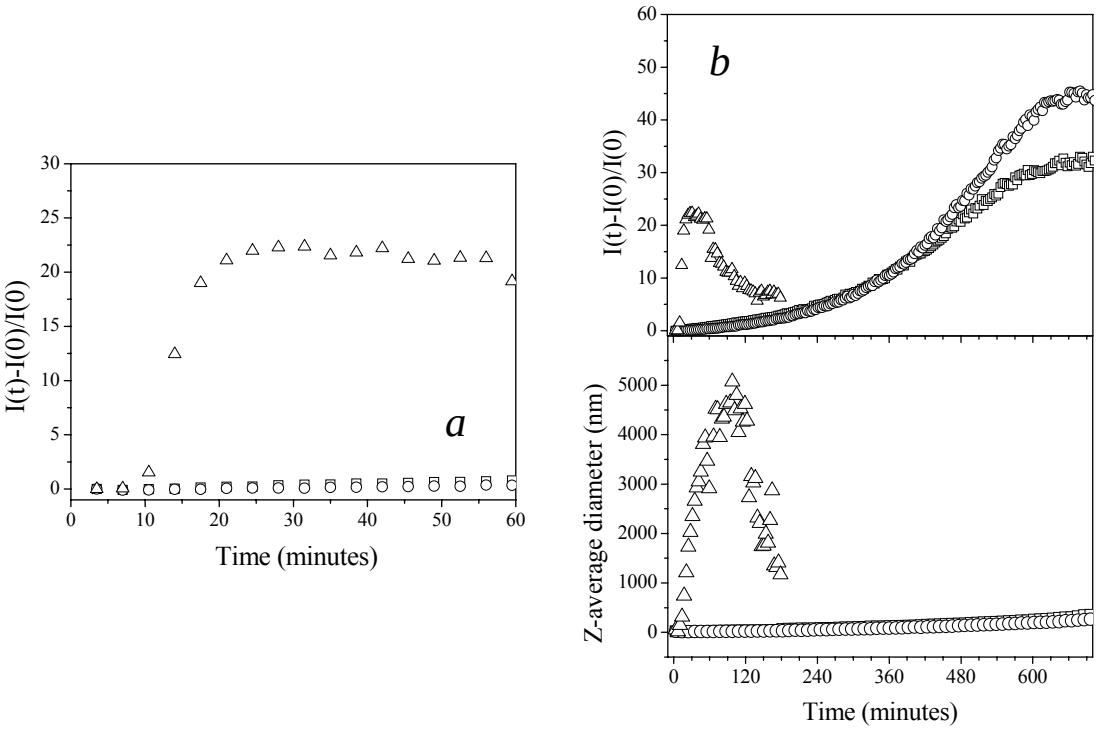

Figure 3.10: (a) Time evolution of the normalized scattered intensity during the first 60 minutes of the kinetic and (b) the whole observed time evolution of (up) the normalized scattered intensity and (bottom) the Z-average diameter of (□) BLG, (○) Cu BLG and (Δ) Zn-BLG at pH = 7 and T = 60°C. The experimental error is smaller than symbol dimension.

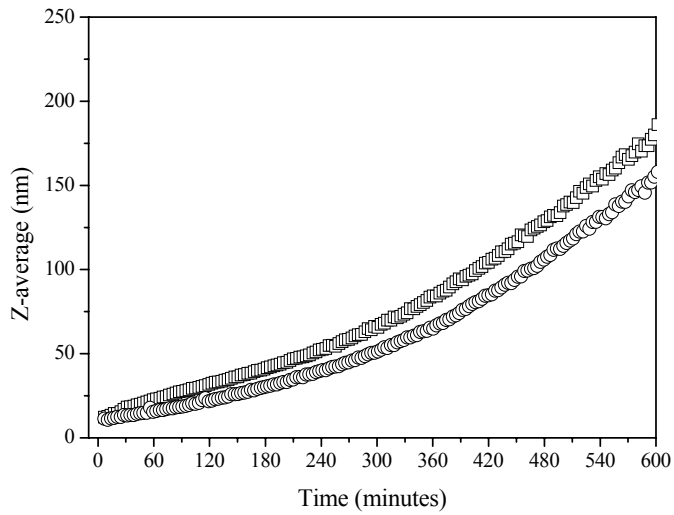

Figure 3.11: Time evolution of the Z-average diameter of (□) BLG and (○) Cu-BLG at pH = 7 and T = 60 °C with a more opportune scale. The experimental error is smaller than symbol dimension.

It is noteworthy that, when the aggregation of Zn-BLG has finished, in the other two samples it has not yet begun. In the Zn-BLG sample, after 10 minutes, the total scattered intensity quickly increases due to the aggregation and after 70 minutes much quickly decreases due to the precipitation. In figure 3.10b is reported the whole time evolution of the light scattered intensity and of the Z-average diameter. The total scattered intensities for BLG and Cu-BLG show behaviours very similar but with a greater increase of the scattered light intensity for Cu-BLG than for BLG, after 400 minutes. The trend of the scattered light intensity of Cu-BLG may be due to different conformational changes induced by the metal presence.

Evaluating the mean dimensions of the aggregates, whose behaviour for both BLG and Cu-BLG as a function of time is reported in figure 3.11 in a more opportune scale, it is evident how, in these experimental conditions, both samples follow a similar evolution of the heat-induced aggregation, producing species with a diameter of about 180 and 150 nm respectively. On the other hand, as it can be seen in figure 3.10, Zn-BLG rapidly produces aggregates with dimension greater than 3000 nm. It is noteworthy that the observed effects of the metals are not dependent on the negative ions composing the metal salt. The same results (data not shown) were obtained in presence of metal salt formed with SO_4.

In figure 3.12, the "mean count rate" of Cu-BLG against the respective z-average diameters is plotted in logarithmic scale. The line was obtained as an extrapolation of the plot relative to Cu-BLG sample. The fractal dimension, as defined at pag. 81, is in this case 1.52, value slightly greater than the BLG one extrapolated by plot reported in figure 3.4. This suggests a Cu-BLG aggregates formation which shape is slightly more open.

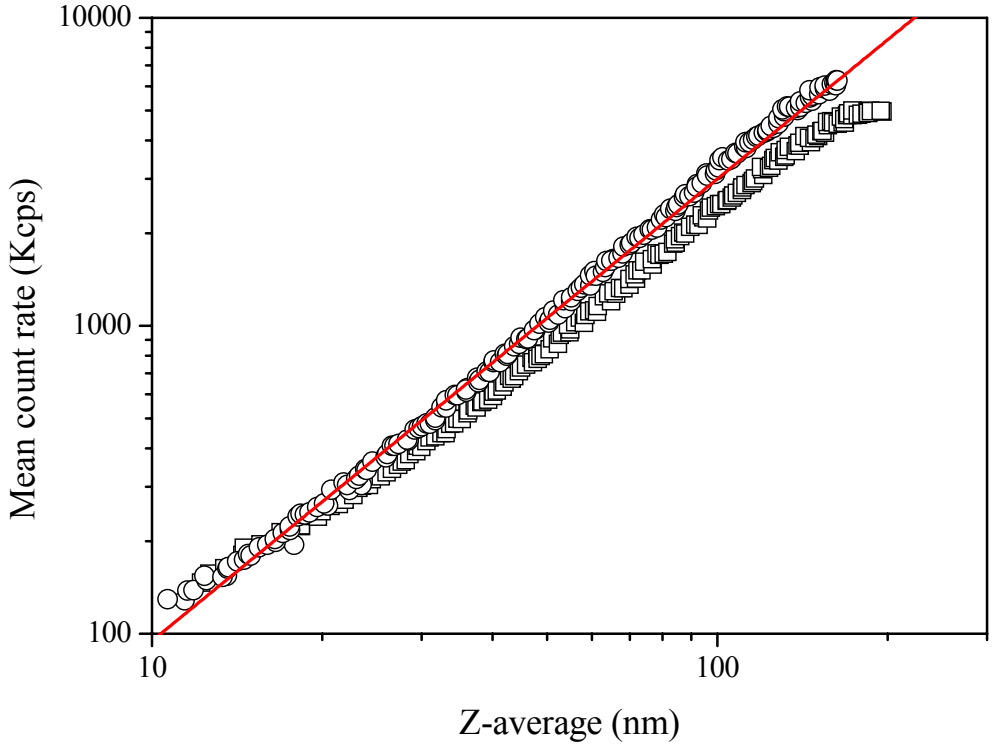

Figure 3.12: Scattering intensity as a function of Z-average diameter for (□) BLG and (o) Cu-BLG at pH = 7 and T = 60 °C. The experimental error is smaller than symbol dimension. The red line shows a linear fit of Cu-BLG plot, Y=*a*+*b*x, where *b*=1.52 ± 0.01.

The analysis of the scattering data, already discussed in paragraph 2.1, permits us to have the distribution of the diameters values in respect to scattered intensity and to particles number into solution at different times. In figure 3.13, the same initial times (continuous line) was chosen for all the samples, while the final times (dashed line), were different for each sample, being 10 hours for BLG and Cu-BLG (figs. 3.13a and 3.13b) and 50 minutes for Zn-BLG (fig. 3.13c). The results obtained for Cu-BLG and BLG are similar, i.e. both samples produce aggregates of the same value of size, which is slightly littler than 200 nm. On the contrary, Zn-BLG produces the biggest final size (over 3000 nm) and a large amount of the aggregates in a shortest time, coherently with the data shown in Fig. 3.10. Analogously, the distributions of the diameter values based on the intensity of the scattered light are shown in figure 3.14. Here, we report three times, those already shown in the previous figure and a time intermediate to the whole investigated time evolution for all samples. Once again the BLG and Cu-BLG are similar, while Zn-BLG has a very different aggregation kinetic. It is noteworthy that, in figure 3.14b, for Cu-BLG after 5.5 hours, the species present a large distribution, while for BLG there is only a narrow distribution around 180 nm. This could explain the increase of the scattered intensity shown by Cu-BLG in figure 3.10a as due to the presence of different species created by the presence of copper, as hypothesized before. We underline that for BLG, Cu-BLG and Zn-BLG, the data of the particles size in respect to the intensity of the light scattering relative to the initial phase of the kinetics (continuous line in figure 3.14) suggest the presence of a small distribution at larger size greater than 200 nm. This may be attributed to clusters of dense liquid, several hundred nanometers in size, which are metastable in respect to the protein solutions and whose formation takes place within a few seconds after the solution preparation **[Pan et al. 2007]**. The fraction of these particles was very small, but as bigger particles cause an increase of the scattered intensity, the presence of this species was revealed too.

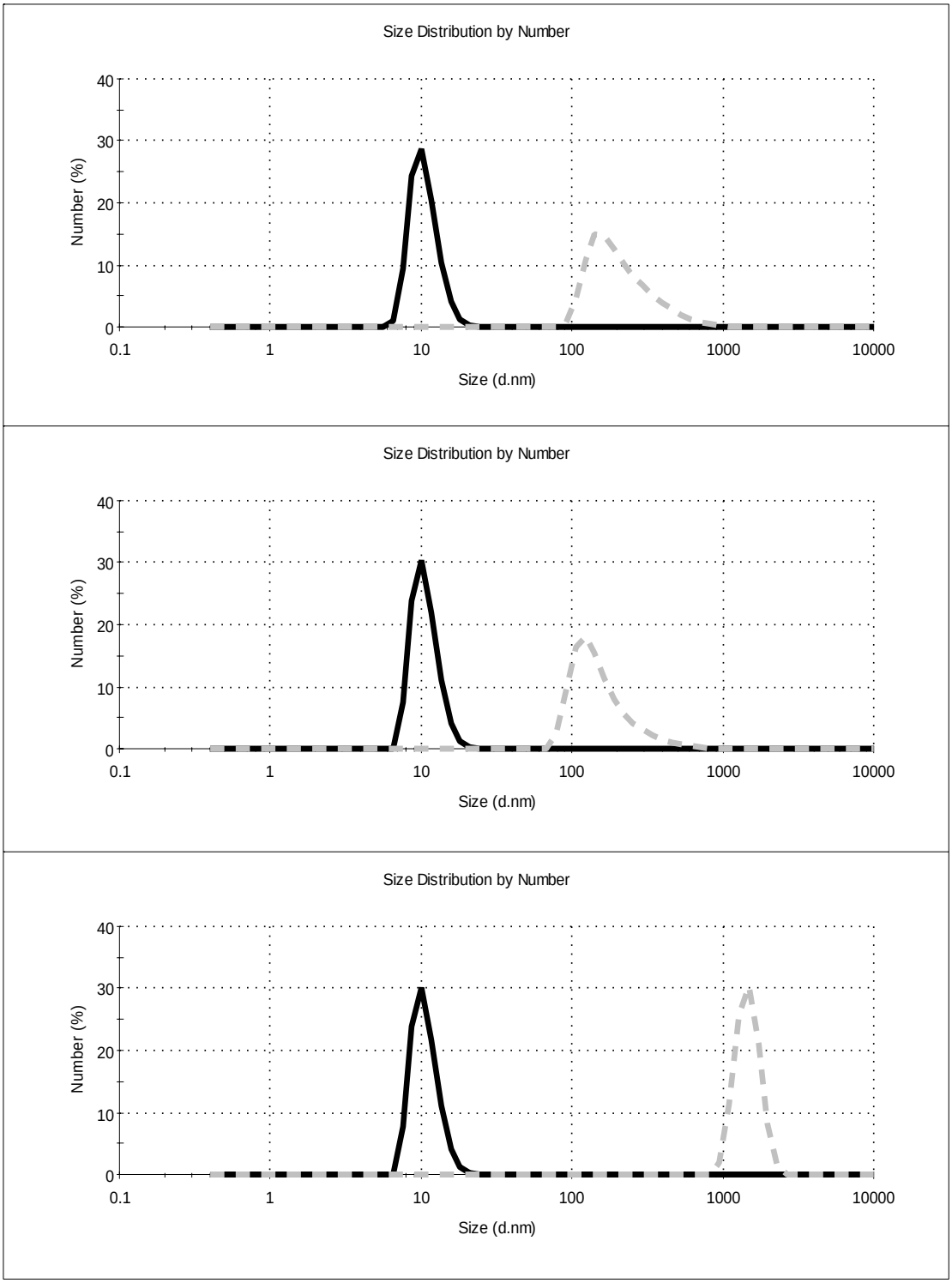

Figure 3.13: Size distribution of the aggregates dimension based on the number of particles into solution at different three times of the scattering kinetic. Monitored times are an initial (t_0 = 3 minutes, black line) and final time (t_f = 11 hours for BLG and Cu-BLG and t_f = 50 minutes for Zn-BLG, dark grey dashed line). (up) BLG, (middle) Cu-BLG and (bottom) Zn-BLG at pH = 7 and T = 60 °C.

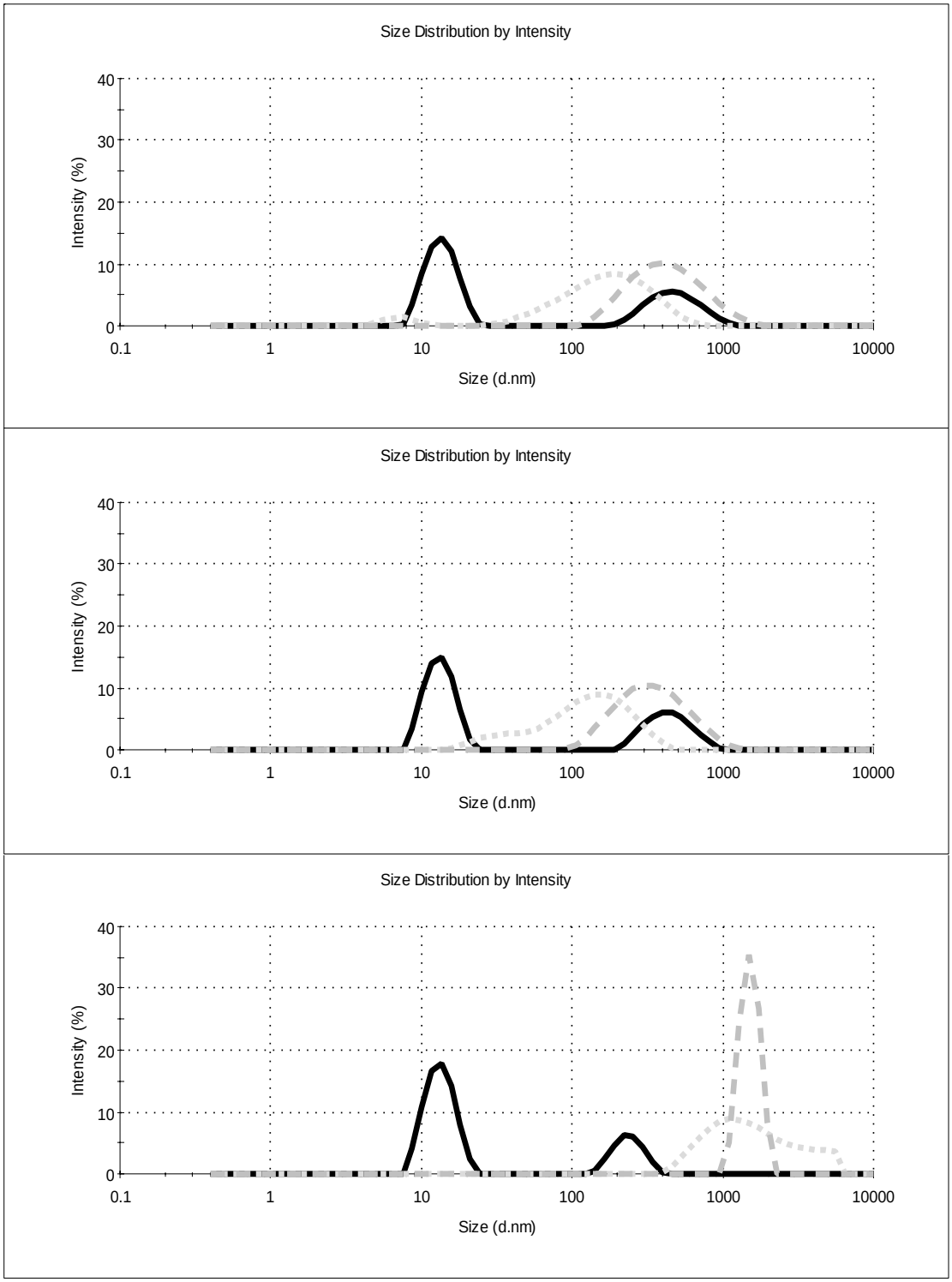

Figure 3.14: Size distribution of the aggregates dimension based on the intensity of scattered light at different three times of the scattering kinetic. Monitored times are an initial (t_0 = 3 minutes, black line), intermediate (t_m = 5.5 hours for BLG and Cu-BLG and t_m = 20 minutes for Zn-BLG, light grey short dashed line) and final time (t_f = 11 hours for BLG and Cu-BLG and t_f = 50 minutes for Zn-BLG, dark grey dashed line). (up) BLG, (middle) Cu-BLG and (bottom) Zn-BLG at pH = 7 and T = 60 °C.

The study carried out on the conformational changes of the secondary and tertiary structures induced by the temperature, as modified by the metal ions, put in evidence the different role played by divalent copper and zinc ions. In particular, the conformational changes of secondary structure induced by temperature are dramatically affected by copper. Figure 3.15 shows the differential absorption spectra of the Amide I' band for all the three samples and highlights the time evolution of the main spectral components of the band. Comparing FTIR kinetics obtained when copper (fig. 3.15b) or zinc (fig. 3.15c) is in solution with FTIR kinetic peculiar of BLG at pH = 7 and at T = 60 °C, it is immediately clear that aggregation occurs in all investigated samples, as marked by the growth of the components around 1620 cm^{-1} and 1685 cm^{-1} and by the decrease of the components in the spectral region 1640 – 1660 cm^{-1}. While Zn-BLG FTIR kinetic is very similar to BLG one, many remarkable differences are evident for Cu-BLG. It is noteworthy that the negative spectral component at 1640 cm^{-1} in the Cu-BLG sample is shifted towards 1635 cm^{-1}, usually assigned to native β-sheets structures and not present in the other two samples. This shift may be related to a possible coordination of the copper, during the aggregation process that can produce different species, as already observed through light scattering. Moreover, the presence of copper determines an increase of the signal in the regions at about 1595 cm^{-1} and at about 1660 cm^{-1} with the consequent lost of the isosbestic points at these two wavenumber values, which are well defined in the native BLG sample. The spectral component at about 1590 cm^{-1} is attributed to asymmetric stretching of CO_2^-, when coordinated with Cu^{2+} **[Mesu et al. 2003]**. The increase of the component at 1660 cm^{-1} may be attributed to the presence of disordered structures induced by copper, whose existence can justify the increase of the fractal dimension formerly estimated.

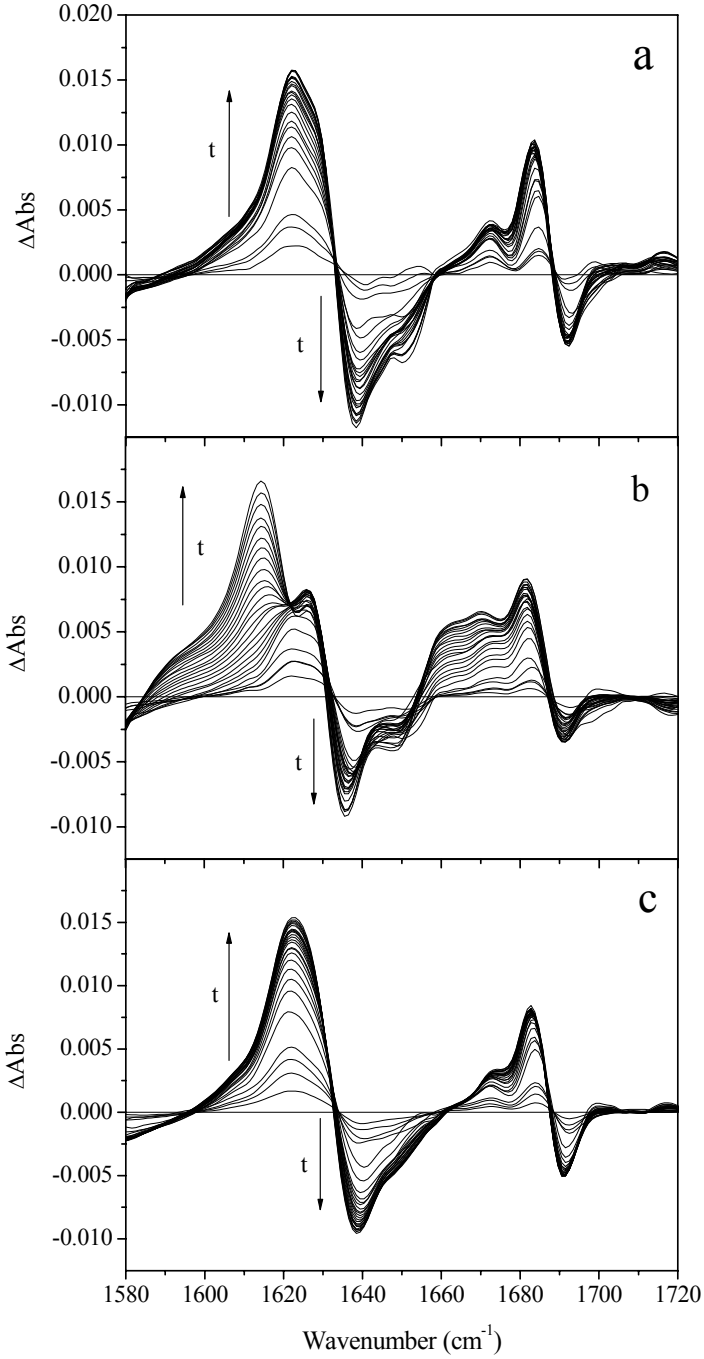

Figure 3.15: FTIR absorption differential spectra in the Amide I′ region of (a) BLG, (b) Cu-BLG, (c) Zn-BLG at pH = 7 during the incubation at T = 60°C for 5 hours. The arrows indicate the Amide I′ changes as a function of time.

A study realized on beta amyloid peptide showed that zinc ion can bind one or two histidines, making itself available for further interaction. This may induce the formation of ordered aggregates, according to a model in which the metal plays the role of a bridge between the imidazole rings of two histidine residues possibly belonging to different peptides **[Stellato et al., 2006]**. In the same study it results that copper is tightly bound to three histidines of the same protein molecules, in a fairly closed structure which ''protects'' the metal against any further interaction (see figures 1.7 an 1.9 in section 1.2.1); this is not supported by the results shown here, which suggest instead that the copper neither promotes nor inhibits the aggregation process (figure 3.10 and 3.11). In a more general way, the influence of metals in the higher or lower stabilization of native structures, after its coordination with histidines, is reported also for several native metallo-proteins. For example, in native enzyme like SOD (superoxide dismutase), that has a active site with the two metals, copper and zinc, the FTIR spectroscopy has revealed the influence of metals on the secondary structure of protein matrix **[Sun et al., 1997]**. The most relevant difference in FTIR kinetic of BLG is induced by copper in the Amide I' spectral region at lower wavenumbers. In this region a very intense component increases as a function of time at 1614 cm^{-1} in spite of the component at 1623 cm^{-1} (as you may see also in figure 3.16a and 3.16b). Both are assigned to the vibration of intermolecular β-sheets that is shifted to lower wavenumbers when the involved H-bonds are stronger. This behaviour, as reported in literature, is attributed to the initial formation of a network of bonds that can move towards gelation **[Allain et al., 1999, Remondetto et al., 2003]**. With respect to the conformational changes of the tertiary structure, our results suggest that metal presence in solution slackens the partial opening of the protein, as it is evident by figure 3.16c, where the time evolution of the peak intensity at 1436 cm^{-1} is shown; its increase is a probe of the H-D exchange. The rate of the time evolution is very similar for Cu-BLG and Zn-BLG. An almost completed opening is reached only for Zn-BLG. The latter is the sample for which the building of greater aggregates occurred in a shorter time.

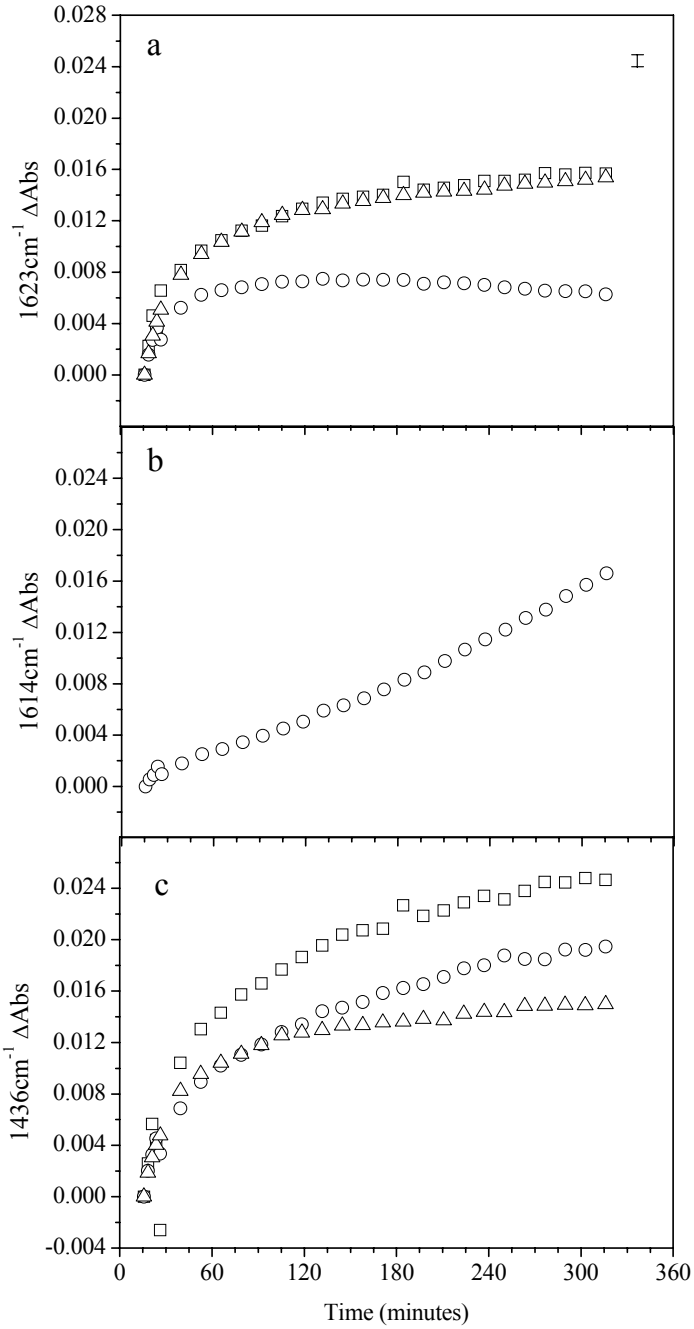

Figure 3.16: Time evolution of the FTIR differential absorption intensity of Amide I′ components: (a) at 1623 cm^{-1} for (□) BLG, (○) Cu-BLG, (Δ) Zn-BLG and (b) at 1614 cm^{-1} for only Cu-BLG; (c) time evolution of the differential absorption intensity of Amide II′ component at 1436 cm^{-1}. Protein was at pH = 7 and T = 60 °C. Error bar shown at the top on the right of (a) is the experimental error estimated for differential absorption values.

These results suggest that Cu^{2+}, through a specific interaction, influences the time evolution of the secondary structure of the native protein more than Zn^{2+}, which instead has a greater influence on the time evolution of the aggregates building. Probably, divalent Zn^{2+} ions act as bridges between the negatively charged carboxylic groups on neighbouring BLG molecules **[Remondetto et al., 2003]**.

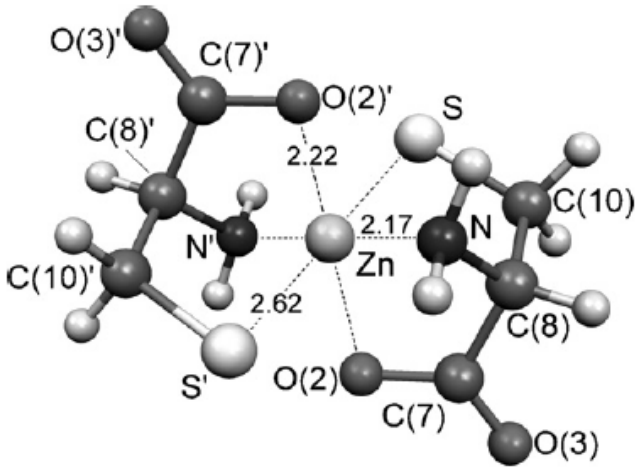

Figure 3.17: Optimized structure of the Zn(Cys)2 complex. Atomic distances are given in Angstroms. [Foley 2007].

A study performed with Raman spectroscopy associated with a theoretical study based on the assignment of the vibrational bands using the density functional theory (DFT) on the interaction between two cysteines and divalent zinc ion at pH=7 in aqueous solution has revealed the deprotonation of the SH and NH_3^+ cysteine groups upon binding to zinc. Moreover it showed a spectral evidence for the participation of CO_2^-; the proposed structural model is shown in figure 3.17 **[Foley et al., 2007]**. In general, it is well known that the increase of the salt concentration changes the distance distribution of the potential repulsive forces (i.e., mainly electrostatic) and thus the energy barrier, which stabilizes the system. The decrease of the potential repulsive force can justify such a fast aggregative process **[Remondetto et al., 2003]**.

Summary. The results shown and discussed in this section highlight that metal ions affect the tertiary and secondary structure changes and the formation of supramolecular aggregates when BLG at pH=7 is subject to heat-treatment at 60°C. It is noteworthy that Cu^{2+} and Zn^{2+} play a different role in conditioning the time evolution of the heat-induced aggregation process. In particular, Cu^{2+} influences mainly the time evolution of the protein secondary structure and of its initial conformational changes, inducing the formation of stronger H-linked bonds, but it does not influence dramatically the trend of aggregates formation. Instead, infrared spectra of Zn-BLG present the same changes of the differential components in respect to BLG ones, but the presence of zinc ions in solution dramatically induces the formation of big aggregates in a shorter time, probably through the making of bridges of zinc between two cysteines of different proteins. A specific interaction between copper and protein is highly consistent with our results.

3.2 β-Lactoglobulin samples at acidic pH values

The aggregation of BLG is very sensitive to the pH value of the solution, since the reactivity and the accessibility of the thiol group depend markedly on the pH. To explore the role of quaternary structure of BLG on the aggregate formation, we have studied the aggregation kinetics with DLS at two acidic pH in which the quaternary structure of BLG changes. Indeed, the quaternary structure of BLG is highly dependent on the pH value and a different initial oligomeric state of BLG can lead to a different aggregation pathway. Moreover, also the charge of the protein changes with pH. At very acidic pH values, BLG has only a positive charge (21 per monomer unit) in contrast with its amphoteric behaviour at neutral pH. The mechanism of aggregation under these conditions is considerably different from that at neutral pH. The disulphide bond interchange, which is involved in the aggregation process at neutral pH, is very unlikely to occur, because the thiol groups are very stable at low pH. Under these conditions, electrostatic interactions between monomers are purely repulsive. Nevertheless, such interactions may be screened to different extents by the addition of salts. Now, the results obtained,

through DLS measurements, from the study on the influence of metal ions presence in solution at acidic pH will be shown. It is noteworthy that the protein molecules and metal ions have the same charge at acidic pH value. Moreover, with the aim to study the role of metal ions during aggregation processes, we have select the copper ion not showing any effect in the time evolution of the aggregates growth of BLG at pH = 7; in these conditions, only an mild increase of the fractal dimension (figure 3.12) revealed the formation of aggregates slightly more open. In particular, the heat-induced aggregation of 3.3mM BLG in presence of two different molar concentration of $CuCl_2$ has been studied at pH 4 and 2.5. Under these experimental conditions, BLG has a different quaternary structure. In particular, solutions of native BLG at pH between 4 and 5 contain native dimers and octamers, the latter enhancing by a decrease in temperature and in ionic strenght **[McKenzie et al., 1967, Carrotta et al., 2003, Verheul et al., 1999]**, while BLG solutions at pH = 2.5 contain mainly monomers.

Considering temperature as a parameter affecting the rate of the aggregation process, it is necessary to determine the more suitable temperature values to study the influence of metal ions on the aggregation in the new different experimental conditions. In figure 3.18 temperature scans of the scattering intensity obtained for 3.3mM BLG at pH 4 and 2.5 are reported. It is clear that the temperature of 60 °C, used to study the kinetic of aggregation at pH = 7, implies a too fast aggregation process. So, the temperature 42 °C was selected for the study of the metal ions influence on the aggregation process of BLG at pH 4, and 50 °C at pH 2.5. According to what said about the dependence on the pH value of the aggregation evolution, the different evolution of the scattering intensity as a function of temperature is evident by the temperature scans shown in figure 3.18. The increase of the scattered light intensity starts at lower temperature values (~42 °C) when the pH value is 4 rather than at pH 2.5 (~ 54 °C); while the growth rate is higher at pH = 2.5.

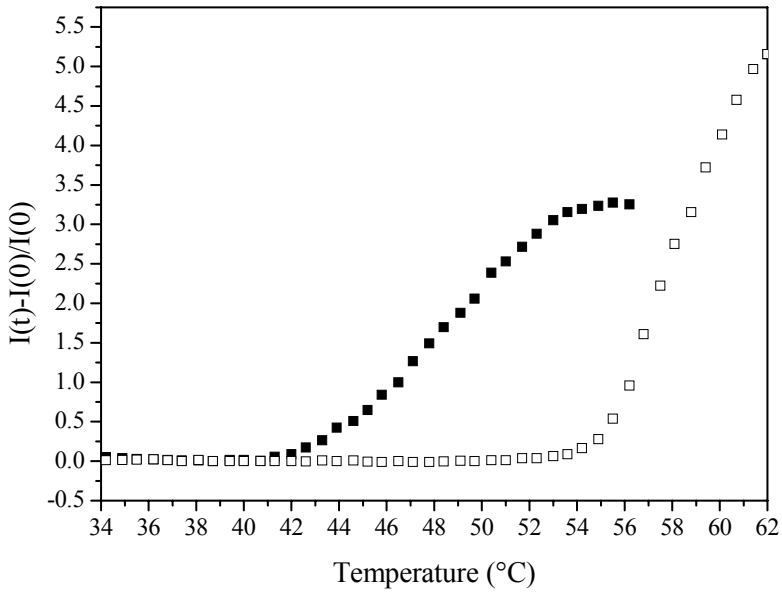

Figure 3.18: Normalized scattered intensity as a function of temperature for BLG at (■) pH = 4 and (□) pH = 2.5. The experimental error is smaller than symbol dimension

In figure 3.19 the scattered light (fig. 3.19a) and Z-average diameter (fig. 3.19b) behaviour of BLG sample at 42 °C and pH = 4 are reported as a function of time, also when 0.5 mM (0.5Cu-BLG) or 3 mM $CuCl_2$ (3Cu-BLG) are in solution. All aggregation kinetics show a little lag-phase, of about 10 minutes, after which the aggregates building is induced by the temperature increase. The light scattering behaviour versus time, shown in figure 3.19a, may indicate that 0.5mM of $CuCl_2$ in solution leads to a slight decrease of the growth rate. BLG with a higher amount of copper (3 mM) in solution shows an appreciable increase in the scattered light in respect to the BLG, before the decrease in the final phase of the kinetic. This decrease should be due to the appearance of the precipitates in solution observed after about 200 minutes (data not shown). The behaviour of the Z-average diameters, reported in figure 3.19b, allows to argue that 3Cu-BLG contains aggregates with greater dimensions, about 90 nm. The presence of copper with molar concentration 0.5 mM in 0.5Cu-BLG sample shows to have an inhibitor effect on the aggregation process, since the decrease of the growth rate is observed in concomitance with the formation of smaller aggregates.

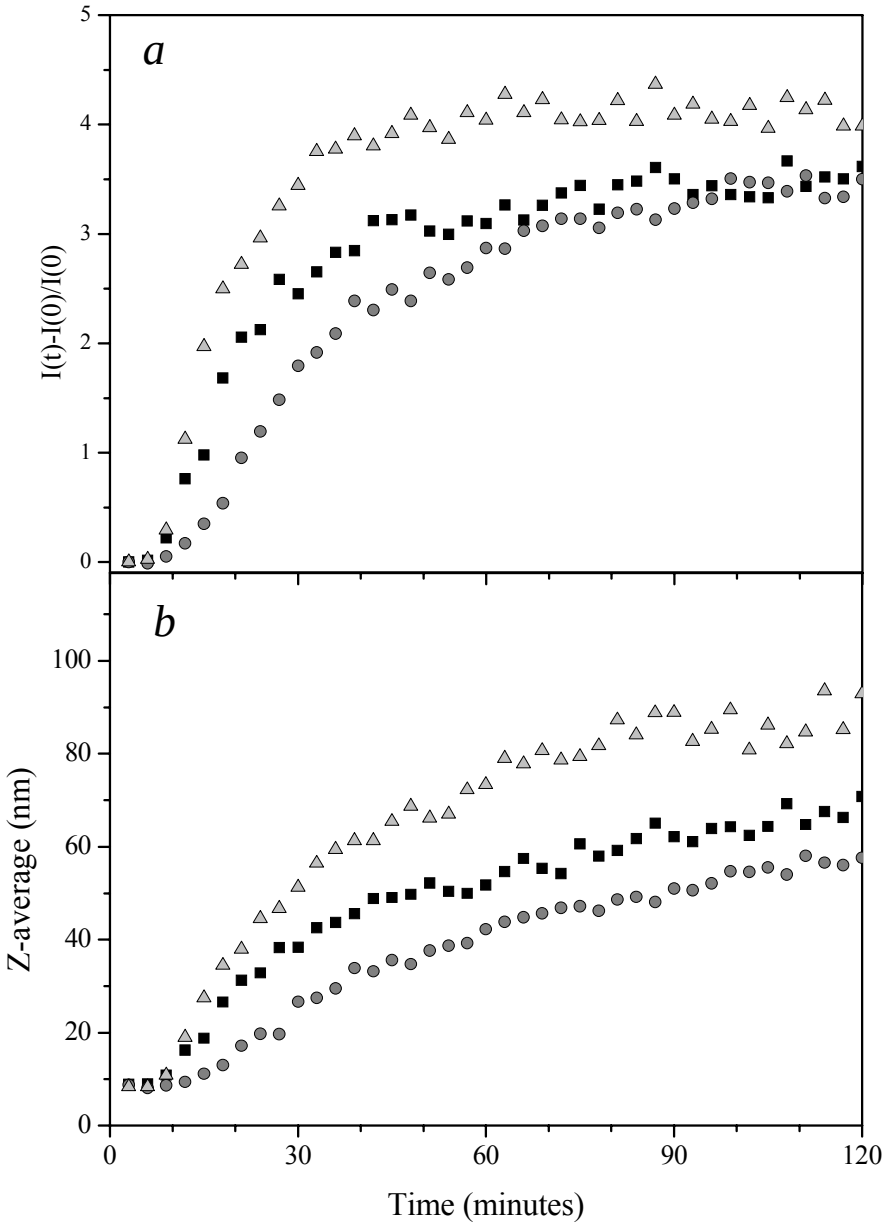

Figure 3.19: (a) Time evolution of the normalized scattered intensity and (b) of the Z-average diameter of (□) BLG, (○) 0.5Cu-BLG and (Δ) 3Cu-BLG at pH = 4 and T = 42 °C. The experimental error is smaller than symbol dimension.

The interpretation of these results should allow to conclude that the presence of 3 mM of copper ions in BLG solution at pH 4 promotes the aggregation process, leading to the formation of slightly greater aggregates. In general, adding salt in solution produces a change of the ionic strength. The influence of the ionic strength reveals itself, not only in the aggregate structure, but also in governing the rate at which native protein units are involved in the formation of oligomers **[de La Fuente et al., 2002]**. The different results obtained at different molar concentration of salt in solution could be attributed to two opposite effects on protein aggregation, effects that would be induced by the change of the ionic strength. First, the increase of ionic strength reduces the intermolecular repulsion between molecules because of the screening of charged groups, thereby increasing the aggregation rate. Second, an increase in ionic strength increases the denaturation temperature of the protein, because positively charged groups can reduce intramolecular repulsion, therefore increasing conformational stability. Since unfolding of BLG molecule is the initial step leading to aggregation, a decrease of the unfolding rate would subsequently lead to a smaller aggregation rate **[de La Fuente et al., 2002]**. Our results show that probably the first effect prevails when the concentration ratio [salt]/[protein] is higher. On the contrary, when the salt concentration is 0.5mM, the predominant effect may be the increase of the conformational stability due to the decrease of the intramolecular repulsion that leading to a decrease of the aggregation rate.

In order to investigate the fractal dimension (as defined at page 81) of the aggregates of BLG, 0.5Cu-BLG and 3Cu-BLG, the plots of the "mean count rate" of all samples as a function of respective Z-average diameters were analysed. These are reported in logarithmic scale in figure 3.20, where a linear fit, suitable for all reported plots, has been carried out between 10 and 40 nm of the z-average. It is evident that the structure of the aggregates is not affected by the metal ions in solution.

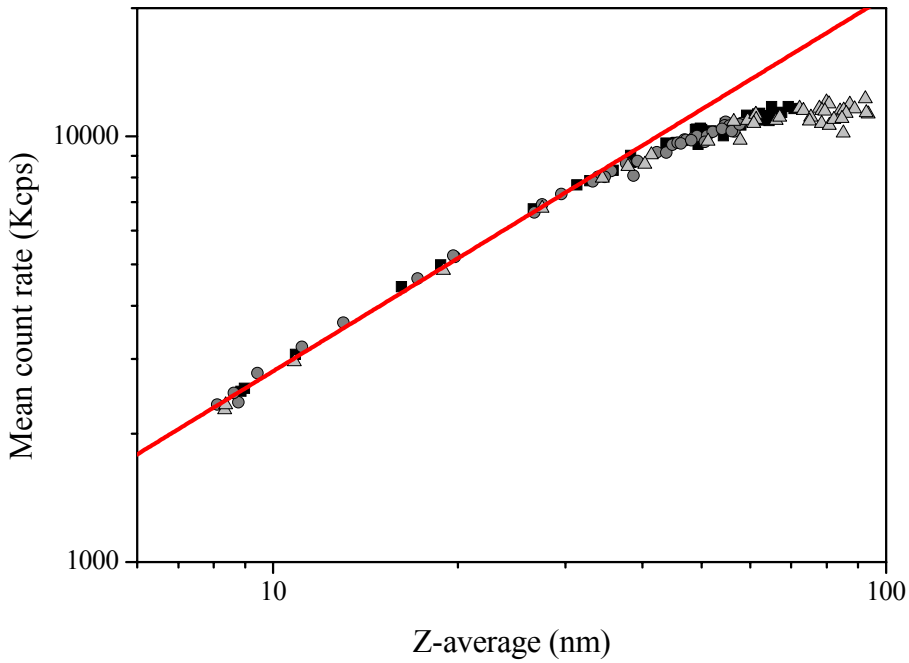

Figure 3.20: Scattering intensity as a function of Z-average diameter for (□) BLG and (o) 0.5Cu-BLG and (Δ) 3Cu-BLG, at pH = 4 and T = 42 °C. The experimental error is smaller than symbol dimension. The red line shows a linear fit, Y=*a*+*b*x, where *b*= 0.90 ± 0.01.

However, the estimated numeric value of the fractal dimension is probably highly affected by the "form factor"[3], which can not be anymore approximated to 1. Indeed, as you will see in the following, the protein solution is polydispersed (figure 3.21) and, as a consequence, the lower values of the scattered intensity are affected by the presence of an other aggregating species, whose dimension is comparable with the source wavelength. For this reason, the obtained slope value is inconsistent with a greater expected value. The fractal dimension depends on the nature of the aggregation process. Globular proteins can make either random or linear aggregation, depending on factors, such as pH [**Hongsprabhas et al., 1999**]. On both sides of the pI of the protein (pI=5.2 for BLG), high electrostatic repulsion will slow down the aggregation rate, thus inducing the formation of linear aggregates.

[3] In fact, the scattered intensity is proportional to the average mass of aggregates times the form factor P(q), which can be approximated with the Fisher-Burford expression **[Nicolai et al., 2003]**:
$P(q)=[1+\frac{2}{3}d_f^{-1}q^2R_H^2]^{-df/2}$,
where, R_H is the hydrodynamic radius and *df* is the fractal dimension of the object.

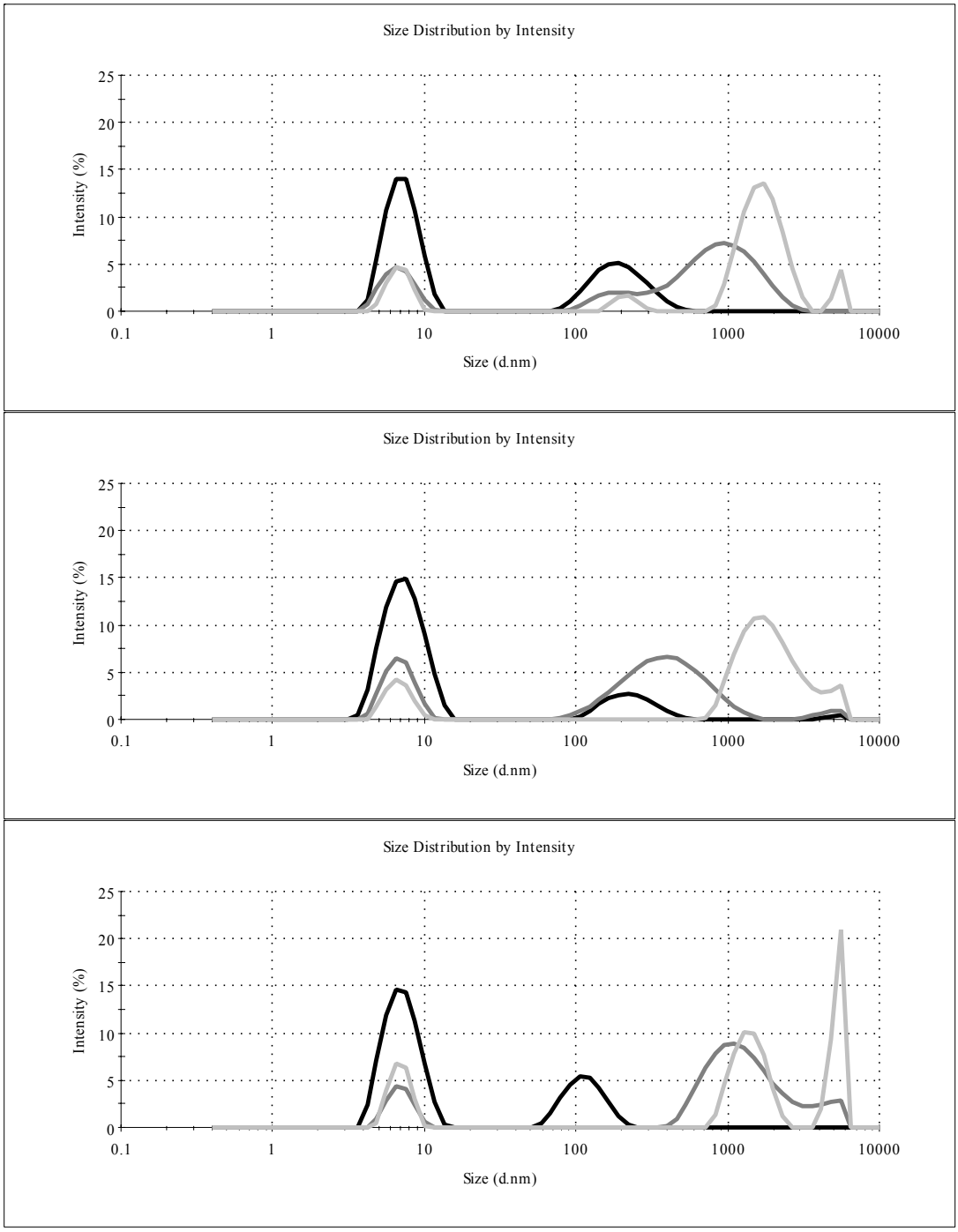

Figure 3.21: Size distribution of the aggregates dimension based on the intensity of scattered light at different three times of the scattering kinetic. Monitored times are an initial (t_0 = 3 minutes, black line), intermediate (t_m = 30 minutes, dark grey line) and final time (t_f = 120 minutes, light grey line). (up) BLG, (middle) 0.5Cu-BLG and (bottom) 3Cu-BLG at pH = 4 and T = 42 °C.

In contrast, at pH 4, that is closer than pH 2.5 to pI, random aggregates should rise [**Bryant et al., 1998, Hongsprabhas et al., 1999, de la Fuente et al., 2002**], with a fractal dimension greater than 2. These speculative observations do not invalidate the obtained result concerning the independence of the aggregates structure by the presence of metal ions in solution, since, as you will see later, the nature of the aggregation process is the same for BLG 0.5Cu-BLG and 3Cu-BLG, even if it is different from that of BLG at neutral pH.

Our data do not allow to establish if the aggregation is based on the links between unfolded monomers units or on the links between little oligomeric units, such as native dimers or octamers at pH=4. To this end, some considerations can be extrapolated by the distribution of the diameter dimension based on the scattered intensity of the different species in solution. Moreover, by the distribution of the diameters dimension based on the number of the particles, it is possible to determine which of these species is predominant. In figure 3.21 the distributions of the aggregates dimension based on the scattered light intensity are shown for BLG, 0.5Cu-BLG and 3Cu-BLG at three different times: immediately after the reaching of thermal equilibrium (t_0, 3 minutes), at an intermediate time (t_m, 30 minutes) and when the plateau is reached (t_f, 120 minutes). Once again, at initial time in all samples two species are present. The first has the several native quaternary structures peculiar of pH = 4 and it extends from 4 to 10 nm and it is centred at a diameter of 8 nm. According to previous studies **[McKenzie et al., 1967, Carrotta et al., 2003, Verheul et al., 1999]**, native quaternary structures present in solution seem to be dimers; on the contrary, no evidence exists of the presence of expected greater native oligomers at this pH value, such as octamers. The second distribution, housing species having diameter of about or larger than 150 nm, may be again attributed to the presence in solution of dense liquid clusters, several hundred nanometers in size, which are metastable and whose formation takes place within a few seconds after solution preparation **[Pan et al. 2007]**.

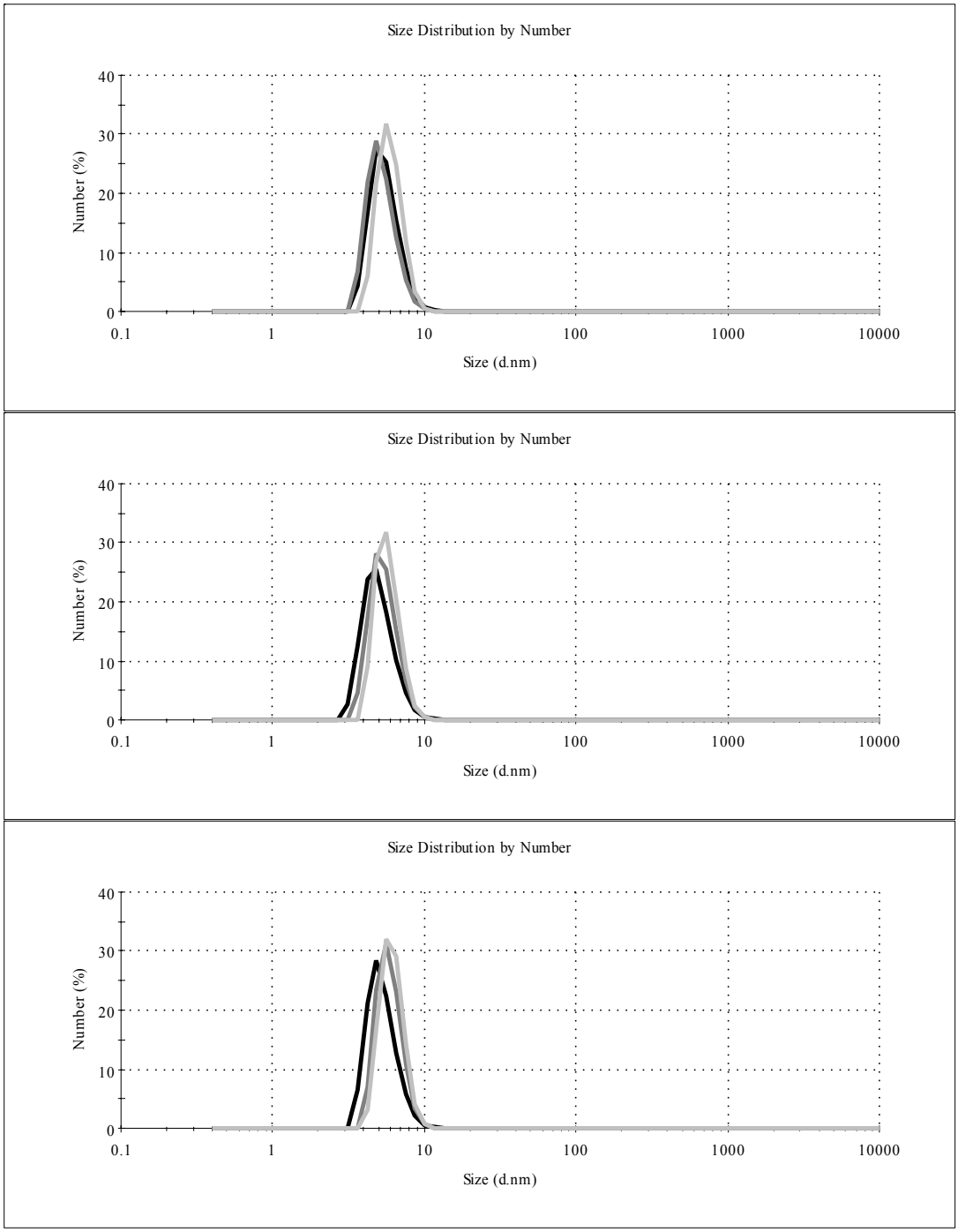

Figure 3.22: Size distribution of the aggregates dimension based on the number of the particles into solution at different three times of the scattering kinetic. Monitored times are an initial (t_0 = 3 minutes, black line), intermediate (t_m = 30 minutes, dark grey line) and final time (t_f = 120 minutes, light grey line). (up) BLG, (middle) 0.5Cu-BLG and (bottom) 3Cu-BLG at pH = 4 and T = 42 °C.

At later times greater species arise, marking the start of the aggregation process. Comparing BLG and 0.5Cu-BLG diameter distributions at the intermediate time, as reported in figure 3.21, it is evident that the species with a diameter of about 1000 nm is present in the BLG solution only but it is absent in 0.5Cu-BLG solution. This is in agreement with the likely increase of the conformational stability induced by the change of the ionic strength producing a decrease in the initial phase of the growth rate of the big aggregates building. A comparison between the BLG and 3Cu-BLG diameters distributions puts in evidence that the screening effect of a greater amount of salt promotes and makes faster the aggregates building. Actually, the number of the bigger species observed at all times and for all samples is smaller than that of the species having diameter of about 10 nm, even though their intensities in figure 3.21 are similar because bigger particles induce an increase of the scattered light intensity. In figure 3.22 the diameter distribution based on the number of particles in solution is reported. Here no component of the species having greater dimension is observed. Thus, heat-treatment at 42 °C of BLG induces the formation of a little relative fraction of aggregates having big dimensions. On the other hand, the component of smaller dimension gets slightly bigger, suggesting an association between monomers and dimers as a function of time faster when 3mM of $CuCl_2$ is in solution, as shown in figure 3.21, comparing the three different distributions at intermediate time. On the contrary of BLG thermal aggregation at neutral pH, the aggregation process at pH 4 occurs involving a low number of protein molecules engaged in the formation of greater species, whose dimensions become comparable with the source wavelength. As already reported, the coexistence of these species does not anymore permit to approximate the factor form to 1 and probably leads to an under estimated value of the fractal dimension.

The influence of metal ions in 3.3 mM BLG solution on the aggregation process was studied also when pH is 2.5; in these experimental conditions, BLG is present as positively charged monomers.

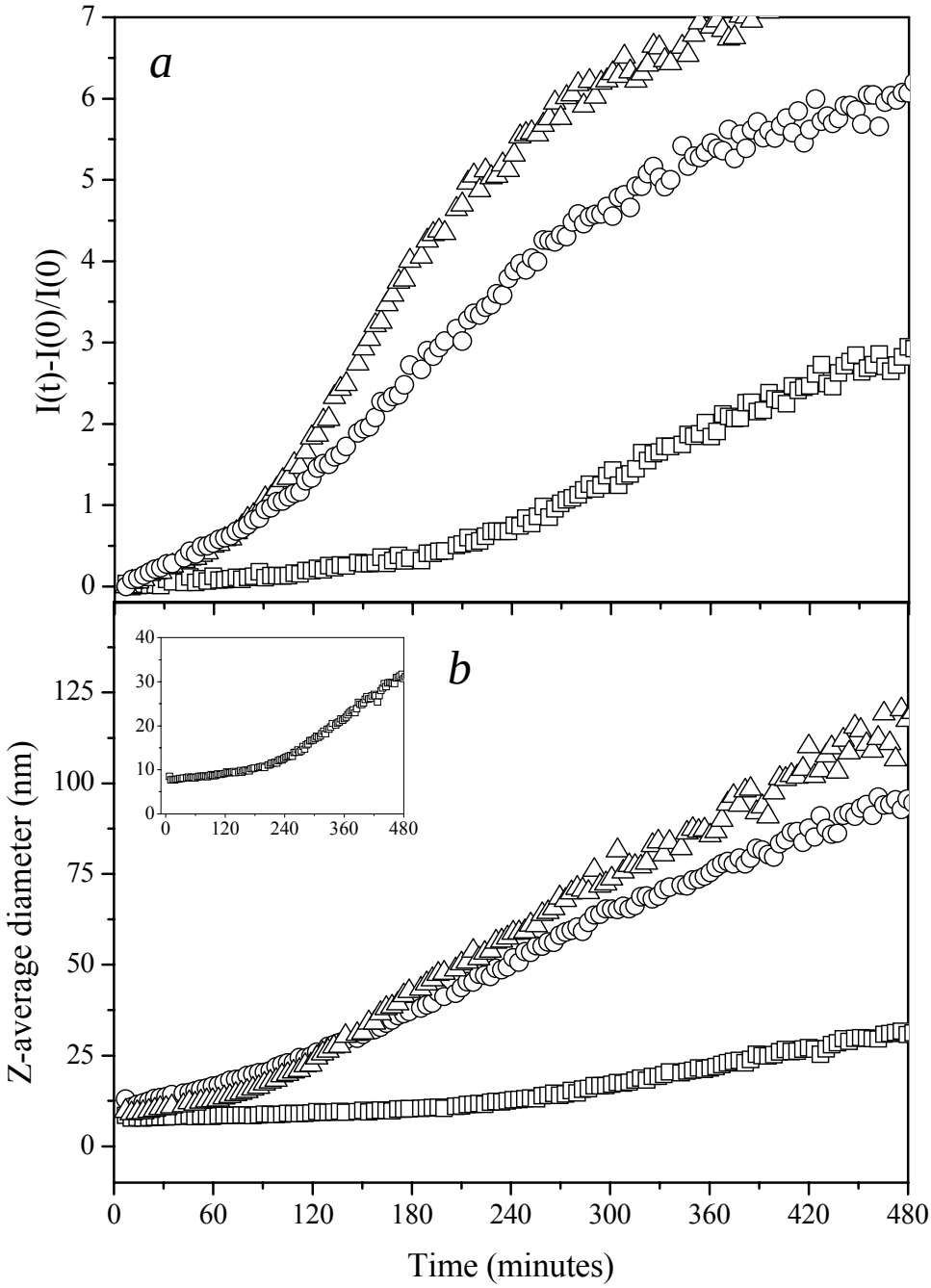

Figure 3.23: (a) Time evolution of the normalized scattered intensity and (b) of the Z-average diameter of (□) BLG, (○) 0.5 mM Cu-BLG and (Δ) 3 mM Cu-BLG at pH = 2.5 and T = 50°C. The inset shows a zoom of a Z-average as a function of time. The experimental error is smaller than symbol dimension.

The temperature chosen for the aggregation kinetic is 50 °C. In figure 3.23 the scattered light (fig. 3.23a) and Z-average diameter (fig. 3.23b) behaviour as a function of time of BLG sample (also when 0.5mM or 3mM $CuCl_2$ are in solution) are reported. The aggregation process of BLG at pH 2.5 is qualitatively different from that at pH = 7. The contribution of the disulfide bonds in the formation of the oligomers at pH 7 can be excluded, because of the high stability of the thiol groups at acidic pH values. In agreement with literature data, the aggregation rate increases with increasing salt concentration, confirming that BLG aggregation at pH 2.5 is strongly dependent on the ionic strength **[Aymard et al., 1999, Schokker et al., 2000]**. The increase of the scattered light as a function of molar concentration of the metal in solution suggests that $CuCl_2$ promotes the aggregation. The increase is remarkable also when the molar concentration of metal is 0.5 mM; probably, the greater positive charge of the protein at pH = 2.5 makes more efficient the effect due to the screening rather than that to the increase of the conformational stability **[de La Fuente et al., 2002]**. The presence of copper in solution increases the growth rate of the scattered light intensity of BLG solution at pH 2.5 and T = 50 °C. The z-average diameter, shown in figure 3.23b, indicates an increase of the average dimension of the aggregates more remarkable when the molar concentration of the metal is higher; this confirms that the increase of the scattered light intensity is due to the building of bigger aggregates and not only to the increase of their number. The average dimension of 0.5Cu-BLG at pH 2.5 is about 90 nm, while the average dimension of 3Cu-BLG at the same pH is about 120 nm. The structure of the associated BLG particles at pH 2.5 and with different concentration of copper ions in solution has also been investigated estimating the fractal dimension of the aggregates by the correlation between the "mean count rate" of the scattered photons and z-average of the aggregates in solution, according to the relation 3.1 at page 81. As it can be seen in figure 3.24, the aggregates structure is substantially independent on the presence of the metals in solution.

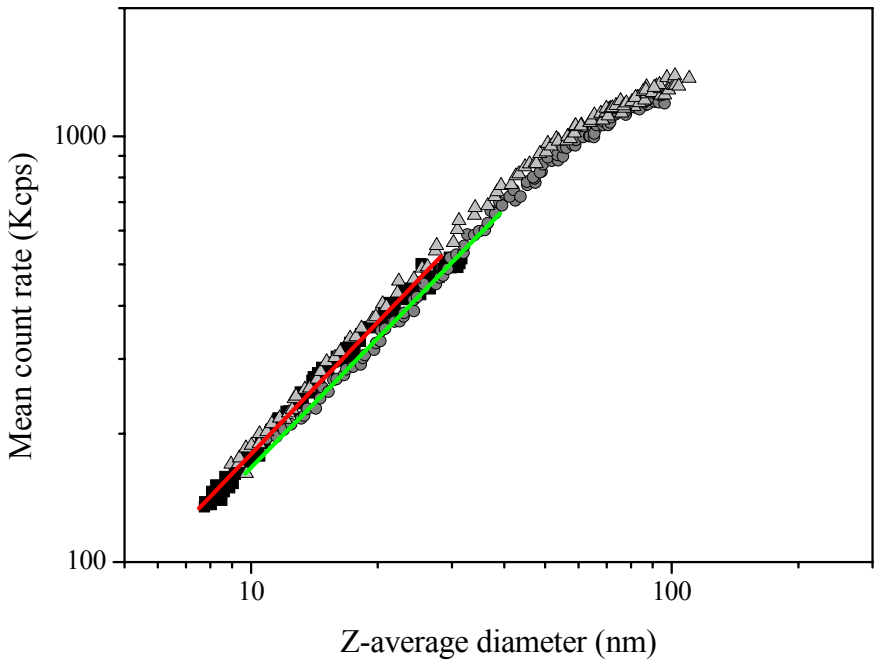

Figure 3.24: Scattering intensity as a function of Z-average diameter for (□) BLG and (o) 0.5Cu-BLG and (Δ) 3Cu-BLG at pH 2.5 and T = 50 °C. The experimental error is smaller than symbol dimension. The lines show the linear fits, Y=*a*x+*b*, for (red line) BLG and 3Cu-BLG, with *a*=1.02 ±0.01, and (green line) 0.5Cu-BLG, with *a*=1.00 ±0.01.

As observed for the BLG aggregation process at pH 4, also at pH 2.5 the nature of the aggregation process (discussed later) does not permit to approximate to 1 in the data analysis the "form factor" *P(q)*, whose expression is reported in the note 3 at page 104. It may be cause of an uncorrected estimation of the fractal dimension, found equal to 1 according the expression 3.1. So, even if we can not to assert that the aggregates formed at pH 2.5 have a linear conformation, we want to underline that the formation of elongated fibril-like aggregates is expected at very acidic pH and at very low ionic strength **[Aymard et al., 1996 and 1999]**.

Their formation should occur via to the association of a monomer with a bigger aggregate according to a more or less "fixed" orientation induced by the charge of the protein molecules at very acidic pH **[Aymard et al., 1999, Schokker et al., 2000, de La Fuente et al., 2002]**. The association between monomers to form new oligomers is less probable, because of the large repulsive interaction between them. The aggregates

revealed at pH 2.5 are smaller than that observed at neutral pH, as expected at low ionic strength **[Schokker et al., 2000]**. In agreement with **Aymard et al., 1999**, the formation of the aggregates can be explained in terms of a nucleation and growth process. Because of the large repulsive interactions between monomers, nucleation is the limiting step, and once a critical size is reached, the growth process could be relatively fast, leading to very large aggregates **[Aymard et al., 1999]**. The nucleation process appears promoted by the presence of copper ions in solution, but probably the critical size was not reached, since in all BLG solutions the presence of very large aggregates (~120 nm) was not observed.

The whole time evolution of diameter distribution of the species in the different BLG solutions, based on the scattered intensity, is shown in figure 3.25 at three representative times. The evolution indicates that the formation of bigger aggregates occurs. In particular, the intensity of the smaller species in the three different samples decreases, while the component of the bigger species increases, the latter being greater with increasing of the copper concentration. Thus, these results suggest that the presence of $CuCl_2$ in solution promotes the aggregation processes. However, the component of smaller dimension is still present in the final phase of the kinetics. Considering that species having small dimension scatter light less efficiently than greater species, their remarkable presence in the final phase of the time evolution of the diameter distribution based on the scattered intensity implies that a wide number of not-aggregated proteins is still in solution and, as a consequence, that the formation of the aggregates is not extended. Indeed, as it can be seen in figure 3.26, the distribution of aggregates dimension based on the number of particles in solution shows that the aggregation process of BLG at pH = 2.5 and at T = 50 °C is characterized by a limited formation of bigger aggregates, and only the species of smaller diameter dimension is revealed as predominant. This species has native quaternary structure peculiar of pH = 2.5 and it extends from 2 to 9 nm and is centred at a diameter of 4 nm.

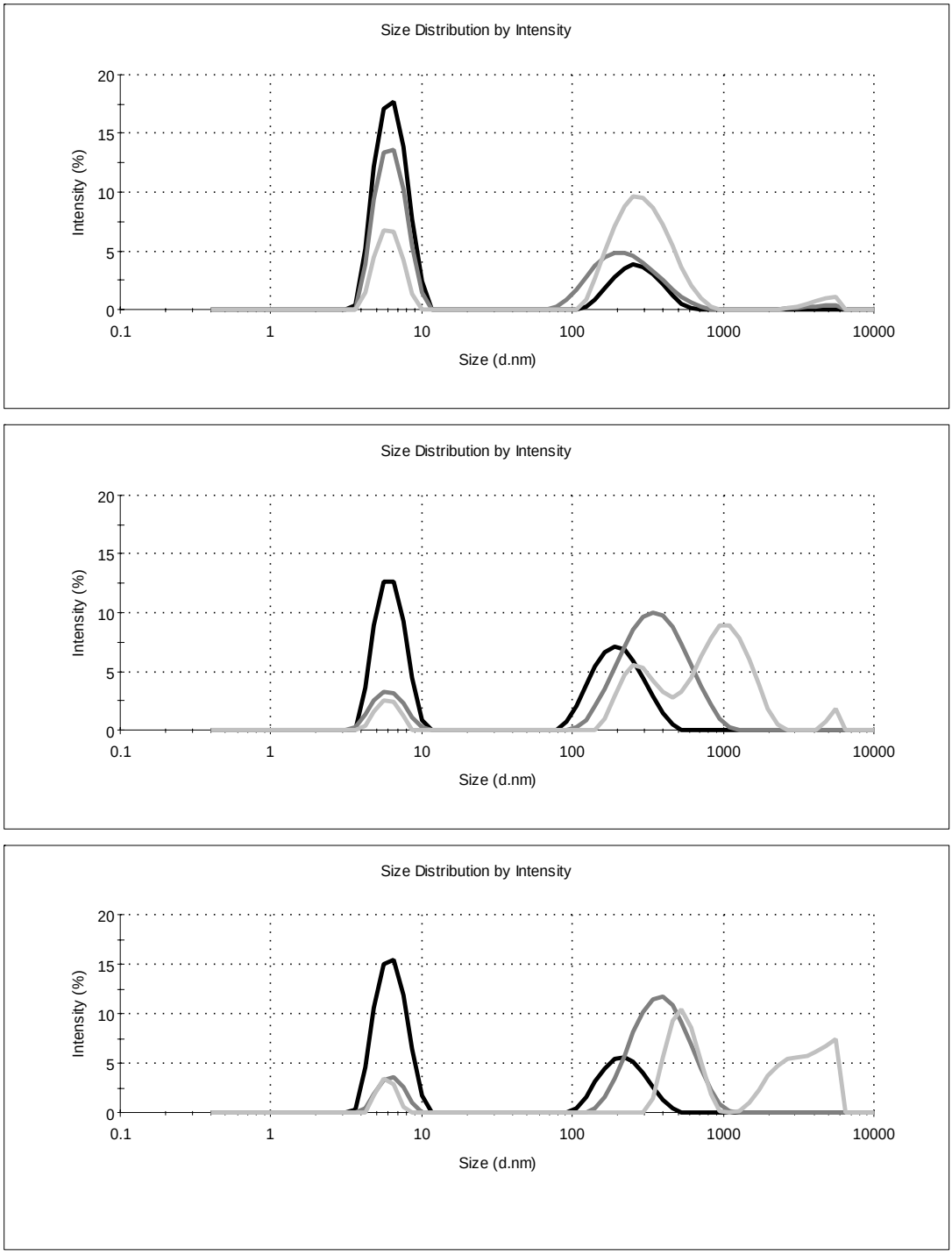

Figure 3.25: Size distribution of aggregates dimension based on the intensity of light scattered, at t_0 = 3 minutes (black line), t_1 = 180 minutes (dark grey line) and t_3 = 360 minutes (light grey line) of the scattering kinetics. (up) BLG, (middle) 0.5Cu-BLG, (bottom) 3Cu-BLG at pH = 2.5 and T = 50 °C.

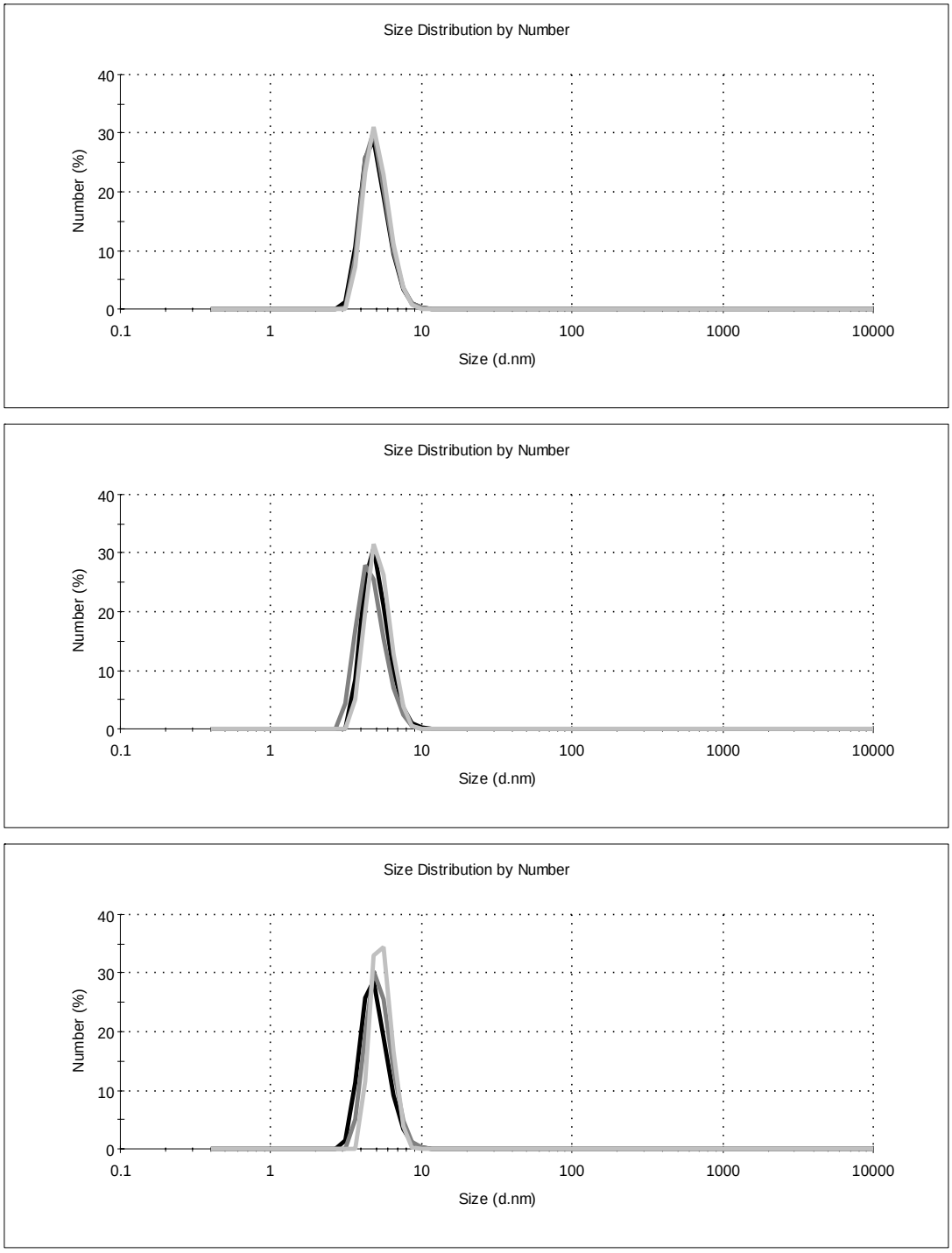

Figure 3.26: Size distribution of aggregates dimension based on the number of the particles into solution, at t_0 = 3 minutes (black line), t_1 = 180 minutes (dark grey line) and t_3 = 360 minutes (light grey line) of the scattering kinetics. (up) BLG, (middle) 0.5Cu-BLG, (bottom) 3Cu-BLG at pH = 2.5 and T = 50 °C.

In accord with the literature **[Aymard et al., 1996, and 1999, Renard et al., 1998, Verheul et al., 1999, Schokker et al., 2000, de la Fuente et al., 2002]**, the native quaternary structures present in solution seem to be prevalently monomers, but also dimers are in solution. This suggests that, at pH 2.5, BLG behaves as a mixture of monomers and dimmers, and even when the ionic strength is low, the purely monomeric form occurs only in a limited range of concentrations **[Aymard et al., 1996]**. The scenario, the same for BLG with and without copper ions in solution, indicates the thermal induced aggregation of BLG at pH 2.5 and at T = 52 °C leads to a not widespread formation of aggregates. The dimension of these aggregates increases with the increasing of the copper concentration in solution. The thermal aggregation process of BLG at acidic pH values results promoted by the presence of metal ions in solution, except for 0.5Cu-BLG at pH = 4, where the addition of 0.5mM of metal probably induces an increase of the conformational stability. The aggregates structure is not affected by metal ions in solution. This scenario is consistent with an aggregation model, in which metal ions promote the aggregates formation, playing the role of bridges between negatively charged carboxylic groups of some amino acids **[Mesu et al., 2006]**, as illustrated in figure 3.27. We can conclude that the large-scale structure of the aggregates is surely governed by the balance between electrostatic interactions and the degree of screening.

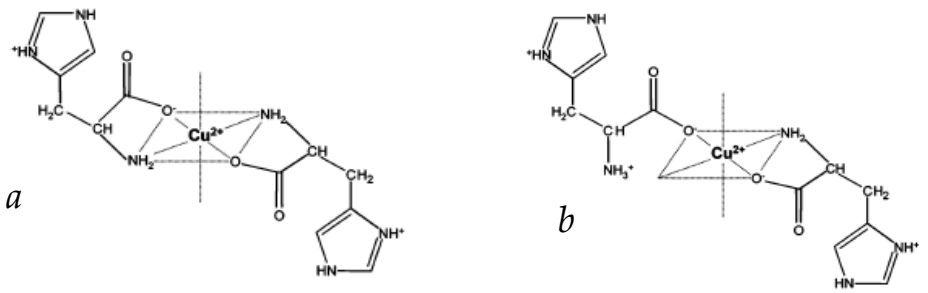

Figure 3.27: Proposed molecular structure of Cu^{2+}/his complex at (*a*)pH~ 4 and (*b*) pH ~ 2.5 . Figure from **Mesu et al., 2006**.

Summary. The results shown and discussed in this section highlight that the presence of Cu^{2+} ions affects slightly the time evolution of the aggregation process and of the growth of the aggregates mean dimension of BLG at pH 4 and 2.5. In particular, only a mitigated formation of aggregates has been observed. The number and the dimension of these aggregates increase with increasing the copper concentration in solution, indicating that the presence of metal promotes the aggregation of BLG. The dimension growth is higher at pH 2.5 rather than at pH 4, suggesting that the electrostatic interactions play a key role in the formation of aggregates. Finally, the structure does not result affected by metal in solution, though being different at different acidic pH values.

Chapter 4

Experimental results: Thermal aggregation of Bovine Serum Albumin

4.1 Bovine Serum Albumin samples at neutral pH

A study analogous to that carried out on the metal effects on the thermal aggregation of BLG has been employed on Bovine Serum Albumin (BSA). Contrary to the BLG quaternary structure, that one of BSA is not dependent on the pH and its secondary structures is essentially α-helix **[Gelamo et al., 2000 and 2002]**. Into domain I it is a single free cysteine (Cys-34) playing a relevant role in the aggregation process at pH near to neutral **[Militello et al., 2003]**. As BLG, BSA has a stable conformational structure at room temperature and it can be considered a model system in order to study the influence of metal ions on the aggregation process at neutral pH. In early years, my research group has carried out studies on the heat-induced conformational changes on the tertiary and secondary structures followed by steady-state fluorescence and CD, in the low concentration regime of the protein **[Militello et al., 2003]**. In addition, the effects of pD changes on aggregation changes on the aggregation kinetics of BSA have been studied in a high concentration regime, in order to see if and how intra and intermolecular interactions can depend

on surface net charge. This latter study has been realized investigating the conformational changes of the tertiary and secondary structures via FTIR and light scattering measurements **[Militello et al., 2004]**. In these works the protein was diluted in a phosphate buffer different by the one used here (MES buffer). The switching of the buffer was necessary because of the observed interactions between phosphate buffer and metals ions leading to the formation of chemical complexes in solution; moreover, this has allowed to evaluate the influence of the buffer on the thermal aggregation process of BSA induced by a temperature increase. In this chapter the results concerning the influence of copper and zinc on the heat-induced aggregation process will be reported. Temperature scans of BSA solution with and without metal ions have been carried out in order to select an opportune temperature for the protein incubation. As metal concentrations, we have selected the following values: 1 mM (the same of BLG solutions) and 0.3 mM, in order to maintain the same ratio of metal/protein concentration, since BSA in solution was 1 mM. From figure 4.1 it is evident that the presence of metal ions in BSA solution does not affect the temperature of the protein unfolding. Moreover, no remarkable differences are observed at varying of metal concentrations. A very slight decrease of the temperature of the protein unfolding is revealed for 1 mM zinc ions in BSA solution. However, in absence of relevant differences in the temperature scan of BSA in presence of metal ions, the temperature of 58 °C was selected, being the same of the above mentioned and used in **Militello et al., 2004**.

Before showing the results relative to the study of metals influence on the thermal aggregation of BSA, the time evolution of the formation of aggregates and the conformational changes of the secondary and tertiary structures characterizing the thermal aggregation process of BSA diluted in 20 mM MES buffer at pD or pH 7.4 (being pD or pH 7 at the incubation temperature) and kept for 8 hours at 58 °C will be described.

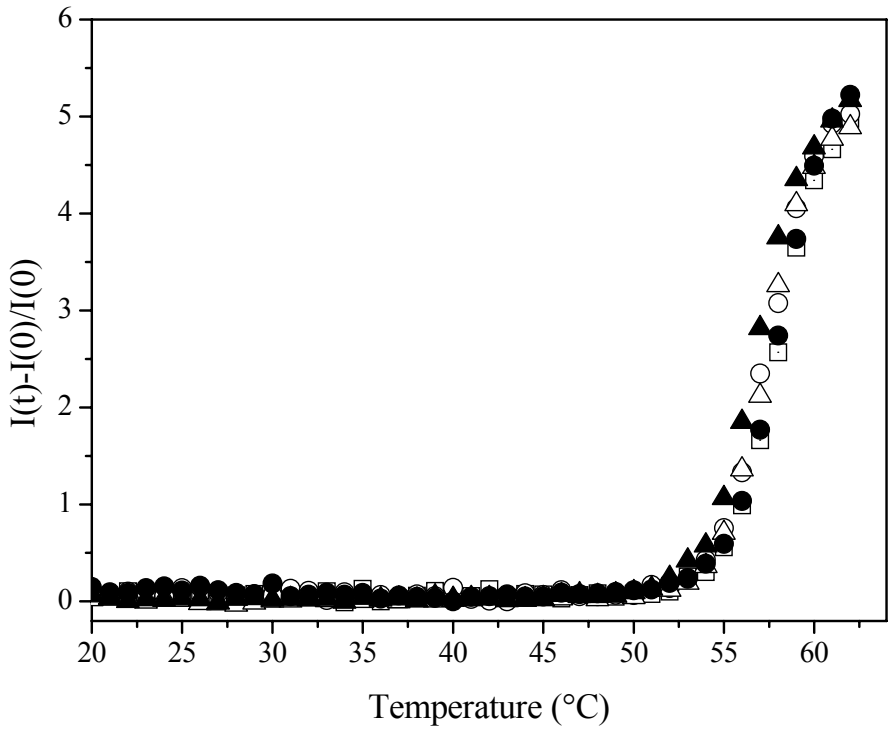

Figure 4.1: Normalized scattered intensity as a function of temperature of 1 mM BSA at pH = 7 (□) in absence of the metal ions, (o) with 0.3 mM Cu^{2+}, (Δ) with 0.3 mM Zn^{2+}, (●) with 1 mM Cu^{2+} and (▲) with 1 mM Zn^{2+}. The experimental error is smaller than symbol dimension.

4.1.1 Thermal aggregation

Figure 4.2 shows the time evolution of the normalized total scattered intensity of native BSA. As can be observed, BSA undergoes the more remarkable changes in the first 20 minutes. During this time, the building of little aggregates with a mean diameter of about 20 nm occurs; their time evolution is shown in figure 4.2b. The analysis of data discussed in paragraph 2.1 allows to obtain the distribution of the diameter values based on the particles number in solution and on the scattered intensity, at different time instants. In figure 4.3, the size distributions based on the light scattered intensity (a) and on the number (b) at the initial (t_0), intermediate (t_m) and final experimental (t_f) times are plotted. As shown in figure 4.3a, after 20 minutes the smallest species embedding the native structure of the protein disappears, while bigger species (prevalently of about 20 nm) appear, suggesting that the aggregation occurs. In particular, after 20 minutes, the main component is centred at about 20 nm as well as the main component after 480 minutes, the latter being narrower because of a relevant component at a greater dimension. This behaviour suggests that the aggregation process of BSA in the selected experimental condition carries out the more remarkable changes in few minutes. As already noted for BLG, also in the distribution of the diameters based on the intensity of BSA, a species having greater dimensions than the BSA native one is present since the first instants of the kinetic; as it was already mentioned, its presence is justified with the probable existence in solution of very few metastable clusters of dense liquid (several hundred nanometres in size) and whose formation occurs within few seconds after the sample preparation **[Pan et al., 2007]**. The distribution of the diameter sizes based on the particles numbers in solution, reported in figure 4.3b, shows that after 8 hours of incubation at 58°C, mainly small aggregates are present in solution, agreement with results reported by **Militello et al., 2004,** indicating that in this case the buffer does not modify the process involved in aggregation. The size distribution based on the particles number in solution (4.3b) allows to argue that only the formation of small oligomers occurs.

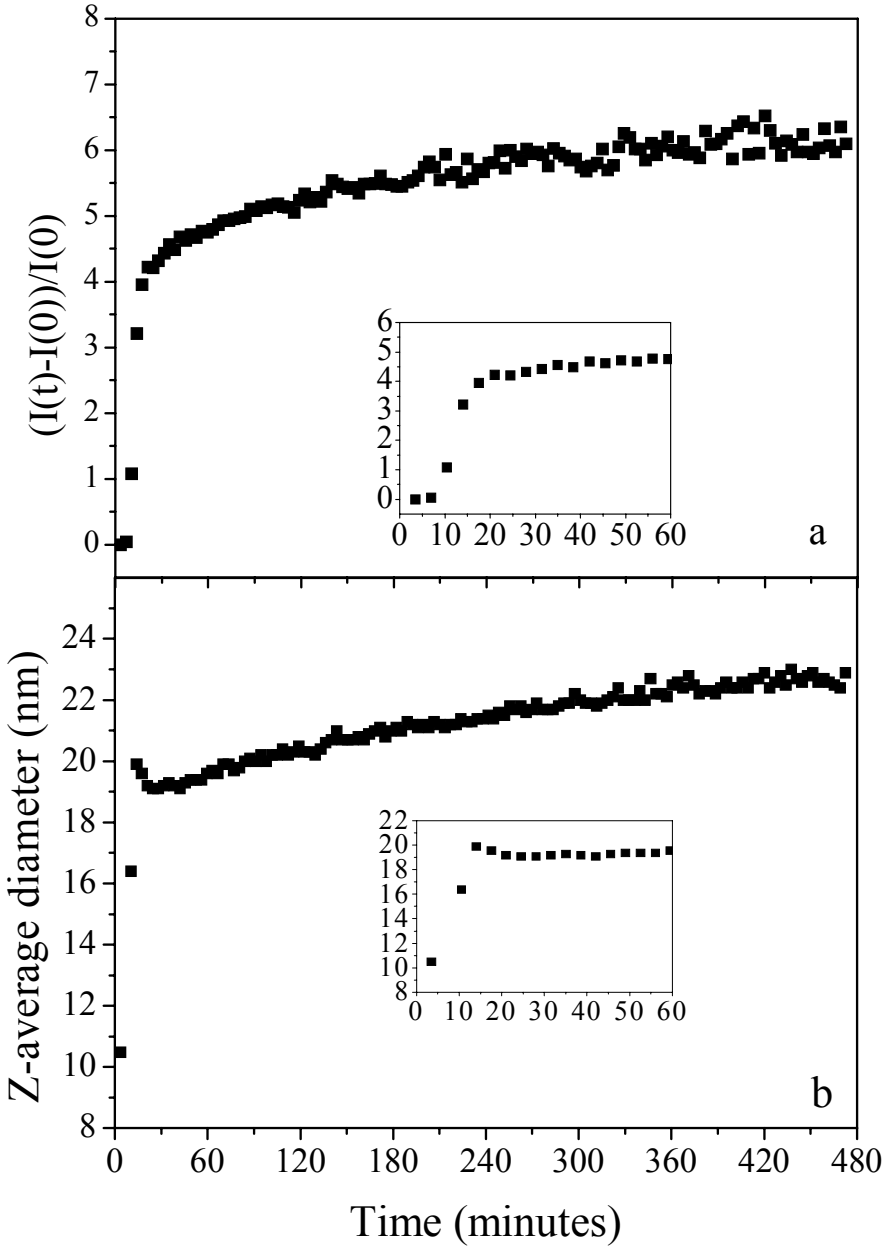

Figure 4.2: (a) Time evolution of the normalized scattered intensity and (b) of the Z-average diameter of 1mM BSA at pH = 7 and T = 58 °C. The insets show a zoom of the scattered intensity and Z-average diameter as a function of time, respectively. The experimental error is smaller than symbol dimension.

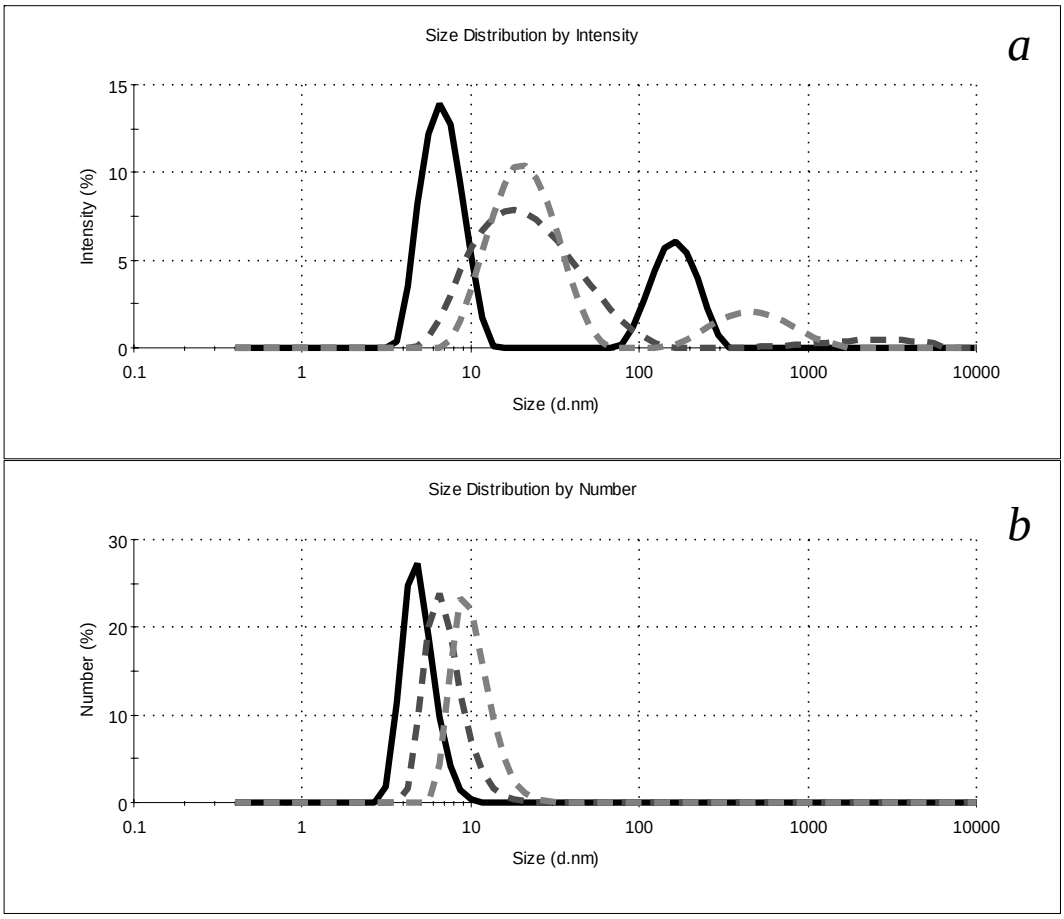

Figure 4.3: Size distributions of BSA aggregates dimension at pH = 7 and T = 58 °C based (*a*) on the intensity of light scattered and (*b*) on the numbers of particles present into solution at different three times of the scattering kinetic. Monitored times are an initial (t_i = 3 minutes, black line), intermediate (t_m = 20 minutes, black dashed line) and final time (t_f = 480 minutes, gray dashed line).

In order to monitor changes in secondary and tertiary structures of the protein in solution, FTIR absorption kinetics in the mid-infrared region have been carried out. In particular, our interest has been focused on the IR absorption band of Amide I and Amide II (see paragraph 2.2.1 for a general description and attribution of these bands). As it has been already said, Amide II band is principally associated to the N-H bending; as a consequence, when the protein is diluted with deuterium too in solution, this band is an efficient probe of the H-D exchange of the hydrogen atoms located in the core of the native protein, the replace being attributable to the heat-induced partial opening of the protein. In figure 4.4a IR differential absorption spectra of BSA solution at different incubation times are shown in the Amide II and II' regions (time increases in the arrows directions). As it can be observed, the signal due to Amide II decreases while that of Amide II' increases and these changes are more remarkable with increasing time. This suggests that a partial unfolding of protein occurs. In figure 4.4b the time evolutions of both Amide II (1540 cm^{-1}) and Amide II' (1450 cm^{-1}) are reported. As it can be observed, the signals reach a plateau in 45 minutes, suggesting that the unfolding of the protein has finished in few minutes. Amide I is an infrared band attributed to an out of phase combination of C = O and C - N stretching of amide groups and it is called Amide I' for the shift towards 1650 cm^{-1} in D_2O. The time evolution of the main spectral components of the band during thermal treatment is a probe of protein structural organization in terms of α–helix, random coil and β–sheet contents and gives information on the intermolecular aggregation through the appearance of two shoulders at about 1620 and 1680 cm^{-1}. Generally, Amide I' band has a composite profile, consisting of different spectral components related to several secondary structures **[Byler et al., 1986, Dong et al., 1990, Cai et al., 1999, Pelton et al., 2000]**. Fig. 4.5a shows the differential absorption spectra of the Amide I' band for BSA protein solution (1 mM) in the IR region between 1580-1720 cm^{-1} recorded at different incubation times (again, time increases in the arrows directions).

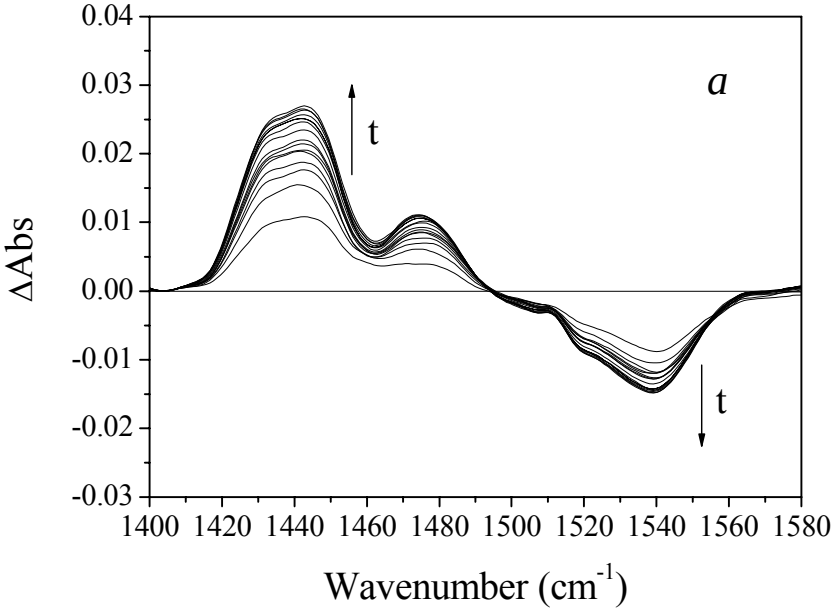

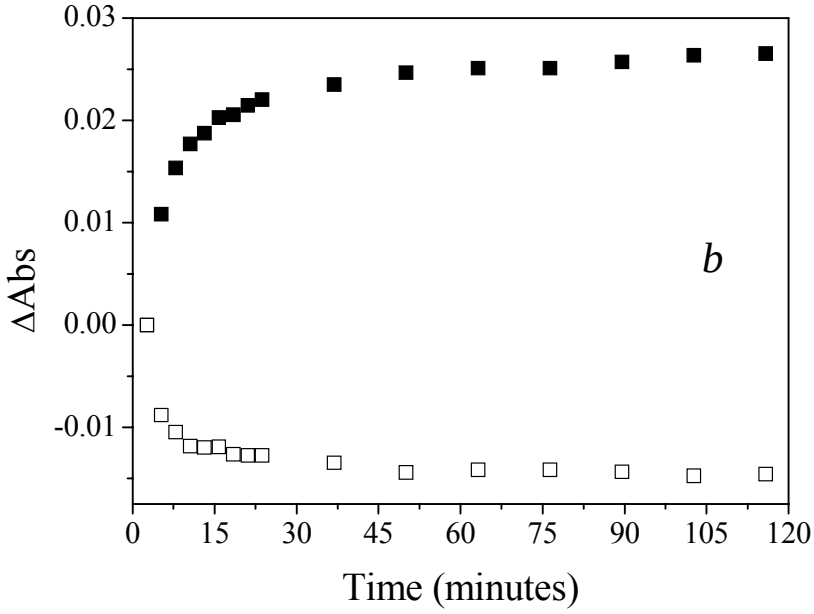

Figure 4.4: (a) FTIR differential absorption spectra in the Amide II and Amide II′ region of BSA at pD = 7 and T = 58 °C; the arrows indicate the Amide II and Amide II′ changes as a function of time. (b) Time evolution of the differential absorption intensity of (■) Amide II′ component at 1442 cm^{-1} and (□) Amide II component at 1540 cm^{-1}.

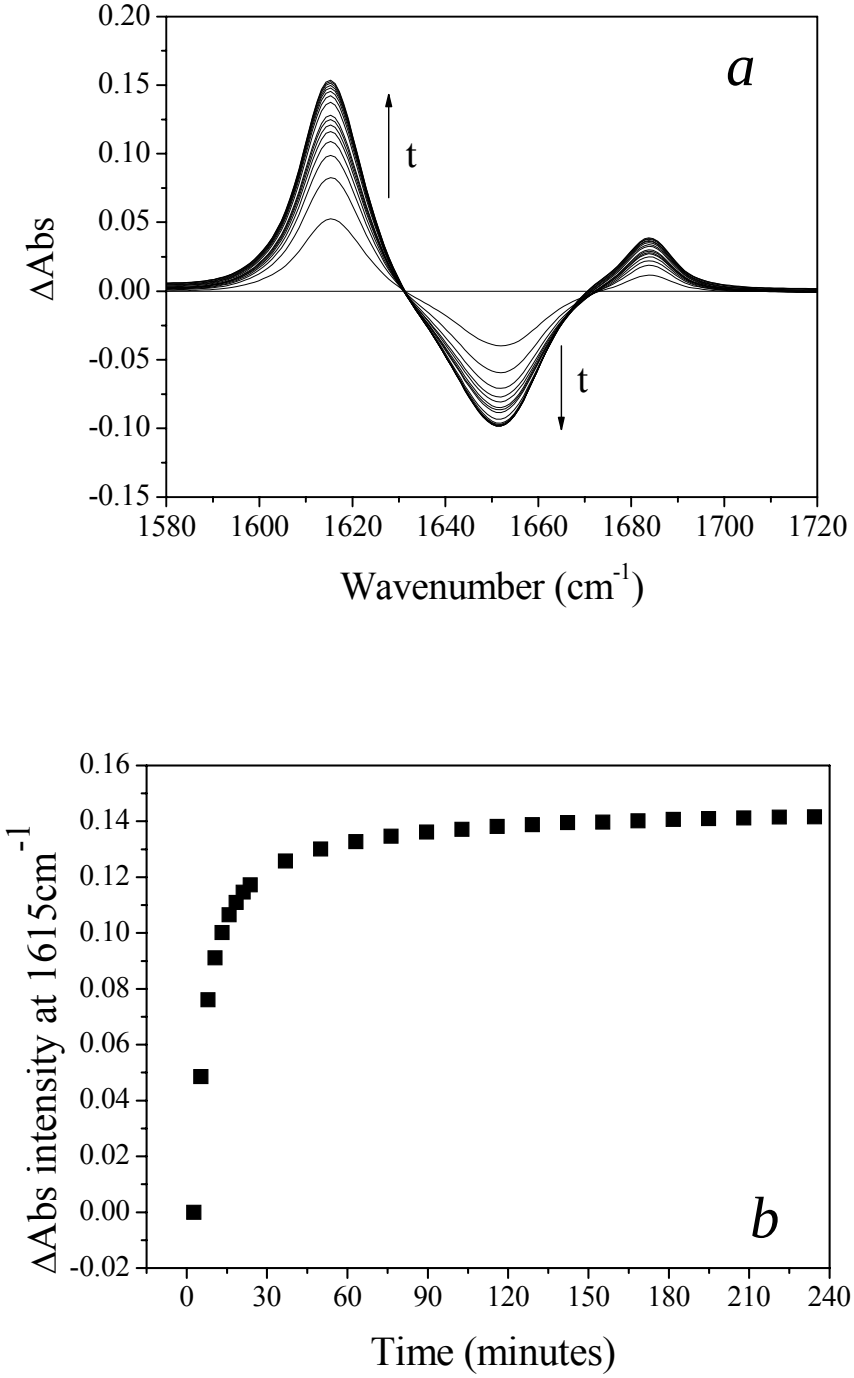

Figure 4.5: (*a*) FTIR absorption differential spectra in the Amide I′ region of BSA at pD = 7 and T = 58 °C; the arrows indicate the Amide II and Amide II′ changes as a function of time. (*b*) Time evolution of the absorption differential intensity of Amide I′ component at 1615 cm^{-1}.

The spectral region between 1630 and 1650 cm^{-1} is attributed to α-helix, disordered random coil and intra-molecular native β-sheet and its decrease is a probe of the conversion from α-helix and intramolecular β-native towards β-aggregated structures **[Fink 1998, Qi et al., 1997, Fang et al., 1997, Levefre et al., 1999, Allain et al., 1999, Militello et al., 2003 and 2004, Remondetto et al., 2003]**. In particular, the bands being probe of the intermolecular aggregation are at around 1614÷1623 and 1685 cm^{-1} and are assigned to vibrations of strongly bound intermolecular β-strands and anti-parallel β-sheets, respectively. In the BSA solution, these bands increase as a function of time, suggesting that aggregation occurs, as confirmed by light scattering data, through the formation of small aggregates. In particular, the spectral component assigned to β-aggregated sheets has its maximum at 1615 cm^{-1}, suggesting the existence of stronger H-bonds, necessary to the network of intermolecular bonds preceding the sample gelation **[Allain et al., 1999, Remondetto et al., 2003, Navarra et al., 2007]**. The time evolution of the latter component is shown in figure 4.5b: we can argue that the partial protein opening, the aggregates building and the formation of stronger H-bonded network are contemporary processes. The appearance of a component at about 1615 cm^{-1} has also been observed for BLG heated at 60 °C in presence of Cu^{2+}; the formation of small dimensions aggregates and the contemporary appearance of a band at 1614 cm^{-1} is to attribute to the initial formation of a network made by very strong intermolecular H-bonds. For BLG, it was argued that, during heating, aggregates of Cu-BLG can choose this alternative path leading to gelation in respect to its usual aggregation process **[Navarra et al., 2007]**. Native BSA seems to have the same behaviour: formation of small aggregates preceding gelation. The behaviour of the component at about 1615 cm^{-1} was expected, considering that BSA solution at concentration of 1 mM and at 58 °C is in the gel region of the phase diagram (see figure 1.18 for more details). Indeed, as it will be reported later, rheological measurements of BSA after an incubation of two hours at 58 °C has revealed that the protein solution presents a weak solid-like character with the elastic modulus, G′, greater than the viscous one, G′′, in the

frequency range 0.1 ÷ 200 rad /s suggesting that after the thermal treatment the globular protein solution is already structured.

As it has been already said, the results here reported are in agreement with those obtained for BSA diluted in phosphate buffer **[Militello et al., 2004]**, indicating that in this case the buffer have not modified the process involved in the aggregates formation. Indeed, at pD values far from the pI of the protein (~ 5), i.e. when the protein has a net charge, the aggregation proceeds in an ordered way: formation of β-aggregates of small dimensions, around 20 nm, originated by α-helix conversions in β-aggregated structures **[Militello et al., 2004]**.

4.1.2 Effects of the presence of copper or zinc

On the basis of these early results, the influence of metal ions on the time evolution of the aggregation process of BSA has been studied at 58°C, pH=7 and with the metal/protein concentration ratio already used for BLG samples. As for BLG, the first step of the investigation is to analyse the dependence of the normalized light scattered intensity as a function of temperature, when the metal is inserted or not in solution with the same metal/protein concentration ratio of the BLG samples (empty symbols in figure 4.1). It is evident that the metal in solution does not affect dramatically the evolution of the scattered light intensity as a function of temperature, not depending on the concentration of both metals. Thus, as it concerns the obtained results on the time evolution of the aggregates growth and of the conformational changes of secondary and tertiary structures in presence of metal in solution, only the ones obtained in the experimental condition of the metal/protein concentration ratio of 0.3:1 will be reported, being the same used for the BLG samples. The activation temperature is about 54°C and it has been estimated via temperature scanning of the scattered intensity. Above this temperature value, the rate of the scattered light growth is very high; thus, a very fast time evolution of the scattering kinetics is expected at 58°C.

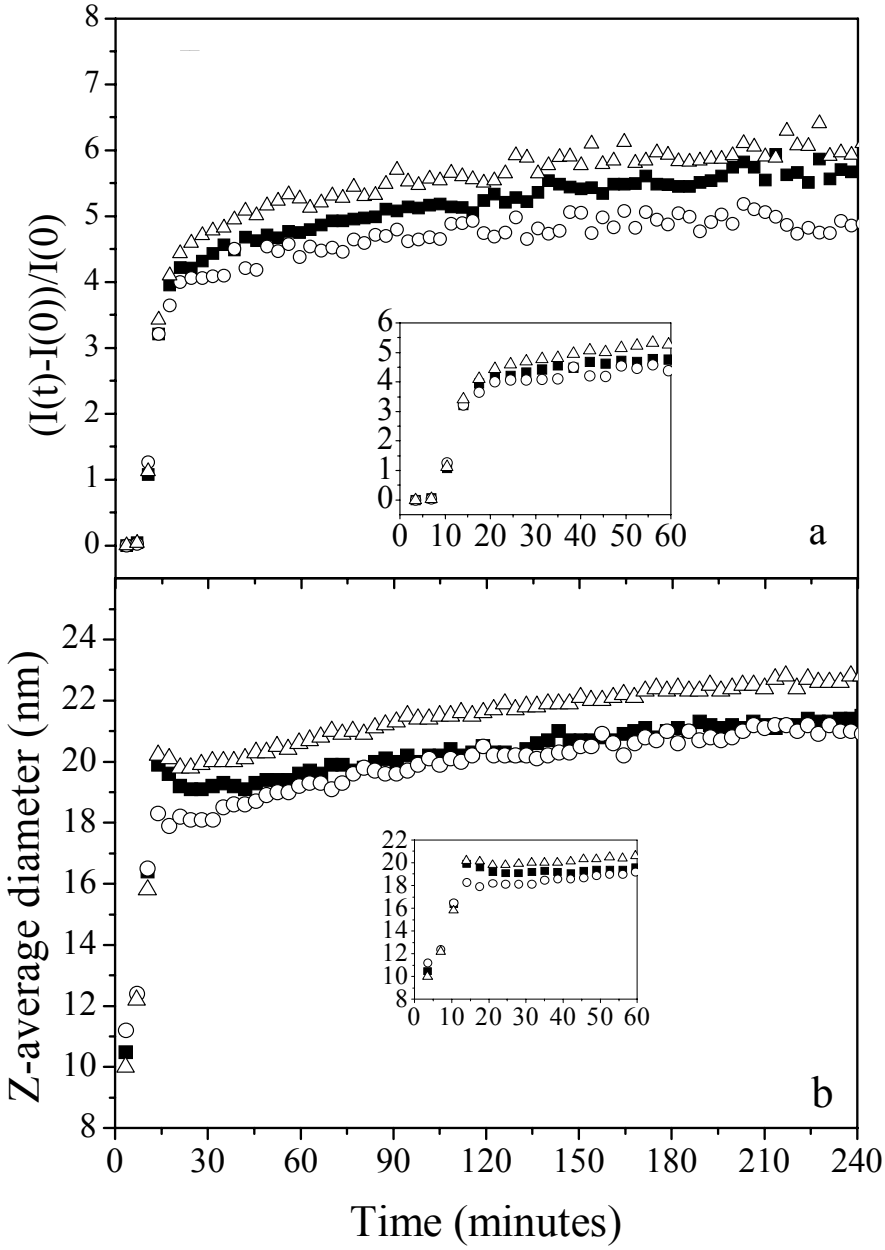

Figure 4.6: (a) Time evolution of the normalized scattered intensity and (b) of the Z-average diameter of (□) BSA, (○) Cu-BSA and (Δ) Zn-BSA at pH = 7 and T = 58°C. The insets show a zoom of the scattered intensity and Z-average diameter as a function of time, respectively. The experimental error is smaller than symbol dimension.

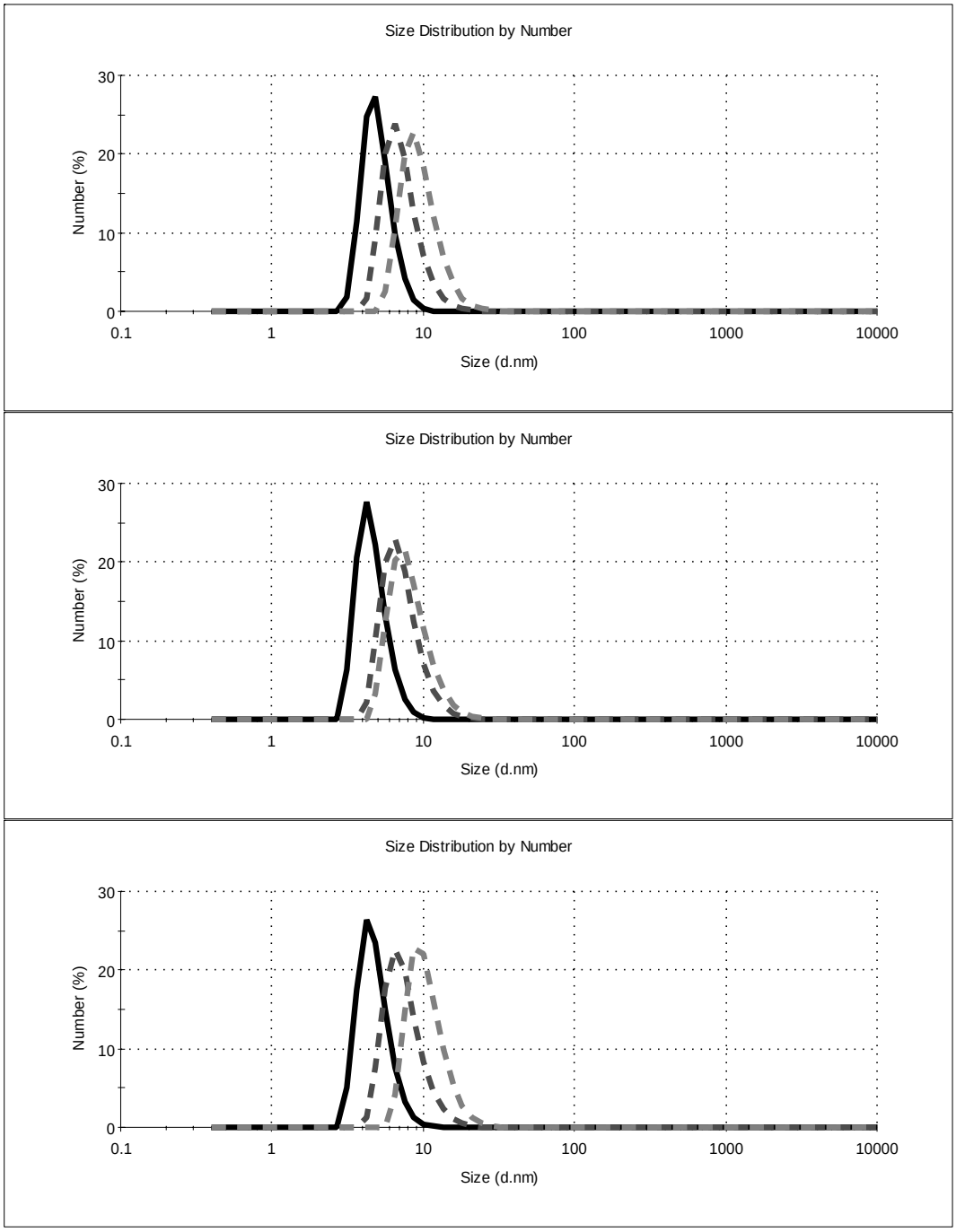

Figure 4.7: Size distribution of the aggregates dimension based on the number of the particles into solution at different three times of the scattering kinetic. Monitored times are an initial (t_0 = 3 minutes, black line), intermediate (t_m = 20 minutes, black dashed line) and final time (t_f = 240 minutes, grey dashed line). (up) BLG, (middle) Cu-BLG and (bottom) Zn-BLG at pH = 7 and T = 58 °C.

The time evolutions of the scattered light intensity and of a z-average diameter at 58°C up to 240 minutes are shown in figure 4.6. During the incubation, in presence of zinc in solution (Zn-BSA), BSA aggregates having greater dimensions are formed. In the reported kinetics no lag-phase is observed and a substantial increase of the scattered light and of Z-average diameter occurs during the first 18-20 minutes, as it can be seen in the insets of figure 4.6. However, also after 20 minutes, the aggregates growth has not completed, as it can be observed by the size distributions of the species in solution based on the number of the particles. In figure 5.7 the aggregates growth is shown at the initial time, t_i, at the intermediate time, t_m, (about 15 minutes after t_i) and after 240 minutes, t_f, for BSA (upper panel), Cu-BSA, (middle panel) and Zn-BSA (bottom panel). It is important to recall that the dimension of BSA aggregates after 240 minutes is not the final dimension. The final dimension has been estimated as about 22 nm and it is reached after about 480 min. According to the evolution time of the z-average in figure 4.6b, the time evolutions of the dimension growth of BSA and Cu-BSA aggregates are very similar; the distributions of the aggregates diameters show that the growth of the Cu-BSA aggregates is slower than that of BSA and Zn-BSA aggregates. The latter have a dimension slightly greater than the others, but fundamentally the features of the time evolution and the dimension of the aggregates of BSA in absence and in presence of metal ions in solution remains unchanged, i.e. about 22 nm. Thus, in last analysis, the presence of the metal ions in solution does not affect dramatically the time evolution of the aggregates growth. Only an initial slight inhibitory effect of copper ions has been observed. However, the diameters distribution based on the number of particles in solution, reported in figure 4.7, probes that there is only one predominant aggregated species having a diameter of about 22 nm. The high rate aggregates formation prevents to fit data in order to determine the fractal dimension of their structure.

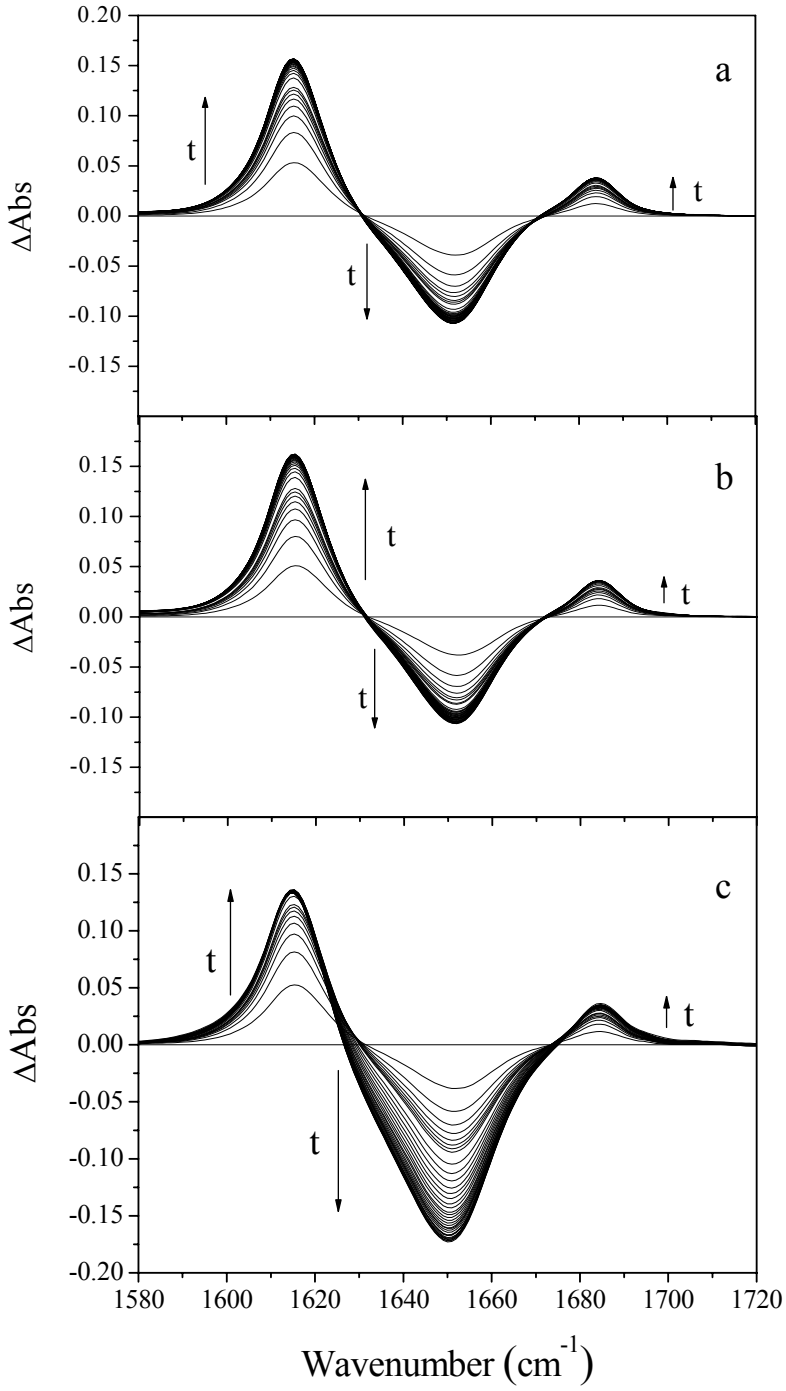

Figure 4.8: FTIR absorption differential spectra in the Amide I′ region of (a) BSA, (b) Cu-BSA, (c) Zn-BSA at pH = 7 during the incubation at T = 58°C for 6 hours. The arrows indicate the Amide I′ changes as a function of time.

As BLG, BSA undergoes conformational changes when subjected to a temperature increase. To investigate the possible modifications induced by metal ions on the conformational changes caused by the temperature increase on the secondary structure, Amide I′ changes of BSA, Cu-BSA and Zn-BSA solutions have been studied at the same experimental conditions. Differential spectra are shown in figure 4.8. It is evident that the behaviour of the Amide I′ changes are very similar in all the investigated cases. The components at about 1615 cm^{-1} and 1680 cm^{-1}, attributed to the vibration of anti-parallel β-aggregated, increase as a function of time, indicating that an aggregation process occurs; simultaneously, the component at about 1650 cm^{-1} decreases, indicating that the conversion of native α-helices in β-aggregated structures has occurred. It is evident a stronger decrease of α-helix structures for Zn-BLG. This can be related to a feature of the zinc ions that will be explained in the following. A study realized on beta amyloid peptide **[Stellato et al., 2006]** has shown that zinc ion forms complex with a more open hexa-coordinated geometry than the penta-coordinated one of the Cu–peptide complex, making itself available for further interaction. Zinc ion can bind two histidine and four oxygen atoms; al least one of four may belong to the water in the solvent (open structure). Finally, it may induce the formation of ordered aggregates, according to a model in which the metal plays the role of a bridge between the imidazole rings of two histidine residues possibly belonging to different peptides **[Stellato et al., 2006]**.

In order to compare the extent of the aggregation process in BSA, Cu-BSA and Zn-BSA solutions, the time evolutions of the components at about 1615, 1650 and 1684 cm^{-1} have been studied, after having normalized the intensity values to the absorption maximum of the Amide I′ bands. Through the changes of these bands, the α/β conversion and the building of intermolecular β-aggregates can be monitored. With respect to the aggregation process, no change is induced by the presence of metal ions in solution.

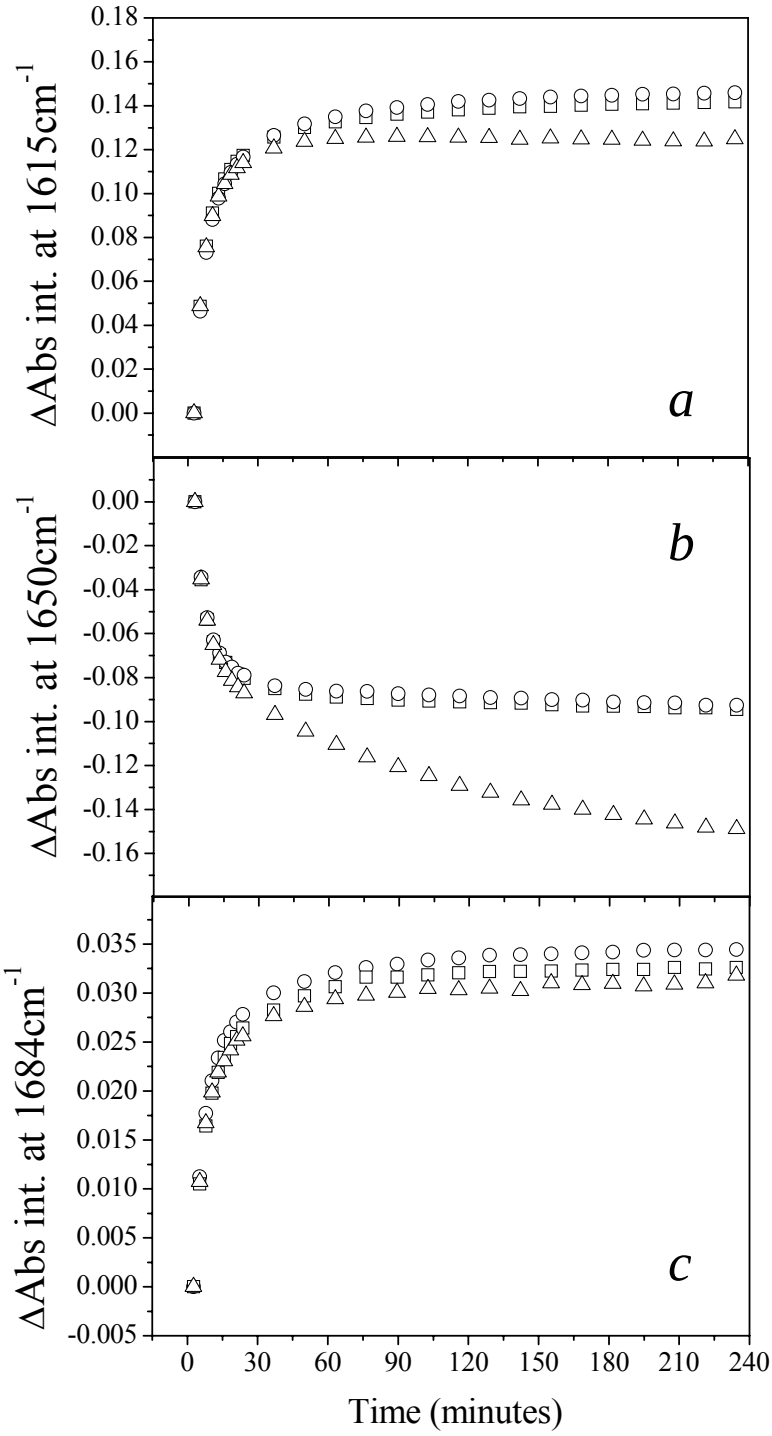

Figure 4.9: Time evolution of the normalized FTIR differential absorption intensity of Amide I′ components: (a) at 1615 cm-1 (up panel), (b) at 1650cm^{-1} (middle panel) and (c) at 1684cm^{1} (bottom panel) for (□) BSA, (○) Cu-BSA, (Δ) Zn-BSA at pH = 7 and T = 58 °C. The experimental error is smaller than symbol dimension.

Through the results obtained by light scattering and FTIR measurements, it can be concluded that the heat-induced aggregation process of BSA at neutral pH incubated at 58 °C is substantially independent on the presence of metal ions in solution. Only a very light inhibitory effect of copper mainly in the first phase of the scattering kinetic, and, on the contrary, a slight promoter effect of zinc have been revealed, suggesting that metals play the same roles assumed during thermal aggregation of BLG at neutral pH. However, in this case, zinc do not induce the aggregates formation with a remarkable increased dimension; this can be due to a higher conformational stability of BSA respect to BLG, probably due to a different secondary structure and/or to a higher number of disulphide bonds present in BSA at neutral pH. Moreover, no evidence of a specific coordination between metal and protein has been observed. It is noteworthy that the conformational changes of the secondary structure monitored by FTIR measurements and the evolution of the aggregates growth monitored by scattering measurements have a similar behaviour as a function of time. The more important changes occur during the first 20 minutes.

Summary. The results shown and discussed in this section highlight that the aggregation process of BSA at pH = 7 induced at 58°C is characterized by the building of β–aggregates having small dimensions that prevalently come from the α-helix changes. The experimental observations allow to observe that this aggregation process is not dramatically affected by Cu^{2+} and Zn^{2+} in solution. This behaviour is probably due to the BSA ability to bind metal ions in inner hydrophobic sites, making them unable to promote aggregation process via bridging or, more simply, screening effects.

Chapter 5

Experimental results: Proteins cold gelation induced by metal ions

5.1 β-Lactoglobulin cold-gels induced by copper or zinc ions

Cold-set gels of BLG induced by different concentration of $CuCl_2$ or $ZnCl_2$ have been studied. In particular, the pre-heating step of the protein solution has been monitored by dynamic light scattering and FTIR kinetics. Then, viscoelastic properties of gels have been investigated via rheological measurements.

5.1.1 Characterization of the BLG pre-aggregates

The experimental conditions of the measurements here presented are described in Chapter 4 concerning the thermal aggregation of BLG at pH 7. In the present section results strictly involved in the characterization of pre-aggregates leading to the gel formation are reported, sending you back to the paragraph 4.1 for more details. Data reported in figure 5.1a illustrate how the mean mass value and the mean diameter of particles in solution increase linearly as a function of time.

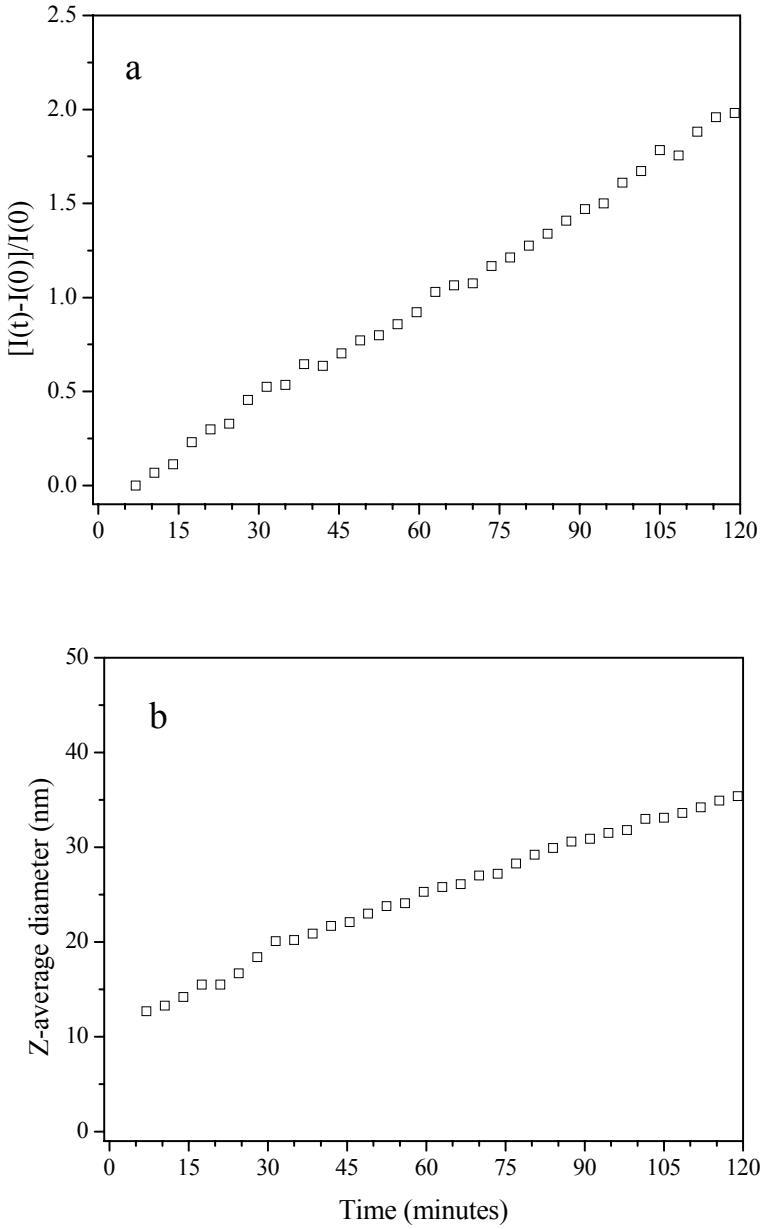

Figure 5.1: (a) Time evolution of the normalized scattered intensity and (b) of the Z-average diameter of BLG at pH = 7 and T = 60 °C. The experimental error is smaller than symbol dimension

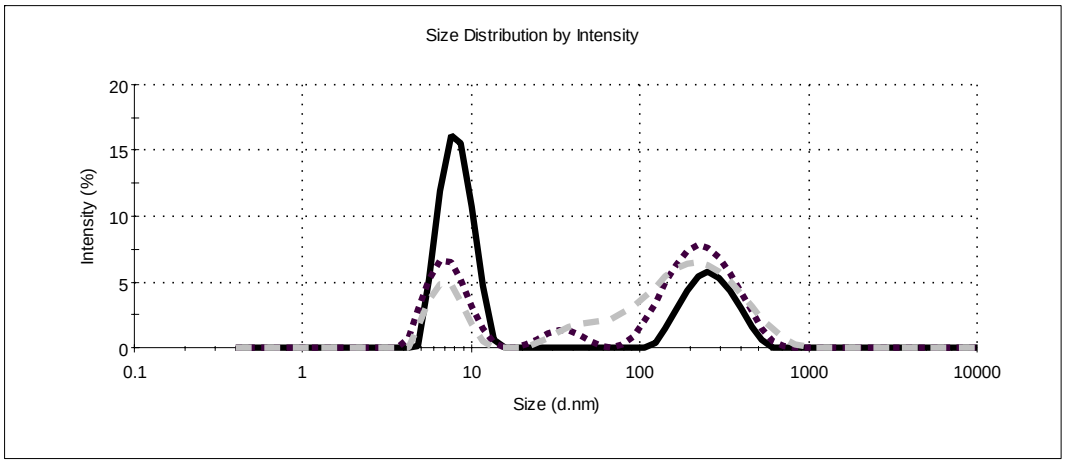

Figure 5.2: Size distribution of aggregates dimension of BLG at pH = 7 and T = 60°C based on the intensity of the scattered light at different three times of the scattering kinetic. Monitored times are t_0 = 3 minutes (black line), t_m = 60 minutes (grey long dashed line) and t_f = 120 minutes (dark grey short dashed line).

Moreover, the diameter size distribution shows that a greater species increases consequently to the decrease of the native species (figure 5.2). This is consistent with a linear association of the native species in solution in agreement with the model of Roefs and de Kruif (1994). The fractal dimension of the aggregates, obtained according to relation 3.1 at page 81, was about 1.5; this value is consistent with an amorphous shape of the greater species, grown via linear association of the native units, whose spatial conformation results by its folding. At the end of the heating treatment, the aggregates have a mean dimension of about 35 nm, suggesting the formation of small aggregates. The infrared spectra in the Amide II / Amide II' and in the Amide I' regions, shown in figures 5.3 and 5.4 respectively, and the time evolution of Amide II' and of the β-aggregated structures, shown in figure 5.5, allow to argue that the aggregates formation is contemporaneous both to the partial unfolding of the several proteins in solution, monitored via the decrease of Amide II and the corresponding increase of the Amide II', and to the conformational changes of the secondary structures proper of the thermal aggregation of BLG. The latter consists prevalently in the conversion of native β–sheets (at ~1634 cm^{-1}) into β-aggregates structures (at ~1623 cm^{-1}), being BLG a protein characterized by the predominant presence of native β-sheets rather than α-helical structures (see paragraph 3.1 for the bands attribution and further comments). Finally, a comparison between the spectra of BLG obtained at room temperature before and after the heat-treatment of the protein is reported in figure 5.6 in order to verify that the changes induced by the heating are irreversible. As it has been already said, the variations of the band shape due both to the increase of the band intensity at ~1625 cm^{-1} and at ~1680 cm^{-1} and to the decrease of the band intensity at ~1635 cm^{-1} indicate that the heating at 60 °C for 2 hours induces irreversible changes on the secondary structure of BLG, leading to the formation of small β-aggregates through the conversion of the native β-sheets and α-helical structures **[Fink 1998, Qi et al., 1997, Fang et al., 1997, Levefre et al., 1999, Allain et al., 1999, Militello et al., 2003 and 2004, Remondetto et al., 2003]**.

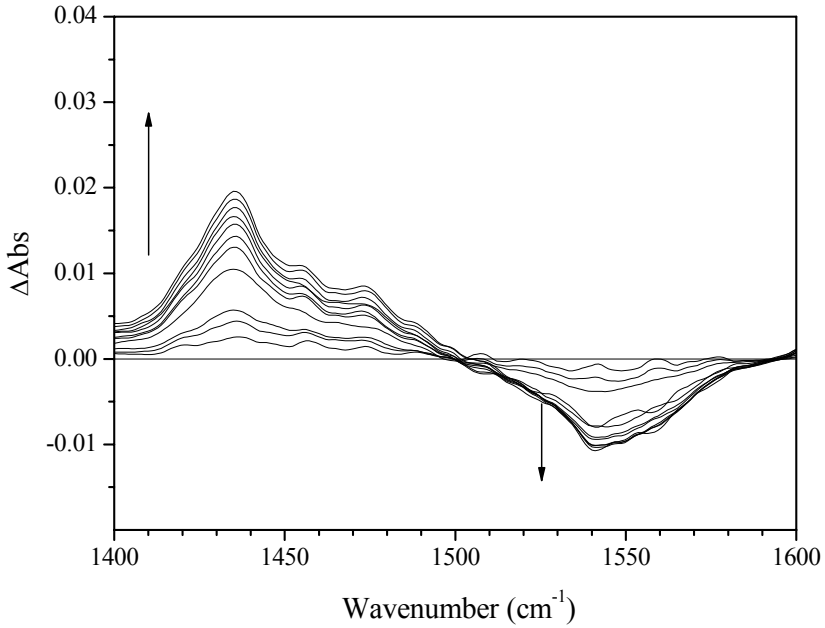

Figure 5.3: FTIR differential spectra of BLG at pH = 7 in the Amide II/Amide II′ during the incubation at T = 60 °C for 2 hours. The arrows indicate the Amide II and Amide II′ changes as a function of time.

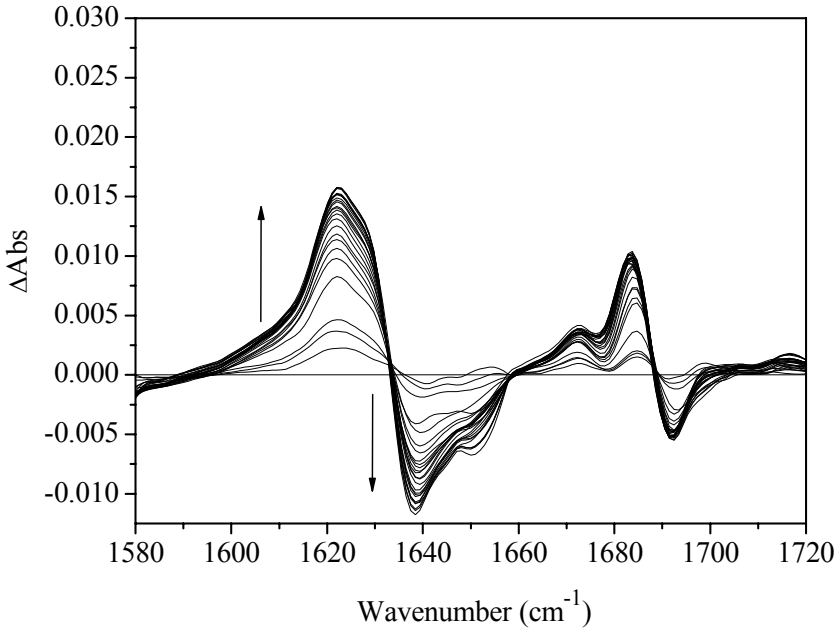

Figure 5.4: FTIR differential spectra of BLG at pH = 7 in the Amide I′ during the incubation at T = 60 °C for 2 hours. The arrows indicate the Amide I′ changes as a function of time.

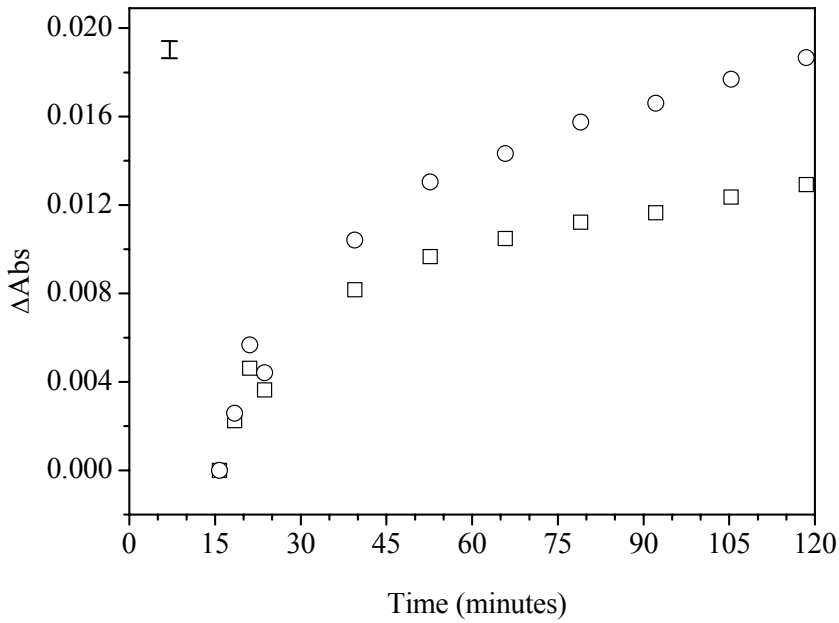

Figure 5.5: Time evolution of the FTIR differential absorption intensity of *(a)* Amide II′ (o) components at 1436 cm^{-1} and of *(b)* Amide I′ (□) at 1623 cm^{-1} of BLG at pH = 7 and T = 60 °C. Error bar at the top on the right is the experimental error estimated for differential absorption values.

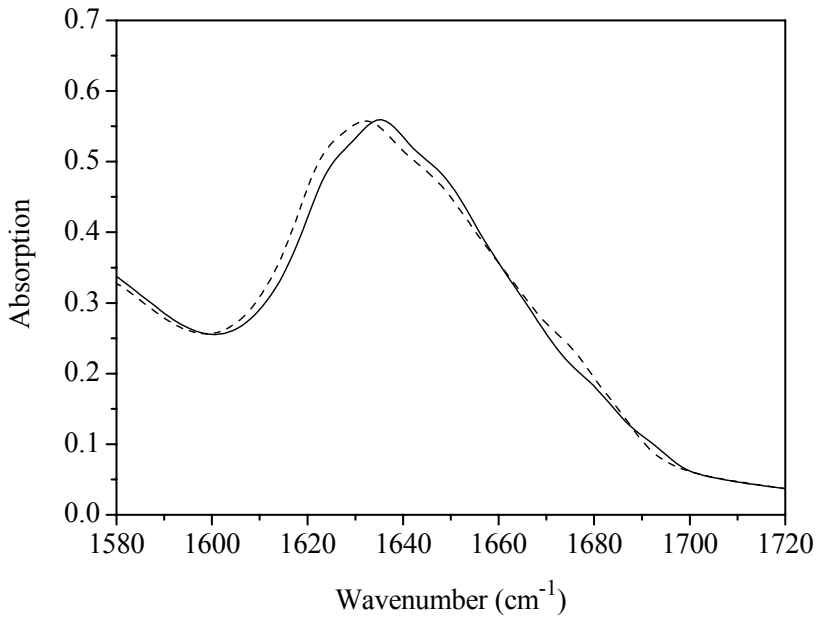

Figure 5.6: FTIR absorption spectra of BLG at pH = 7 realized at room temperature before (continuous line) and after (dashed lines) the heating for 2 hours at T = 60 °C.

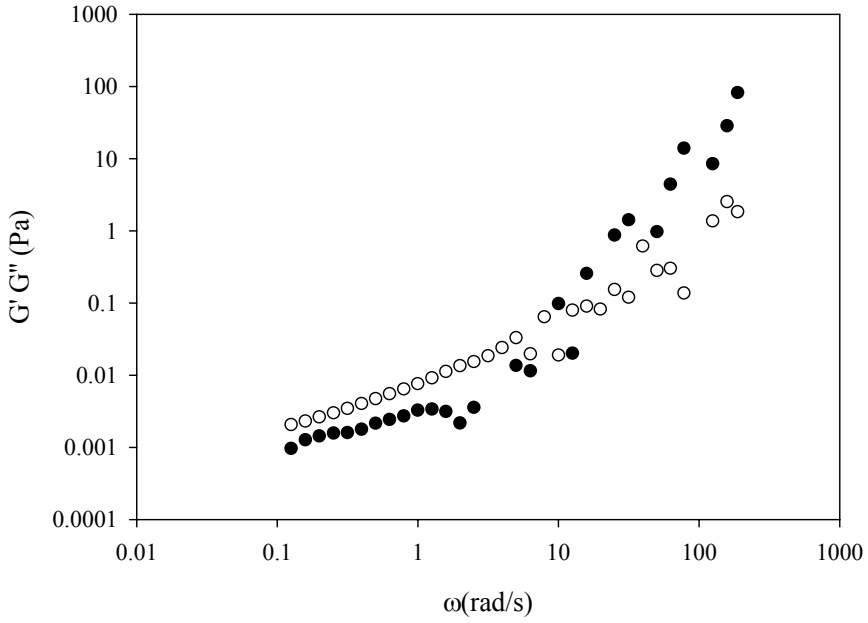

Figure 5.7: Elastic G′ (●) and viscous G′′ (o) modulus as a function of oscillation frequency of BLG solution at pH = 7, after incubation at 60 °C for 2 hours. The frequency sweep has been realized at 20 °C.

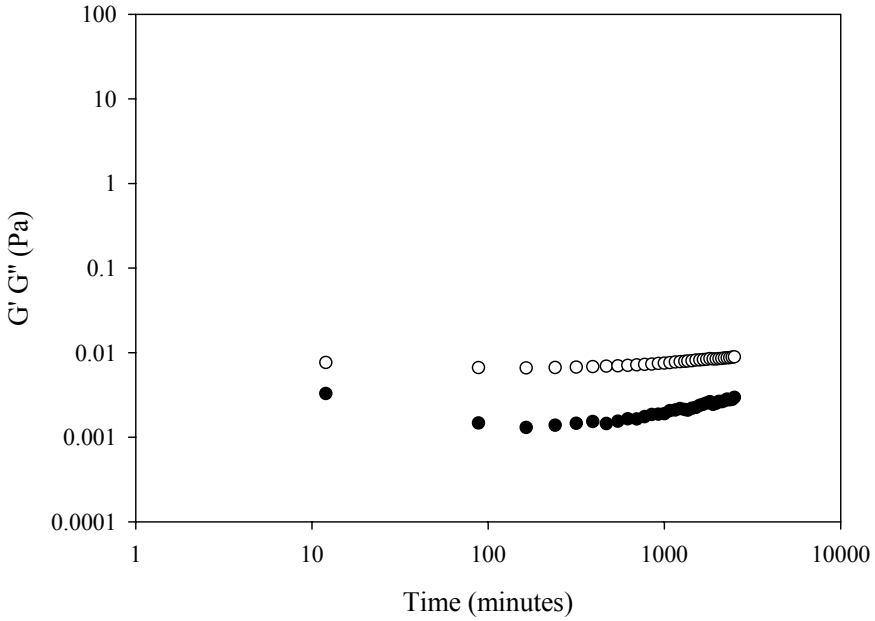

Figure 5.8: Elastic G′ (●) and viscous G′′ (o) modulus as a function of time of BLG solution at pH = 7 after incubation at 60 °C for 2 hours. Kinetic measurements have been realized at 20 °C.

The viscoelastic properties of pre-heated BLG solution have also been investigated at 20 °C with the aim to verify the absence of a solid-like character of the solution immediately after the heating. Mechanical spectra, reported in figure 5.7, show that the protein solution does not present a solid-like character. In fact, the elastic modulus, G′, is smaller than the viscous one, G′′, in the frequency range 0.1 ÷ 200 rad/s; this result indicates that after thermal treatment the globular protein solution is not yet structured. The aging of the pre-heated BLG solution has been analysed in order to verify if the gel formation occurred as a function of time. The evolution of G′ and G′′, reported in figure 5.8, indicates that G′ is smaller than G′′ during the whole observation time. After 33 hours from its cooling, the pre-heated BLG solution does not show any gel formation.

5.1.2 Gels characterization

The addition of metal ions in pre-heated protein solution at room temperature induces the formation of gels. In figure 5.9, from left to right, is shown the macroscopic aspect of three gel samples obtained at a protein concentration of 3.3 mM after addition of 10 mM of zinc ions (10Zn-BLG), 30mM of zinc ions (30Zn-BLG) and 30 mM of copper ions (30Cu-BLG). We do not report here a picture of the gel of 10Cu-BLG. It was obtained at the same concentration of the protein and induced by 10 mM of copper ions (10Cu-BLG), and it appeared having a consistence similar but a more marked blue colour in respect to 30Cu-BLG. All samples appeared non homogeneous and not transparent.

The viscoelasticity of networks formed adding metal ions to the pre-heated BLG solution has been investigated using small deformation dynamical rheological measurements. In particular, the behaviour of the storage modulus (G′) and loss modulus (G′′) as a function of frequency and of time, at a fixed frequency, has been evaluated immediately after the addition of the gelling agents.

Figure 5.9: Gels of 3.3 mM BLG induced by zinc and copper ions at different concentration; from left to right: 10Zn-BLG, 30Zn-BLG and 30Cu-BLG.

The behaviour of the G′ and G′′ of BLG metal ions-induced gels as a function of time is reported in figure 5.10. In figure 5.11 data relative to the pre-heated BLG solution and to the acid-induced gel of BLG are inserted together with the 30Zn-BLG for comparison. Rheological measurements, carried out immediately after the addition of the gelling agent to the cooled BLG solution, show that the G′ values are larger than G′′ ones, confirming the gel formation. Moreover, G′ values are higher than those relative to the BLG pre-heated solution shown again in figure 5.11. This result indicates that all the investigated samples have an elastic character stronger than that measured in the pre-heated BLG solution. As illustrated in figure 5.10, the formation of BLG gels induced by metal occurs within 10 minutes; both the storage and loss moduli do not present a lag time, but a short approach towards the respective asymptotic equilibrium values. Gelation process of metal-induced gels is different from that of acid-induced gels. The comparison between 30Zn-BLG and A-BLG shown in figure 5.11 puts well in evidence the gradual increase of G′ in the acid-induced gel (A-BLG) due to the gradual decrease induced by acid of the pH value toward pI of the protein.

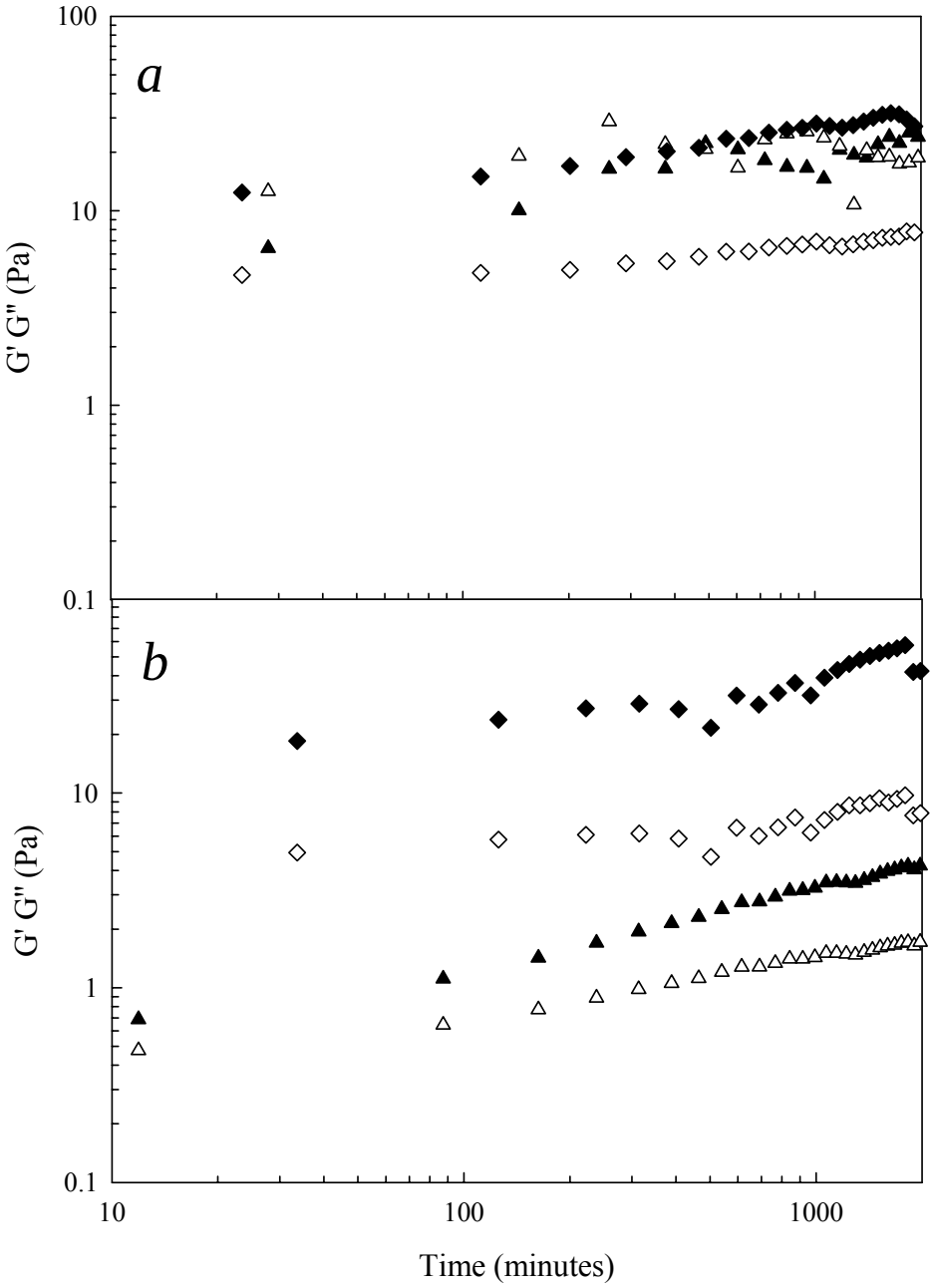

Figure 5.10: Elastic G′ (full symbols) and viscous G′′ (empty symbols) modulus as a function of time of (*a*) Cu-BLG and (*b*) Zn-BLG gels. The metal ions concentration was (Δ) 10 mM and (◊) 30 mM. Kinetic measurements have been realized at 20 °C.

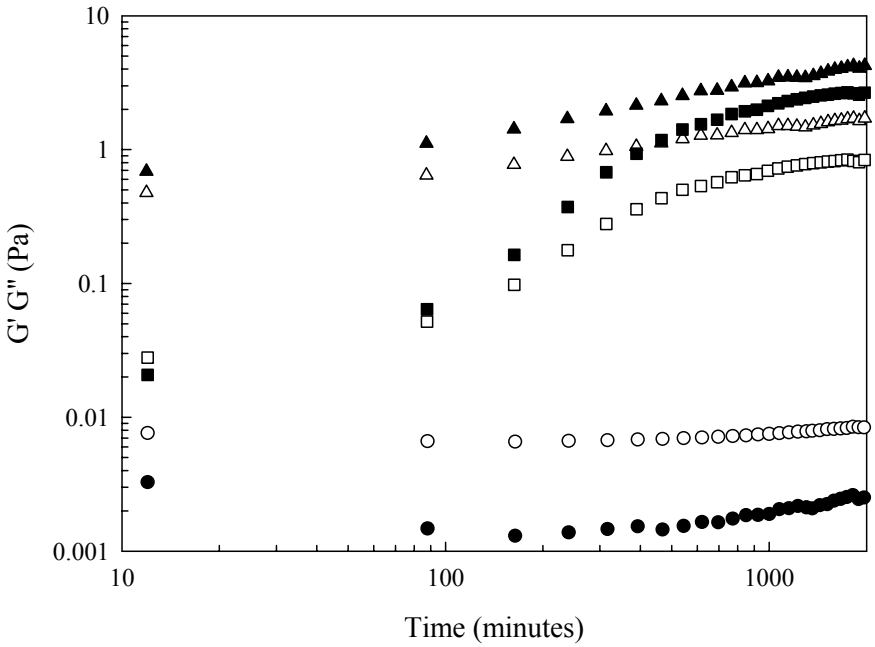

Figure 5.11: Elastic G′ (full symbols) and viscous G′′ (empty symbols) modulus as a function of time of (○) pre-heated BLG solution, (□) acid-induced BLG gel and (Δ) 30Zn-BLG. Kinetic measurements have been realized at 20 °C.

Gels induced by adding copper, both 10 and 30 mM (figure 5.10a), have comparable G′ but different G′′ values, the lower being that obtained at 30 mM Cu, suggesting that in this case a gel with predominant elastic character has been obtained. The decrease of the G′ value after about 1000 minutes in the 10Cu-BLG sample is probably caused by skidding of the instrument cone on the gel because of syneresis process in BLG gels. When $ZnCl_2$, at the two concentrations used here, was added to pre-heated BLG solution, gel formation was induced in both cases. In particular, as shown in figure 5.10b, at 30 mM Zn G′ values are higher than those measured at 10 mM, indicating a larger elastic behaviour for the former gel. Moreover, for 30Zn-BLG a difference between the G′ values and the G′′ values larger than in 10Zn-BLG is observed, confirming once again the more elastic character of the former **[Chen et al., 1999]**. Our data do not agree with the results reported in **Remondetto et al., 2003**. After the addition of Fe ions to the pre-heated BLG solution, they observe a decrease of the elastic behaviour of the cold-induced gels when the iron concentration increases. This discrepancy can be due to the formation of different

typologies of gel in dependence on the iron concentration. At low iron concentration, 10 mM, the authors report the formation of a gel with a filamentous structure, while at higher concentration, 30 mM, the formation of a gel with a random-aggregated structure was observed **[Remondetto et al., 2002 and 2003]**. In the former case, the gel appears transparent, in the latter opaque and brittle. On the contrary, no gels studied in this thesis were transparent, suggesting the formation of random-aggregated structures promoted by an electrostatic screening effect due to the introduction of charges in solution. From this point of view, the pre-aggregate conformation could have affected the final gel obtained after metal addition. As far as this aspect is concerned, it is also important to underline that the incubation temperature used by **Remondetto et al., 2003** is higher than the denaturation temperature of the protein. It is well known that the temperature and the prolonging of the heating time affect the number and the properties of the pre-aggregates **[Baussay et al., 2004, Ju et al., 1998]** and that a solution of native whey protein must be heated up to a temperature higher than at least 70 °C before the molecules unfold and aggregate into filamentous structures **[Barbut et al., 1993, Bryant et al., 1998]**.

The effect of the different kind of metal ions on the viscoelastic properties of gels has been investigated in equal conditions of metal concentration. The gels induced by 10 mM and 30 mM of metal ions are compared in figure 5.12. We may observe that:

- the gels formed at an ions concentration of 10 mM show a different behaviour depending on metal type, copper or zinc;
- at a concentration of 10 mM, gel formed in presence of Cu^{2+} exhibits a G' value higher than that obtained in presence of Zn^{2+};
- at a concentration of 30 mM, both Cu^{2+} and Zn^{2+} have an analogous effect on the rheological properties of gels.

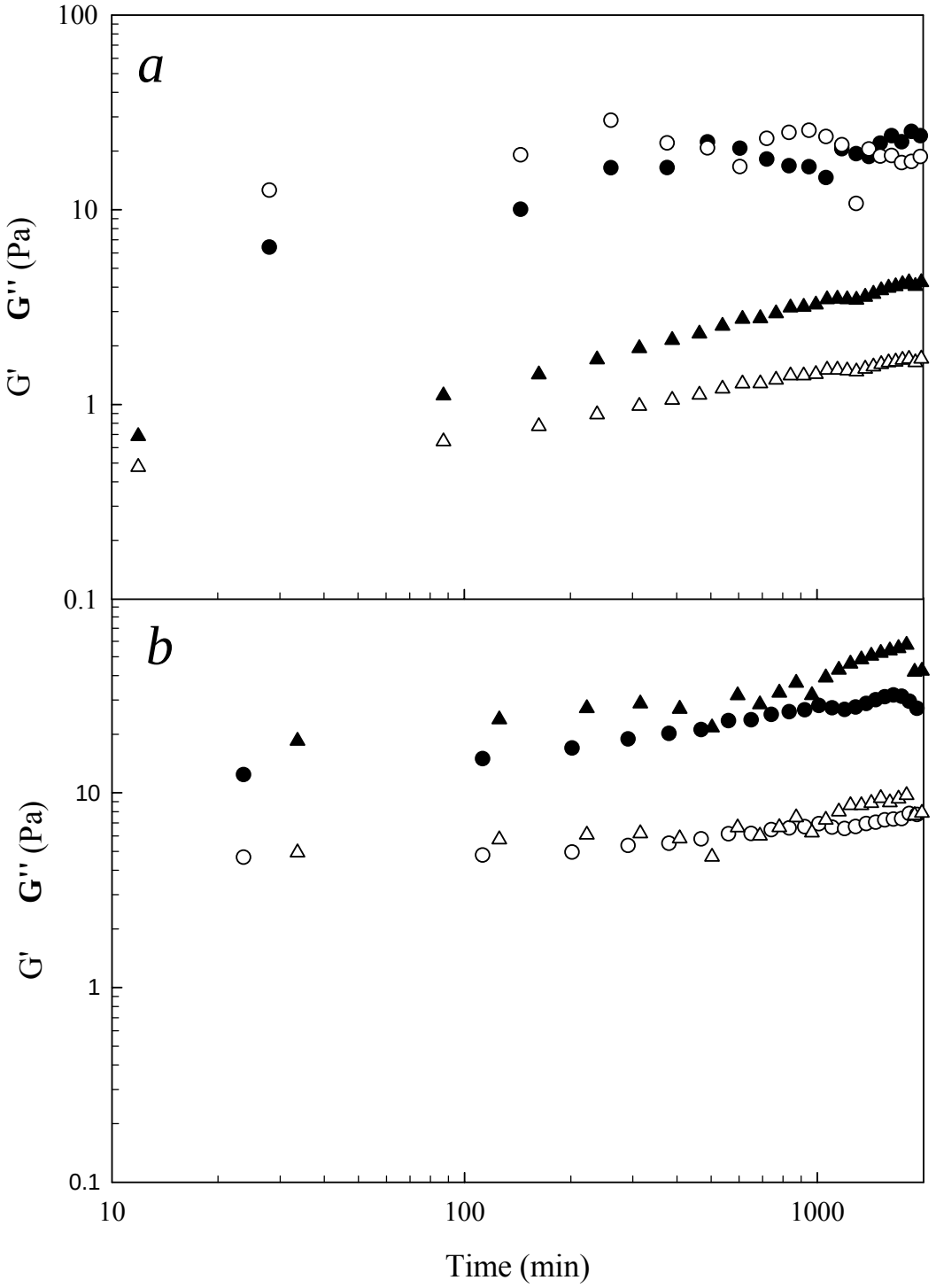

Figure: 5.12 Elastic G′ (full symbols) and viscous G′′ (empty symbols) modulus as a function of time of BLG gel induced by (*a*) 10 mM or (*b*) 30 mM of (o) $CuCl_2$ or (Δ) $ZnCl_2$. Kinetic measurements have been realized at 20 °C.

The reason of the different behaviour of the 10Cu-BLG sample can be explained on the base of the results obtained and already discussed in chapter 4 by the FTIR and dynamic light scattering study of the thermal aggregation of BLG in presence of copper. In fact, those data allowed to conclude that copper did not affect markedly the size evolution of the aggregates but induced the formation of β-aggregates more strongly H-bonded to the network as revealed by the contribution at 1614 cm^{-1} illustrated in figure 3.15b. The appearance of the shoulder at about 1590 cm^{-1} attributed to the asymmetric stretching of CO^{2-} when coordinated with Cu^{2+} **[Mesu et al. 2003]** suggested a direct interaction of copper with a specific site of the protein. This specific interaction may also occur between the partial unfolded pre-aggregates in the cooled BLG solution and copper ions and, as a consequence, it may account for the premature solid-like character of the solution (very high values of the elastic modulus, G') not yet attributable to a gel state (similar values of the viscous modulus, G'' and G'), which may be reached only for longer times. The data concerning the gels induced by 30 mM of metal ions, reported in figure 5.12b, show that the G' and G'' have similar values and similar evolutions, indicating that the same levels of elasticity and viscosity are attained in the networks not depending on the fact that the inserted metal is copper or zinc. In the light of the considerations reported here, the cold-set gels of 3.3 mM BLG with a marked solid-like character are formed at higher concentration of metal. However, all the cold-gels induced by the metals, here investigated, have not reached their final state, since the respective rheological data do not show the presence of a final plateau.

An observation of the dried gels after about 24 hours from their formation has been carried out with an optical reflected light microscope, Olympus BX51, 20x, 40x. The gels were dried keeping them at 30 °C for about 10 minutes. Different studied gels showed a very similar aspect. The structure of each one was not homogeneous, as demonstrated by the observation of several zones in the same sample. As an example of this lack of homogeneity, the micrographs of the 10 mM

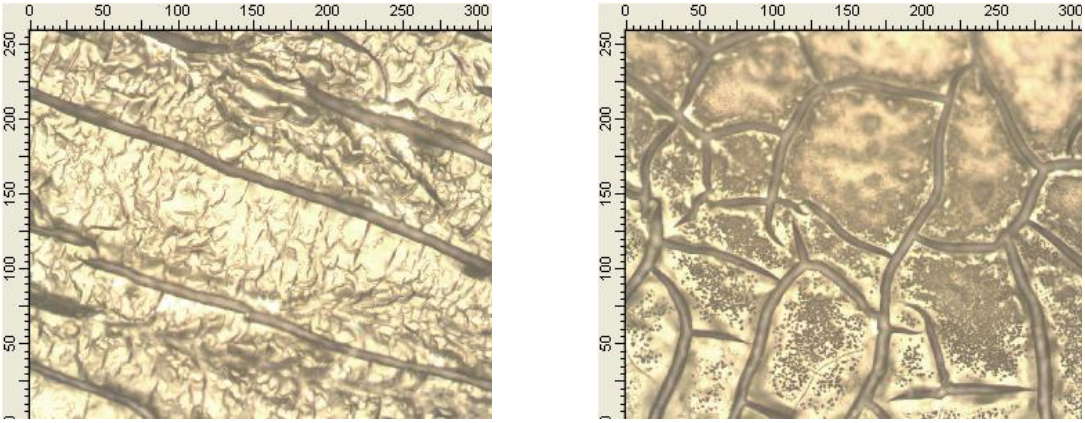

Figure 5.13: Optical micrographs of dried cold induced gels of 3.3 mM BLG at pH 7 induced by 10 mM copper in two several zones of the sample. The scale is in µm.

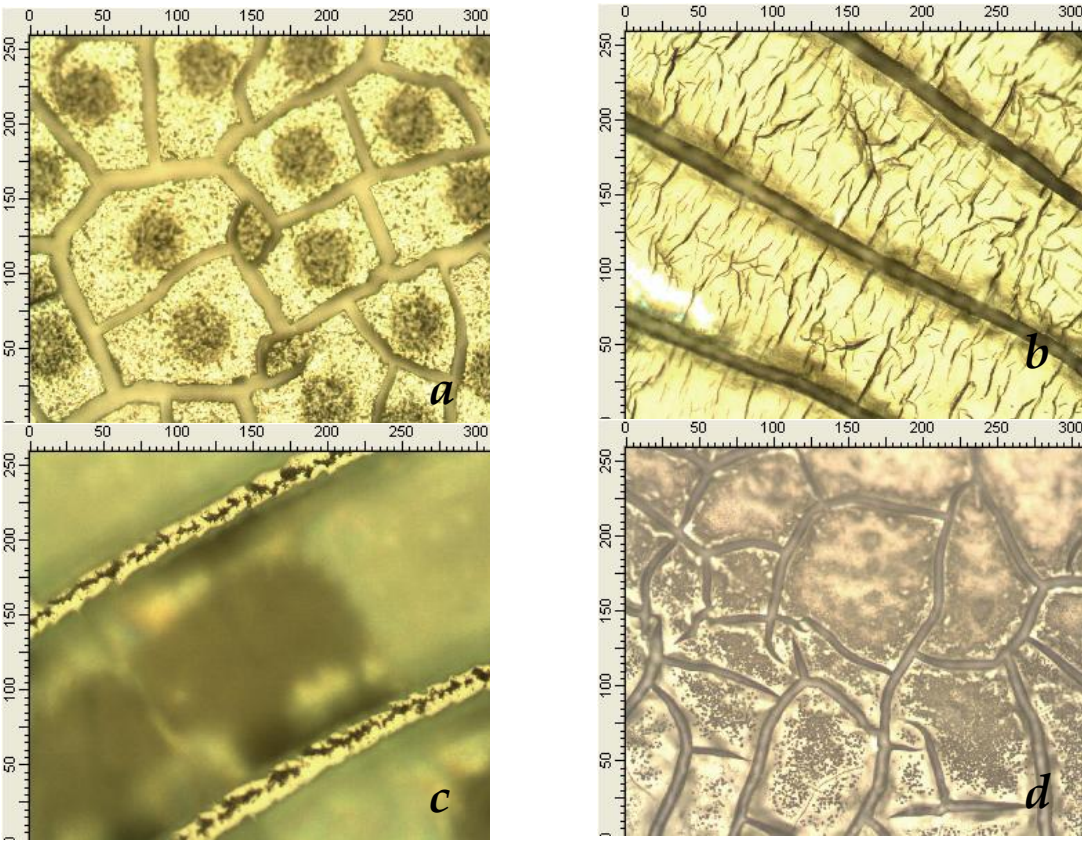

Figure 5.14: Optical micrographs of dried metal ions induced gels of 3.3 mM BLG at pH 7: (*a*) 30Zn-BLG, (*b*) 10Zn-BLG, (*c*) 30Cu-BLG, (*d*) 10CuCl2. The scale is in µm.

Cu-BLG sample realized in two different zones are shown in figure 5.13. These images indicate the presence of cracks in the dried gels. Moving towards the centre, these cracks entwined enclosing some beads of the protein aggregates. Figures 5.14b and c, obtained with a different focus, put in evidence the environment around the cracks and their inner side, respectively. In particular, figure 5.14c reveals the presence of proteins aggregates in the cracks zones appearing as fibril-like structures.

FTIR measurements have been carried out, at room temperature on cold-set gels of BLG induced by metal ions after about 24 hours from their formation. After an opportune normalization, necessary to eliminate changes due to a different concentration of the several aliquots of non-homogeneous gels, these spectra are reported in figure 5.15 together with the BLG spectrum realized at room temperature before and after the incubation of the solution at 60 °C for 2 hours. As a consequence of the normalization procedure, only qualitative considerations can be argued on bands shape. The latter is very similar in the spectra of several studied gels, indicating that no dependence of the band shape on the ionic force[4] is revealed here, once again contrary to the results obtained by FTIR spectra realized on cold-gels of BLG induced at different iron concentrations **[Remondetto et al., 2003]**. Those authors ascribed the observed differences to the formation of gels with a filamentous or random-aggregated structure. However, the lack of significant differences between the FTIR spectra of these gels does not contrast with the differences early observed by rheological measurements. Indeed, the absence of differences in the secondary structure of the gel proteins does not eliminate the possibility of a conformational change at a different supramolecular structure, which can lead to changes in macroscopic properties monitored by rheological measurements. A comparison between FTIR spectra of the cold-gels and the FTIR

[4] Ionic force is defined as follows:

$$\mu = \frac{1}{2}\sum_{i=1}^{n} C_i \times Z_i^2 \ ,$$

where C_i is active ionic concentration and Z_i is ionic charge.

spectrum of BLG solution after the protein incubation at 60 °C for 2 hours shows that differences in the secondary structure of the protein have been induced with the formation of gels. In particular, the contributions related to α-helical structures, to random coil and to anti-parallel β-sheets increase markedly, while the absorption at lower wavenumbers decreases slightly, indicating that the amount of β-aggregated structures decreases slightly with the formation of gels.

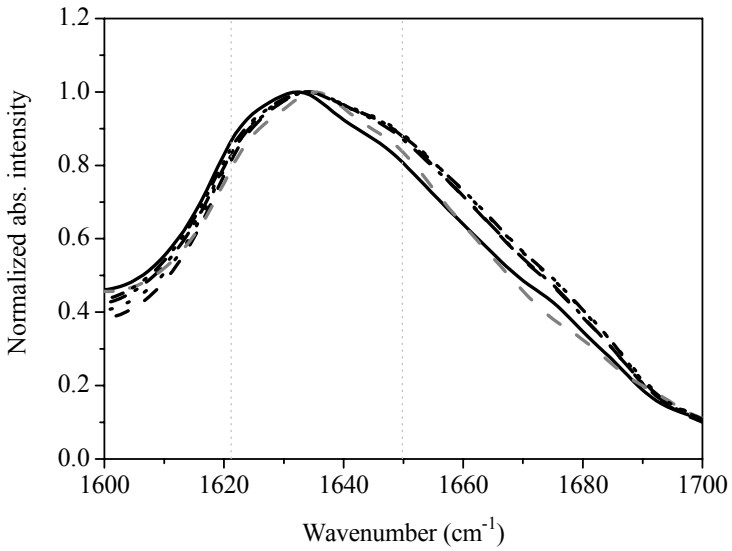

Figure 5.15: FTIR spectra of cold-gels: 10Zn-BLG (dashed line), 30Zn-BLG (dotted line) and 30Cu-BLG (dashed and dotted line); and FTIR spectrum of BLG solution before (dashed grey line) and after (continuous line) 2 hours of incubation at 60 °C. Light grey short dashed lines in the graph indicate, from left to right, the crucial spectral zones assigned to β-aggregated and α-helical structures.

Changes of the secondary structures due to the presence of metal ions in solution are irreversible as evidenced by comparison of the FTIR spectra of gels and native BLG solution (Figure 5.15). FTIR results suggest that the gels are not produced by simple association of structural units constituted by aggregated molecules formed in the pre-heated step, but a rearrangement of the secondary structure of the protein is involved during gel formation. This rearrangement is probably caused by electrostatic interactions increased because of the presence of metal ions in solution. Work is in progress in order to clarify this aspect.

5.2 Bovine Serum Albumin cold-gels induced by copper or zinc ions

On BSA cold-gels we have accomplished a study analogous to the one carried out on BLG cold-gels. The experimental conditions were the same except for the molar concentration of the protein that is 1 mM for BSA.

5.2.1 Characterization of the BSA pre-aggregates

The BSA solutions have been heated for 2 hours at 58 °C. The description of the time evolution of the growth of the aggregates and of the changes of the secondary and tertiary structures induced by heating during the protein incubation has already been reported in paragraph 5.1.1, where the thermal aggregation of BSA in the same experimental conditions has been studied via Dynamic light scattering and FTIR absorption measurements. Thus, we send you back to the paragraph 5.1.1 for more details on the thermal aggregation process of BSA, while here we want only to summarize the results presenting again some crucial graphs.

The time evolution of the normalized scattered light intensity of native BSA reported in figure 5.16 and the size distribution reported in figure 5.17 at three different times show that, after about 18 minutes, BSA molecules have undergone the partial unfolding process, making them able to build small oligomeric aggregates with a mean diameter of about 20 nm after 2 hours of incubation at 58° C. Changes of the secondary and tertiary structures of protein in solution have been monitored by kinetics in the infrared region. In particular, our interest has been focused on the IR absorption band of Amide I e Amide II/Amide II'. We remind that Amide II band is principally associated to the N-H bending **[Miyazawa 1960]**; as a consequence, it is an efficient probe of the H-D exchange of the hydrogen atoms located in the core of the native protein, the exchange being attributable to the heat-induced partial opening of the protein; heating induced modifications on Amide I band allow to have information on the conformational changes of the secondary structure of the protein **[Cai et al., 1999, Pelton et al., 2000]**.

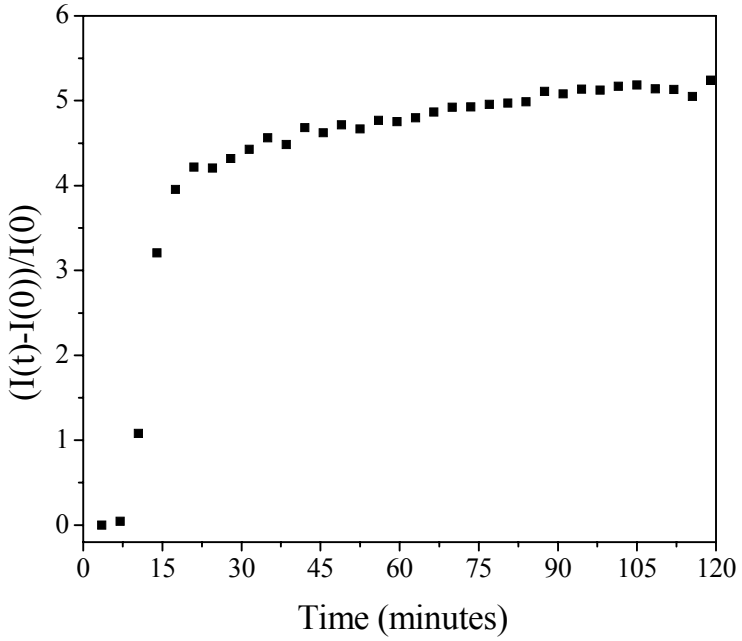

Figure 5.16: Time evolution of the normalized scattered intensity of BSA at pH = 7 and T = 58 °C. The experimental error is smaller than symbol dimension.

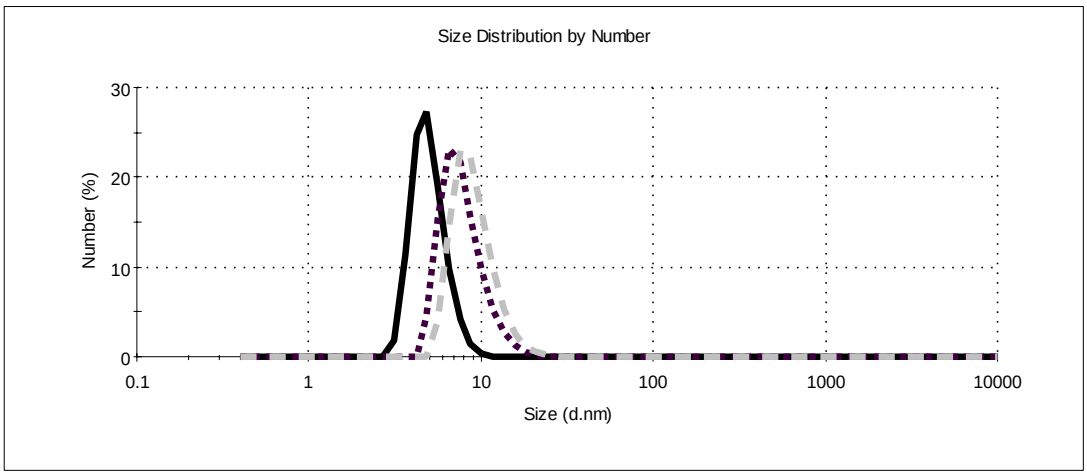

Figure 5.17: Size distribution of BSA aggregates dimension at pH = 7 and T = 58 °C based on the number of the particles present into solution at different three times of the scattering kinetic. Monitored times are an initial (t_i = 3 minutes, black continuous line), intermediate time (t_m = 20 minutes, black short dashed line) and final time (t_f = 120 minutes, gray long dashed line).

A comparison between spectra at the beginning and at the end of the heating step of BSA solution and the differential absorption spectra realized at several times during the protein incubation are reported in figure 5.18. The time evolutions of the absorption intensity of both Amide II (1540 cm^{-1}) and Amide II′ (1450 cm^{-1}) and time evolution of the differential absorption intensity of the component at about 1615 cm^{-1} assigned to strong H-bonded β-aggregated structures **[Allain et al., 1999, Remondetto et al., 2003]** are reported in figures 5.19 and 5.20 respectively. The shown data allow to argue that the formation of small aggregates observed via dynamic light scattering occurs simultaneously to the partial unfolding of the protein and to the formation of β-aggregated structures, originating from the conversion of the α-helical structures as shown and explained in paragraph 5.1.1. In particular, we want again to underline that the spectral component assigned to β–sheets of BSA induced by heating has its maximum at 1615 cm^{-1} instead of 1623 cm^{-1}, which is the value usually assigned to the β-aggregated structures **[Boye et al., 1996, Allain et al., 1999, Remondetto et al., 2003]**. This suggests the existence of stronger H-bonds in solution, probably due to a premature formation of a weak network **[Allain et al., 1999, Remondetto et al., 2003, Navarra et al., 2007]**. This interpretation is coherent with the behaviour outlined in the phase diagram of BSA solution, shown in figure 3.4 **[San Biagio et al., 1996]**.

In order to make sure that changes induced by the heating treatment were not reversible, IR measurement in the same spectral region, on sample kept for 2 hours at 58°C and then cooled at room temperature, has been made. The comparison between this spectrum and that at room temperature before heating shows that the observed changes are not reversible (figure 5.21). The decrease of the contribution related to α-helical structures (at about 1656 cm^{-1}) and the presence of the contribution at about 1615 cm^{-1}, in respect to the not-treated sample, have been observed.

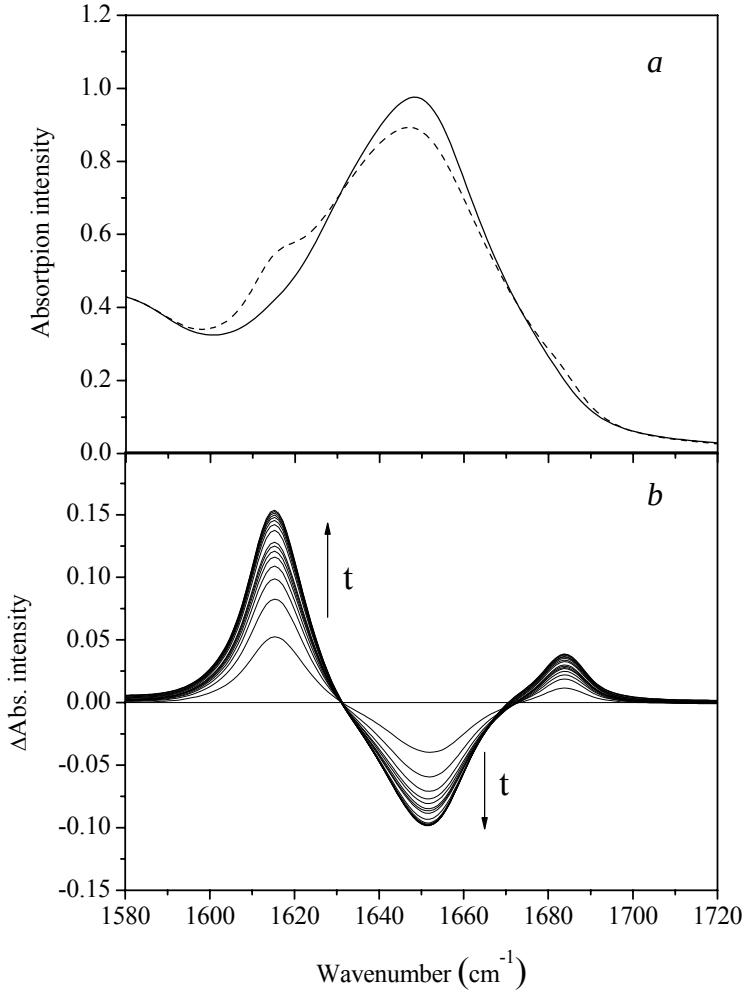

Figure 5.18: (a) FTIR absorption spectra in the Amide I′ region for BSA at pH = 7 and T = 58 °C at the start (continuous line) and at the end (dashed line) of 2 hours heating; (b) correspondent differential spectra.

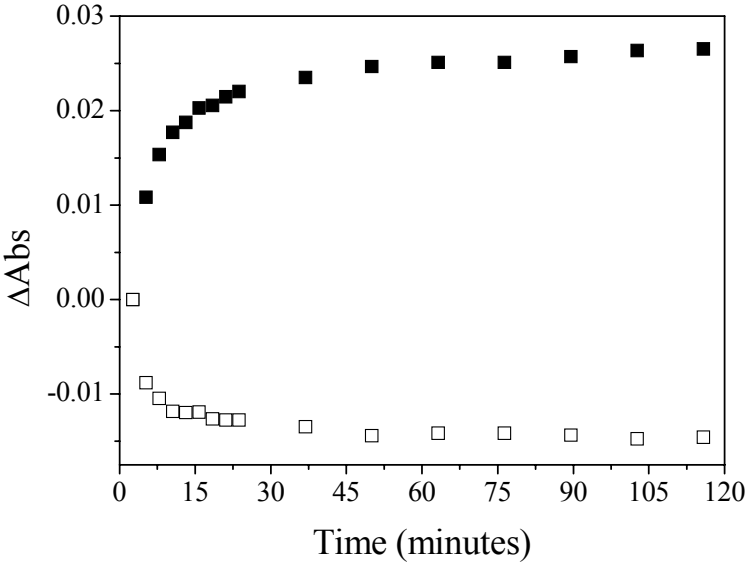

Figure 5.19: Time evolution of the FTIR differential absorption intensity of (■) Amide II′ component at 1442 cm^{-1} and (□) Amide II component at 1540 cm^{-1} of BSA at pH = 7 and T = 58 °C. The experimental error is smaller than symbol dimension.

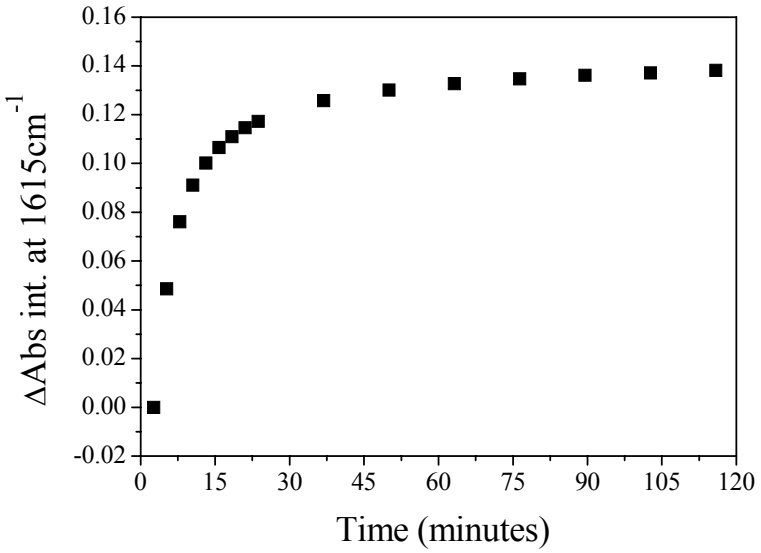

Figure 5.20: Time evolution of the FTIR differential absorption intensity of Amide I′ component at 1615 cm^{-1} of BSA at pH = 7 and T = 58 °C. The experimental error is smaller than symbol dimension.

Moreover, the shift of the band maximum is caused by the further increase of the contribution at 1615 cm^{-1} attributed to intermolecular β-aggregated structures, thus indicating that the formed β-sheets are more pronounced on cooling. The observation of the band at about 1615 cm^{-1} indicates the presence of β-aggregated structures characterized by stronger H-bonds **[Allain et al., 1999, Remondetto et al. 2003]** due to a probable initial formation of a network. This suggested to study the viscoelastic properties of the BSA solution after heating but before metal ions addition. Mechanical spectra (Fig. 5.22), at room temperature immediately after the incubation period, show that the protein solution presents a weak solid-like character with the elastic modulus, G′, greater than the viscous one, G′′, in the frequency range range 0.1 ÷ 200 rad /s thus suggesting that after thermal treatment the globular protein solution is already structured. In order to observe the behaviour of BSA in absence of metal ions, a kinetic measurement has been made. The protein solution, kept for 2 hours at 58 °C and then cooled, has been placed on the rheometry plate; the elastic (G′) and viscous (G′′) moduli were recorded in function of time. After 24 hours only a weak gel is formed with a low G′ value, as shown in figure 5.23.

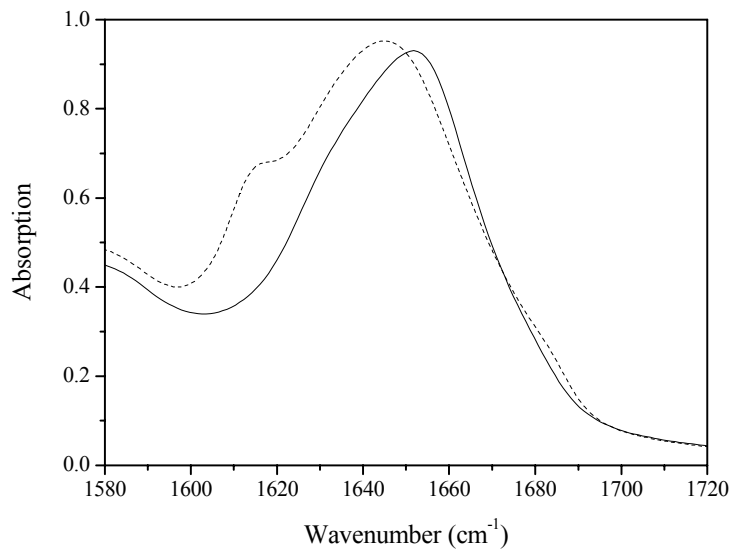

Figure 5.21: FTIR absorption spectra of BSA at pH = 7 at room temperature before (continuous line) and after (dashed lines) heating at T = 58 °C for 2 hours.

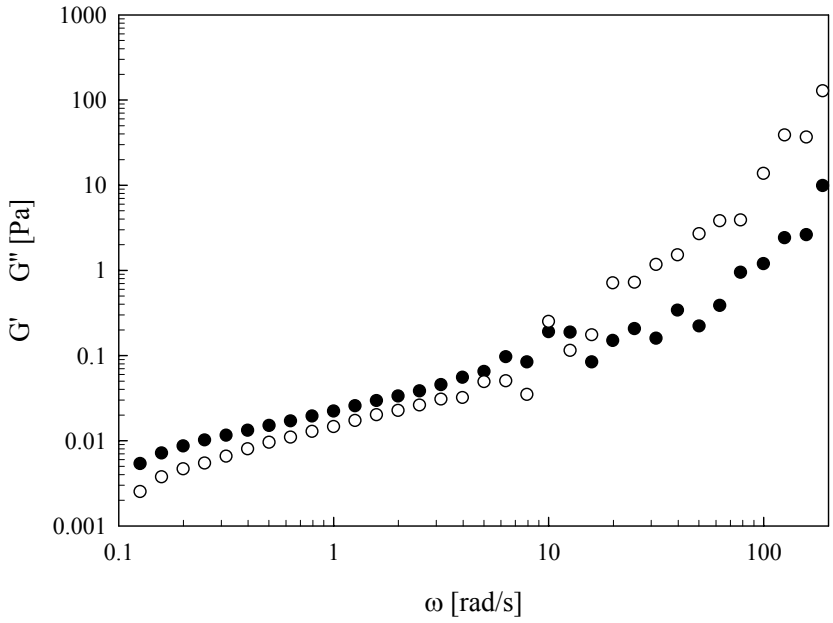

Figure 5.22: Elastic G′ (●) and viscous G′′ (o) modulus as a function of oscillation frequency of BSA solution at pH = 7, after incubation at 58 °C for 2 hours. The frequency sweep has been realized at 20 °C.

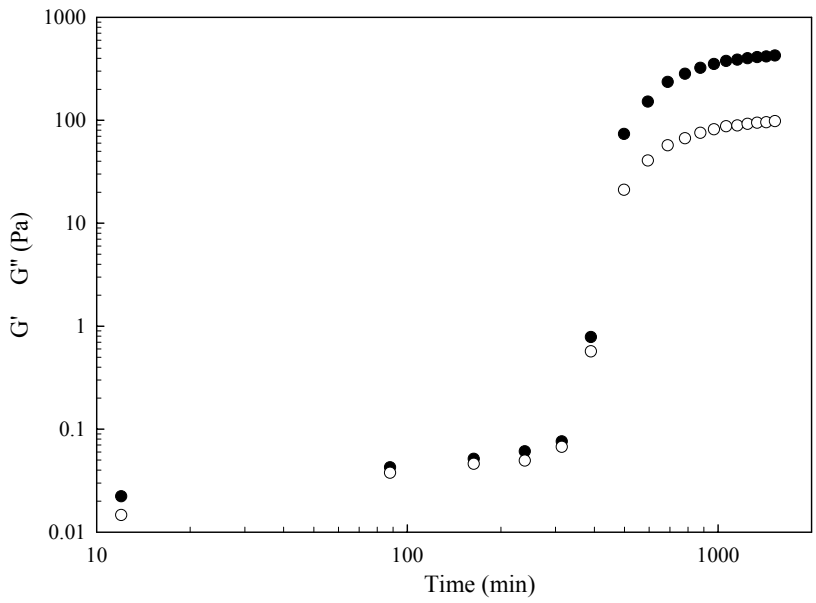

Figure 5.23: Elastic G′ (●) and viscous G′′ (o) modulus as a function of time of BSA solution at pH = 7 after incubation at 58 °C for 2 hours. Kinetic measurements have been realized at 20 °C.

5.2.2 Gels characterization

The addition of metal ions in pre-heated protein solution at room temperature has induced the formation of gels, whose pictures are reported in figure 5.24. In this figure, from left to right, are represented gels obtained from BSA 1 mM after the addition of:

- 0.42% (w/w) glucono-δ-lactone, an acidifier, (A-BSA)
- 10 mM of copper ions (10Cu-BSA)
- 30 mM of copper ions (30Cu-BSA)
- 10 mM of zinc ions (10Zn-BSA)
- 30mM of zinc ions (30Zn-BSA).

The gel induced by the addition of glucono-δ-lactone (0.42% w/w) has been made according to the procedure described in **Alting et al. 2003b**. The addition of an acidifier causes a gradual lowering of pH value of the pre-heated protein solution towards its isoelectric point, reducing the electrostatic interaction between proteins and promoting gel formation. All gels appeared not homogeneous and not transparent.

Figure 5.24: Gels of 1 mM BSA induced by an acidifier and by two different metal ions at two concentration; left to right: A-BSA, 10Cu-BSA, 30Cu-BSA, 10Zn-BSA and 30Zn-BLG.

As for BLG gels, the viscoelasticity of the networks formed through addition of metal ions to the pre-heated BSA solution has been investigated using small deformation dynamical rheological measurements. In particular, the behaviour of the storage modulus (G′) and loss modulus (G′′) as a function of oscillation frequency and time has been measured immediately after the addition of the gelling agents. The behaviour of the G′ and G′′ of BSA cold-set gels induced by metal ions as function of time is reported in figure 5.25. After few minutes, the addition of metal ions induces the formation of a network with a marked solid-like character, as revealed by the remarkable values of G′, always greater than G′′. It is worth noting that the difference between G′ and G′′ values is larger for the zinc induced gels than for the copper ones. G′ values are noticeably higher than those characterizing the kinetic measurement of the only pre-heated BSA solution realized in the same experimental conditions and shown in figure 5.23. This confirms the increase of the connectivity of the network after the addition of metal ions in solution. Moreover, it must be noted that the elastic character of the BSA gels is sensibly higher than those of the corresponding BLG ones. However, the data reported in figure 5.25 show a decrease of the elastic behaviour when the metal concentration is increased. This behaviour has been observed by other authors **[Doi 1993, Remondetto et al., 2003]**, and it has suggested a different supramolecular arrangement in dependence of the metal ions concentration. Indeed, at pH far from pI, the addition of large ion amount is capable to shield the charge present on the surface of proteins, reducing the energy barrier that prevents their approach. The resulting network is coarse, opaque and brittle. On the other hand, at low ion concentration an ordered assembly occurs, whose growth takes place in a "preferential" direction. Gel obtained in the last case are transparent and elastic as evident by the greater G′ value. However, the results obtained here are not in agreement with this explanation, since no BSA metal ions induced gels were transparent.

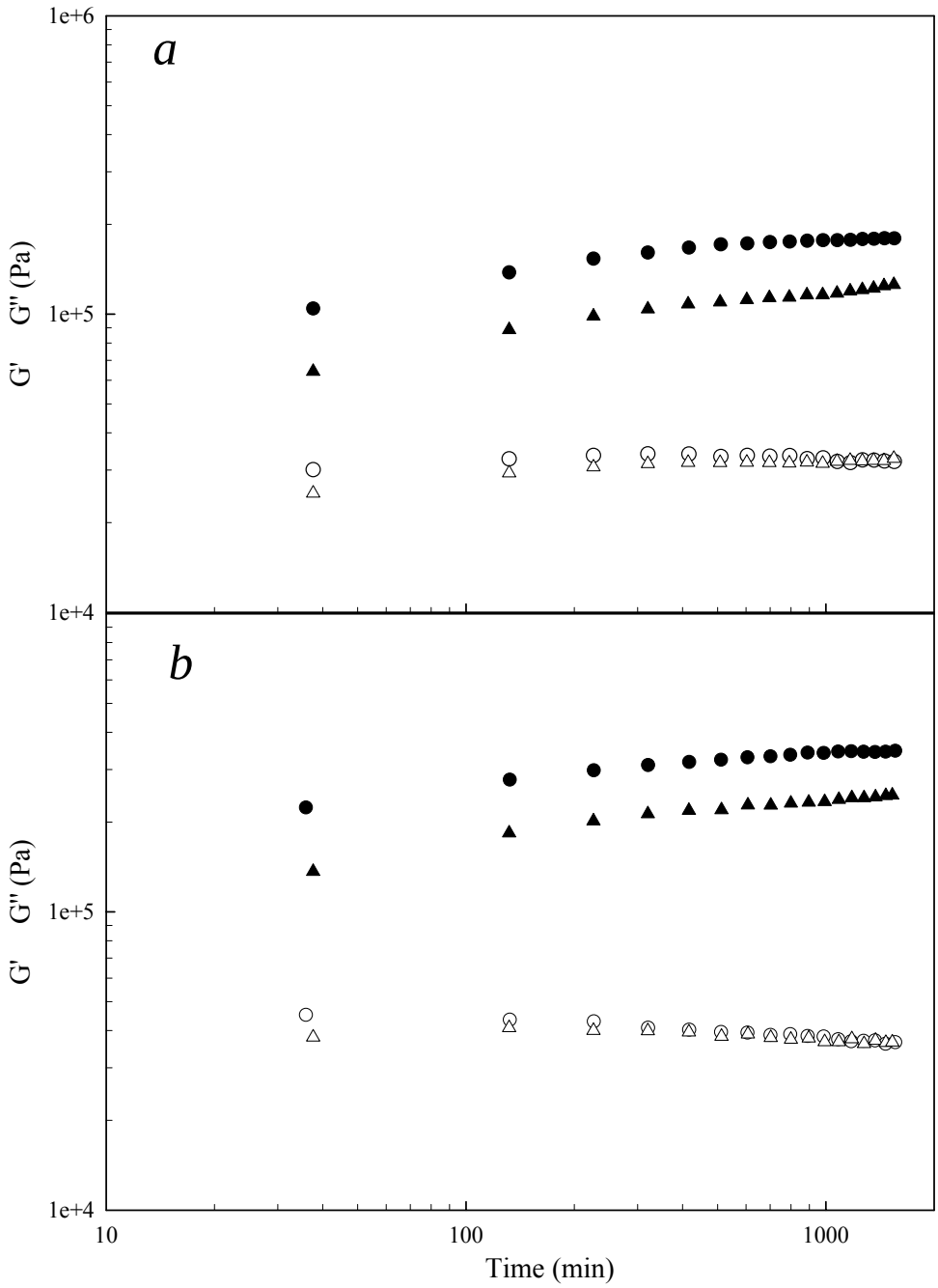

Figure 5.25: Elastic G′ (full symbols) and viscous G′′ (empty symbols) modulus as a function of time of BSA gel induced by (*a*)$CuCl_2$ or (*b*) $ZnCl_2$ with concentration (o) 10 mM or (Δ) 30 mM. Kinetic measurements have been realized at 20 °C.

During the heating step, the protein and the pre-aggregates are negatively charged, being the solution pH far from the isoelectric point of the BSA; addition of divalent cations causes a decrease of the potential repulsive forces between the pre-aggregates, promoting the formation of a network. Several hypothesis may explain this behaviour: *i)* divalent cations act as bridges between the negatively charged carboxyl groups on neighbouring protein molecules; *ii)*, altering the ionic force, cations allow an electrostatic screening effect between protein molecules; obviously, both hypothesis can be valid simultaneously **[Iyer et al., 1996, Hongsprabhas 1997a, 1997b, 1997c and 1999, Bryant et al., 1998, Marangoni et al., 2000, Remondetto et al., 2003]**. Indeed, in the first case the increase of metal concentration should induce a greater and greater lowering of the potential barrier, promoting more and more the proteins aggregation and the gel formation. As a consequence, the increase of the elastic character of gels when the metal concentration decreases suggests that both the shielding action exerted by ions against the charges present on the protein surface and the "bridging" effect due to ability of the ion in coordinating different oligomeric structures play an important role in the network formation. Moreover, this hypothesis is supported by some results obtained by preliminary measurements. These have been carried out on gels induced by the addition of monovalent ions at the same concentration of the divalent ions used earlier, and they have shown no remarkable increase of the elastic modulus. This suggests that probably a greater concentration is necessary in order to reach the same effect induced by the addition of divalent ions, in agreement with the results of other authors **[Kitabatake et al., 1996, Bryant et al., 2000]**. Thus, the formation of gels is due both to the bridging effect of metal ions and to the modification of the ionic force consequent to the presence of the metal ions in solution. The former effect is probably due to bridging action of the copper and zinc, which can bond the histidines or cysteines with a very high affinity **[Mesu et al., 2006, Foley et al., 2007]**. Moreover, Serum albumin is capable to bind an extraordinarily wide range of metabolites, medicine and other organic compounds. BSA forms covalent adducts

with various metal ions, such as Cu^{2+}, Ni^{2+}, Zn^{2+}, and Co^{2+}. The binding of these metals to serum albumin has been widely reported **[Zhou et al., 1994, Sadler et al., 1996, Liang et al., 2001, Liu et al., 2005]**.

Finally, in figures 5.25a and b data obtained in presence of copper and zinc at the same salt concentration are reported. A comparison between the data shown in the latter mentioned figure evidences that addition of zinc ions induces the formation of a more elastic network as illustrated by a G' value of Zn-BSA greater than that of Cu-BSA cold gels. The reasons of such behaviour are not clear yet, but this result surely indicates that the alteration of the ionic force, not involved in the formation of gels at the same concentration of different divalent cations, is not the only cause of the different elastic character of the gels. Studies realized on the coordination of copper or zinc ions in β-amyloides peptides have shown that zinc ion can bind one or two histidine, making itself available for further interaction; this may induce the formation of ordered aggregates, according to a model in which the metal plays the role of a bridge between the imidazole rings of two histidine residues possibly belonging to different peptides **[Stellato et al., 2006]**. By the same study results that copper is tightly bound to three histidines of the same protein molecule in a closed structure, which ''protects'' the metal against any further interaction **[Stellato et al., 2006]**. We can suppose that: i) zinc has a greater effect in promoting gelation because of its wider ability in building bridges between BSA aggregates and/or ii) Cu2+ has a low "effective" concentration since some ions can be used in intramolecular bonds and coordination, becoming them not available to the network construction **[Stellato et al., 2006, Miura et al., 2000, Suzuki et al., 2001]**. Thus, because of BSA nature as sequestrator of many ligands, we hypothesize that some metallic ions could be busy in specific interactions with proteins. An affinity between copper and BSA greater than that between zinc and BSA can explain the greater elastic character of zinc-induced gels in respect to copper-induced gels when the metal ions concentration is the same.

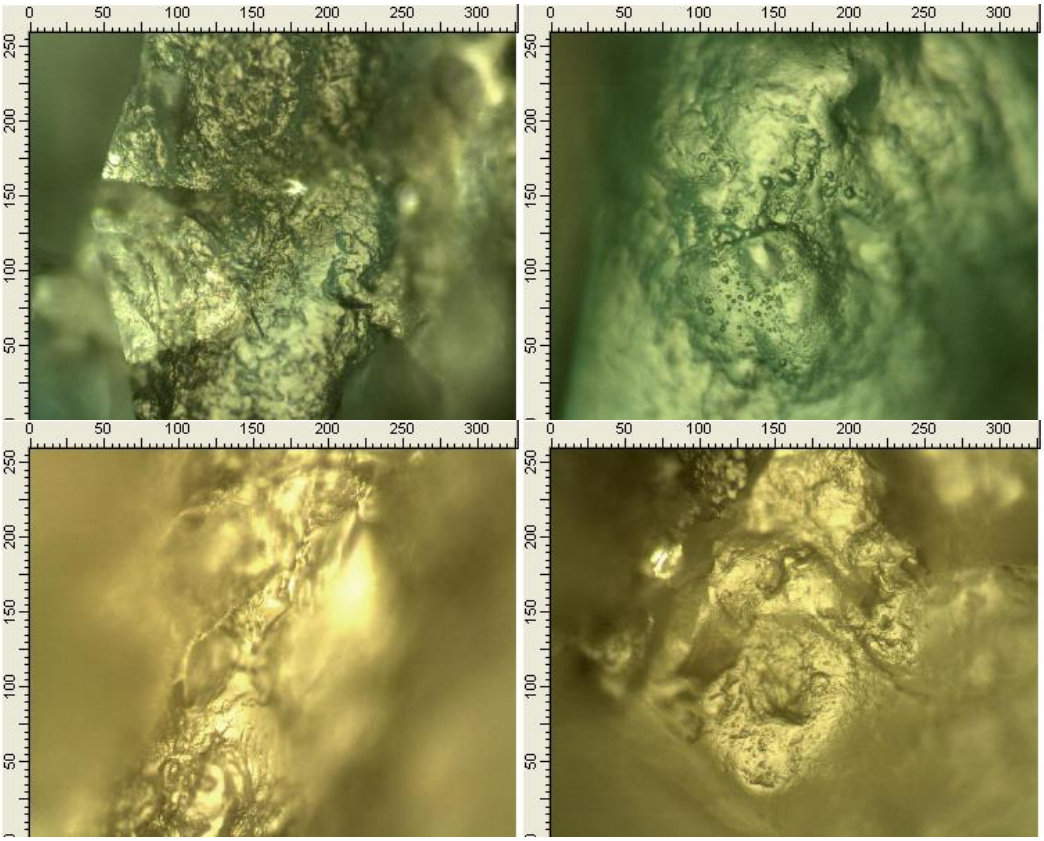

Figure 5.26: Optical micrographs of dried metal ions induced gels of 1 mM BSA at pH 7: (*a*) 10Cu-BSA, (*b*) 30Cu-BSA, (*c*) 10Zn-BSA, (*d*) 30Zn-BSA. The scale is in μm.

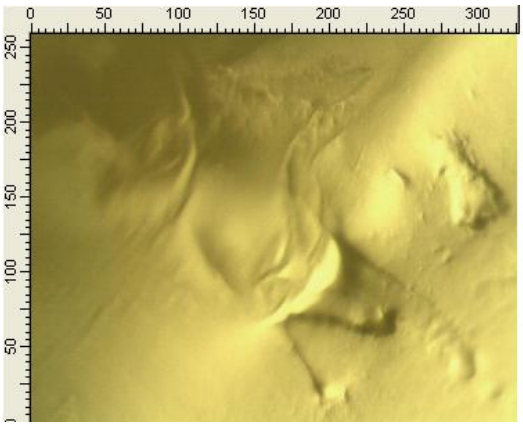

Figure 5.27: Optical micrographs of dried 1 mM BSA cold-set gels of 1 at pH 7 induced by glucono-δ-lactone (0.42% w/w). The scale is in μm.

An observation of the dried gels after about 24 hours from their formation has been carried out with an optical reflected light microscope, Olympus BX51, 20x, 40x. The gels were dried keeping them at 30 °C for about 10 minutes. Four pictures of the gels are reported in figure 5.26. They had a very similar aspect; no evident differences in the gels structure as a function of metal concentration and kind were observed. A different structural aspect is evident in the cold-set BSA gel induced by the acidifier, whose photo is reported in figure 5.27. The A-BSA gel has a less coarse structure in respect to the metal induced gels of BSA.

FTIR measurements have been realized at room temperature on these gels and their spectra are shown after an opportune normalization necessary to eliminate changes due to a different concentration of the several aliquots of non-homogeneous gels. We stress again that, as a consequence of the normalization procedure, only qualitative considerations can be argued about the bands shape. In figure 5.28 the spectra of gels induced by metals are reported together with the spectrum of BSA solution after the incubation at 58 °C for 2 hours. As for BLG cold-induced gels by metal ions, the comparison between gels spectra and BSA solution spectrum realized at room temperature after heat-treatment shows that a rearrangement of the secondary structure occurs during the gel formation. This is probably caused by the electrostatic interactions due to the presence of metal ions in solution. However, it is evident that the relative contribution of the absorption related to strongly H-bonded β-aggregated structures at 1615 cm^{-1} increases, suggesting the formation of a stronger network during making of the gel. The band profiles in the BSA gels spectra are very similar in all the observed cases. The differences of intensity in the spectral region assigned to the vibrational activity of random coils and antiparallel β-sheets show an increase of the absorption intensity with the increase of the metal concentration. However, the band is more intense for the zinc-induced gels.

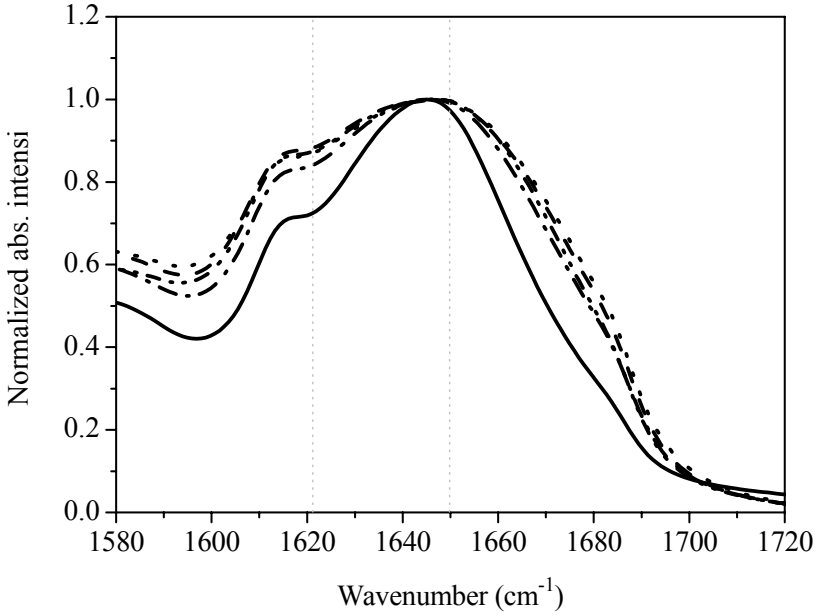

Figure 5.28: FTIR spectra of cold-induced gels: 10Zn-BSA (dashed line), 30Zn-BSA (dotted line), 10Cu-BSA (dashed dotted line) and 30Cu-BSA (dashed dotted dotted line); and FTIR spectrum of BSA solution after (continuous line) 2 hours of incubation at 58 °C. Light grey short dashed lines in the graph indicate the crucial spectral zones assigned to β-aggregated and α-helical structures.

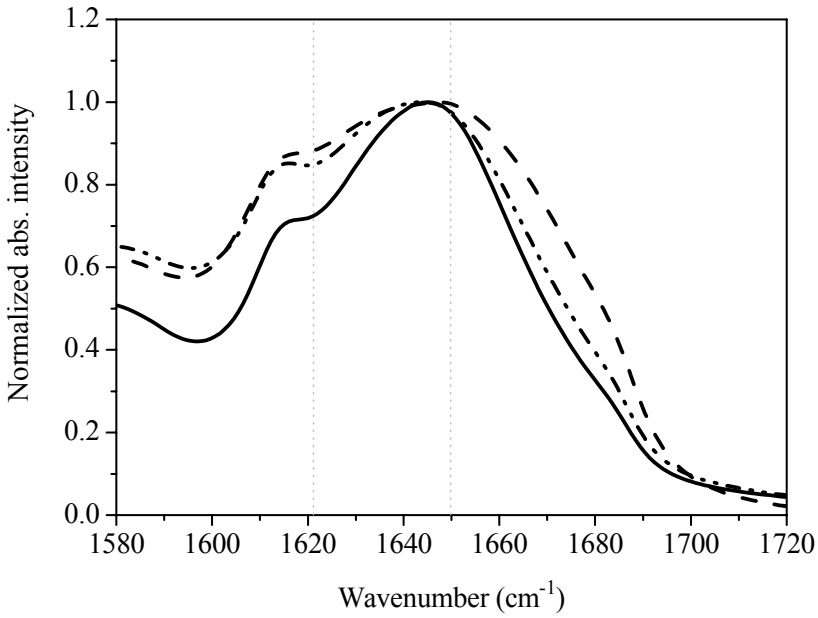

Figure 5.29: FTIR spectra of pre-heated BSA solution (continuous line), of 10Zn-BSA (dashed line) and of A-BSA (dotted line).

This result, in relation with the behaviour of the elastic modulus, G′, as a function of kind of metal ion inducing protein gelation, suggests that the intensity of the contributions on the right side of Amide I′ band may be dependent on the ionic strength in the gel and strongly affected by the different metal efficiency to form gels. This behaviour could be explained by an increased structural contraction resulting from the effects of the ionic forces that lead to an increase in the molecular interactions in the aggregates **[Remondetto et al., 2003]**. The FTIR spectrum of BSA cold-induced gels by glucono-δ-lactone is reported in figure 5.29 in comparison with a Zn-BSA 10 mM spectrum and with a BSA solution spectrum after heating. The rearrangement occurring during the gel formation induced by the addition of an acidifier to the pre-heated solution of BSA is slighter in respect to the one induced by metal ions; however, its existence in A-BSA gel suggests that the rearrangement and the electrostatic interactions because of the ions presence in solution can be related. Indeed, the A-BSA gel is induced by the gradual lowering of pH value of the pre-heated protein solution towards its isoelectric point, reducing the electrostatic interaction between protein molecules. Finally, the absorption intensity at 1615 cm^{-1} is very similar in the A-BSA and Zn-BSA gels, suggesting that they are both characterized by a comparable amount of β-aggregated structures strongly H-bonded to the gel network.

Chapter 6 - Conclusions

In this Ph.D. thesis the aggregation processes and the cold-set gels of some model proteins have been studied, focusing the interest on the effects induced by metals on the aggregation pathway peculiar of the protein and on the gels properties. In particular, the model proteins used for this investigation are β-Lactoglobulin (BLG) and Bovine Serum Albumin (BSA). Both have been widely studied and their aggregation pathways characterized in different experimental conditions (Chapter 1), with a relevant scientific contribution resulting from many studies carried out by the molecular biophysics group at the Dept. of Physical and Astronomical Sciences (DSFA) in Palermo. These two proteins have different dimensions, different secondary structure (BSA constituted predominantly by α-helices, while BLG by β-sheets) and a different conformational stability as a function of pH values and of incubation temperatures. BSA preserves its monomeric conformation as a function of pH values and it has a more compact structure, due to the presence of a greater number of disulfide bonds.

As it is more widely discussed in the first chapter, recent studies have indicated that metal ions have an active role in the aggregation processes of biological systems and are able to induce cold gels. In particular, it has been observed that the senile plaques typical of Alzheimer disease contain high quantities of metal ions, such Cu^{+2}, Fe^{+3} e Zn^{+2}. Moreover, these accelerate the fibrils formation originating by beta amyloid peptide, i.e. the main component of the plaques. This result has suggested that metal ions may have a key role in the etiology of different pathologies (amyloidos) such as Parkinson's, Alzheimer and Creutzfeldt-Jacob diseases. Moreover, other studies have put in evidence the ability of metal ions to induce the formation of cold-gels, whose structural properties can be modulated varying the concentration of metal ions. Recently, the interest towards this kind of gels has widely increased, since they represent an alternative way to

obtain gels from proteins allowing immediate applications in food technology, pharmaceutics and engineering. This procedure may also be very important in biotechnology and, in particular, in tissue engineering because the last gelation step does not require high temperatures, enabling, in this conditions, the cell growth. The use of BSA and BLG, which are whey proteins (being BLG the most abundant), adds value to this thesis, since the information obtained on the metal induced gels nature may find application in the field of food technology. Thus, the research work carried out during my Ph.D. has tried to clarify the role played by metal ions in these processes. Our attention has been focused on metal induced conformational changes of the secondary and tertiary structures and on the properties of the aggregates, in dependence of the kind and the conformation of the protein and of the kind and concentration of the metals. In this scenario, a deeper understanding of the mechanisms through which metal ions affect protein aggregation processes is fundamental both for basic researches and for biomedical and food-technological applications.

Metal effects on thermal aggregation processes

With respect to the study of the metal effects on the thermal aggregation of proteins, the experimental approach was based on the study of the conformational changes of the secondary and tertiary structures via FTIR spectroscopy and on the study of the growth and structure of the aggregates via dynamic light scattering. In particular, the metal effects on the aggregation kinetic evolution have been investigated on BLG and BSA at neutral pH and on the BLG at different pH values, leading to several conformations of the protein. At acidic pH, the contribution of different concentrations of metals has been investigated. The main results are reported in the following.

- The study carried out on BLG at neutral pH has shown that metal ions affect the tertiary and secondary structure changes and the time evolution of the supramolecular aggregates formation. It has been observed that Cu^{2+} and

Zn^{2+} play a different role in conditioning the time evolution of the heat-induced aggregation process. In particular, Cu^{2+} influences mainly the time evolution of the protein secondary structure and of its initial conformational changes, inducing the formation of stronger H-linked bonds but not influencing dramatically the trend of aggregates formation. On the other hand, Zn^{2+} determines similar weak effects on the conformational changes of BLG, but it dramatically induces the formation of big aggregates in a shorter time. Thus, it has been found that zinc promotes the aggregation of BLG at neutral pH, probably through the making of metal bridges between two cysteines of different proteins, suggesting that the extent of the aggregation is due to the increased electrostatic interactions. The fractal dimension of the aggregates of BLG and Cu-BLG is very similar and suggests the formation of "fibrils-like" aggregates assuming a slightly more open geometry in presence of copper. FTIR results suggest the existence of specific interactions between copper and protein reducing the screening effect of copper ions and causing the different observed behaviour of both metals.

- The effect of the presence of copper in solution during thermal aggregation of BLG at acidic pH has been investigated at different concentration of metal. The obtained results have shown that the presence of Cu^{2+} ions affects slightly the time evolution of the aggregation process and of the growth of the mean dimension of BLG aggregates at pH 4 and 2.5. In particular, only a mitigated formation of aggregates has been observed. The number and the dimensions of these aggregates increase with increasing the copper concentration in solution, indicating that the presence of the metal promotes the aggregation of BLG. The dimension growth is higher at pH 2.5 rather than at pH 4, suggesting that the electrostatic interactions play a key role in the formation of the aggregates. Finally, the aggregates structure does not result affected by the metal in solution, being diverse at different acidic pH values. In particular, the fractal dimension value obtained at pH = 2.5 is

compatible with the formation of very elongated fibrils-like aggregates at very acidic pH values.

- The study of the metal effect in thermal aggregation of BSA carried out at neutral pH and 58 °C allows to argue that the aggregation process is substantially independent on the presence of metal ions in solution. In particular, during the first phase of the scattering kinetic only a slight inhibitory effect of copper has been observed together with a weak promoter effect of zinc. For these reasons it can be argued that the two metals play the same role that in the thermal aggregation of BLG at neutral pH. However, it is important point out that zinc does not induce the aggregates formation with a remarkable increased dimension: this behaviour is probably due to the BSA ability to bind metal ions in inner hydrophobic sites, making them unable to promote aggregation process via bridging or, more simply, screening effects. However, no evidence of a specific coordination between metal and protein has been observed by FTIR masaurements. It is noteworthy that the conformational changes of the secondary structure monitored by FTIR measurements and the evolution of the aggregates growth monitored by scattering measurements have a similar behaviour as a function of time. The most relevant changes occur during the first 20 minutes.

The study of the metal ions effects on thermal aggregation of some model proteins has allowed to get some important information. Different metals can induce different changes in the aggregation features of the same protein in the same experimental conditions (copper and zinc influence on BLG or BSA thermal aggregation at neutral pH). At acidic pH of the protein solution, when the electrostatic interactions play the fundamental role in the promoting of aggregation, the effects depend on the concentration of the metal. Moreover, the study of thermal aggregation at neutral pH influenced by the presence of copper and zinc of two different proteins has put in evidence that the extent of the effects is highly

dependent on the protein nature, though the roles played by the different metals seem to be the same. However, in all the cases here investigated the presence of the metals does not affect the structure of the aggregates, leaving unchanged their fractal dimension both when inserting metals in solution during the protein incubation and when changing the kind and the concentration of metal.

Metal effects on intrinsic properties of cold-induced gels

As far as the study of the cold gels induced by metal ions is concerned, the nature of gels of BLG and BSA induced at room temperature by the presence of copper or zinc has been characterized. To my knowledge, these kinds of gels have been realized and studied for the first time during my Ph.D. The experimental approach has consisted first in the characterization of the pre-aggregates of gels by FTIR and dynamic light scattering measurements, which gave information respectively on the secondary and tertiary structures of the aggregated proteins and on the structure and the dimension of these pre-aggregates. With respect to cold gels formed in the second phase of the cold gelation process, their viscoelastic properties have been investigated immediately after the addition of the metals in solution for more than 24 hours via rheological measurements. After 24 hours the secondary structure of the gelled proteins has been monitored via FTIR measurements and a visual inspection of these gels has been realized with an optical microscope. The main results are reported in the following.

- Cold gels of BLG induced by copper or zinc ions at different concentrations of the metals are formed by pre-aggregates in protein solution at neutral pH characterized by a dimension of about 35 nm and by a fractal dimension of 1.5, consistent with the pre-aggregate formation via linear association of the native units, whose spatial conformation results by its folding. BLG cold gels are not transparent and not homogeneous. Moreover, it has been observed that in the gels induced by metal ions the gelation is very fast, since G′ gets its final value during the first minutes after the addition of metal to the pre-

heated protein solution. The elastic character of BLG copper induced gels does not depend on metal concentration, while BLG gel induced by 10 mM $CuCl_2$ has a higher viscous character. The elastic and viscous characters of BLG cold-gels induced by zinc increase with the increase of zinc concentration. In last analysis, the cold set gels of 3.3 mM BLG with a marked "solid-like" character are formed at the higher concentration of the metals, resulting similar changing the metal kind. Finally, the comparison with BLG gel induced by gluconic acid shows a much lower rate of the gel origination and a lower elastic character of the latter. Visual inspection of BLG cold-gels induced by metal ions has shown a scenario consistent with gels having a mixed structure between filamentous and random aggregated types. The monitoring of the Amide I' after 24 hours the induction of gels has shown that a rearrangement of the secondary structures of the protein has occurred also in respect to one of the pre-aggregates into pre-heated solution.

- Cold gels of BSA induced by copper or zinc ions at different concentrations are formed by pre-aggregates in protein solution at neutral pH characterized by a dimension of about 20 nm. The pre-heated solution of BSA shows a weak "solid-like" character, coherently with the behaviour delineated in the phase diagram of BSA solution deducted by San Biagio et al., 1996. The addition of metal ions induces a much higher elastic character after only few minutes. In general, the gels show to have a similar viscous character, while the elastic character is similar only when the metal concentration added to pre-heated solution is the same. The same metal induces a gel with a higher elastic character with the decrease of the metal concentration. This behaviour supports the hypothesis that a different value of the ionic force plays a more important role than that of metal ions bridging action in the gels formation. Visual inspection of BSA cold-gels show a similar scenario consistent with random aggregated structure; the gel induced by gluconic acid has got a less

coarse structure respect to the metal induced gels of BSA. As it has been already said for BLG gels, the monitoring of the Amide I' 24 hours after the induction of gels has shown that a further rearrangement of the secondary structures of the protein has occurred also in respect to one of the pre-aggregates into pre-heated solution.

The characterization of cold gels induced by metals has allowed to realize some important considerations on the intrinsic properties of the gels and on the interactions nature on which the gels formation is based on. First, it is evident that the elastic character of gels has not the same dependence on the metal concentration with the change of the protein. Moreover, it has been observed that different divalent ions at the same concentrations do not always induce a similar elastic character to the gel. The reasons of such behaviour are not clear yet, but this result surely indicates that the alteration of the ionic force, not involved in the formation of gels at the same concentration of different divalent cations, is not the only cause of the different elastic character of the gels. The morphological structure of the metal-induced gels of a same protein kind appears independent on the concentration of the metal ions added to pre-heated solution; while different structures have been observed between BLG and BSA gels. In all gels monitored, as a consequence of their formation, a rearrangement of the secondary structures of the protein has occurred also respect to one of the pre-aggregates into pre-heated solution.

References

Allain A.F., Paquin P., Subirade M. Relationships between conformation of β-lactoglobulin in solution and gel states as revealed by attenuated total reflection Fourier transform infrared spectroscopy. Biol Macromol 26 (1999), 337-344.

Alting A.C., Hamer R.J., de Kruif C.G., Visschers R.W. Formation of disulfide bonds in acid-induced gels of preheated whey protein isolate. J. Agric. Food Chem. 48 (2000), 5001-5007.

Alting A.C., de Jongh H.J.J., Visschers R.W., Simons J.F.A. Physical and chemical interactions in pH-induced aggregation and gelation of food proteins. J. Agric. Food Chem. 50 (2002), 4674-4681.

Alting A.C., Hamer R.J., de Kruif C.G., Paques M., Visschers R.W. Hardness of cold set whey protein gels determined by the amount of thiol groups rather than by the size of the aggregates. Food Hydrocolloids 17 (2003a), 469-479.

Alting A.C., Hamer R.J., de Kruif C.G., Visschers R.W. Cold-set protein gels; interactions, structure and rheology as a function of protein concentration. J. Agric. Food Chem 51 (2003b), 3150-3156.

Alting, A.C. Cold gelation of globular proteins. Thesis Wageningen University, The Netherlands, 2003

Alting A.C., Weijers M., de Hoog E.H.A., van de Pijpekamo A.M., Cohen Stuart M.A., Hamer R.J., de Kruif C.G. and Visschers R.W. Acid-Induced Cold Gelation of Globular Proteins: Effects of Protein Aggregate Characteristics and Disulfide Bonding on Rheological Properties. J. Agric. Food Chem 52 (2004), 623-631.

Arai S, Hirai M, Reversibility and Hierarchy of Thermal Transition of Hen Egg-White Lysozyme Studied by Small-Angle X-Ray Scattering. Biophys J 76 (1999), 2192-2197.

Atwood C. S., Moir R. D., Huang X., Scarpa R. C., Bacarra N. M., Romano D. M., Hartshorn M. A., Tanzi R. E. & Bush A. I.. Dramatic aggregation of Alzheimer aβ by Cu(II) is induced by conditions representing physiological acidosis. J. Biol. Chem. 273 (1998), 12817–12826.

Aymard P., Durand D., Nicolai T. The effect of temperature and ionic strength on the dimerisation of β-Lactoglobulin. Int J Biol Macromol 19 (1996), 213-221.

Aymard P., Durand D., Nicolai T., & Gimel J. C. Fractality of globular protein aggregates: from the molecular to the microscopic level. Fractals, 5 (1997), 23-43.

Aymard P., Nicolai T, Durand D. Static and Dynamic Scattering of β-Lactoglobulin Aggregates Formed after Heat-Induced Denaturation at pH 2. Macromolecules 32 (1999), 2542-2552.

Bal W., Christodoulou J., Sadler P.J.and Tucker A. Multi-metal binding site of serum albuminJournal of Inorganic Biochemistry, 70(1) (1998) 33-39.

Barbut, S.; Foegeding E.A. Ca2+-induced gelation of pre-heated whey protein isolate. J. Food Sci. 58 (1993), 867-871.

Barnes H.A., Hutton J.F. and Walters K. Rheology Series, 3: An Introduction to Rheology. Elsevier Science 2001.

Barone G., Giancola C., Verdoliva A. DSC studies of the denaturation and aggregation of serum albumin. Thermochim. Acta 199 (1992), 197–205.

Barone G, Capasso S, Del Vecchio P, De Sena C, Fessas D, Giancola C, Graziano G, Tramonri P. Thermal denaturation of bovine serum albumin and its oligomers and derivatives pH dependence. J Thermal Analysis 45 (1995), 1255–1264.

Bauer R. Hansen S. and Øgendal L. Detection of Intermediate Oligomers, Important for the Formation of Heat Aggregates of β-Lactoglobulin. Int. Dairy Journal 8 (1998), 105-112.

Bauer R., Carrotta R., Rischel C. and Øgendal L. Characterization and Isolation of Intermediates in β-Lactoglobulin Heat Aggregation at high pH. Biophys. J. 79 (2000), 1030-1038.

Baussay K., Le Bon C., Nicolai T. Durand D., Busnel J.P. Influence of the ionic strength on the heat-induced aggregation of the globular protein β-Lactoglobulin at pH 7. Int J Biol Macromol 34 (2004), 21-28.

Bell, A.E. Gel structure and food biopolymers. In T. Hardman(Ed.), Gel structure and food biopolymers 251–274. New York, Elsevier Applied Science, (1989).

Berg J.M. Shi Y. The Galvanization of Biology: A Growing Appreciation for the Roles of Zinc. Science 271 (1996), 1081-1085.

Berne B.J. and Pecora R. Dynamic light scattering. Wiley Interscience New York,New York (1976).

Bertran J., Rodriguez-Santiago L. and Sodupe M. The different Nature of Bonding in Cu^{+}-Glycine and Cu^{+2}-Glycine. J. Phys. Chem. B 103 (1999) 2310-2317.

Bohren C.F., Huffman D.R., Absorption and Scattering of Light by Small Particles, Wiley, New York, 1983.

Bouhallab S., Henry G., Caussin F., Croguennec J., Fauquant J., Mollè D., Copper-catalyzed formation of disulfide-linked dimer of bovine β-Lactoglobulin, Lait 84 (2004), 517-525.

Boye J.I., Ismail A.A. Alli I. Effect of Physico-Chemical Factors on the Secondary Structure of β-Lactoglobulin. J. Dairy Res. 63 (1996), 97-109.

Bransden B.H., Joachi C.J. Physics of atoms and molecules. John Wiley & Sons, New York, 1983.

Brewer S.H., Glomm W.R., Johnson M.C., Knag M.K., Franzen S. Probing BSA binding to citrate-coated gold nanoparticles and surfaces. Langmuir 21 (2005), 9303–9307.

Brownlow S., Cabral J.H.M., Cooper R., Flower D.R., Yewdall S.J, Polikarpov I., North A.C.T. & Sawyer L. Bovine β-lactoglobulin at 1.8 Å resolution - still an enigmatic lipocalin. Structure, 5 (1997), 481-495.

Bryant C.M. and McClements D.J. Molecular basis of protein functionality with special consideration of cold-set gels derived from heat-denatured whey. Trends in Food Science and Technology 9 (1998), 143-151.

Bryant C.M. and McClements D.J. Influence of NaCl and CaCl2 on Cold-Set Gelation of Heat-denatured Whey Protein. J. Food Sci. 65 (2000), 801-804.

Bulone D, San Biagio PL, Palma-Vittorelli MB, Palma MU. The role of water on hemoglobin function and stability. Science 259 (1993), 1335–1336.

Bush AI, Pettingell WH, Multhaup G, Paradis M, Vonsaltel J, Gusella JF, Beyreuther K, Masters CL and Tenzi RE, Rapid induction of Alzheimer's Aβ amyloid formation by zinc. Science 265 (1994), 1464-1467.

Bush, A. I., Moir, R. D., Rosenkranz, K. M. and Tanzi, R. E. Response. Science 268 (1995), 1921-1923.

Byler D.M., Susi H. Examination of the secondary structure of proteins by deconvolved FTIR spectra. Biopolymers. 25, (1986), 469–487.

Cai S., Singh B.R. Identification of b-turn and random coil amide III infrared bands for secondary structure estimation of proteins. Biopolymers 80 (1999), 7-20.

Carrotta R. Bauer R., Waninge R. and Rischel C. Conformational characterization of oligomeric intermediates and aggregates in β-Lactoglobulin heat aggregation. Protein Science 10 (2001), 1312-1318.

Carrotta R., Arleth L., Pedersen J.S., Bauer R. Small-Angle X-Ray Scattering Studies of Metastable Intermediates of β-Lactoglobulin Isolated After Heat-Induced Aggregation. Biopolymers 70 (2003), 377-390.

Carrotta R., Di Carlo M., Manno M., Montana G., Picone P., Romancino D., and San Biagio P. L., Toxicity of recombinant {beta}-amyloid prefibrillar oligomers on the morphogenesis of the sea urchin Paracentrotus lividus. FASEB J. 20 (2006), 1916-1917.

Carter D.C. Ho J.X. Structure of Serum Albumin. Adv. Protein Chem. 45 (1994), 153-203.

Channu B.C., Kalpana H.N., Eregowda G.B., Dass C., Houghton P.J. and Thimmaiah K.N., Interaction of substituted phenoxazine chemosensitizers with bovine serum albumin. Journal of Pharmaceutical and Biomedical Analysis 21 (1999), 775-785.

Cheftel J.-C., Cuq J.-L. & Lorient D. (1985). Protéines Alimentaires. In: Biochimie - Propriétés Fonctionnelles - Valeur Nutritionnelle - Modifications Chimiques, pp.156-192.Technique et Documentation Lavoisier, Paris.

Chen J., & Dickinson E. Effect of monoglycerides and diglycerol-esters on viscoelasticity of heat-set whey protein emulsion gels. Int. J. Food Sci. and Technol., 34 (1999),. 493–501.

Chiti F. Webster P., Taddei N., Clark A., Stefani, M. , Ramponi, G. & Dobson, C. M.. Designing conditions for in vitro formation of amyloid protofilaments and fibrils. Proc. Natl. Acad. Sci. USA 96 (1999), 3590-3594.

Chiti F. Taddei N., Baroni F., Capanni C., Stefani M., Ramponi G., Dobson C.M. Kinetic partitioning of protein folding and aggregation. Nature Struct –biol 9 (2002), 137-143.

Clark, A. H.; Saunderson, D. H. P.; Suggett, A. Infrared and Laser-Raman Spectroscopic studies of thermally-induced Globular Protein Gels. Int J Peptide Protein Res 1981, 17, 353-364.

Cleary J. P., Walsh D. M., Hofmeister J. J., Shankar G.M., Kuskowski M. A., Selkoe D. J. & Ashe K. H., Natural oligomers of the amyloid-β protein specifically disrupt cognitive function. Nat. Neurosci. 8, (2005) 79–84.

Comai M., Dalla Serra M., Potrich C., Menestrina G., Cu2+ and Zn2+ effects on beta-amyloid aggregation and structural conformation. Biophys J 84 (2003), 337a.

Curry S., Brick P. and Franks N.P. Fatty acid binding to human serum albumin: new insights from crystallographic studies. Biochimica et Biophysica Acta (BBA) - Molecular and Cell Biology of Lipids 1441 (1999), 131-140.

D'Alfonso L., Collini M. and Baldini G. Does β-Lactoglobulin Denaturation Occur via an Intermediate State? Biochemistry 41 (2002), 326-333.

Danielsson J., Pierattelli R., Banci L. and Graslund A., High-resolution NMR studies of the zinc-binding site of the Alzheimer's amyloid β-peptide. FEBS Journal 274, (2007) 46–59.

Danscher, G., Jensen, K. B., Frederickson, C. J., Kemp, K., Andreasen, A., Juhl, S., Stoltenberg, M., and Ravid, R. Increased amount of zinc in the hippocampus and amygdala of Alzheimer's diseased brains: A proton-induced X-ray emission spectroscopic analysis of cryostat sections from autopsy material. J. Neurosci. Methods 76 (1997), 53–59.

de la Fuente M.A, Singh H., and Hemar Y. Recent advances in the characterisation of heat-induced aggregates and intermediates of whey proteins. Trends in Food Science and Technology 13 (2002), 262-274.

Dill K.A. Dominant Forces in Protein Folding. Biochem 29 (1990), 7133-7155.

Dobson C.M: Protein misfolding, evolution and disease. Trends Biochem Sci 24 (1999), 329-332.

Dobson C.M: Principles of protein folding, misfolding and aggregation. Seminars in Cell & Developmental Biology 15 (2004), 3-16.

Doi E. Gels and gelling of globular proteins. Trends Food Sci Tech 1 (1993) 1-5.

Doi, E.; Kitabatake, N. Structure and Functionality of Egg Protein. In Food proteins and their applications. Damadoran, S., Paraf, A. Eds.; Marcel Dekker Inc.: New York, 1997; pp325-340.

Donato L., Garnier C., Novales B. and Doublier J.-L., Gelation of globular protein in presence of low methoxyl pectin: effect of Na+ and/or Ca2+ ions on rheology and microstructure of the systems. Food Hydrocolloids 19 (2005), 549-556.

Donato L., Alexander M. and Dalgleish D.G. Acid Gelation in Heated and Unheated Milks: Interactions between Serum Protein Complexes and the Surfaces of Casein Micelles. J. Agric. Food Chem. 55 (2007), 4160-4168.

Dong, A., Huang, P., and Caughey, W. S. Protein Secondary Structures in Water from Second-Derivative Amide I Infrared Spectra. Biochemistry 29 (1990), 3303–3308.

Dong A., Matsuura J., Manning M.C., and Carpenter J.F. Intermolecular β-Sheet Results from Trifluoroethanol-Induced Nonnative α-Helical Structure in β-Sheet Predominant Proteins: Infrared and Circular Dichroism Spectroscopic Study. Arch. Biochem. Biophys. 355 (1998), 275–281.

Doucet D., Otter D.E., Gauthier S.F. and Foegeding E.A. Enzyme-Induced Gelation of Extensively Hydrolyzed Whey Proteins by Alcalase: Peptide Identification and Determination of enzyme Specificity. J. Agric. Food Chem. 51 (2003), 6300-6308.

Dufour E., Robert P., Renard D., Llamas G. Investigation of β-Lactoglobulin Gelation in Water/Ethanol Solutions. Int. Dairy J. 8 (1998), 87-93.

Elofsson U.M., Dejmek P., Paulsson M.A. Heat-Induced Aggregation of β-Lactoglobulin Studied by Dynamic Light Scattering. Int. Dairy Journal 6 (1996), 343-357.

Esler W.P., Stimson E.R., Jennings J.M., Ghilardi J.R., Mantyh P.W. and Maggio J.E. Zinc-imduced aggregation of human and rat beta-amyloid peptides in vitro. J. Neuroche. 66 (1996), 723-732.

Euston S.R. Ur-Rehman S., Costello G. Denaturation and aggregation of β-lactoglobulin—a preliminary molecular dynamics study. Food Hydrocolloids 21 (2007), 1081–1091.

Fandrich M., Fletcher M.A., Dobson C.M., Amyloid fibrils from muscle myoglobin-even an ordinary globular protein can assume a rogue guise if conditions are right. Nature, 410 (2001), 165-166.

Fandrich M. and Dobson C. M. The behaviour of polyamino-acids reveals an inverse side chain effect in amyloid structure formation. EMBO J. 21 (2002), 5682-5690.

Fang Y. and Dalgleish D.G. Conformation of β-Lactoglobulin Studied by FTIR: Effect of pH, Temperature, and Adsorption to the Oil-Water Interface. J Colloid Interface Sci. 196 (1997), 292-298.

Fang Y. and Dalgleish D.G. The conformation of α-Lactalbumin as a function of pH, heat treatment and adsorption at hydrophobic surfaces studied by FTIR. Food Hydrocolloids 12 (1998), 121-126.

Fessas D., Iametti S., Schiraldi A. and Bonomi F. Thermal unfolding of monomeric and dimeric β–lactoglobulins. Eur. J. Biochem. 268 (2001), 5439-5448.

Fink A.L. Protein aggregation: folding aggregates, inclusion bodies and amyloid. Folding & Design 30 (1998),:R9–R23.

Fitzgerald, D. J. Zinc and Alzheimer's disease. Science 268 (1995), 1920.

Flower D.R. The lipocalin protein family: structure and function, Biochem. J. 318 (1996) 1-14.

Flower D.R., North A.C.T. and Sansom C.E. The lipocalin protein family: structural and sequence overview, Biochimica et Biophysica Acta (BBA) - Protein Structure and Molecular Enzymology 1482, (2000), 9-24.

Foguel D, Suarez MC, Ferrão-Gonzales AD, Porto TCR, Palmieri L, Einsiedler CM, Andrade LR, Lashuel HA, Lansbury PT, Kelly JW, Silva JL, Dissociation of amyloid fibrils of α-synuclein and transthyretin by pressure reveals their reversible nature and the formation of water-excluded cavities. Proc Natl Acad Sci USA 19 (2003), 9831-9836.

Foley S. and Enescu M. A Raman spectroscopy and theoretical study of zinc-cysteine complexation, Vibrational Spectroscopy 44(2) (2007), 256-265.

Foster J.F. In: Rosenoer VM, Oratz M, Rothschield MA (eds) Albumin structure, function and uses. Pregamon Press, Oxford, pp 53–84, (1977).

Fox P.F. The milk protein system. In: Developments in Dairy Chemistry - 4. Functional Milk Proteins, pp. 1-53. Fox P.F. (Ed.), Applied Science Publishers. New York (1989).

Fox J.H., Kama A.J., Lieberman G., Chopra R., Dorsey K., Chopra V., Volitakis I., Cherny R.A., Bush A.I., Hersch S. Mechanisms of Copper Ion Mediated Huntington's Disease Progression. PLoS ONE 2(3) e334 (2007), doi:10.1371/journal.pone.0000334.

Garai K., Sengupta P., Sahoo B., Maiti S., Selective destabilization of solubile β oligomers by divalent metal ions. Biochem. Biophys. Res. Commun. 354, (2006) 210-215.

Garai K., Sahoo B., Kaushalya S.K., Desai R. and Maiti S., Zinc Lowers Amyloid-β Toxicity by Selectively Precipitatimg Aggregation Intermediates. Biochemistry. 46, (2007) 10655-10663.

Gelamo E.L. and Tabak M., Spectroscopic studies on the interaction of bovine (BSA) and human (HSA) serum albumins with ionic surfactants. Spectrochimica Acta A: Molecular and Biomolecular Spectroscopy 56 (2000), 2255-2271.

Gelamo E.L., Silva C.H.T.P., Imasato H., Tabak M., Interaction of bovine (BSA) and human (HSA) serum albumins with ionic surfactants: spectroscopy and modelling, Biochim. Biophys. Acta 1594 (2002), 84–99.

Giancola C, De Sena C, Fessas D, Graziano G, Barone G. DSC studies on bovine serum albumin denaturation. Effects of ionic strength and SDS concentration. Int J Biol Macromol 20 (1997), 193–204.

Gimel J.C., Durand D., & Nicolai T. Structure and distribution of aggregates formed after heat-induced denaturation of globular proteins. Macromolecules 27 (1994), 583–589.

Goers, J.; Permyakov, S.E.; Permyakov, E.A.; Uversky, V.N.; Fink, A.L. Conformational prerequisites for alpha-lactalbumin fibrillation. Biochemistry 2002, 41, 12546-12551.

Gosal W.S., Ross-Murphy S.B. Globular protein gelation. Current Opinion in Colloid & Interface Science 5 (2000), 188-194.

Gosal W.S., Clark A.H. and Ross-Murphy S.B.Fibrillar β-Lactoglobulin Gels; Part 1. Fibril Formation and Structure. Biomacromolecules 5 (2004a), 2408-2419.

Gosal W.S., Clark A.H. and Ross-Murphy S.B.Fibrillar β-Lactoglobulin Gels; Part 2. Dynamic Mechanical Characterization of Heat-Set System. Biomacromolecules 5 (2004b), 2420-2429.

Grdadolnik J., Marechal Y. Bovine serum albumin observed by infrared spectrometry. I. Methodology, structural investigation, and water uptake. Biopolymers. 2001 ;62 (1):40-53.

Griffin W.C., Griffin M.C.A, Martin S.R. & Price J. Molecular basis of thermal aggregation of bovine betalactoglobulin A. J. Chem. Soc. Faruday Trans. 89 (1993), 3395-3405.

Gunasekaran S., Xiao L. & Ould Eleya, M. M. Whey protein concentrate hydrogels as bioactive carriers. Journal of Applied Polymer Science 99 (2006), 2470–2476.

Gunasekaran S., Ko S., Xiao L. Use of whey proteins for encapsulation and controlled delivery applications. J. Food Eng. 83 (2007), 31-40.

Hambling, S. G., McAlpine, A. & Sawyer, L. β-Lactoglobulin, in Milk proteins (Fox, P.F., ed.) pp. 141 -190, Elsevier, London (1992).

Hoffmann M.A.M., Roefs S.P.F.M., Verheul M., van Mil P.J.J.M. & de Kruif, K.G.. Aggregation of β-lactoglobulin studied by in situ light scattering. Journal of Dairy Research, 63 (1996), 423– 440.

Hoffmann M.A.M. and van Mill P.J.J.M. Heat-Induced Aggregation of β-Lactoglobulin: role of the free thiol group and disulphide bonds. J Agric Food Chem 45 (1997), 2942-2948.

Hoffmann M.A.M. and van Mill P.J.J.M. Heat-Induced Aggregation of β-Lactoglobulin as a Function of pH. J Agric Food Chem 47 (1999), 1898-1905.

Hongsprabhas P. and Barbut S.Effects of N-ethylmaleimide and CaCl2 on cold gelation of whey protein isolate. Food Res Int 30 (1997), 451-455.

Hongsprabhas P. and Barbut S. Ca^{2+}-Induced cold gelation of whey protein isolate: effect of two stage gelation. Food Res Int 30 (1998a), 523-527.

Hongsprabhas P. and Barbut S. Structure-forming Processes in Ca^{2+}-Induced Whey Protein Isolate Cold Gelation. Int Dairy J 7 (1998b), 827-834.

Hongsprabhas P., Barbut S. and Marangoni A.G: The Structure of Cold-Set Whey Protein Isolate Gels Prepared with Ca^{++}. Lebensm.-Wiss. u.-Technol. 32 (1999), 196-202.

Hoshi M., Sato M., Matsumoto S., Noguchi A., Yasutake K., Yoshida N. & Sato K. Spherical aggregates of β-amyloid (amylospheroid) show high neurotoxicity and activate tau protein kinase I / glycogen synthase kinase- 3beta. Proc. Natl. Acad. Sci. USA 100, (2003) 6370–6375.

House E., Collingwood J., Khan A., Korchazkina O., Berthon G. & Exley C., Aluminium, iron, zinc and copper influence the in vitro formation of amyloid fibrils of Aβ42 in a manner which may have consequences for metal chelation therapy in Alzheimer's disease. J. Alzheimer's Dis. 6 (2004), 291–301.

Howell N.K. Protein-Protein Interactions in "Biochemistry Food Proteins" (B.J:F. Hudson, ed.) Elsevier Applied Science (1992), 35-74.

Huang X., Atwood C. S., Moir R. D., Hartshorn M. A., Vonsattel J. P., Tanzi R. E. & Bush A. I., Zinc-induced Alzheimer's Abeta1–40 aggregation is mediated by conformational factors. J Biol Chem 272, (1997) 26464–26470.

Iametti S., De Gregori B., Vecchio G. and Bonomi F. Modifications occur at different structural levels during the heat denaturation of β-lactoglobulin. Eur. J. Biochem. 237 (1996), 106-112

Ipsen, R.; Olsen, K.; Skibsted, L.H.; Qvist, K.B.; Gelation of whey protein induced by high pressure, Milchwissenschaft, 2002, 11/12, 650-653.

Israelachvili J. Intermolecular abd Surface Forces. (2nd edn.) Academic Press. (1992).

Iyer H.V. and Przybycien T.M. A Model for Metal Affinity Protein Precipitation. J. Colloid Interface Sci. 177 (1996), 391-400.

Jaenicke R., Protein structure and function at low temperatures, Phylos. Trans. R. Soc. Lond. B 326 (1990), 535–551.

Jimenez J.L. Guijarro J.I., Orlova E., Zurdo J., Dobson C.M., Sunde M. Saibil H.R. Cryo-electron microscopy structure of an SH3 amyloid fibril and model of the molecular packing. EMBO J. 18 (1999), 815–821.

Ju Z.Y. and Kilara A. Effects of Preheating on Properties of Aggregates and of Cold-Set Gels of Whey Protein Isolate. J. Agric. Food Chem. 46 (1998), 3604-3608.

Kaiser J. Alzheimer's: could there be a zinc link? Science 265 (1994), 1365.

Kavanagh G.M., Ross-Murphy B.S. Rheological characterization of Polymer Gels. Prog Polym. Sci. 23 (1998), 533-562.

Kavanagh G.M., Clark A.H., Ross-Murphy B.S. Heat-induced gelation of globular proteins: part 3. Molecular studies on low pH β-lactoglobulin gels. Int. J. Biol. Macromol. 28 (2000), 41–50.

Kawahara M. Neurotoxicity of aluminium and its implication in neurodegenerative disease. Biomed Res Trace Elements 12 (2001), 207-216.

Kawahara M. Aluminum-Induced Conformationl Changes of β-Amyloid Protein and the Pathogenesis of Alzhaimer's Disease. J Health Science 49 (2003), 341-347.

Kelly JW, The alternative conformations of amyloidogenic proteins and their multi-step assembly pathways. Curr Opin Struct Biol 8 (1998), 101-106.

Kinsella, J.E. and Whitehead, D.M. Proteins in Whey: Chemical, Physical, and Functional Properties. Adv. Food Nutr. Res. 33, (1989) 343-438.

Kitabatake, N., Fujita, Y. and Kinkawa, Y.-I. Viscous Sol and Gel Formation from Process Whey Protein Below 25°C. J. Food Sci. 61 (1996), 500-503.

Kitabatake N., Wada R. & Fujita Y. Reversible conformational change in β-lactoglobulin A modified with N-ethylmaleimide and resistance to molecular aggregation on heating. Journal of Agricultural and Food Chemistry 49 (2001), 4011–4018.

Koning M.M.G. and Visser H. in "Protein Interactions" (H. Visser, ed.) VCH Publishers (1992), 1-24.

Kontopidis G., Holt C. & Sawyer L. The Ligand-binding Site of Bovine β-Lactoglobulin: Evidence for a Function?. Journal of Molecular Biology, 318 (2002), 1043-1055.

Kontopidis G., Holt C., and Sawyer L. Invited Review: β-Lactoglobulin: Binding Properties, Structure, and Function. J. Dairy Sci. 87 (2004), 785–796.

Kosa T., Maruyama T., Otagiri N., Species differences of serum albumins: II chemical and thermal stability, Pharm. Res. 15 (1998), 449–454.

Kusumoto Y., Lomakin A., Teplow D. B., and. Benedek G.B Temperature dependence of amyloid β–protein fibrillization. Proc. Natl. Acad. Sci. USA, 95, (1998), 12277–12282.

Le Bon C., Nicolai T. and Durand D. Kinetics of Aggregation and Gelation of Globular Proteins after Heat-Induced Denaturation. Macromolecules 32 (1999), 6120-6127.

Lefevre T., Subirade M. Structural and interaction properties of β-Lactoglobulin as studied by FTIR spectroscopy. Int. J. Food Sci. and Techn. 34 (1999), 419–428.

Lefevre T., Subirade M. Molecular differences in the formation and structure of fine-stranded and particulate beta-lactoglobulin gels. Biopolymers 54 (2000), 578-586.

Lefevre T., Subirade M. Formation of intermolecular β-sheet structures: a phenomenon relevant to protein film structure at oil–water interfaces of emulsions. Journal of Colloid and Interface Science 263 (2003), 59–67.

Leung Sok Line V., Remondetto G.E. and Subirade M., Cold gelation of β-lactoglobulin oil-in-water emulsions. Food Hydrocolloids 19 (2005), 269-278.

Li H. and Thomas G.J. Jr. Cysteine Conformation and Sulphydryl Interactions in Proteins and Viruses. 1. Correlation of the Raman S-H Band with Hydrogen Bonding and Intramolecular Geometry in Model Compounds. J Am Chem Soc 113 (1991), 456-462.

Liang H., Huang J., Tu C.Q., Zhang M., Zhou Y.Q., Shen P.W. The subsequent effect of interaction between Co2+ and human serum albumin or bovine serum albumin. J. Inorg. Biochem. 85, (2001), 167-171.

Librizzi F., Rischel C.,The kinetic behavior of insulin fibrillation is determined by heterogeneous nucleation pathways, Protein Science 14 (2005), 3129 –3134.

Librizzi F., Foderà V., Vetri V., Lo Presti C., Leone M. Effect of confinement on insulin amyloid fibrils formation. Eur Biophys J 36 (2007), 711-715.

Liu T.X., Relkin P., Launay B. Thermal denaturation and heat-induced gelation properties of β-Lactoglobulin. Effects of some chemical parameters. Termochim Acta 246 (1994), 387-403.

Liu X., Xia Y., Fang Y. Effect of metal ions on the interaction between bovine serum albumin and berberine chloride extracted from a traditional Chinese Herb *coptis chinensis franch*. J. Inorg. Biochem 99 (2005), 1449-1457.

Lovell, M. A., Robertson, J. D., Teesdale, W. J., Campbell, J. L., and Markesbery W. R. Copper, iron and zinc in Alzheimer's disease senile plaques. J. Neurol. Sci. 158 (1998), 47–52.

Lovell M.A., Xie C. and Markesbery W. R. Protection against amyloid beta peptide toxicity by zinc. Brain Res. 823 (1999), 88-95.

Maggio, J. E., Esler, W. P., Stimson, E. R., Jennings, J. M., Ghilardi, J. R. and Mantyh, P. W. Zinc and Alzheimer's disease. Science 268 (1995), 1920-1921.

Manno M, Emanuele A, Martorana V, Bulone D, San Biagio PL, Palma-Vittorelli MB, Palma MU. Multiple interactions between molecular and supramolecular ordering. Phys Rev E 59 (1999), 2222–2230.

Manno M, Emanuele A, Martorana V, San Biagio PL, Bulone D, Palma-Vittorelli MB, McPerson DT, Xu J, Parker TM, Urry DW. Interaction of processes on different length scales in a bioelastomer capable of performing energy conversion. Biopolymers 59 (2001), 51–64.

Manno M, San Biagio PL and Palma MU, The Role of pH on Instability and Aggregation of Sickle Hemoglobin Solutions. Proteins 55 (2004), 169–176.

Mantyh PW, Ghilardi JR, Rogers S, De Masters E, Allen CJ, Stimson ER, Maggio JE, Aluminum, iron and zinc ions promote aggregation of physiological concentrations of β-amyloid peptide. J Neurochem 61 (1993), 1171-1174.

Marangoni A. G., Barbut S., McGauley S. E., Marcone M. and Narine S. S., On the structure of particulate gels--the case of salt-induced cold gelation of heat-denatured whey protein isolate, Food Hydrocolloids 14 (2000), 61-74.

McClements, D.J. and Keogh, M.K. Physical Properties of Cold-Setting Gels Formed from Heat-Denatured Whey Protein Isolate J. Sci. Food. Agric. 69 (1995), 7-14.

McKenzie, H. A.; Sawyer, W. H. Effect of pH on beta-lactoglobulins. Nature 1967, 214, 1101–1104.

Mesu J. G., Visser T., Soulimani F., van Faassen E. E., de Peinder P., Beale A. M. and Weckhuysen B. M., New Insights into the Coordination Chemistry and Molecular Structure of Copper(II) Histidine Complexes in Aqueous Solutions. Inorg. Chem. 45 (2006), 1960-1971.

Mie G., Beitrage zur optik truber medien, speziell kolloidaler metallosungen, Ann. Phys. 25 (1908) 377–445.

Militello V, Vetri V and Leone M, Conformational changes involved in thermal aggregation processes of Bovine Serum Albumin, Biophys. Chem. 105 (2003), 133-141.

Militello V., Casarino C., Emanuele A., Giostra A., Pullara F., Leone M., Aggregation kinetics of bovine serum albumin studied by FTIR spectroscopy and light scattering, Biophys. Chem. 107 (2004), 175–187.

Miura T., Suzuki K., Kohata N., Takeuchi H., Metal binding modes of Alzheimer's amyloid β-peptide in insoluble aggregates and soluble complexes, Biochemistry 39 (2000) 7024–7031.

Miyazawa T. Perturbation Treatment of the Characteristic Vibrations of Polypeptide Chains in Various Configurations. J Chem Phys 32 (1960), 1647-1651.

Morante S., Gonzalez-Iglesias R., Potrich C., Meneghini C., Meyer-Klaucke W., Menestrina G., Gasset M. Inter- and intraoctarepeat Cu(II) site geometries in the prion protein: implications in Cu(II) binding cooperativity and Cu(II)-mediated assemblies. J Biol Chem 279 (2004),11753–11759.

Moreira P., Pereira, C., Santos M.S. and Oliveira C. Effect of zinc ions on the cytotoxicity induced by the amyloid beta-peptide. Antioxid. Redox Signal. 2 (2000), 317-325.

Multhaup, G., Schlicksupp, A., Hesse, L., Behler, D., Ruppert, T., Masters, C. L. and Beyreuther, K. The Amyloid Precursor Protein of Alzheimer's Disease in the Reduction of Copper(II) to Copper(I). Science 271 (1996), 1406-1409.

Mulvihill, D.M. and Kinsella, J.E. Gelation characteristics of whey proteins and beta-lactoglobulin. Food Technology41(9) (1987), 102-111.

Mulvihill, D.M. and Kinsella, J.E. Gelation of beta-lactoglobulin: Effects of sodium chloride and calcium chloride on the rheological and structural properties of gels. J. Food Sci. 53 (1988), 231- 236.

Navarra G., Leone M., Militello V. Thermal aggregation of β-lactoglobulin in presence of metal ions. Biophys Chem 161 (2007), 52-61.

Nicolai T., Durand D. and Gimel J.C. Light Scattering: Principles and Development (Brown, W., ed) pp. 201–231, Clarendon Press, Oxford (1993).

Otte J., Zakota M. and Qvist K.B. Involvement of Disulfide Bonds in Bovine β-Lactoglobulin B Gels Set Thermally at Various pH. J Food Sci 65 (2000), 384-389.

Ozaki Y., Mizubo A., Itoh K. and Iriyama K. Inter- and Intramolecular Disulfide Bond Formation and Related Structural Changes in the Lens Proteins. J Biol Chem 262 (1987), 15445-15551.

Paik S.R., Shin H.J., Lee J.H., Chang C.S., Kim J., Copper(II)-induced self-oligomerization of α-synuclein, Biochem. J. 340 (1999) 821–828.

Pan W., Galkin O., Filobelo L., Nagel R.L., Vekilov P.G., Metastable mesoscopic clusters in solutions of sickle-cell hemoglobin, Biophys. J. 92 (2007), 267–277.

Panick G., Malessa R. and Winter R. Differences between the Pressure- and Temperature-Induced Denaturation and Aggregation of β-Lactoglobulin A, B, and AB Monitored by FT-IR Spectroscopy and Small-Angle X-ray Scattering. Biochemistry 38 (1999), 6512-6519.

Papiz M.Z., Sawyer L., Eliopoulos E.E., North A.C.T., Findlay J.B.C., Sivaprasadarao R., Jones T.A., Newcome M.E. & Kraulis, P.J. The structure of β-lactoglobulin and its similarity to plasma retinol-binding protein, Nature 324 (1986), 383-385.

Pelton J.T., Mec Lean L.R. Spectroscopic Methods for Analysis of Protein Secondary Structure. Analytical Biochemistry 277 (2000), 167–176

Pérez M.D. & Calvo M. Interaction of β-lactoglobulin with retinol and fatty acids and its role as a possible biological function for this protein: a review. Journal of Dairy Science, 78 (1995), 978-988.

Pervaiz S. and Brew K. Homology and structure-function correlations between α1-acid glycoprotein and serum retinol-binding protein and its relatives. FASEB J. 1 (1987), 209-214.

Peters T., Serum albumin, Adv. Protein Chem. 37 (1985), 161-245.

Peters TJ All about albumin biochemistry, genetics, and medical applications. Academic Press, San Diego, (1996).

Phillips, L.G.; Whitehead, D.M.; Kinsella, J.E. Structure-Function Properties of Food Proteins; San Diego, Academic press, 1994, pp179-204.

Piazza R., Iacopini S. and Galliano M. BLGA protein solutions at high ionic strength: Vanishing attractive interactions and "frustrated" aggregation. Europhys. Lett., 59 (2002), 149–154.

Provencher S.W. CONTIN: A general purpose constrained regularization program for inverting noisy linear algebraic and integral equations. Comput. Phys. Commun. 27 (1982), 229-242.

Putnam F.W. The plasma protein structure, functions and genetic control. Academic Press, New York, pp 133–172, (1975).

Qi X.L., Holt C., McNulty D., Clarke D.T., Brownlow S. and Gareth R. Jones G.R. Effect of temperature on the secondary structure of b-lactoglobulin at pH 6.7, as determined by CD and IR spectroscopy : a test of the molten globule hypothesis. Biochem. J. 324 (1997), 341-346.

Qin K., Coomaraswamy J., Mastrangelo P., Yang Y., Lugowski S., Petromilli C., Prusiner S.B., Fraser P.E., Goldberg J.M., Chakrabartty A., and Westaway D. The PrP-like Protein Doppel Binds Copper The Journal of Biophysical Chemistry 278 (2003), 8888–8896.

Raman B., Ban T., Yamaguchi K., Sakai M., Kawai T., Naiki H. & Goto Y., Metal ion dependent effects of clioquinol on the fibril growth of an amyloid {beta} peptide. J Biol Chem 280, (2005) 16157–16162.

Rebane K.K. Impurity Spectra of Solids. Plenum Press, New York, 1970.

Religa, D. Strozyk D., Cherny R.A., Volitakis I., Haroutunian V., Winblad B., Naslund J., Bush A.I., Elevated cortical zinc in Alzheimer disease, Neurology 67 (2006) 69–75.

Relkin P. Reversibility of heat-induced conformational changes and surface exposed hydrophobic clusters of β-lactoglobulin: their role in heat-induced sol-gel state transition. Biological Macromolecules, 22: (1998), 59-66.

Remondetto G.E., Paquin P. and Subirade M. Cold Gelation of β-Lactoglobulin in the Presence of Iron. J. Food Sci. 67 (2002) 586-595.

Remondetto G. E., Subirade M., Molecular mechanisms of Fe2+-induced β-Lactoglobulin cold gelation, Biopolymers, 69 (2003), 461-469.

Renard D., Lefebvre J., Griffin M.C.A. Griffin W.G. Effects of pH and salt environment on the association of β-Lactoglobulin revealed by intrinsic fluorescence studies. Int J Biol Macromol 22 (1998), 41-49.

Renard D., Lefebvre J., Robert P., Llamas G., Dufour E. Structural investigation of β-Lactoglobulin gelation in ethanol/water solutions. Int J Biol Macromol 26 (1999), 35-44.

Roefs S.P.F.M. and de Kruif K.G. A model for the denaturation and aggregation of β-Lactoglobulin. Eur J Biochem 226 (1994), 883-889.

Sadler P.J, Tucke A. r, Viles J.H. Involvement of a lysine residue in the N-terminal Ni2+ and Cu2+ binding site of serum albumins 220(1) (1994),193-200.

Sadler P.J. and Viles J.H. ^{1}H and ^{113}Cd NMR Investigations of Cd^{2+} and Zn^{2+} Binding Sites on Serum Albumin: Competition with Ca^{2+}, Ni^{2+}, Cu^{2+}, and Zn^{2+}. Inorg. Chem. 35 (1996), 4490-4496.

San Biagio PL, Palma MU. Spinodal lines and Flory-Huggins free-energies for solutions of human hemoglobin HbS and HbA. Biophys J 60 (1991), 508–512.

San Biagio P.L., Bulone D., Emanuele A., Palma M.U., Self-assembly of biopolymeric structures below the threshold of random cross-link percolation, Biophys. J. 70 (1996) 494–499.

San Biagio PL, Martorana V, Emanuele A, Vaiana SM, Manno M, Bulone D, Palma-Vittorelli MB, Palma MU, Interacting processes in protein coagulation. Proteins 37 (1999), 116–120.

Sawyer L. & Kontopidis G. The core lipocalin, bovine β-lactoglobulin. Biochimica et Biophysica Acta - Protein Structure and Molecular Enzymology, 1482 (2000), 136-148.

Schokker E.P., Singh H., Pinder D.N., Norris G.E., & Creamer L.K. Characterisation of intermediates formed during heat induced aggregation of β-lactoglobulin at neutral pH. Int. Dairy Journal 9 (1999), 791–800.

Schokker E.P., Singh H., Pinder D.N. & Creamer L.K. Heat-induced aggregation of β-lactoglobulin AB at pH 2.5 as influenced by ionic strength and protein concentration. Int. Dairy Journal 10 (2000), 233–240.

Sittikijyothin W., Sampaio P. and Goncalves M.P., Heat-induced gelation of [beta]-lactoglobulin at varying pH: Effect of tara gum on the rheological and structural properties of the gels, Food Hydrocolloids. 21 (2007), 1046-1055.

Stellato F., Menestrina G. Dalla Serra M., Potrich C., Tomazzolli R., Meyer-Klaucke W. Morante S., Metal binding in amyloid β-peptides shows intra- and inter-peptide coordination modes. Eur Biophys J 35 (2006), 340–351.

Stewart A.J., Blindauer C.A., Berezenko S, Sleep D., Sadler P.J. Interdomain zinc site on human albumin.100(7) (2003), 3701-3706.

Subirade M., Loupil F., Allain A.F. and Paquin P. Effect of Dynamic High Pressure on the Secondary Structure of β-Lactoglobulin and on its Conformation Properties as Determined by Fourier Transform Infrared Spectroscopy. Int. Dairy Journal 8 (1998), 135-140.

Sun W.Y., Fang J.L., Cheng M., Xia P.Y., Tang W.X. Secondary Structure Dependence on Metal Ions of Copper, Zinc Superoxide Dismutase Investigated by Fourier Transform IR Spectroscopy. Biopolymers 42 (1997), 297–303.

Sunde M., Blake C.C.F. The structure of Amyloid fibrils by electron microscopy and X-ray diffraction. Adv Prot Chem 50 (1997), 123-159.

Suzuki K. Miura T., Takeuchi H., Inhibitory effect of copper(II) on zinc(II)-induced aggregation of amyloid β-peptide, Biochem. Biophys. Res. Commun. 285 (2001) 991–996.

Taboada P., Gutierrez-Pichel M., Mosquera V. Effects of the molecular structure of two amphiphilic antidepressant drugs on the formation of complexes with human serum albumin. Biomacromolecules 5 (2004), 1116–1123.

Tadros, T.F. Correlation of viscoelastic properties of stable and flocculated suspensions with their interparticle interactions. Advances in Colloid and Interface Science 68 (1996), 97–200.

Taneva S.G., Kaiser U., Donchev A.A., Dimitrov M.I., Mantelle W., Muga A. Redox-Induced Conformational Changes in Plastocyanin: An Infrared Study. Biochemistry 38 (1999), 9640-9647.

Tanford C., Bunville L.G., Nozaki Y. The Reversible Transformation of β-Lactoglobulin at pH 7.5 J Am Chem Soc 81 (1959), 4032–4036.

Tjernberg L. O., Callaway D. J. E., Tjernberg A, Hahne S., Lilliehook C., Terenius L., Thyberg J. and Nordstedt C., A Molecular Model of Alzheimer Amyloid β-Peptide Fibril Formation. J. Biol. Chem. 274 (1999), 12619-12625.

Totosaus, A.; Montejano, J.G.; Salazar, J.A.; Guerrero, I. A review of physical and chemical protein-gel induction. Int. J. Food Sci. Technol. 37 (2002), 589-601.

Uversky VN, Fink AL, Conformational constraints for amyloid fibrillation: the importance of being unfolded. Biochim Biophys Acta 1698 (2004) 131-153.

Vaiana SM, Manno M, Emanuele A, Palma-Vittorelli MB, Palma MU, The role of solvent in protein folding and in aggregation. J Biol Phys 27 (2001), 133–145.

Vaiana SM, Palma-Vittorelli MB, Palma MU. Time scale of protein aggregation dictated by liquid-liquid demixing. Proteins 51 (2003), 147–153.

Vaiana SM, Emanuele A, Palma-Vittorelli MB, Palma MU. Irreversible Formation of Intermediate BSA Oligomers Requires and Induces Conformational Changes Proteins 55 (2004), 1053–1062.

Van Camp, J., Messens, W., Clement, J. and Huyghebaert, A. Influence of pH and Calcium Chloride on the High-Pressure-lnduced Aggregation of a Whey Protein Concentrate J. Ag. Food Chem. 45 (1997), 1600-1607.

Veerman C., Baptist H., Sagis L.M.C. and van der Linden E. A New Multistep Ca^{2+}-Induced Cold Gelation Process for β-Lactoglobulin. J. Agric. Food Chem. 51 (2003a), 3880-3885.

Veerman C, Sagie LMC, Heck J, van der Linden E. Mesostructure of fibrillar bovine serum albumin gels. Int J Biol Macromol 31 (2003b), 139–146.

Vendruscolo M., Zurdo J., MacPhee Cait E. and Dobson C.M. Protein folding and misfolding: a paradigm of self-assembly and regulation in complex biological systems. Phil. Trans. R. Soc. Lond. A 361 (2003), 1205-1222.

Verheul M., Pedersen J.S., Roefs S.P.F. & de Kruif K.G. Association Behavior of Native β-Lactoglobulin. Biopolymers, 49 (1999), 11-20.

Vetri V, Militello V, Thermal induced conformational changes involved in the aggregation pathways of beta-lactoglobulin. Biophys Chem 13 (2005), 83–91.

Vetri V, Librizzi F, Leone M, Militello V, Thermal aggregation of bovine serum albumin at different pH: comparison with human serum albumin. Eur Biophys 36 J (2007a), 717-725.

Vetri V, Canale C, Relini A, Librizzi F, Militello V, Gliozzi A, Leone M, Amyloid fibrils formation and amorphous aggregation in concanavalin. A Biophys Chem 125(1) (2007b), 184–90.

Visschers R.W., de Jongh H.H.J. Disulphide bond formation in food protein aggregation and gelation. Biotech Advances 23 (2005), 75-80.

Wang L., Colon W., Effect of Zinc, Copper and Calcium on the Structure and Stability of Serum Amyloid A. Biochemistry 46(18), (2007) 5562-5569.

Weissbluth, Atoms and Molecules. Academic Press, New York, 1978.

Wilkins D.K., Grimshaw S.B., Receveur V., Dobson C.M., Jones J. A. and Smith L. J. Hydrodynamic radii of native and denatured proteins measured by pulse field gradient NMR techniques. Biochemistry, 38 (1999), 16424-16431.

Wong, D.W.S. Mechanism and Theory in Food Chemistry. Avi, Van Nostrand Reinhold, Eds, New York, 1989, pp48-62.

Wong D.W.S., Camirand W.M. & Pavlath A.E. Structures and Functionalities of Milk Proteins. CRC Critical Reviews in Food Science & Nutrition, 36 (1996), 807-844.

Yan Y., Zhang J., He H. and Zhou H. Oligomerization and Aggregation of Bovine Pancreatic Ribonuclease A:Characteristic Eents Observed by FTIR Spectroscopy. Biophys J 90 (2006), 2525-2533.

Yoshiike Y., Tanemura K., Murayama O., Akagi T., Murayama M., Sato S., Sun X., Tanaka N. & Takashima A., New insights on how metals disrupt amyloid beta-aggregation and their effects on amyloid-beta cytotoxicity. J. Biol. Chem. 276 (2001), 32293–32299.

Yu N., DeNagel D.C., Pruett P.L. and Kuck J.F.R. Disulfide Bond Formation in the Eye Lens. Proc Natl Acad Sci USA 82 (1985), 7965-7968.

Zhang Y., Wilcox D.E. Thermodynamic and spectroscopic study of Cu(II) and Ni(II) binding to bovine serum albumin7(3) (2002), 327-337.

Zhou Y., Wang Y., Hu X., Huang J., Hao Y., Liu H. and Shen P. Equilibrium dialysis of metal-serum albumin. I. Successive stability constants of Zn(II)-serum albumin and the Zn^{2+}-induced cross-linking self-association, Biophys. Chem. 51 (1994), 81-87.

Ziegler, G.R. and Foegeding, E.A. The Gelation of Proteins. Adv. Food Nutri. Res. 34 (1990), 203-298.

Acknowledgements

I wish to devote some pages to acknowledge the people who have contributed to my research work during Ph.D. These people have supplied me with the support of useful discussions and collaborations, which have been necessary to achieve the capabilities of autonomous research and to increase my knowledge of the fascinating Biophysics field.

First, I wish to express my gratitude to my supervisor, Prof. Maurizio Leone, which has shared with me his vast experience. I wish also to acknowledge Prof. Valeria Militello, who has been my second, but not less important, supervisor and has supplied me with scientific support in proteins biology and biophysics; moreover, being a mother like I am, she has known to understand the signs of my tiredness and in those moments she has supplied me with significant encouragement and moral support. Obviously, I thank all the others members of my biophysical research group, Fabio Librizzi, Valeria Vetri and Vito Foderà, for useful discussions and suggestions. I am particularly indebeted with Fabio for the crucial suggestions that have helped me in the interpretation of the dynamic light scattering data discussed in this thesis.

I am grateful to all the professors and colleagues in Palermo. In particular, I wish to thank Prof. Marco Cannas and Eleonora Vella for reading the first draft of the thesis and giving me many helpful suggestions.

A part of my work would not have been accomplished without the collaboration of Dr. Daniela Giacomazza, who has made possible the realization of the rheological measurements at Biophysics Institute of C.N.R., U.O. Palermo (Italy) and has shared with me her experience in the rheological field through precious and stimulating discussions.

I wish to thank Prof. Roberto Boscaino for having introduced me in these last years to the amorphous materials physics, sharing with me his knowledge and his passion for science.

Gianluca Napoli is acknowledged for useful technical assistance.

I confirm to my husband's family and mine my deep gratefulness. In particular, to the former my sincere thankfulness goes to have taken care with much love of my son, Alessandro, almost every day allowing me to devote myself quietly to the draft of this Ph.D. thesis.

Finally, I owe a great debt to my husband, Giancarlo. Nothing of what I have accomplished would have been possible without his caring support. However, I believe that the greatest acknowledegement should be for Alessandro, who has unconsciously already done some renunciations, because of the achievement of this important goal for his mother.

This research was directly supported by M.I.U.R. and C.N.R. fellowships. Partial indirect support was obtained by P.O.R. 2000-2006, Misura 3.15, Azione C and by a National Project (PRIN2005) of the Italian Ministry of University Research.